Author:
Zhang, Chao

Title:
Analysis and Design of FRP-Reinforced Indeterminate Structures

Analysis and Design of FRP-Reinforced Indeterminate Structures

by

Chao Zhang

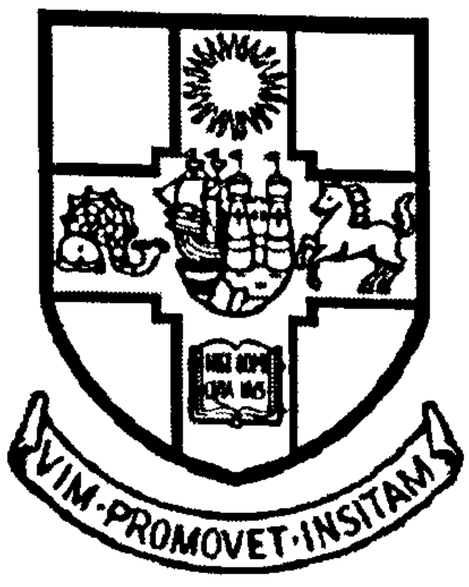

A dissertation submitted to the University of Bristol in accordance with the requirements of the degree of Doctor of Philosophy in the Faculty of Engineering, Department of Civil Engineering

May 2010

To my parents
Shenfu and Jiying

Abstract

There has been limited research on statically indeterminate fibre reinforced polymer (FRP) – strengthened structures. Indeterminacy can give rise to self-equilibrating moments that influence first yield and failure loads, the latter due to potential FRP buckling and end-peel on account of offsets between points of contraflexure and nearby FRP curtailments. For thin-walled metallic structures, buckling failure is also a concern. The nature and extents of these complex effects have not thus far been investigated.

In this PhD study, closed-form algebraic expressions are presented for the self-equilibrating moments, due to differential settlement between supports, developed in 2-span continuous structures. The expressions were written to clearly show how the moments depend on the support-to-member stiffness ratios and on the distribution of stiffness along the member for service and ultimate limit states. Four 2-span carbon FRP (CFRP)-plated steel beam specimens with varying layouts of plates and plate thicknesses have been fabricated and loaded to failure. The instrumentation (strain gauge and displacement transducer) layouts have enabled investigation of several important aspects related to structural indeterminacy and those related to FRP-plated thin-walled metallic structures. One novelty is that the steel stiffeners have been adhesively bonded (rather than welded) to the steel main beams. This proved successful in inhibiting web/flange buckling. In addition, a computational technique was developed for time-efficient prediction of ultimate loads of ductility-deficient indeterminate structures, which was then incorporated into an iterative procedure to create an analysis-design process for indeterminate structures of varying ductility levels.

- The key findings of the research include:

- There exists a 'sensitive zone' for support stiffnesses, within which the moments change rapidly with support stiffnesses and particular care should be taken for test set-up in the lab and also for bridges in practice;

- Adhesive bonding the steel stiffeners to the test beam has worked very efficiently to prevent local flange/web buckling. Local buckling was prevented up to a load of at least 36% higher than the failure load for the beam of similar section but without any stiffeners. This technique is an alternative to welding and allows for safe application of strain gauging at the section of stiffening;

- The general nonlinear stiffness variation can be approximated in a piecewise linear manner. The choice of the number of linear stiffness segments depends on how rapidly the stiffness changes and the precision level specified. A 2-to-5-piece linear stiffness approximation generally gives sufficient representation of the nonlinear stiffness variation;

- This technique has been illustrated by way of examples, which cover a wide range of structural ductility under different types of loading. Convergence was attained after 4-8 iterations in all cases, suggesting that standard structural analysis software for linear beam analysis may well be used confidently for analysing nonlinear problems;

- An iterative procedure has been developed entailing multiple detailing and ultimate analysis loops for the structure to create an analysis-design process for ductility-deficient indeterminate structures. The new analysis-design process has been illustrated by way of examples including a FRP-plated continuous RC beam, a traditional RC continuous beam and a three-storey three-span plane frame. Quick attainment of reinforcement details in all cases suggest that this may well constitute a design procedure applicable to structures of varying levels of ductility. Design based on constant EI may lead to structures with a load deficiency of 12.9% and 9.2% for Examples 1 and 3, respectively; and
- Through thickness strain variation and/or local bending of plates are important in the evaluation of the average shear bond stresses, especially for thick plates. Using outer surface strains only (which is common in the research environment) could lead to unreasonable prediction of interfacial shear stresses.

It is concluded that the self-equilibrating moments should be properly accounted for in designing and analysing FRP-plated indeterminate structures, and that the rigid bond section analysis and piecewise linear stiffness variation can be incorporated into the proposed iterative procedures to construct a reliable analysis and design approach for indeterminate structures of varying ductility levels.

Acknowledgements

I would like to express my sincere gratitude to my supervisor Dr. Wendel Sebastian, for his invaluable advice and guidance throughout the course of this research. He has provided the unfailing source of encouragement that is so essential for the completion of the project, particularly when I was somewhat unsettled at one stage. I am particularly indebted to him for his encouragement for me to pursue the PhD, for his efforts at securing the funding for this PhD study, and for his patient and critical readings of the draft chapters towards completion of this thesis.

I would like to thank the former Overseas Research Students Award Scheme (ORSAS), the University of Bristol and the Department of Civil Engineering for granting me a scholarship. I am also grateful to Professor David Blockley and to Professor Colin Taylor for granting me financial support and for their kindness towards me during my study.

Many thanks are due to all the members of the administration staff at Department of Civil Engineering, in particular Anne Thorpe, Joanna Allsop, Chris Hawkins and Andy Gayner, who have made my study at the department such an enjoyable experience. Special thanks go to Peter Whereat, Dave Hooper, and all the members of the Structures Lab for their help in fabrication and testing of the specimens and all the fun that came along.

I am grateful for help rendered upon my first arrival and then during my stay at this city by my colleague Dr. Jianru Yu. Further gratitude is due to my colleagues and friends for their friendship and encouragement through my time at Bristol, in particular Dr. Matthew Dietz, Dr. Wendy Daniel, Dr. Adam Crew, Dr. Jitendra Agarwal, Dr. Luiza Dihoru, Joel Ross and Said Macharkah. I also wish to acknowledge my appreciation to my work colleagues Dr. Lee Canning and Professor Sam Luke at Mouchel for their valuable advice and encouragement.

Finally, I will always have special gratitude and love to my parents and my sisters.

Declaration

The accompanying dissertation is submitted for the Degree of Doctor of Philosophy in the Faculty of Engineering at the University of Bristol. The work was carried out in the Department of Civil Engineering, University of Bristol, under the supervision of Dr. W. M. Sebastian.

I declare that the work in this dissertation was carried out in accordance with the Regulations of the University of Bristol. The work is original, except where indicated by special reference in the text, and no part of the dissertation has been submitted for any other degree. Any views expressed in the dissertation are those of the author.

The dissertation has not been presented to any other University for examination either in the United Kingdom or overseas.

Signed: Date: May 2010

chaozhang

Chao Zhang

Publications based on this work

The following publications are based on some of the material presented in this thesis.

Sebastian, W. M. and Zhang, C., "Analysis of concrete structures across the ductility spectrum", *Magazine of Concrete Research*, 2008, Vol. 60, No.9, pp.685-690.

Zhang, C. and Sebastian, W. M., "External FRP strengthening of statically indeterminate metallic structures", *Proc. 4th International Conference on FRP composites in Civil Engineering (CICE 2008)*, 2008, Zurich, Switzerland (in CD form).

Table of Contents

List of Tables

List of Figures

Number *Page*

Notation

A_p	Cross sectional area of the FRP plate
$A_{p,hog}$	Cross sectional area of the hogging FRP plate
$A_{p,sag}$	Cross sectional area of the sagging FRP plate
A_{sc}	Area of the steel reinforcement in compression
$A_{s,hog}$	Area of the steel reinforcement in hog
$A_{s,hog}$	Area of the steel reinforcement in sag
A_{st}	Area of the steel reinforcement in tension
b	Width of the section
b_w	Width of the web
C_P, C_W	Moment parameter under point load and distributed load
C_{PN}, C_{PL}	Point load moment parameters for nonlinear and linear regimes
C_{WN}, C_{WL}	UDL moment parameters for nonlinear and linear regimes
c_{cs}	Cover to the centroid of the compression steel
d_c	Depth of the compression concrete
E_a	Young's modulus of adhesive
E_c	Young's modulus of concrete
E_{el}	Elastic energy
EI	Reference flexural stiffness
$EI(x)$	Section stiffness along the member;
E_p	Young's modulus of FRP
E_s	Young's modulus of steel
E_{tot}	Total energy
f_c'	Uniaxial cylinder strength of concrete
f_{cu}	Cube strength of the concrete
f_r	Modulus of rupture of the concrete
f_t	Tensile strength of adhesive
f_y	Yielding stress of steel
	Bulk modulus of concrete

K_0	
h	Depth of the section to the centroid of the plate
k	Support stiffness
k_1, k_2	Stiffness of support 1 and of support 2
G_0	Shear modulus of concrete
L	Span of the beam
$m(x)$	Virtual moment
$M(x)$	Real moment
M_2	Moment at the centre support section
$M_{flexible}$	Moment at centre support section with flexible supports
M_{rigid}	Moment at centre support section with rigid supports
M_u	Ultimate moment capacity
P	Point load
$\overline{P_e}$	Non-dimensional load capacity as relative to the design load when designed to constant EI
$\overline{P_u}$	Non-dimensional ultimate load capacity
R	Support reaction force
t_p	Thickness of the FRP plate
w	Distributed load
$\alpha_1, \alpha_2, \alpha_3, \alpha_4$	Stiffness ratio relative to the reference stiffness
β_1, β_2	Dimensionless stiffness of supports 1 and 2
δ	Differential settlement of supports
ε	Strain
ε_c	Strain in the concrete
ε_i	Inner surface strain of the FRP plate
ε_o	Outer surface strain of the FRP plate
ε_{pl}	Strain in the bonded plate
ϕ_p	Local curvature of the FRP plate
$\gamma_1, \gamma_2, \gamma_3, \gamma_4$	Relative lengths of different segments to the span
γ_m	Partial safety factor for materials
λ	Position parameter of the point load

μ	Support stiffness ratio
μ_{du}	Ductility index
σ_a	Average normal stress in the adhesive
σ_c	Compressive stress in the concrete
ς	Parameter to describe the linear stiffness variation
τ_a	Average shear stress in the adhesive
ξ	Parameter to describe the linear stiffness variation
ζ_P	Self-equilibrating moment parameter for point load case
ζ_W	Self-equilibrating moment parameter for distributed load case
Δx	Distance between two locations along the FRP plate
$\Delta\varepsilon_p$	Difference in longitudinal strain between two locations along the FRP plate
Π	$=\gamma_1+\gamma_2$
Ψ	$=\gamma_1+\gamma_2+\gamma_3$
$(M_{hog})_{EI.const}$	Theoretical hogging moment from linear elastic analysis assuming constant flexural rigidity
$(M_{hog})_{test}$	Experimental hogging moment

Chapter 1

Introduction

1.1 Introduction

The lower bound theorem of plasticity underpins traditional design of statically indeterminate reinforced concrete (RC) structures via the procedure outlined in Figure 1-1. Uncracked analyses for ultimate load cases are followed by dimensioning and/or reinforcement detailing – with moment redistribution for less onerous detailing – to give sufficient ductility via steel yield at peak moment locations. The ductility guarantees sufficient rotation capacity – and therefore sufficient actual moment redistribution capacity – for the design loads to be achieved and so no checks on load capacity are required for the detailed structure.

If the structure is ductility-deficient, then detailing to uncracked analysis and redistribution may be unsafe so an alternative approach is needed. There is more urgency to this need as fibre-reinforced polymer (FRP) composites have been increasingly used for strengthening concrete structures. Owing to their lack of ductility and potential debonding failures, composite materials diminish the moment redistribution capacity of the concrete structure within which they serve as flexural reinforcement. For statically indeterminate structures, this reduction in moment redistribution capacity dictates that the actual failure loads can fall well below the intended failure loads.

One such approach, outlined in Figure 1-2, entails an iterative loop where analysis is conducted to quantify the load capacity of the detailed structure, with any deficiency in capacity triggering a re-detailing of the structure.

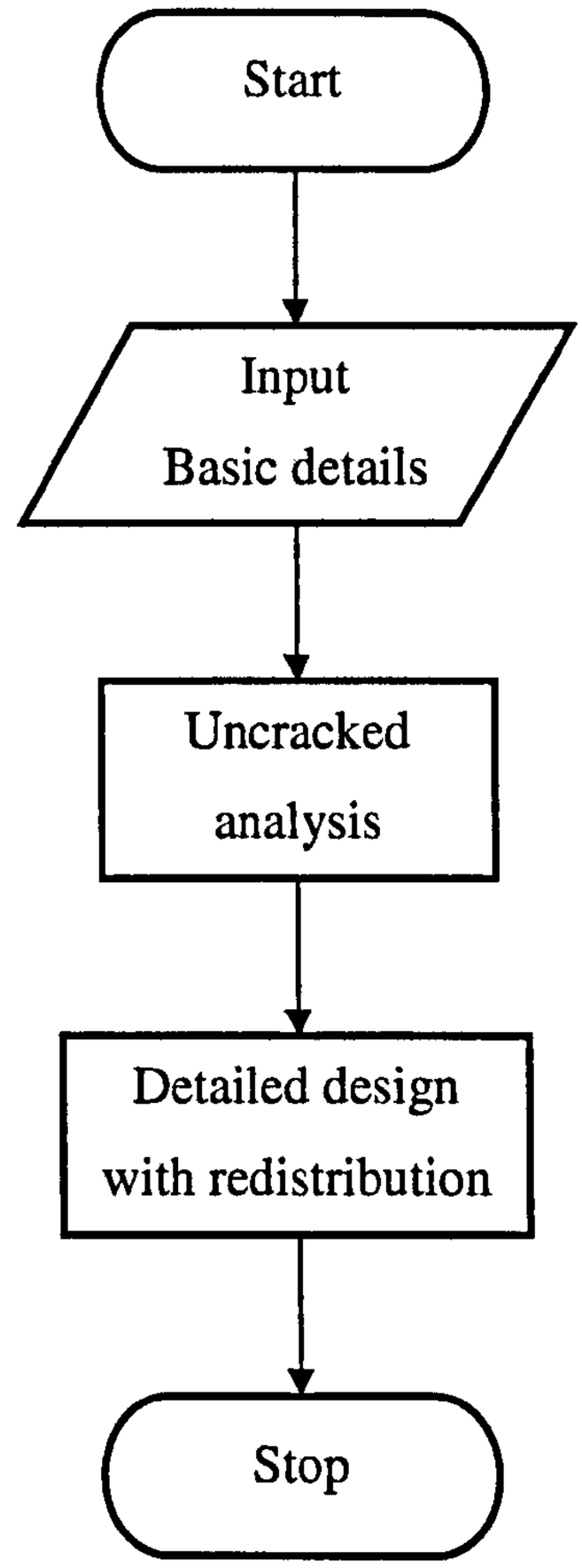

Figure 1-1 - Traditional analysis and design approach for indeterminate reinforced concrete structures

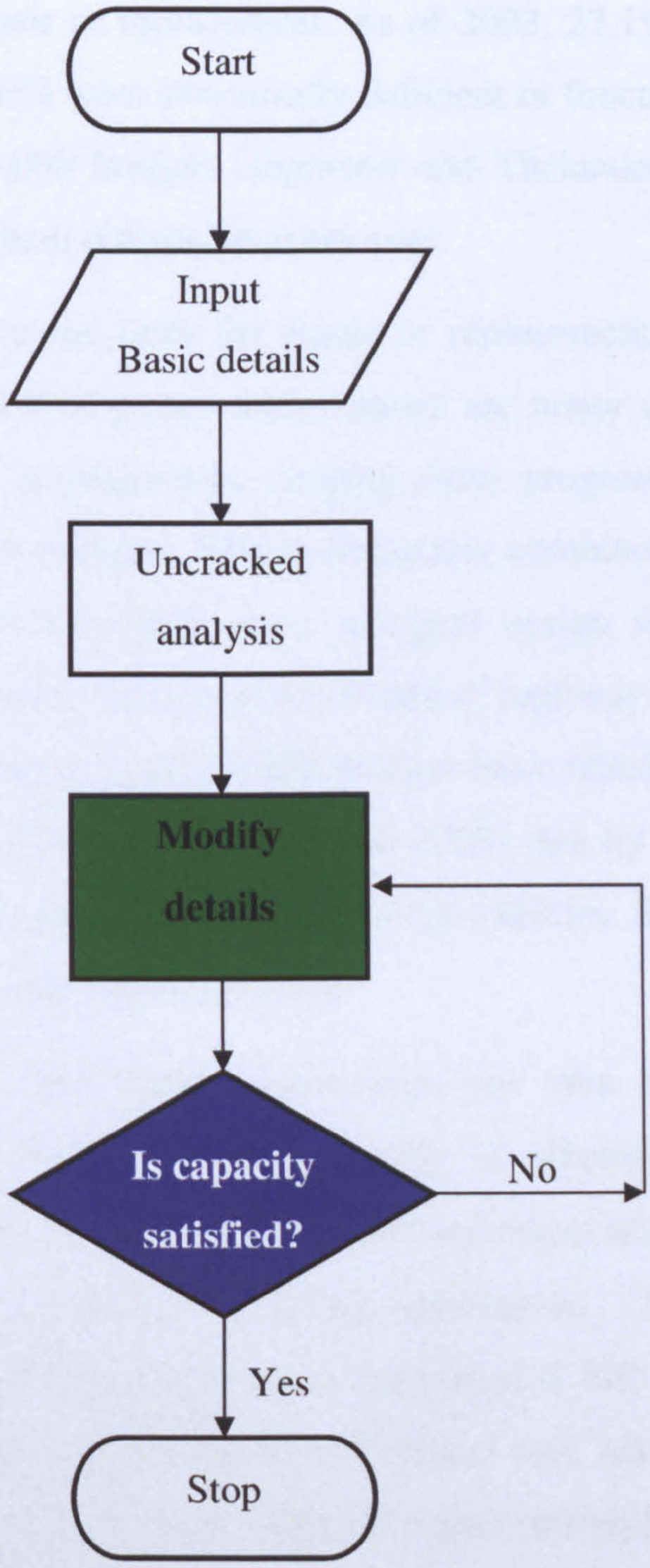

Figure 1-2 - New analysis and design approach for FRP reinforcing of indeterminate reinforced concrete structures

1.2 Market for FRP strengthening – the background

Of all the civil infrastructures that will be needed 20 years from now, about 85-90% of these are probably already built (Nordin and Taljsten 2006). A big part of these structures are in need of repair or replacement. As of 2003, 27.1% of the bridges in the United States (ASCE 2005) were structurally deficient or functionally obsolete. In Russia, one-third of the 60,000 bridges (Jeppsson and Thelandersson 2003) are in poor condition, with 1% of them collapsing every year.

Several reasons contribute to the need for repair or replacement. Corrosion due to environmental attack and lack of proper maintenance are major causes for the poor condition of bridges, with consequences ranging from progressive weakening of structural elements to sudden collapse. This is frequently combined with the need for upgrading so that structures can meet more stringent design requirements which mainly derived from continuous increase in the weight of highway vehicles and traffic density. In the United Kingdom, some 40,000 bridges have failed to meet European Union Requirements (Jeppsson and Thelandersson 2003) that by 1999 all European highways should have been capable of carrying 44 ton vehicles. Sub-standard design and construction errors also play important parts.

The remedial actions for these suspect structures can take the form of either demolition and rebuilding, or strengthening (repair or rehabilitation) of existing structures. Either way, the cost is high. ASCE (2005) estimated that it would cost $9.4 billion a year for 20 years to eliminate all bridge deficiencies. The replacement cost for damaged bridges in the United Kingdom is estimated at $10 billion, with nearly $230 million per year spent on maintenance (Bonacci and Maalej 2000). A total $900 billion is estimated by ISIS Canada (2008) to repair and replace the deteriorated civil infrastructure throughout the world.

It is not always practically feasible or financially economic to demolish and rebuild a deficient structure. In Hooks and Cooper (2003), concrete box beams in Kentucky were strengthened at a cost of $105,000 while replacement would have cost $450,000. The challenge facing both the research and engineering community is to develop simple and cost-effective rehabilitation methods, making use of new technology and new materials. One method that has gained increasing popularity during the last two decades is the use of FRP composites, usually adhesively bonding fibre reinforced

polymer (FRP) plates/sheets to the surface(s) of a structure. Despite the higher material cost compared to conventional construction materials, it is now generally accepted that civil engineering structures can be rehabilitated using FRPs for 40-60% of the cost of conventional methods (ISIS Canada 2005) over the structures' life span.

Advantages including high strength-to-weight ratio, durability, resistance to electrochemical corrosion, availability in any length and ease of handling have made the FRP strengthening system significantly simpler and quicker. This is particularly important for highways or bridges because of the high costs of lane closures and possession times on major highways and railway lines. As an example, upgrading work of a major highway in New York City had to be carried out at night because of the requirement for road to be fully open during the day. The penalty for failure to reopen the carriageway in the morning was $30,000 per hour in 1997, with a penalty of $20,000 per day for overrun of the complete project (Concrete Society 2004).

1.3 Uses of FRPs in Civil Engineering

The use of fibre reinforced polymer (FRP) composite materials in the Civil Engineering industry started in the 1980s, initially for flexural strengthening of reinforced concrete (RC) beams or slabs, and confinement of RC columns. As this technique has been successfully implemented in numerous field projects around the world, extensive research work has been undertaken, and is still ongoing to further develop its applications, both for strengthening purposes and in new build structures.

FRP materials are usually processed in factory into semi-finished products and components, which are then transported to site for erection. There are four basic areas of application: FRP-reinforced concrete, repair and strengthening of existing structures, hybrid structures in which both FRP and traditional (such as steel or concrete) materials are used, and all-composite new structures made entirely of FRP materials.

The use of FRP bars to replace steel bars can be beneficial in aggressive environments such as coastal environments, or in areas where the seasonal use of de-icing salts causes traditional steel reinforcement to corrode, or in concrete structures which may be required to be devoid of metal.

In new hybrid structures, FRP components are used to replace those made of conventional materials, mainly due to their light weight and better durability. Two common examples are bridges constructed of FRP bridge decks used with steel or concrete girders, and FRP cable-stayed structures. All-composite new structures, by contrast, are constructed exclusively of FRP materials.

The use of FRP for strengthening existing structures still represents one major area of application in Civil Engineering. It is now generally well accepted by the construction industry and a number of design guidance documents have been prepared in various parts of the world. The materials used include aramid, carbon or glass fibres; the components are in various forms such as plates, sheets, rods, or straps; and the FRP may be installed unstressed or prestressed. To date, applications have been reported on flexural, shear, torsional, confinement and seismic strengthening of concrete, steel, cast iron, aluminium, timber and masonry structures.

However, their use for the last two decades has mainly been an imitation of the use of other conventional construction materials rather than fully utilizing their potential and unique characteristics. As an example, the strengthening level is generally limited in currently available design guidance documents for FRP-strengthened RC structures, in order to fulfil the ductility requirements specified in existing codes and standards for reinforced concrete structures. TR 55 (Concrete Society 2004) permits up to a maximum of 30% moment redistribution into FRP-strengthened part of the structure if it can be demonstrated that there exists sufficient rotation capacity within the strengthened zone and within the surrounding structure to allow such redistribution to take place. Moment redistribution out of FRP-strengthened zones, however, is not recommended.

In practice, most applications for FRP-strengthening of RC structures have been on strengthening statically determinate (one-span simply supported) structures and there has been very limited design of FRP strengthening for indeterminate structures. The very few applications on statically indeterminate structures were reported in Schuman *et al.* (2003) and Luke and Canning (2004). Shown in Figure 1-3 is a typical view of the approach viaduct of West Gate Bridge, Melbourne, strengthened with carbon FRP (CFRP) sheets/laminates.

Figure 1-3 - Typical view of approach viaduct of West Gate Bridge, Melbourne (Irwin and Rahman 2002)

1.4 Objective of the research

Despite the superior characteristics of the materials and the great potential it has shown, the technique of adhesively bonding FRP composites for strengthening concrete or metallic structures is still relatively new to design engineers. Its applications in some areas are still novel where the technique should be further developed before full confidence can be gained. In particular, research on FRP-strengthening of indeterminate structures is limited to date. Also, from a structural mechanics point of view, there are still issues that have not been thoroughly addressed or remain to be agreed on. Overall, their use so far has been mainly an imitation of the use of other conventional construction materials and more research is still required before FRP will become a mainstream construction material.

This PhD reports on the results of one such research programme. This study aims, by considering the stiffness profiles of the structure, to develop an analysis and design approach that is independent of the ductility levels and will be applicable to both FRP-strengthened continuous RC and metallic structures. There are six main objectives, as follows:

- Understanding different (premature) failure modes and their implications for the structural ductility of FRP-plated structures.
- Understanding the mechanics of development of self-equilibrating stress resultants and their potential effects on indeterminate FRP-plated structures.
- Development of an analytical model that is capable of predicting the structural behaviour of FRP-plated 2-span continuous members under both service and ultimate loads.
- Experimental investigation of the structural behaviour of the FRP-plated 2-span continuous steel beams.
- Development of a computational technique for time-efficient prediction the ultimate load capacity of ductility-deficient indeterminate structures;
- Development of an iterative procedure entailing multiple detailing and ultimate analysis loops for the structure to create a design process for ductility-deficient indeterminate structures.

In the following section, a brief description of the structure of this thesis is presented.

1.5 Layout of the thesis

The thesis consists of 7 chapters. Chapter 2 reviews the research work to date on the brittle failure behaviours of FRP-strengthened components and the implications of these failures for the ductilities of the FRP-plated structures. Different failure modes together with strength models developed by various researchers are described and the resulting lack of agreement in specific areas is highlighted. Approaches to quantify and measures to improve the ductility of FRP-plated structures are reviewed, after

which treatment of this issue in currently available design guidelines is discussed. General lack of research on FRP-plated indeterminate structures is highlighted.

Chapter 3 presents closed-form algebraic expressions for the self-equilibrating moments, due to differential settlement, in FRP-plated 2-span continuous beams. A general framework of ideas is presented to help rapidly establish whether self-equilibrating moments should be considered in interpreting output data from lab tests on 2-span continuous members and in design/assessment of 2-span continuous bridges. A deflection-based approach is proposed to estimate the support stiffnesses.

Chapter 4 reports on tests performed on FRP-plated 2-span continuous steel I-beams. The design of the experiments, fabrication of the specimens, and instrumentation, are described. Important observations and data from the tests are presented and discussed. The analytical models developed in Chapter 3 are applied to the test specimens to give insight into the phenomena observed during the tests. It is worth noting that some of the presentation and discussion of the experimental results given in Chapter 4 has been included in *Proc. 4th International Conference on Composites in Civil Engineering (CICE)* (Zhang and Sebastian 2008).

Chapter 5 presents a computational technique for time-efficient prediction of ultimate load of indeterminate structures. The technique is illustrated by way of examples including a ductility-compromised frame and multi-span continuous beams which possess varying levels of ductility. Then, the technique is extended to incorporate effects of states of self-stress and to investigate behaviours in the pre-failure non-linear regime. Note that some of the material presented in Chapter 5 was published in *Magazine of Concrete Research* (Sebastian and Zhang 2008).

Chapter 6 is devoted to the development of an iterative procedure entailing multiple detailing and ultimate analysis loops for the structure to create an analysis-design process for FRP strengthening of ductility-deficient indeterminate structures. The design procedure is applied to three examples including a FRP-plated continuous RC beam which is ductility-deficient, a continuous RC beam which is of sufficient ductility for the traditional design approach to be applied, and a 3×3 steel RC frame strengthened with FRP sheets.

Chapter 7 summarises the work done and the main results from this research programme. Conclusions are drawn and suggestions for continuation of the work are presented.

Chapter 2

Literature Review

2.1 Introduction

The background and current state of the use of FRPs in Civil Engineering have been introduced in Chapter 1 and the lack of ductility of FRP-plated structures highlighted. This chapter further examines the general failure behaviours of FRP-plated structures and the implications of these behaviours for the ductilities of these structures. Work to date on FRP-plated indeterminate structures is reviewed. The review aims to demonstrate that despite efforts by various researchers, there are still some very important areas specific to FRP-plated indeterminate structures on which significant further light must be shed. In particular, this chapter highlights the urgent need for further work in the following areas.

- Development of a reliable strength model capable of predicting both failure modes and failure loads of FRP-plated structures.
- Gaining a fundamental quantitative understanding of the mechanics of development of self-equilibrating stress resultants for FRP-plated indeterminate structures and their potential effects in indeterminate spans.
- Development of a significantly enhanced understanding of the stress redistributions in the approach to failure of FRP-plated indeterminate metallic structures.
- Development of a new analysis and design approach that is independent of the ductility level of the structure.

In the remainder of the chapter, a brief overview is first given of the use of FRP in flexural strengthening. Different failure modes together with various strength models developed by researchers for premature debonding are then discussed. Approaches to quantify and measures to improve the ductility of FRP-plated structures are reviewed,

after which the treatment of these issues in currently available design guidelines is discussed. Research into and applications of FRP-strengthened indeterminate structures to date are then reviewed. Finally, conclusions are drawn from the extensive discussions of this chapter. The outstanding issues raised in bullet point form above are discussed and emphasized in detail, so the need for the work reported in the remainder of this thesis is established.

2.2 Use of FRP for flexural strengthening

In the context of flexural strengthening, which represents one major area for the use of FRP materials in Civil Engineering, the main application is still for reinforced concrete (RC) beams or slabs. Two systems are commonly used (as shown in Figure 2-1). One system is adhesively bonding FRP laminates (plates, sheets or strips) to the external surface(s) of the reinforced concrete substrate. Another method is the near-surface mounting (NSM) technique, which involves embedding composite bars or strips in narrow adhesive filled groves which are cut into the existing structure. NSM repair methods may be appropriate in applications when environmental exposure of externally bonded composites may adversely affect the bond between the FRP and the substrate concrete. In certain cases, the NSM strengthening technique can be more convenient due to better reinforcement anchoring systems and the minimal surface preparation work (Nanni *et al.* 1999). This technique has been successfully applied for flexural strengthening of RC (Alkhrdaji *et al.* 1999; Hogue *et al.* 1999), timber (Gentile and Rizkalla 1999) and masonry (Tumaialan *et al.* 1999) structures. The current study focuses on the FRP plate bonding technique, although the principles of the analysis and design procedures proposed are equally applicable to structures strengthened using the NSM technique.

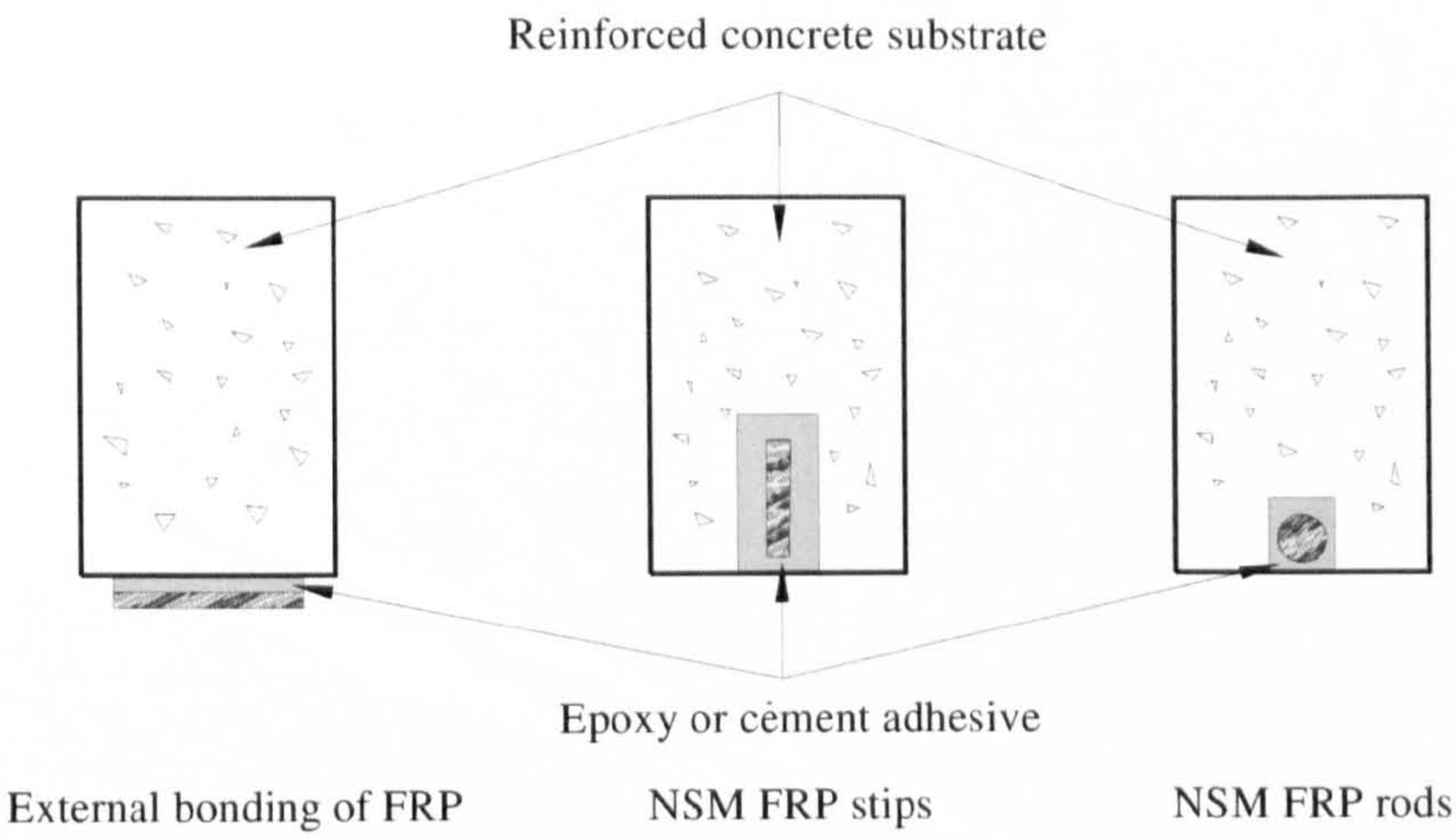

Figure 2-1 - Cross sections comparing different strengthening systems

The FRP plate bonding technology was first investigated at the Swiss Federal Laboratory for Materials Testing and Research (EMPA) (Meier and Kaiser 1991) where tests on RC beams strengthened with carbon FRP (CFRP) plates started in 1984. Since then, extensive research and laboratory work has been carried out throughout the world (Saadatmanesh and Ehsani 1991; Hollaway 1993; Chajes *et al.* 1994; Arduini *et al.* 1997; Quantrill *et al.* 1996; Quantrill and Hollaway 1998; Garden *et al.* 1997; Varastehpour and Hamelin 1997). The results have shown that this method is effective in enhancing the ultimate (flexural and/or shear) capacities (as high as 230% increase has been reported), reducing deflections and controlling crack widths in reinforced concrete members (Meier and Kaiser 1991; Hutchinson and Rahimi 1993, 1996; Taylor *et al.* 1999).

To date, the FRP plate bonding technique has been widely applied in practice to both bridges and buildings in the United Kingdom (an example is shown in Figure 2-2) and other parts of the world. Economic advantage of this technique has been confirmed in many applications (Kliger 1996; Alexander and Cheng 1996; Hollaway and Leeming 2001; Luke *et al.* 2002). Studies carried out for Network Rail (Concrete Society 2004) have indicated that strengthening with FRP materials is approximately 30% cheaper than the equivalent strengthening using steel plates.

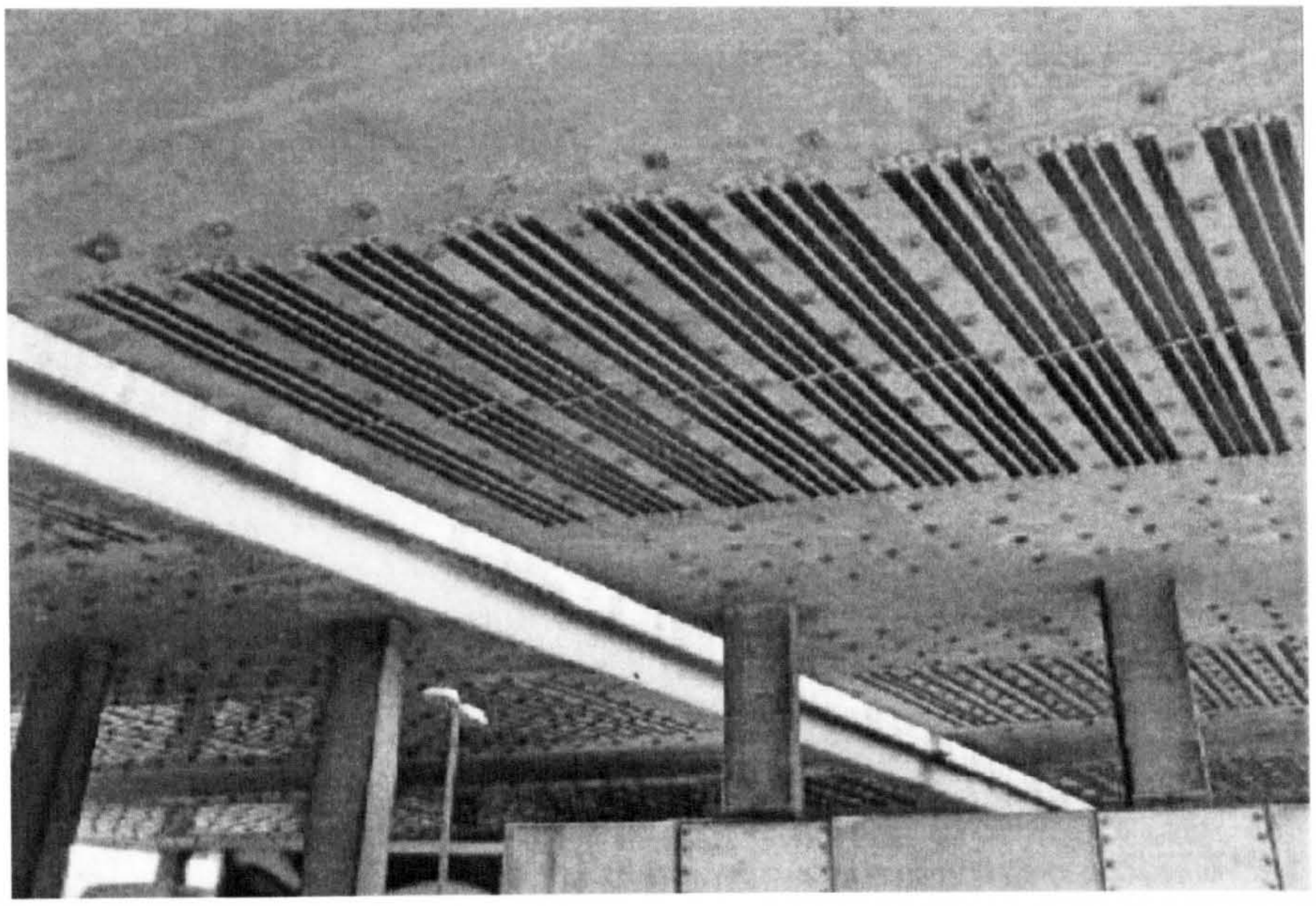

Figure 2-2 - CFRP plate bonding of M60 Barnes Bridge in Greater Manchester (Keble *et al.* (2001))

Although bonding FRP plates/sheets to a beam can increase its ultimate strength, it does not significantly change the cracking load or the behaviour of the beam under service loads. This is due to a number of reasons. First, the pre-existing strains in the structure due to dead load or other loads often cannot be released during strengthening. Second, the structure may already have been cracked at the time of strengthening. Finally, the reinforcement – being in typically small percentages – does not impact significantly on the stiffness of the uncracked section. The material is more efficiently used by prestressing as it contributes under both the ultimate and service loads. The economic benefit of prestressing was noted in Triantafillou and Deskovic (1991). A large amount of work has been reported in this area over the years by many researchers (Meier and Kaiser 1991; Saadatmanesh and Ehsani 1991; Triantafillou *et al.* 1992; Meier 1995; Izumo *et al.* 1997; Garden *et al.* 1998; Quantrill and Hollaway 1998; Lees *et al.* 1999; Wu *et al.* 1999; Ferrier *et al.* 2001; Wight *et al.* 1995, 2001; El-Hacha *et al.* 2001, 2004; Woo *et al.* 2008). However, this technique has not been used widely in practice because it normally requires anchorage systems – which are expensive, difficult to install and more importantly, could have severe consequences

in the event of failure of the system (Stocklin and Meier 2001) – at the ends of the prestressing plate/sheets to prevent debonding. A new technique for prestressing the CFRP laminates has been proposed by Stocklin and Meier (2001) to gradually reduce the stress level near the ends of the CFRP laminate.

The successful application of adhesively bonding FRP to RC structures has invoked great interest in its application to metallic structures. This technique has the advantage of avoiding the welding work normally required with strengthening steel structures using steel plates. It, however, presents a different but in no means easier set of problems, such as the likelihood of lateral and local buckling, higher stiffness or area requirement in order to provide significant contribution relative to the parent material and the resulting high interfacial stresses to transfer the load between the FRP plates and metallic substrate.

The investigations for application of the FRP plate bonding technique in strengthening metallic structures started in the mid-1990s (Karbhari and Shulley 1995; Sen *et al.* 1995; Edberg *et al.* 1996; Mertz and Gillespie 1996) and has been the focus of continued research efforts (Liu *et al.* 2001; Tavakolizadeh and Saadatmanesh 2003; Patnaik and Bauer 2004). Figure 2-3 shows the installation of CFRP plates at Slattocks Canal Bridge, an historic steel bridge constructed in 1935. Continuing efforts by the research and practicing communities (Luke 2001; Miller *et al.* 2001; Hollaway and Cadei 2002; El Damatty *et al.* 2003; Luke and Canning 2004; Sebastian 2005; Colombi and Poggi 2006; Lenwari *et al.* 2006; Youssef, 2006; Zhao and Zhang 2007; Benachour *et al.* 2008), together with the recent availability of high modulus CFRP (Schnerch and Rizkalla 2008), have led to a more promising vision for the application of the FRP bonding technique in this field. However, strengthening metallic structures is still relatively novel, with applications mainly being adhesively bonding FRP strips to the soffit of the metallic structures (Luke 2001; Miller *et al.* 2001; Sen *et al.* 2001; Holloway and Cadei 2002; Phares *et al.* 2003; Mosallam 2004; Lenwari *et al.* 2006; Moy and Bloodworth 2007).

Figure 2-3 - Installation of CFRP plate at Slattocks Canal Bridge

(Courtesy of Mouchel, UK)

As the use of FRP materials is becoming more widely accepted, several design guidance documents have been prepared. Most design documents currently available are for strengthening of RC structures, such as ACI 440.2R-02 (American Concrete Institute 2008), fib Bulletin 14 (Federation International du Beton 2001), TR 55 (Concrete Society 2004), JSCE Recommendations (Japan Society of Civil Engineers, 2001), ISIS Canada Design Manual No. 4 (Neale 2001) and those by Teng *et al.* (2002) and by Oehlers *et al.* (2004c). Relatively few guidance documents have so far been developed for strengthening of metallic structures (Moy 2001; Cadei *et al.* 2004). Design guidelines were also developed by authorities for use within specific industries, such as BD 85/08 developed by the Highways Agency (2008) for strengthening of concrete and metallic highway bridges. For individual products, application guidelines or manufacturer design handbooks may also be available.

Despite the continuous efforts by the research and practicing communities and the increasing acceptance of this technology by the construction industry, these uses of FRPs have been viewed mainly as 'an imitation of the use of other conventional

construction materials' (Rizkalla *et al.* 2006). From the structural mechanics point of view, there are still issues that have not been thoroughly addressed or remain to be agreed upon. One such issue is the impact on structural performance of the reduction in ductility of plated structures due to application of FRP. In the following section, a review is given of the general failure behaviour of FRP-plated RC and steel structures. Particular attention is paid to premature debonding failures, which represent one major cause of the reduction in ductility of FRP-plated structures. Various strength models developed by many researchers are presented and discussed in detail.

2.3 Failure behaviour of FRP-plated structures

2.3.1 Failure modes

From extensive testing of externally bonded FRP-plated members over the last two decades, a number of failure modes, from ductile to very brittle, have been observed. Despite an almost unanimous agreement on the different mechanisms, the names used for each mechanism may differ between researchers. Here they are classified into two types – Type 1 includes modes exhibiting composite action up to failure of the strengthened beam and Type 2 includes modes where failure is due to the loss in composite action. A schematic representation of typical failure modes of FRP-strengthened RC and steel-I beams is shown in Figure 2-4.

The plated RC beam may reach its shear limit prior to any kind of flexural failure, especially in beams of low shear span/depth ratios (Jones 1980; Hollaway and Leeming 2001) or when the flexural strength of the beam has been increased by externally bonded FRP laminates to a point where the shear capacity of the beam is reached before the beam fails in flexure (Hollaway and Leeming 2001; Bonacci and Maalej 2001; Esfahani *et al.* 2007). In present discussion, this type of failure is assumed to be prevented by corresponding shear reinforcement and is thus not included.

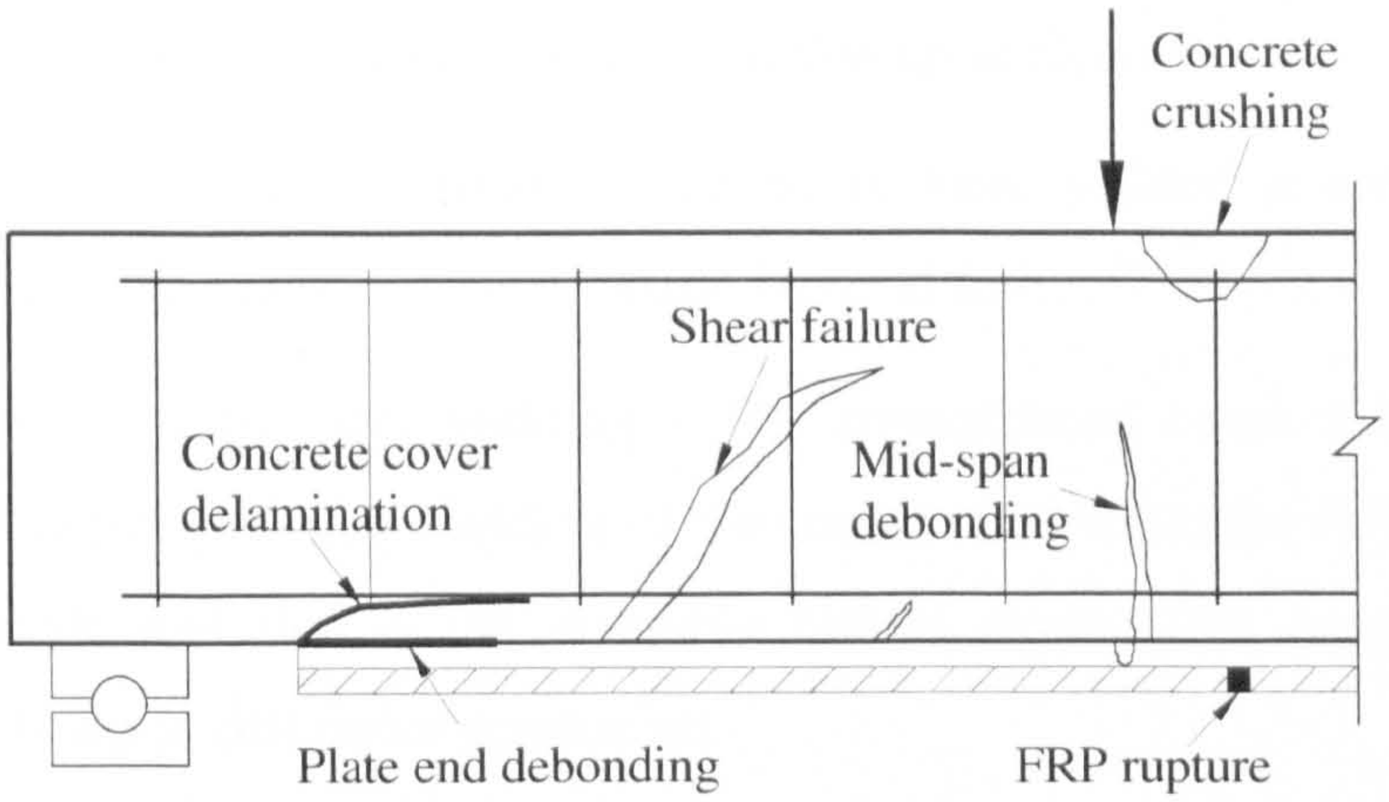

(a)

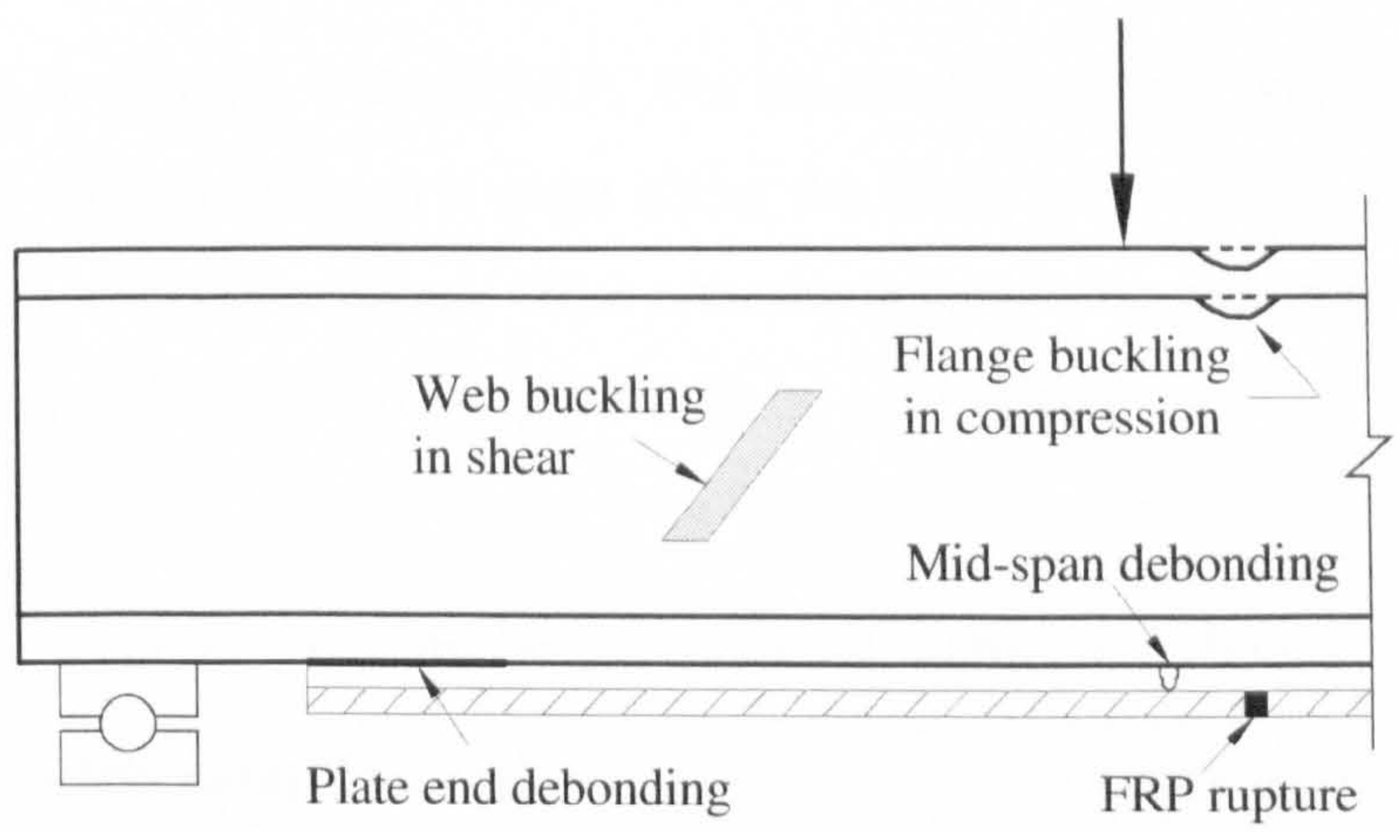

(b)

Figure 2-4 - Typical failure modes for (a) FRP-plated RC beams; and (b) FRP-plated steel I-beams

2.3.1.1 Failure modes of FRP-plated RC structures

Type 1 failure: beams exhibiting composite action up to failure

The steel reinforcement is normally assumed to have yielded at failure to ensure efficient strengthening and to prevent brittle flexural failure

- Concrete crushing after steel yielding - The strengthened beam fails by concrete crushing in compression after yielding of the tensile steel while the FRP is intact. The failure is ductile and this is the desirable failure mode. This happens when the strengthened beam is still under-reinforced.

- FRP rupture after yielding of steel in tension - For relatively low ratios of both steel and FRP reinforcement, the beam may fail by FRP rupture after yielding of the tensile steel prior to concrete crushing. The FRP reinforcement must be well anchored, so debonding is prevented, for this failure to take place (Bonacci and Maalej 2001).

- Steel yielding in sections with no FRP - For beams strengthened with very short plates, steel yielding can progress to a point along the beam where there is no FRP and a crack has formed in the concrete. This effectively causes formation of a plastic hinge at the ends of the plate (Mayo *et al.* 2000; Seim *et al.* 2001).

Type 2 failure: beams exhibiting loss of composite action at failure

(debonding failures)

- Plate end (PE) debonding failure - There are two PE debonding failures, namely concrete cover delamination and end peel. Concrete cover delamination is defined by a crack formed in the concrete at or near the FRP plate end, propagating to the level of tension reinforcement and then progressing longitudinally along the level of the reinforcement, resulting in separation of the concrete cover (Figure 2-5). End peel occurs in the concrete layer adjacent to the concrete-to-adhesive interface. It starts at the ends of the plates and propagates inwards along the beam.

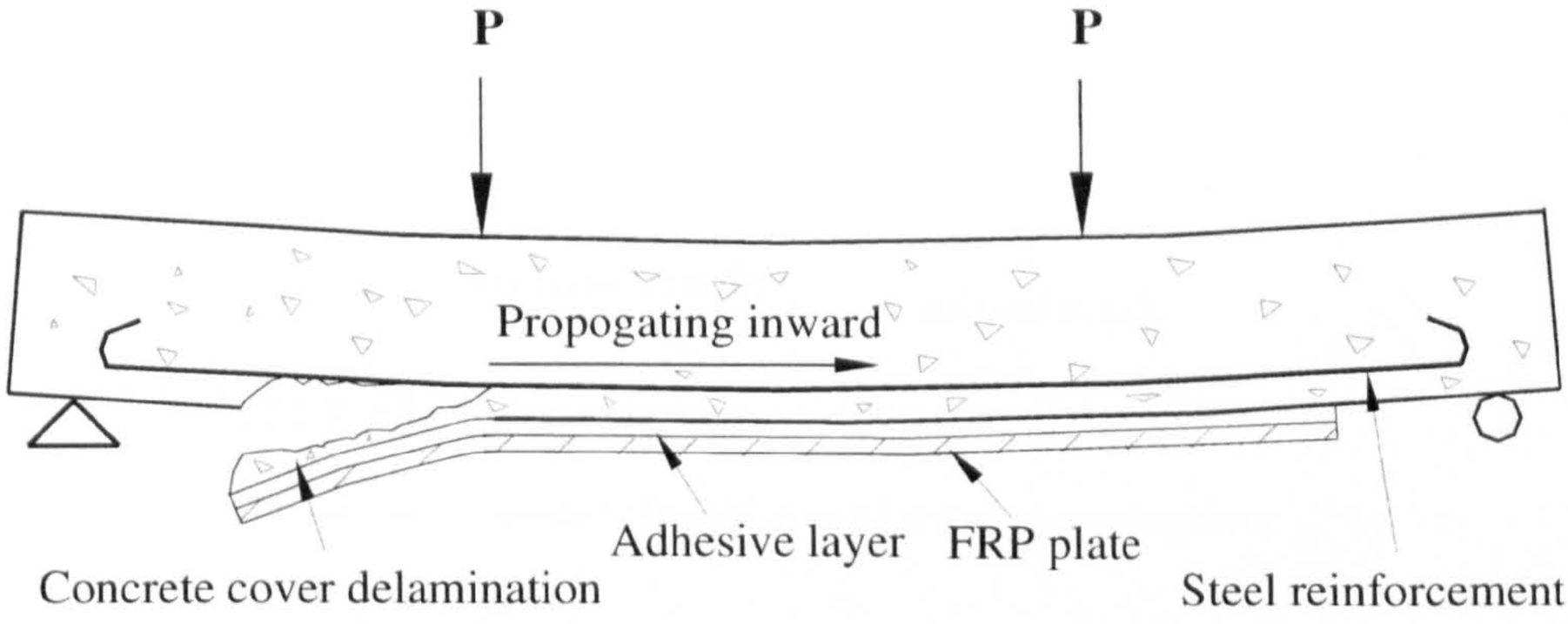

Figure 2-5 - Plate end debonding

It is generally believed to be the result of high interfacial shear and normal stresses near the plate end that exceed the strength of the weakest material, usually the concrete (Smith and Teng 2002a). Of the two distinct modes of PE debonding failures, concrete cover separation is far more common than plate end interfacial debonding (Smith and Teng 2002b).

PE debonding is associated with those regions of the beam where the flexural forces are small and where a critical diagonal crack has not occurred, so that the section at which PE debonding occurs can be assumed to behave in a linear fashion, that is linear elastic sectional analyses can be used albeit that the concrete has cracked in tension.

- Mid-span debonding failure due to flexural or flexural/shear crack - This type of debonding initiates as a result of high interfacial stresses due to the applied loading and/or stress concentrations at the toe of the crack or at substrate discontinuity. Failure is induced due to propagation of a flexural crack in the concrete parallel to the bonded plate and adjacent to the concrete-to-adhesive interface, starting from the critically stressed portion toward one of the ends of the plate (Arduini and Nanni 1997; Bizindavyi and Neale 1999; Rahimi and Hutchinson 2001; Sebastian 2001) (Figure 2-6). It is called mid-span debonding or inclined crack (IC) debonding. In the present study, the two names are synonymous and are used interchangeably.

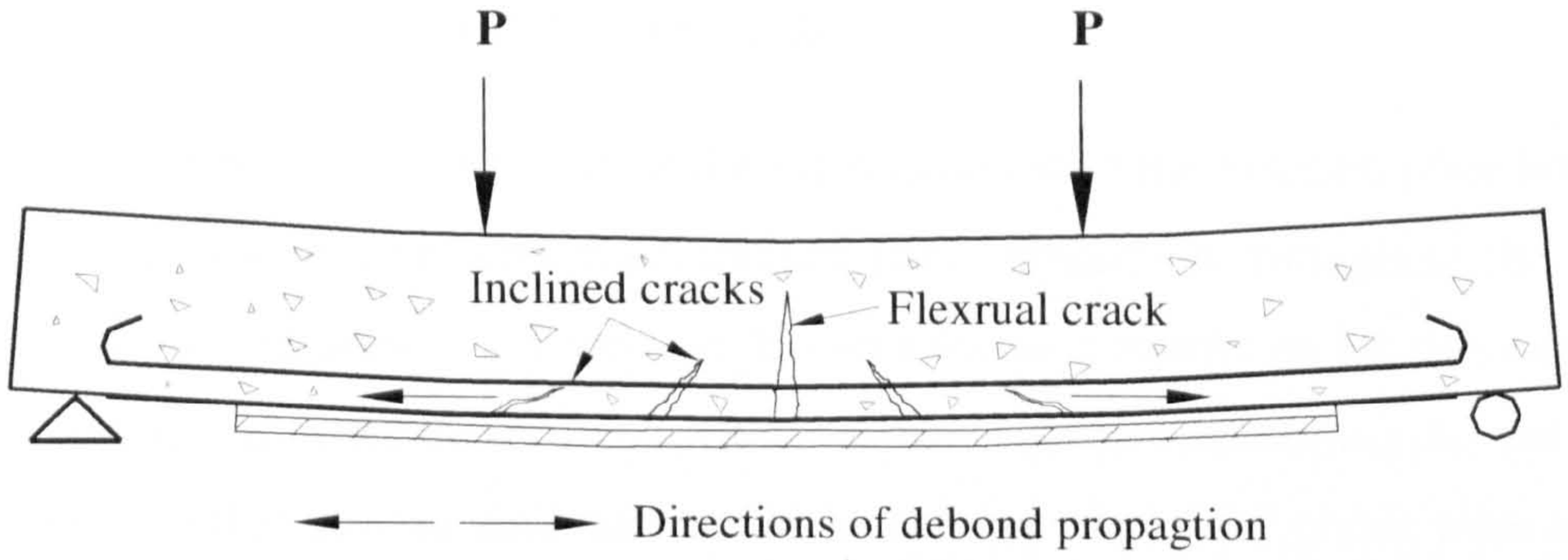

Figure 2-6 - Mid-span debonding

IC debonding is associated with regions of the beam that are subject to ultimate failure of the beam (flexural and shear failure), which requires the sections to behave in a nonlinear fashion.

Though described as the common anchorage failure mode for plates/strips bonded on beam sides for shear strengthening (Teng *et al.* 2002) and also a possible failure mode in beams strengthened with bonded soffit plate (Smith *et al.* 2001; Teng *et al.* 2002), IC debonding was not found in laboratory tests until towards the end of the 20th century when FRP plates/sheets were increasingly used to replace steel plates.

2.3.1.2 Failure modes of FRP-plated steel structures

When FRP materials are used to strengthen steel members, high stiffness and/or area is often required in order to provide significant contribution relative to the parent material. This, in turn, results in potentially high interfacial stresses to transfer the load between the FRP plates and metallic substrate.

The debonding failure modes are similar to those in FRP-plated RC structures. However, for thin-walled steel I-section beams, buckling is also a major concern. Sayed-Ahmed (2006) numerically investigated the potential use of FRP strips on compression webs to delay the onset of local buckling. Zhao *et al.* (2006) carried out a series of tests and reported significantly improved buckling behaviour for CFRP-strengthened rectangular hollow sections.

2.3.2 Strength models for debonding failures

Premature debonding has been one of the main issues with the external plate bonding technique and has attracted enormous interest from researchers throughout the world over the last two decades. Early work in this area focused mainly on PE debonding as it is a common failure mode for steel-plated beams. Mid-span debonding did not come into much attention until around the turn of the century when FRP plates were largely used to replace steel plates. Since then, extensive research has been carried out on this failure mode.

The continuous effort from the research community has led to better understanding on the mechanics of these different failure modes and also development of various strength models to predict debonding failures. In this section, strength models are reviewed for PE and IC debonding in FRP-strengthened RC structures. The limited number of strength models for FRP-strengthened steel beams are also investigated, after which some remaining issues are discussed.

2.3.2.1 PE debonding Strength models for FRP-plated RC structures

A large number of strength models have been developed for plate-end debonding (plate end interfacial debonding or concrete cover separation) failures during the last decade of the past century. Some of these models were developed for steel plates and directly used for FRP plates (Oehlers 1992; Ziraba *et al.* 1994; Jansze 1997; Raoof and Zhang 1997) or modified from models developed for steel plates (Wang and Ling 1998; Ahmed and Van Gemert 1999; Raoof and Hassanen 2000), and others were developed specifically for FRP plates (Varastehpour and Hamelin 1997; Saadatmanesh and Malek 1998; Tumialan *et al.* 1999).

A comprehensive review of different models was conducted by Smith and Teng (2002a). They classified the models into three categories based on their approaches, namely: (a) shear capacity based models (Oehlers 1992, Jansze 1997, Ahmed and Van Gemert 1999), in which the debonding failure strength is related to the shear strength of the concrete with no or only partial contribution from the steel shear reinforcement and given as the shear force acting at the plate end, with or without taking into account the effect of any coexistent moment; (b) concrete tooth models (Raoof and Zhang 1997, Wang and Ling 1998, Raoof and Hassanen 2000), which make use of the

concept of a concrete 'tooth' between two adjacent cracks deforming like a cantilever under the action of horizontal shear stresses at the base of the beam; and (c) interfacial stress based models (model I of Ziraba *et al.* 1994, Varastehpour and Hamelin 1997, Saadatmanesh and Malek 1998, Tumialan *et al.* 1999b), which generally make use of interfacial stresses from an existing closed-form solution and a concrete failure criterion (Mohr-Coulomb failure criterion, modulus of rupture of the concrete, concrete splitting tensile strength). Model II of Ziraba *et al.* (1994) in fact combines approaches (a) and (c).

These different models were then assessed in Smith and Teng (2002b) using a test database containing the test results of 59 beams reported to have failed by plate end debonding. They concluded that of the three approaches mentioned above, the shear capacity based models appears to be the most robust while only Oehler's (1992) model provides safe though overly conservative predictions. They then proposed a simple model applicable to FRP-strengthened beams by modifying the Oehler's (1992) model through calibration with the test database, which is suitable for direct application in design, and can be easily included in any national code. For a detailed discussion of these models, the reader is referred to Smith and Teng (2002a,b).

El-Mihilmy and Tedesco (2001) studied the concrete cover separation failure mode of FRP-strengthened RC beams. An analytical procedure for calculating shear and normal stresses at the plate curtailment was developed using linear elastic theory and statistical analysis of test data. Zhao (2005) studied plate end failures in FRP-strengthened RC beams and proposed two separate models for wet lay-up and pultruded FRP plated beams. The models were based on a regression analysis of test data. More recently, Bahn and Harichandran (2008) modified Roberts' (1989) model for predicting the failure loads of RC beams strengthened with carbon FRP (CFRP) and mortar patch anchorages.

2.3.2.2 IC debonding Strength models for FRP-plated RC structures

While PE debonding is a common concern for steel plated beams and has been a subject of interest from the early 1990s, mid-span debonding, although long known to be one of the possible failure modes, had received much less attention for a long time. This is partly due to the fact that mid-span debonding was not observed in laboratory tests until towards the end of the 20th century when FRP plates/sheets were

increasingly used to replace steel plates (Arduini and Nanni 1997; Wu *et al.* 1997). Since then, there has been a general shift of focus and increasing research (Sebastian 2001; Leung 2001; Rahimi and Hutchinson 2001; Smith *et al.* 2001; Seracino 2001; Niu and Wu 2001; Teng *et al.* 2002, 2003, 2004) is being carried out in this area.

Various strength models have been developed to predict IC debonding failures and they can be categorised into three groups, namely anchorage strength models (Adhikary and Mutsuyoshi 2001; Chen and Teng 2001; Teng *et al.* 2002, 2003, 2004; Ulaga *et al.* 2003; Oehlers and Seracino 2004c; Lu *et al.* 2005; Dai *et al.* 2005), mechanics based models (Wang and Ling 1998; Matthys 2000; Leung and Tung 2001; Harmon *et al.* 2003; Rosenboom and Rizkalla 2008) and empirical models (Said and Wu 2008).

Anchorage strength models, based on the analogy of IC debonding failure to debonding failures observed in simple lap shear tests, represent the vast majority of the bond strength models currently available. They were divided into three subcategories in Chen and Teng (2001), namely empirical models that are based directly on the regression of test data (Hiroyuki and Wu 1997; Maeda *et al.* 1997), fracture mechanics based models from analysis using linear or nonlinear Fracture mechanics (Blaschko *et al.* 1998; Yuan and Wu 1999; Yuan *et al.* 2001; Neubauer and Rostasy 1997) and design proposals that generally make some simple assumptions (Brosens and Van Gemert 1997; Chaallal *et al.* 1998; Khalifa *et al.* 1998). The differences between bending and shear tests, such as the presence of bending deformations and internal steel reinforcement in bending and the interaction of multiple flexural cracks in bending, are normally accounted for by using an additional factor calibrated through bending test data (Teng *et al.* 2003).

Toutanji *et al.* (2007) reviewed various anchorage strength models and applied them to a database consisting of 351 concrete prisms with bonded FRP and tested in longitudinal shear. They concluded that models using effective bond length in their expressions for bond strength generally predicted results more efficiently than others and recommended models by Chen and Teng (2001), Khalifa *et al.* (1998), Yang *et al.* 2001; Lu *et al.* (2005) and Yuan and Wu (1999) be used as basis for developing strength models for IC debonding.

Mechanics based models, which normally involve an elementary beam analysis and the evaluation of interfacial shear stresses, were also developed by different

researches (Wang and Ling 1998; Matthys 2000; Leung and Tung 2001; Harmon *et al.* 2003). Rosenboom and Rizkalla (2008) reviewed some of the analytical models together with some empirical and anchorage strength models and assessed them using a test data base consisting of 51 beams or slabs, in which 47 failed due to mid-span debonding and four failed due to FRP rupture. They then proposed an analytical model that characterises the interface shear stress based on two distinct sources: the applied loading and stress concentrations at the toes of flexural cracks which predict well most of the test results collected in the database.

Based on a statistical analysis of 200 flexural test results with IC debonding failures, Said and Wu (2008) proposed a simple empirical model for predicting the load-carrying capacity of FRP-strengthened flexural members due to IC debonding failure.

2.3.2.3 Debonding Strength models for FRP-plated steel structures

In contrast to the significant research effort into and numerous models available for FRP-strengthened RC structures, the research into this area for FRP-strengthened metallic structural components is more recent and only limited strength models are available. In one such model developed by Lenwari *et al.* (2006), stress intensity factors at the steel/adhesive corner are proposed as the failure criterion for the purpose of predicting debonding strength. Its application, however, is limited to the same spew-fillet angle and the stresses near the plate end must be sufficiently low to justify the assumptions of linear elasticity for the materials.

The ICE design and practice guide for FRP composites (Moy 2001) suggests different approaches of analysis depending on the substrate metallic materials - elastic analysis for cast iron, and elasto-plastic analysis for steel and good wrought iron. The long-term design allowable strain for CFRP is between 0.1% and 0.3% and the shear stress in the adhesive, evaluated using standard engineering formulae, is assessed against permissible values for the adhesive used.

CIRIA Guidance Document 595 (Cadei *et al.* 2004) takes a similar approach to analysis in terms substrate materials. For adhesive joint analysis, two approaches are suggested, namely the elastic, stress-based approach and the fracture mechanics approach. The elastic, stress-based approach evaluates the stress distributions along the adhesive joint and compares the principal stress to the strength of the adhesive.

The strength of the adhesive can be determined from the lap-shear test result and need to allow for the bond effects. The fracture mechanics approach considers the energy released during the propagation of a crack along the adhesive joint. The energy release rate at failure which characterises the strength can be determined using standard mechanics tests. The method is easy to use, however, it does not fully address the temperature effects and more development is required for beams of non-constant cross-section.

2.3.3 Discussions

Various strength models have been compared with experimental test databases constructed by various researchers such as, among others, Toutanji *et al.* (2006), Said and Wu (2008) for IC debonding, Smith and Teng (2002a,b) for plate end debonding, and Saxena *et al.* (2008) for both types of debonding. A common finding in these studies is that the results predicted from various models are largely dispersed. Interestingly, large disparities exist between results from the improved models that give better performance according to their separate databases.

Figure 2-7 shows the change in debonding strength (in terms FRP strain) for IC debonding with concrete compressive strength from the improved models proposed by Toutanji *et al.* (2006) and Said and Wu (2008), assuming same FRP axial stiffness per unit width. The differences are clearly seen. The high level of dispersion in results from different models indicates that thorough understanding of the debonding mechanism and the effects of various parameters has yet to be gained.

It should be noted that the design codes and guidelines are mostly based on the strength models discussed in the previous sections and some of them were developed by the same people, and so the same issue exists with design codes and guidelines. For example, in a recent study by Aram *et al.* (2008), a discrepancy of up to 250% was reported between different codes and guidelines for predicting debonding failure load.

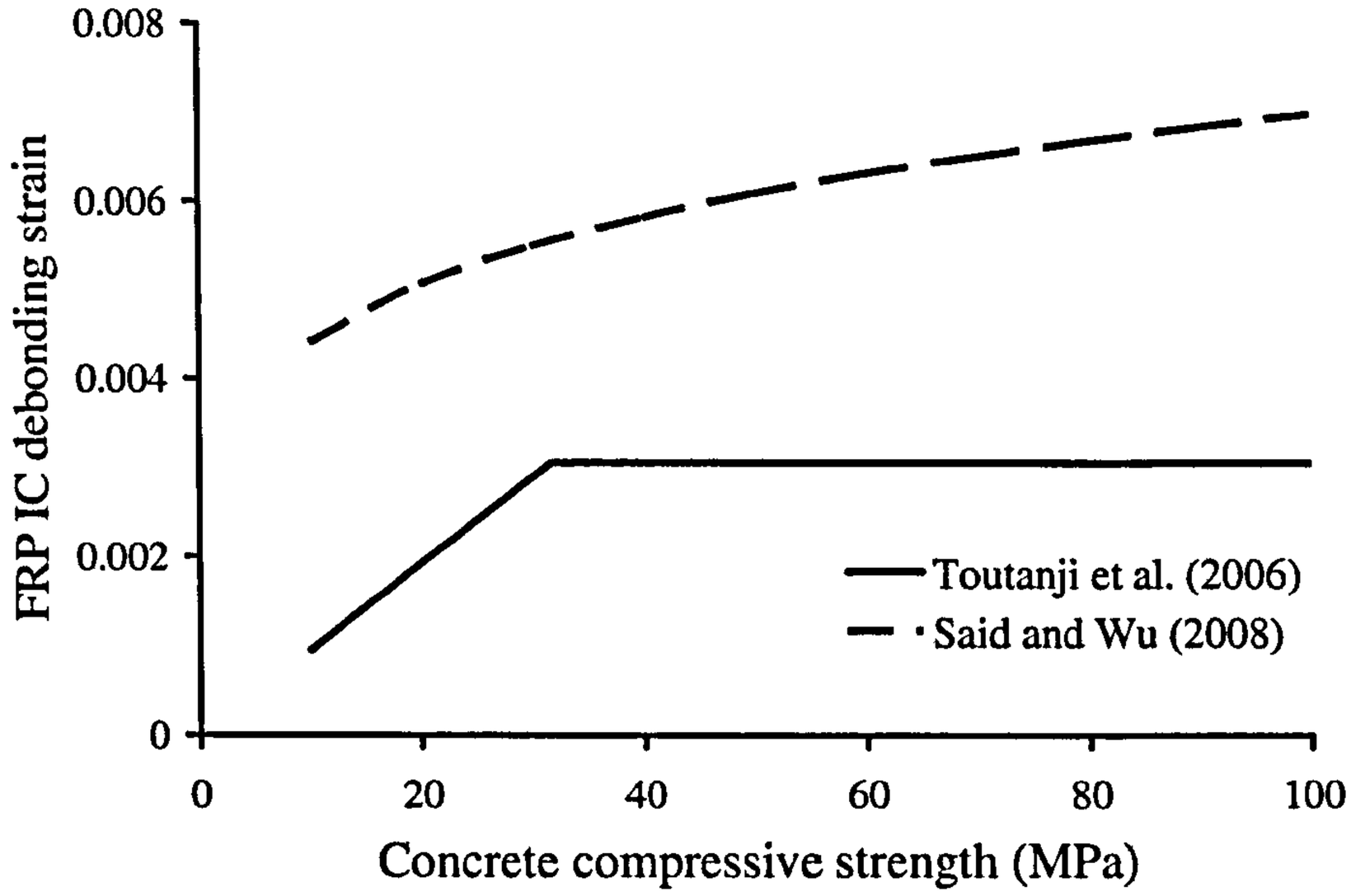

Figure 2-7 - FRP IC-debonding strength

The above discussed models were developed to predict plate end interfacial debonding, concrete cover delamination, or IC debonding. While these models are helpful in post-test analysis of failure modes, there is no approach which can precisely predict the failure mode along with the debonding load prior to test (Saxena *et al.* 2008). Colotti *et al.* (2004) developed a strut-and-tie model that is capable of predicting the ultimate beam load-carrying capacity as well as the associated mode of failure. The study is concerned primarily with plate end debonding, although plate rupture failure is also included. The failure modes are limited to plate end interfacial debonding, concrete cover delamination and shear failure.

The research into FRP-plated metallic structure is limited to date. This is clearly reflected in the number of strength models available as discussed in the previous sections, and also in the smaller number of field applications reported in the literature. In practice, there are large numbers of old metallic structures dating back to the 19th and early 20th centuries including railway bridges, industrial buildings etc. According to Karbhari and Shulley (1995), of all the structurally deficient bridges in the United States, over 58% are constructed of steel. Much of the railway infrastructure in the UK is over 60 years old, much of which is of cast iron or steel (Moy and Bloodworth

2007). More research is needed in this area before FRP plate bonding technology can gain the same level of acceptance with the engineering industry as has been accomplished for RC structures.

In this section, typical failure modes and various strength models for debonding failures have been presented for FRP-plated structures. In addition to these studies, efforts have been put into both developing measures to prevent these debonding failures and thus increase the ductility of FRP-plated structures, and also into quantifying the ductility of FRP-plated structures. These will be reviewed in the following section.

2.4 Ductility of FRP-plated structures

2.4.1 Quantification of ductility of FRP-plated structures

Consideration of ductility is of predominant importance to structural designers, as it provides warning of impending failure, and more importantly, allows for stress redistribution in statically indeterminate structures.

The ductility of conventional steel reinforced concrete members is not usually evaluated directly but is incorporated in the simplified design equations and guaranteed either by limiting reinforcement ratio to be substantially below the balanced reinforcement ratio (the ratio at which steel yielding and concrete crushing occur simultaneously (American Concrete Society 2005)), or by limiting the neutral axis depth to various values (Canadian Standards Association 1994; Standards Australia 1994; British Standards Institution 1995).

These approaches, however, are not sufficient for FRP-strengthened RC members, which are characterised by the brittle nature of the strengthening material and brittle debonding failure mechanisms. Attempts have been made by many researchers (Grace *et al.* 1998; Spadea *et al.* 2001; Bencardino *et al.* 2002; De Lorenzis *et al.* 2004; Duthinh and Starnes 2004; Tann *et al.* 2004) to quantify the ductility of FRP-strengthened structures. The approaches generally fall into two main categories, namely ductility index approach and moment redistribution approach.

2.4.1.1 Ductility index approach

The ductility index approach has been used for conventional steel RC structures. The indices commonly used include deformation (deflection, curvature) index and energy index. The generic action-deformation curve (moment-curvature or load-deflection) of a conventional RC member (Figure 2-8) is characterised by a yielding plateau, the length of which is indicative of the capacity of the section or the member to dissipate energy before failure. The ductility indices are normally defined by the deformation (deflection, curvature) or the total energy at failure divided by those of the reference point (normally the point of steel yield). This is viable as the conventional RC beam has a clear reduction of slope when the steel yields.

A similar definition is not appropriate, however, when dealing with FRP-plated RC members. Firstly, it might be difficult, or even impossible to clearly identify the point where internal steel starts yielding as the generic action-deformation curve may not exhibit an apparent change of slope, which is particularly true for RC members with high FRP reinforcement ratio (Tann *et al.* 2004). Secondly, even if the point at which internal steel starts yielding can be identified, the post-yielding branch of the action-deformation curve increases, rather than levelling off as is the case for conventional RC members (De Lorenzis *et al.* 2004). The slope is dependent, for a given steel reinforcement ratio, on the amount and stiffness of the FRP reinforcement. Furthermore, the ability of a FRP-strengthened member to undergo large deformations does not necessarily suggest high ductility, as pointed out in Tann *et al.* (2004). Therefore, an energy-based method appears to be preferred for determining the ductility index of FRP-strengthened beams.

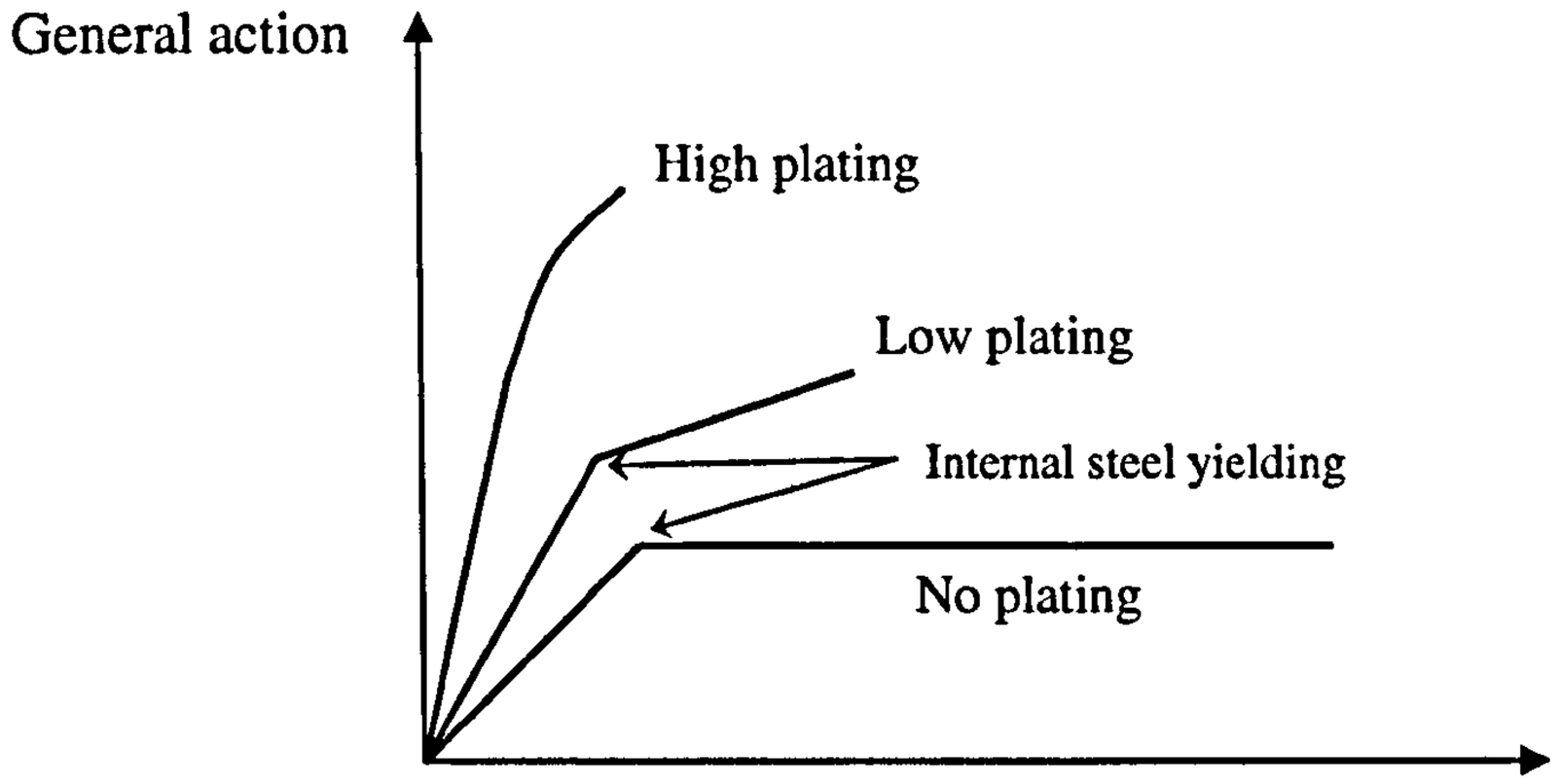

Figure 2-8 - General action-deformation curve for RC members

The energy-based method was first proposed by Naaman and Jeong (1995) for RC members with internal reinforcement and the ductility was expressed by:

$$\mu_{du} = \frac{1}{2}\left(\frac{E_{tot}}{E_{el}} + 1\right) \tag{2-1}$$

where E_{tot} and E_{el} are the total and elastic energy respectively.

Different expressions were then developed (Grace *et al.* 1998; Spadea *et al.* 2001; De Lorenzis *et al.* 2004) for FRP-plated RC structures. There is, however, no fundamental difference from the Naaman and Jeong (1995) procedure. Tann *et al.* (2004) recommended that the Naaman and Jeong (1995) approach should be used before a more rigorous approach for the determination of elastic energy is developed.

2.4.1.2 Moment redistribution approach

The moment redistribution approach is primarily for statically indeterminate structures, for which the ductility may be indicated by the moment redistribution capacity. Oehlers *et al.* (2004a, b) applied the idea in continuous steel- and FRP-plated RC members. They investigated the moment redistribution capacity of such

members experimentally and concluded that (both steel- and FRP-) plated beams have a scope for moment redistribution, while also advising that the neutral axis approach adopted by most national standards should only be used for metal-plated beams in which concrete crushing precedes debonding. They then went on to develop a mathematical model (flexural rigidity approach) based on the maximum strain at debonding to quantify the amount of moment redistribution that can occur in steel or FRP externally bonded plated beams that debond prior to concrete crushing. From a parametric study, they concluded that substantial amounts of moment redistribution can occur in steel plated sections if designed with care; however, CFRP plated sections show a very limited ability to redistribute moment. In their study, the moment redistribution is defined as the change in moment from the elastic moment based on constant flexural rigidity. The percentage redistribution of moment from the hogging region is given by

$$\%MR = \frac{(M_{hog})_{EI.const} - (M_{hog})_{test}}{(M_{hog})_{EI.const}} \times 100 \qquad (2\text{-}2)$$

Where, for a specific load, $(M_{hog})_{EI.const}$ is the theoretical hogging moment from a linear elastic analysis which assumes constant flexural rigidity EI and $(M_{hog})_{test}$ is the experimental hogging moment. Liu *et al.* (2006) modified the flexural rigidity approach and suggested a 'linear flexural rigidity approach' that allows for the variation in EI along the beam to accommodate beams with near surface mounted (NSM) plates, which can be used to determine the moment redistribution at any stage of loading and for any failure mechanism.

In a separate study by Coccia et al. (2008), the application of FRP sheets reduced the moment redistribution ratio by 20% (one sheet) up to 50% (four sheets). They proposed a simplified redistribution ratio, which is fundamentally similar to that proposed by Oehlers *et al.* (2004a, b).

2.4.1.3 Rotational component approach

Oehlers *et al.* (2008) developed a conceptual model that represents all the rotational components that contribute to the ductility of FRP-plated RC structures, namely flexural cracks induced rotation, slip (between the reinforcing bars and the concrete

and between the FRP plate and the concrete) induced rotation, rotation due to flexural bending, and rotation due to yield penetration. A limit was then placed on the rotational capacity based on the work by Fantilli *et al.* (2002) and Debernardi and Taliano (2002).

2.4.2 Measures to improve ductility

There are forms of FRP strengthening that exhibit ductile behaviour such as FRP sheet wrapped columns (Bisby *et al.* 2005; Toutanji *et al.* 2010). For FRP-plated members, however, the ductility is usually limited. This is attributed to the linear elastic nature of the materials and more importantly, the previously discussed premature debonding failures. Thus, the measures to improve ductility are mainly based on delaying or inhibiting premature debonding failures.

In an effort to inhibit such failures, many methods have been suggested, such as termination of FRP plates near the supports (Ritchie *et al.* 1991; El-Mihilmy and Tedesco 2001), use of rubber modified resins (Gao *et al.* 2003, 2004), tapering of the ends of the plates (Gao *et al.* 2006a,b; Pan *et al.* 2008), and the use of external end anchorage (Garden and Hollaway 1998; Lamanna *et al.* 2004; Martin *et al.* 2008) in the form of bolts, steel/FRP jackets or FRP wrappings.

Ideally, FRP plates should be terminated at the zero-moment sections (supports in simply supported structures and points of contraflexure in statically indeterminate structures). This is not always practically possible as in one span (simply supported) bridges bearings are used (Sebastian 2001) and in (mostly statically indeterminate) multi-span bridges, indeterminacy gives rise to self-equilibrating moments as a result of which points of contraflexure shift along the member.

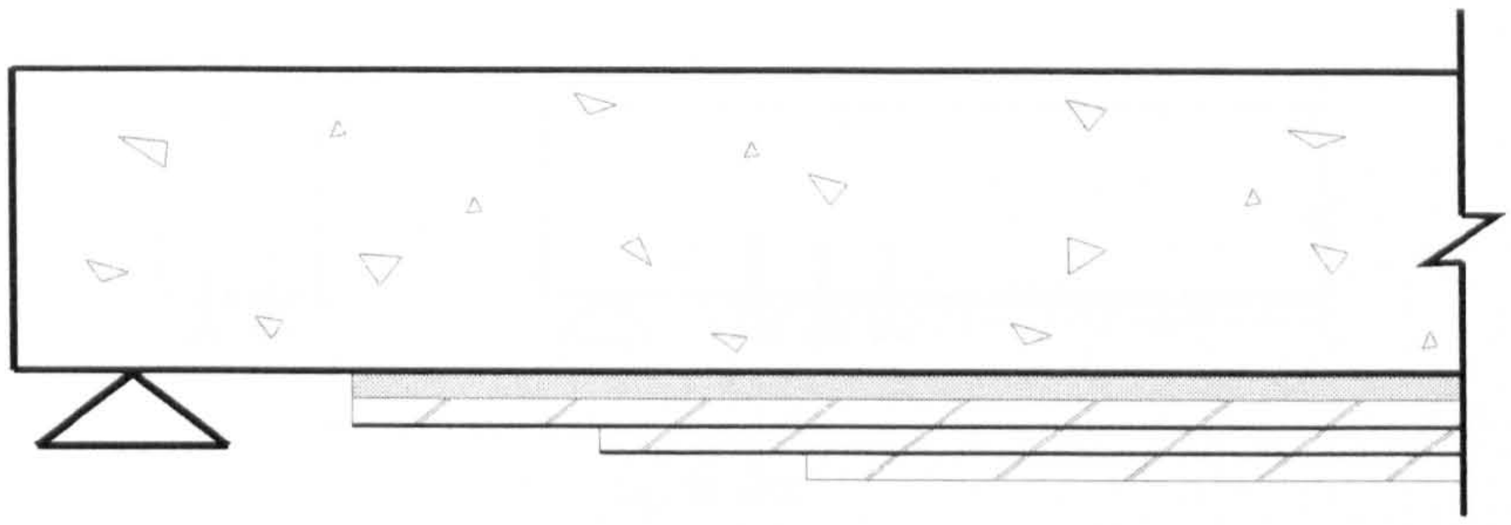

Figure 2-9 - End tapering of FRP plate

There has been significant interest in the use of end tapered plates (Figure 2-9) for strengthening RC and metallic structures (Gao *et al.* 2006b; Pan *et al.* 2008; among others). While numerical and analytical studies (Miller *et al.* 2001; Deng *et al.* 2004; Gao *et al.* 2006a) suggest potential benefits of reducing the stress concentrations and thus enhancing the load carrying capacity, this has not been fully supported by experimental results. Plate debonding still occurred even when the end tapered plates were used (Hutchinson & Rahimi 1993), and in Sebastian & Luke (2007) tapered plates separated from the steel beam while the constant thickness plates did not. This may well have been due to the presence of bond defects, but it also indicates that more work is still needed to identify the beneficial mechanisms and parameters affecting the performance of tapered plates.

Effects of external anchorage on the strengthening performance have been studied intensively (Ritchie *et al.* 1991; Meier *et al.* 1993; Sharif *et al.* 1994; Arduini & Nanni 1997; Garden and Hollaway 1998; De Lorenzis *et al.* 2001). The anchorage is available in different forms - bolts, jackets and FRP wraps, all illustrated in Figure 2-10. The use of bolts requires multi-directional FRP in order to prevent longitudinal splitting failure of the FRP, and to provide sufficient bearing stiffness at the position of the bolts (Concrete Society 2004). Arduini & Nanni (1997) commented that wrapping FRP fabric completely around the beam section (Figure 2-10 (c)) over the entire length of the member is an effective way of anchoring unidirectional fibre plates.

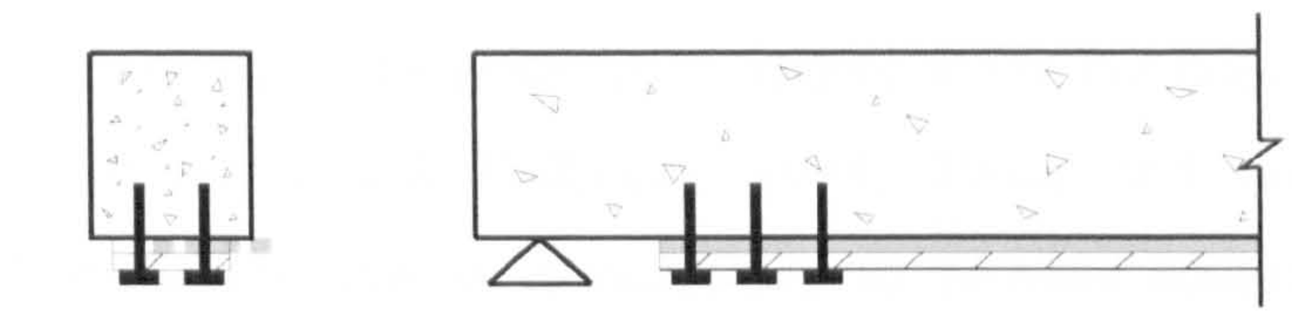

(a) Bolts

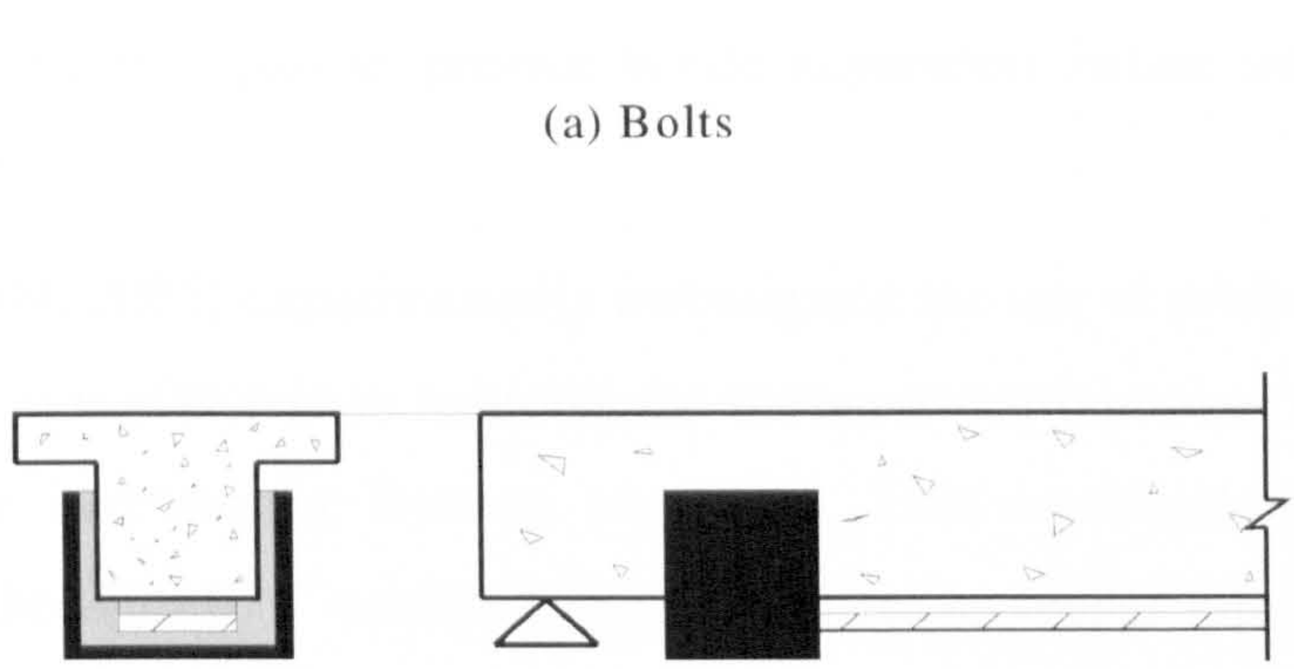

(b) U-jacket

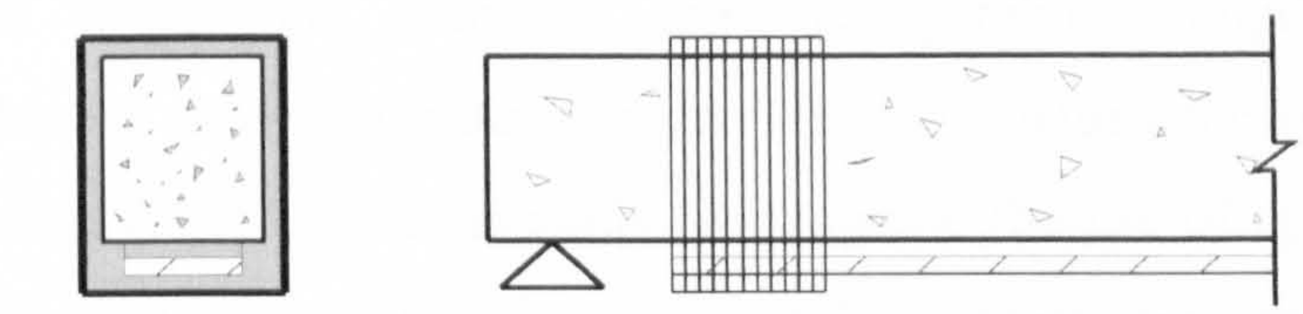

(c) FRP wrap

Figure 2-10 - External anchorage systems

It was, however, recognised that this technique is somewhat limited where the top surface of concrete beam is not accessible due to monolithic connection to an existing slab, in a T-section beam for example. In such cases, only a partial fabric wrap is used, to give a U-jacket around the lower part of the web of the beam section (Figure 2-10 (b)). It is worth noting that the wrapped fabric or the jacket solution (Figure 2-10 (b) and (c)) serves the dual role of inhibiting both conventional shear failure and brittle separation failure. Previous laboratory testing work has shown a mixed degree of success. For example, Sharif *et al.* (1994) observed experimentally that both bolts and jackets effectively inhibit separation failure, while Swamy *et al.* (1999) reported test results indicating no positive influence from the provision of anchor bolts. As end

anchorage has most structural benefits under a low shear span/depth ratio in which case plate end debonding is the more likely failure mode but does not prevent mid-span debonding (Garden and Hollaway 1998; Pham and Al-Mahaidi 2004), researchers acknowledged that it is necessary to provide additional intermediate anchorages along the span to prevent brittle separation failure initiating anywhere along the span.

Gao *et al.* (2004, 2005) experimentally investigated the use of rubber modified epoxy and found that it is effective in reducing the stress concentrations at the plate ends and enhancing the interlaminar fracture toughness. This ameliorating effect is partly attributed to the ability of modified resin to penetrate deeper into the concrete than unmodified resin.

More recently, powder actuated fasteners have also been used to attach the FRP plates to concrete beams (Lamanna *et al.* 2004; Quattlebaum *et al.* 2005; Martin *et al.* 2008). Attached FRP strips were found to show comparable strengthening and such strengthened beams showed greater ductility than that with adhesive bonding. Bahn and Harichandran (2008) experimentally investigated the use of epoxy mortar patch end anchorages on the structural behaviour of RC beams strengthened with carbon CFRP sheets and found that this method is very effective in delaying or preventing premature debonding failures.

Methods to delay or inhibit premature debonding normally lead to more ductile behaviour in the strengthened structures. However, as claimed in Spadea *et al.* (2001), careful design of the end and other anchorages can make major contributions in regaining a substantial part of the lost ductility property, but is unable to restore the strengthened beams to the original levels of ductility. The results from the experiments using powder actuated fasteners (Martin *et al.* 2008) showed that this method improved the flexural capacity of the specimens with little or no loss in ductility, but the technique is still relatively novel and test results are very limited. In addition, some of the methods mentioned are not always practically viable.

2.4.3 Ductility considerations in current design guidance documents

In this section, approaches adopted in major design guidelines in different parts of the world are reviewed for preventing debonding failures together with the general rules in regard to moment redistribution in FRP-plated structures. The design guidance documents discussed here include TR 55 (Concrete Society 2004) in the UK, fib Bulletin 14 (Federation Internationale du Beton 2001) in Europe, JSCE Recommendations (Japanese Society of Civil Engineers 2001) in Japan and ACI 404.2R-08 (American Concrete Institute 2008) in the United States for FRP-strengthened RC structures, and ICE design and practice guide for FRP composites (Moy 2001) and CIRIA Guidance Document 595 (Cadei *et al.* 2004) for metallic structures. Plate end debonding and mid-span debonding are discussed separately below for FRP-strengthened RC structures. Debonding for FRP-strengthened metallic structures was already discussed in previous sections and so is not included here.

2.4.3.1 PE debondig in FRP-plated RC structures

In the fib Bulletin 14 (Federation Internationale du Beton 2001), plate end debonding is considered through verification of the end anchorage, using methods mainly based on fracture mechanics and bond stress-slip relationships (e.g. Taljsten 1994; Neubauer and Rostasy 1997). The axial force in the FRP plates anywhere along the span is restricted to the ultimate bond force taking into consideration the anchorage length.

TR 55 (Concrete Society 2004) takes a similar approach with plate end debonding. Based on some experimental findings, it allows greater FRP force than the FRP anchorage capacity in the span of the strengthened beam provided there is a gradual build-up of stress outside the anchorage region. It limits the longitudinal shear stress between the FRP and the substrate at the ultimate limit state to 0.8 N/mm^2. This should be checked near the plate ends, where any changes in section occur, at positions where there are discontinuities in shear force, such as at the position of load points, and at locations where steel reinforcement has yielded.

JSCE recommendations (Japanese Society of Civil Engineers 2001) suggest a procedure to calculate the flexural and axial load-carrying capacity of members that fail due to peeling of the continuous fibre, based on two main parameters: fracture energy and effective bonding length. It is worth noting that FRP sheets are commonly used in this area compared with FRP plates or strips in other parts of the world and

mid-span debonding is the dominant mode in this case due to the fact that these sheets are relatively thin. Therefore, it is mainly developed for the consideration of IC debonding, even though checks are also carried out in anchorage zones. This will be covered in the following section.

ACI 404.2R-08 (American Concrete Institute 2008) is mainly concerned with mid-span debonding but it does state that a limitation is placed on the strain level developed in the laminate to prevent cover delamination or FRP debonding. This, again, will be discussed in more detail in the following section.

2.4.3.2 IC debonding in FRP-plated RC structures

Three different approaches are recommended in the fib Bulletin 14 (Federation Internationale du Beton 2001) for design against mid-span debonding. In Approach 1, the effective FRP strain is limited to a constant value between 0.0065 and 0.0085, which, as is stated, may lead to uneconomical use of FRP especially when strengthening large spans. In Approach 2, which is more complicated (too complex to be a practical engineering model) and is based on the interface shear stress–slip law (Niedermeier 2000), debonding is treated in a unified way at both the anchorage zone and any point along the FRP-concrete interface. It gives the maximum axial tensile force that can be taken by FRP. Approach 3, based on the model proposed by Matthys (2000), prevents mid-span debonding by limiting shear stress at the FRP-concrete interface to the bond shear strength of concrete.

In TR 55 (Concrete Society 2004), mid-span debonding failure is avoided by limiting the design strains in the FRP. The strain in the FRP at the ultimate limit state should nowhere exceed 0.008.

The JSCE recommendations (Japanese Society of Civil Engineers 2001), based on the fracture energy model proposed by Wu and Niu (2000), limit the stress in the continuous fibre sheet at the location of flexural cracking caused by the maximum bending moment to a value related to the interfacial energy (G_f) and axial stiffness per unit width of the FRP sheets to prevent debonding. It also suggests that the flexural capacity and axial load-carrying capacity of members failing due to debonding of the continuous fibre sheets may be calculated in such a way that the maximum difference

in tensile stress occurring in the continuous fibre sheet over the effective bonding length is limited to the above mentioned value.

ACI 404.2R-08 (American Concrete Institute 2008) takes an empirical approach for avoiding premature debonding failures, by limiting the allowable strain in the FRP to a value depending on the axial stiffness of the FRP composites per unit width.

2.4.3.3 Moment redistribution in FRP-plated RC structures

In currently available design guidance documents, the reduction in ductility after the application of FRP composites is either limited so that the requirement in traditional design is still fulfilled as in fib Bulletin 14 (Federation Internationale du Beton 2001), or is compensated with a higher reserve of strength as in ACI 440.2R-08 (American Concrete Institute 2008), or a combination of both as in TR 55 (Concrete Society 2004). Moment redistribution in the strengthened part of the structure is, in general, not allowed. TR 55 (Concrete Society 2004) permits up to a maximum of 30% moment redistribution into FRP-strengthened parts of the structure if it can be demonstrated that there exists sufficient rotation capacity within the strengthened zone and within the surrounding structure to allow such redistribution to take place. Moment redistribution out of FRP-strengthened zones, however, is not recommended.

- The main consequence of the treatment of ductility is that the strengthening level provided by the external FRP reinforcement is rather limited. Naaman *et al.* (1999) recommended an increase in moment due to strengthening be limited up to 20% of the balance moment (the moment at which steel yielding and concrete crushing occur simultaneously) and shown to be reasonable in Duthinh and Starnes (2004).

2.5 FRP-plated indeterminate structures

Despite some unresolved issues as discussed above, the behaviour of statically determinate (single span simply supported) beams strengthened with composite materials is now considered to be well known. On the contrary, there is a general lack of study on FRP-plated indeterminate structures, although several real structures (including frame buildings and multi-span continuous bridges) targeted for

strengthening are statically indeterminate. In this section, work on FRP-plated indeterminate structures is first reviewed, after which some unique features introduced by structural indeterminacy are discussed.

2.5.1 FRP-plated indeterminate structures

Sharma (1992) repaired eight 2-span continuous reinforced concrete beams (previously failed in flexure) with fibro-ferrocrete and found that the responses of the repaired beams were similar to those of original beams. They also reported that the performances of the beams repaired with fibro-ferrocrete were superior to and more consistent than those of beams repaired with normal concrete and steel reinforcement. Grace *et al.* (1998) tested seven T-section 2-span continuous beams internally reinforced with different types of FRP bar and stirrup, and found that failure modes and ductility varied between different FRP reinforcement arrangements which gave the same load capacities as steel reinforcement in conventional beams.

Grace *et al.* (1999) were among the first to report tests on continuous beams strengthened with externally bonded FRP. They tested five 2-span T-section RC beams with different strengthening arrangements and investigated the effects of flexural and shear strengthenings. They concluded that using FRP laminates to strengthen continuous beams is effective in reducing deflections, increasing load capacity, and leads to smaller and better distributed cracks. They also found that the use of CFRP plates may lead to premature separation in the concrete cover.

El-Refaie *et al.* (2001, 2003a,b, 2004) tested four reinforced concrete 2-span beams strengthened with externally bonded CFRP plates or sheets, to study the effects of the position and form of the CFRP composites. They concluded that using the CFRP composites to strengthen reinforced concrete continuous beams is an effective method and that the performances of the beams strengthened with plates or sheets of equivalent strength were similar. Mid-span soffit and central support strengthening were observed as the most effective arrangement for high stiffness and capacity.

In practice, very few projects have been reported on strengthening indeterminate structures through the use of externally bonded FRP composites (Luke and Canning 2004). Shuman *et al.* (2003) described the rehabilitation of a 5-span cast-in-place concrete T-girder bridge using FRP composites. FRP composites were applied to

provide additional flexural reinforcement. In the West Gate bridge strengthening project (Irwin and Rahman 2002), FRP laminates were used for flexural, torsional and shear strengthening to accommodate the largely increased traffic density and flow.

2.5.2 Deflections of FRP-reinforced structures

Research into deflections of FRP-reinforced structures has focused on FRP-reinforced concrete structures. For FRP-reinforced concrete members, the replacement of steel with FRP bars often leads to substantial decrease in stiffness after cracking due to their relatively low modulus of elasticity. The design of FRP-reinforced concrete members is typically governed by serviceability requirements (Razaqpur *et al.* 2000; Mota *et al.* 2006). There are two approaches commonly adopted for deflection calculations, namely effective moment of inertia approach and moment-curvature approach.

The effective moment of inertia approach usually makes use of the Branson Equation (originally developed for steel reinforced concrete members) with modifications made to give a better fit with test data of FRP-strengthened concrete members (Toutanji and Saafi 2000; Yost *et al.* 2003; Bischoff 2007). The main factors have been found to be the modulus of elasticity of the FRP (ACI 2003), the relative reinforcement ratio (ACI 2004), or both the two factors (Toutanji and Saafi 2000; Yost *et al.* 2003; Mota *et al.* 2006). Rizkalla and Mufti (2001) suggested a different form of equation to calculate the effective moment of inertia. It uses the uncracked moment of inertia of the section transformed to concrete instead of the moment of inertia of the gross section. The moment curvature approach involves the use of the moment curvature diagram (of the section) and the virtual work principle (Razaqpur *et al.* 2000; CSA 2002; Al-Saidy *et al.* 2004). When a moment curvature relationship is known, the virtual work principle can be used to calculate the deflection of structural members under any load:

$$\delta = \int_0^L m(x)\frac{M(x)}{EI(x)}dx \qquad (2\text{-}3)$$

where L = beam span; $EI(x)$ = section stiffness along the member; $m(x)$ and $M(x)$ = virtual and real moments, respectively. This approach is especially suited for

structures where moment curvature relationships are in simple forms such as linear, bilinear or tri-linear.

For FRP-strengthened metallic structures, both Moy (2001) and Cadei *et al.* (2004) take a transformed section approach to evaluate the stiffness of the strengthened section.

Most of the study has been on one span simply supported beams. This limits any approach available for FRP-plated continuous members. The ACI Committee 318 (2005) suggested the use of either the effective moment inertia of the midspan section or the average of the critical positive and negative moment sections for deflection calculations (as suggested by Portland Cement Association 1996). Modification was made by Habeeb and Ashour (2008) to give a better fit of their test data.

2.5.3 Unique features of FRP-plated indeterminate structures

Indeterminacy introduces unique features which render structural response to load more complex that of determinate structures. One unique feature is that self-equilibrating moments develop from causes such as differential settlement between supports, thermal gradients and plasticity-inducing load histories. Another unique feature is that the total (including self-equilibrating) moments developed under load depend not only on the loads but also on the support and internal stiffness profiles of an indeterminate (but not of a determinate) structure.

Under a given load, the self-equilibrating moments and the internal stiffness profile both influence the moment diagram, so affecting the magnitudes/locations of peak moment and also the locations of contraflexure (Sebastian 2003) along individual structural members. As a result, serviceability limit state (SLS) issues such as loads and locations at onset of nonlinearity (first yield, etc at locations of peak moment), and ultimate limit state (ULS) issues such as end peel and local buckling of FRP plates due to offsets between plate curtailments and nearby points of contraflexure (Sebastian 2006a), are complex nonlinear problems.

To illustrate how curtailment - contraflexure offsets influence end-peel tendencies of the plate from the beam, consider a beam (specimen B1 in Chapter 4) analysed via Roberts' staged approach (Roberts 1989). This approach entails algebraic expressions for the shear and normal bond stresses which can trigger end-peel failure. These

expressions, derived for single span simply supported beams, apply equally to continuous beams, with the section of contraflexure (zero moment) in the continuous member replacing the end section of a single span simply supported beam. Application to the present test specimen leads to Figure 2-11, which shows how the end-peel bond stresses vary with the offset between FRP plate curtailment and nearby sections of contraflexure in the beam, although it should be noted that the moments and shear forces themselves will vary with this offset as the change in the plate layout induces a change in the stiffness distribution along the beam. It is clear that the shear and normal bond stresses increase dramatically with this offset. As the offset doubles from 100 mm to 200 mm, the shear and normal stresses almost double from 6.5 N/mm^2 to 12 N/mm^2 and from 5.5 N/mm^2 to 9.5 N/mm^2 respectively. Note that end-peel was indeed observed at the compressive ends of the base FRP plates in this example specimen (discussed in Chapter 4).

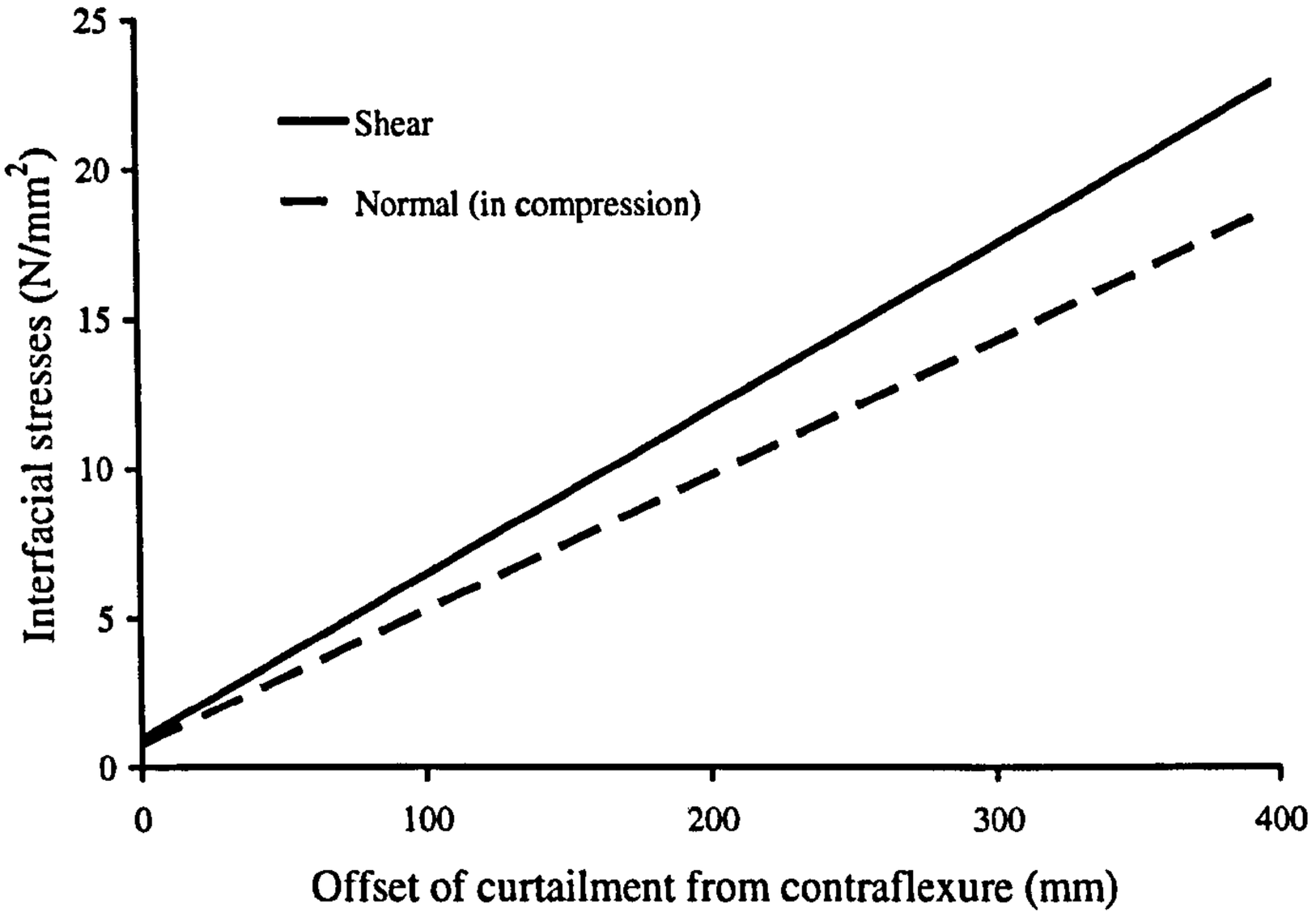

Figure 2-11 - Effect of curtailment offset from contraflexure on interfacial stresses

Clearly, it is important to understand the mechanics of development of self-equilibrating stress resultants and their potential effects on indeterminate FRP-reinforced structures. Also, the ductility issues identified in the previous sections have not yet been thoroughly addressed in the above investigations.

2.6 Conclusions

From the extensive discussions of this chapter, the following points have emerged:

- The elastic nature of the FRP composites and the premature debonding failures often reduce the ductilities of FRP-strengthened structures. Although a large number of strength models have been developed for both plate end debonding and mid-span debonding, there is a high level of dispersion in the results from different models and thorough understanding of the failure mechanisms is still to be gained.
- Design using procedures for traditional statically indeterminate reinforced concrete (RC) structures may be unsafe for FRP-plated RC structures. Quantification of the ductility of FRP-plated structures remains largely an unresolved issue. Design guidance documents currently available either limit the strengthening level of the FRP reinforcement to provide sufficient ductility of the strengthened structure or use a bigger safety factor against debonding failures to compensate for the reduction in ductility. Therefore, there is an urgent need to develop a new design and analysis approach that is independent of the ductility levels of the structures, in order to use these innovative materials to their full potential.
- Research – both analytical and experimental – into FRP-plated indeterminate (particularly metallic) structures is limited to date. The development of self-equilibrating moments and their potential effects in the indeterminate spans have not thus far been addressed. Development of an analytical model to address this issue is therefore timely.
- Most research to date has focused on FRP-plated RC structures and less work has been conducted on FRP-plated metallic structures. Virtually no documents have been found on the general behaviour of FRP-plated indeterminate metallic structures. So an

experimental programme on FRP-plated continuous steel beams has important and far-reaching implications.

These outstanding issues have guided the approach adopted in the present PhD study. In the following chapter, closed-form algebraic expressions are presented for the self-equilibrating moments due to differential settlement, in FRP-plated 2-span continuous beams. A general framework of ideas is presented to help rapidly establish whether self-equilibrating moments should be considered in interpreting output data from lab tests on 2-span continuous members and in design/assessment of 2-span continuous bridges. A deflection-based approach is proposed to estimate the support stiffnesses. Chapter 4 reports on tests performed on FRP-plated 2-span continuous steel-I beams. Important observations and data from the tests are presented and discussed. The design of the instrumentation layouts to investigate the stiffness profiles of the system is also discussed in detail. Chapter 5 presents a computational technique for time-efficient prediction of ultimate loads of highly indeterminate structures. Chapter 6 is then devoted to the development of an iterative procedure entailing multiple detailing and ultimate analysis loops for the structure to create an analysis-design process for ductility-deficient indeterminate structures. Finally, Chapter 7 summarises the main findings of this research programme and puts forward suggestions for continuation of the work.

Chapter 3

Analysis of FRP-Plated Continuous Beams

3.1 Introduction

In Chapter 2 it was identified that research – both analytical and experimental – into FRP-plated indeterminate structures is limited to date. Indeterminacy introduces unique features including the following:

- Self-equilibrating moments develop from causes such as differential settlement between supports, thermal gradients and plasticity-inducing load histories;
- Total (including self-equilibrating) moments developed under load depend not only on the loads but also on the support and internal stiffness profiles of an indeterminate (but not of a determinate) structure.

These features render structural responses – both at the serviceability limit state (SLS) and at the ultimate limit state (ULS) – more complex than that of determinate structures.

Clearly, it is important to understand the mechanics of development of self-equilibrating stress resultants and their potential effects on indeterminate FRP-plated structures. Investigations on statically indeterminate structures, as identified in Chapter 2, have entailed 2-span continuous beams. This looks set to continue in the lab. Also, 2-span bridges are common in practice. To that end, the present chapter presents closed-form nonlinear algebraic expressions for self-equilibrating moments due to differential settlement between supports of 2-span continuous structures. Differential settlement of supports (Figure 3-1) is considered here as it is commonly a major cause of self-equilibrating moments.

In what follows, purpose-derived algebraic expressions are first presented for the total moments in loaded 2-span continuous structures as clear functions of the support-to-member stiffness *ratios* and of the stiffness distributions along the structures. Stiffness layouts representative of both service and ultimate limit states are considered. The results are verified by comparison with limited test data from literature. By subtracting the rigid support moments (for the same loads) from these total moments, the self-equilibrating moments are obtained. Parametric studies are then carried out to illustrate, via appropriate 3D plots, how certain ranges of the stiffness ratios can give rise to significant self-equilibrating moment effects including early nonlinearity and contraflexure shift. Based on these studies, a general framework of ideas is presented to help rapidly establish whether self-equilibrating moments should be considered in interpreting output data from lab tests on 2-span continuous members and in design / assessment of 2-span continuous bridges. Finally, a deflection-based approach is proposed to estimate the support stiffnesses.

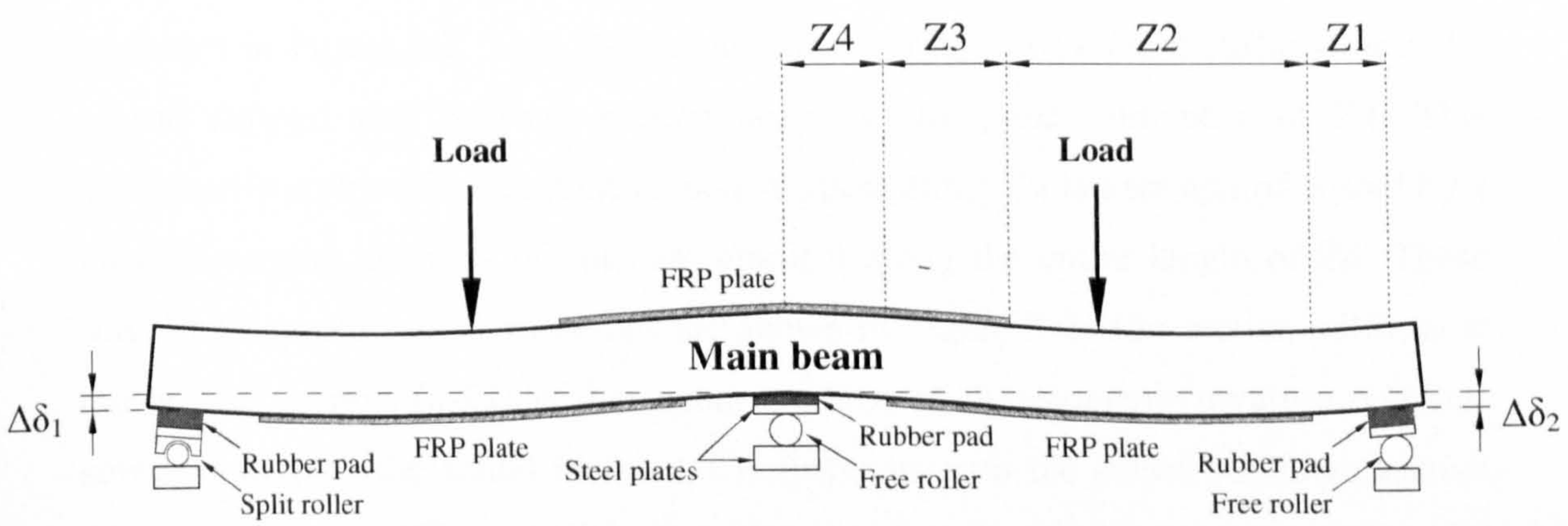

Figure 3-1 - FRP-plated 2-span continuous member

3.2 Theoretical analysis

FRP plates are commonly applied to the tension faces of structural members, giving the typical layout for the 2-span beam shown in Figure 3-1. In the linear regime of behaviour (up to the serviceability limit state SLS), the beam's constituent materials are elastic and section stiffness is typically constant along any zone with a fixed material layout. This leads to 4 different stiffness zones for each span as shown in Figure 3-1, namely the original beam only along zone Z1, the beam with base FRP plate along Z2, the beam with top and base plates along Z3, and the beam with top plate along Z4. During the nonlinear behaviour (up to the ultimate limit state ULS), loss of material stiffness (steel yield, compression concrete softening, etc) typically becomes less pronounced with distance outwards from peak moment sections, giving increase of overall section stiffness from these peak moment locations outwards; section stiffness remaining constant in other zones as explained above for the linear regime.

During the nonlinearity, softening of sections might occur along a part of Z4 nearest the central support, with constant (elastic) section stiffness along the remainder of Z4 as shown in Figure 3-2. This gives a nonlinear variation of section stiffness near the central support and constant section stiffness along the remainder of Z4. This nonlinear-in-series-with-constant section stiffness along Z4 is here approximated by a linearly varying stiffness of constant gradient along the entire length of Z4. These actual and approximated variations are shown in Figure 3-2. The section stiffness at the central support (α_4EI) is the secant gradient of the moment-curvature relations corresponding to the actual moment. Comparisons with the actual nonlinear section stiffness variation (FE analysis) show that this linear variation permits very useful insight into the important features of structural behaviour.

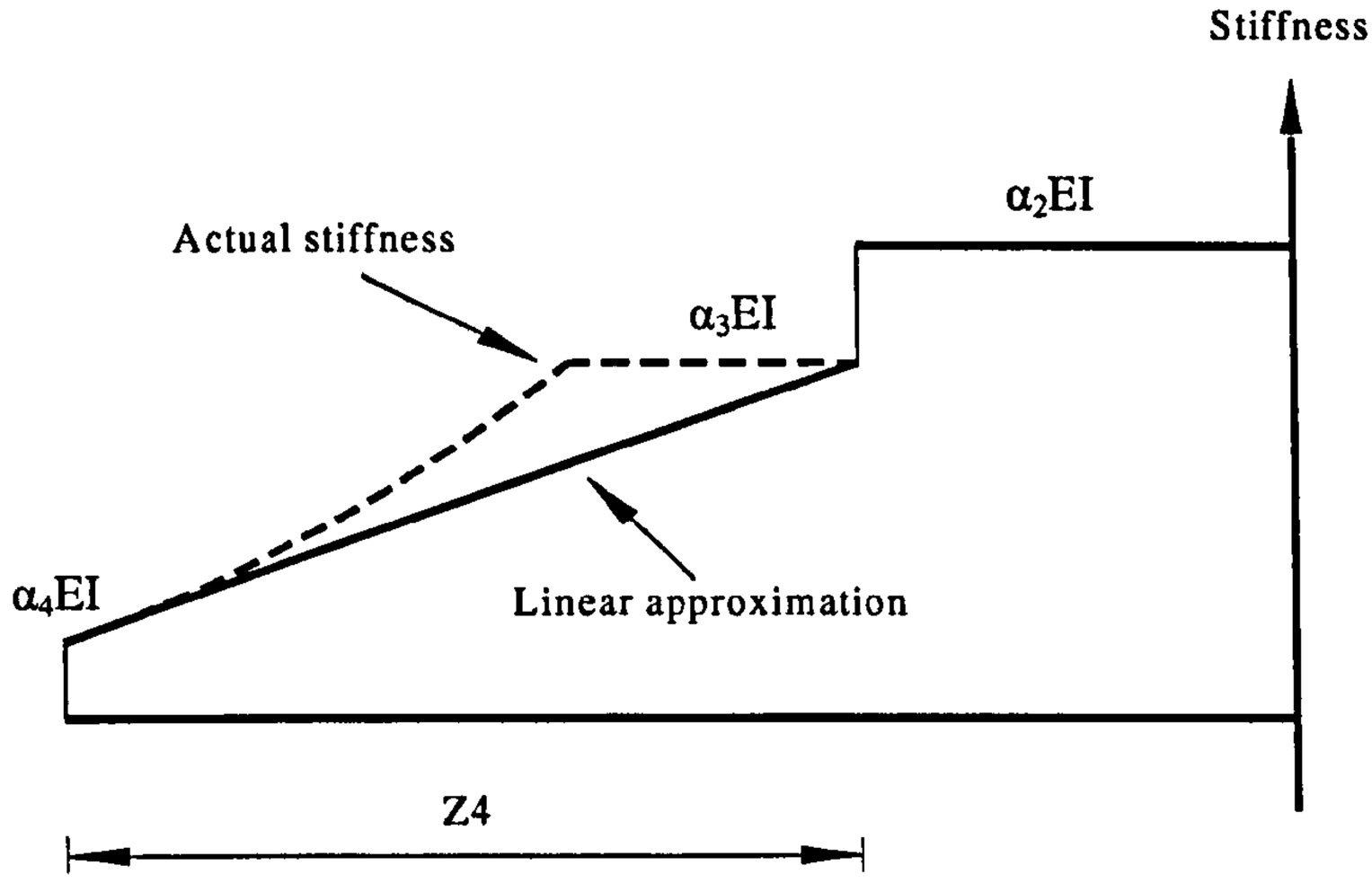

Figure 3-2 - Approximation of stiffness variation

Uniformly distributed loading and a point load are separately considered. Symmetry is assumed about the centre support. For one span Figure 3-3 (a) defines the point load's location, the stiffness zones and the sprung supports. The length of each zone is expressed relative to the span L via parameters γ_1 to γ_4. Each support stiffness, k (the quotient of load and deflection at the support), is as follows:

$$k = \beta \frac{EI}{L^3} \qquad (3\text{-}1),$$

where β is a stiffness multiplier (β_1, β_2 for the end and centre supports respectively, see Figure 3-3 (a)), while the function EI/L^3 is used for dimensional consistency on moments and to ensure that the supports are defined in terms of the same reference stiffness as are the zones Z2 – Z4. Figure 3-3 (b) defines the stiffness zones during nonlinear behaviour as discussed above. The section bending stiffness (EI) of zone Z1 is used as a reference. Parameters α_1 to α_4 define the section stiffnesses of the other zones relative to the reference stiffness.

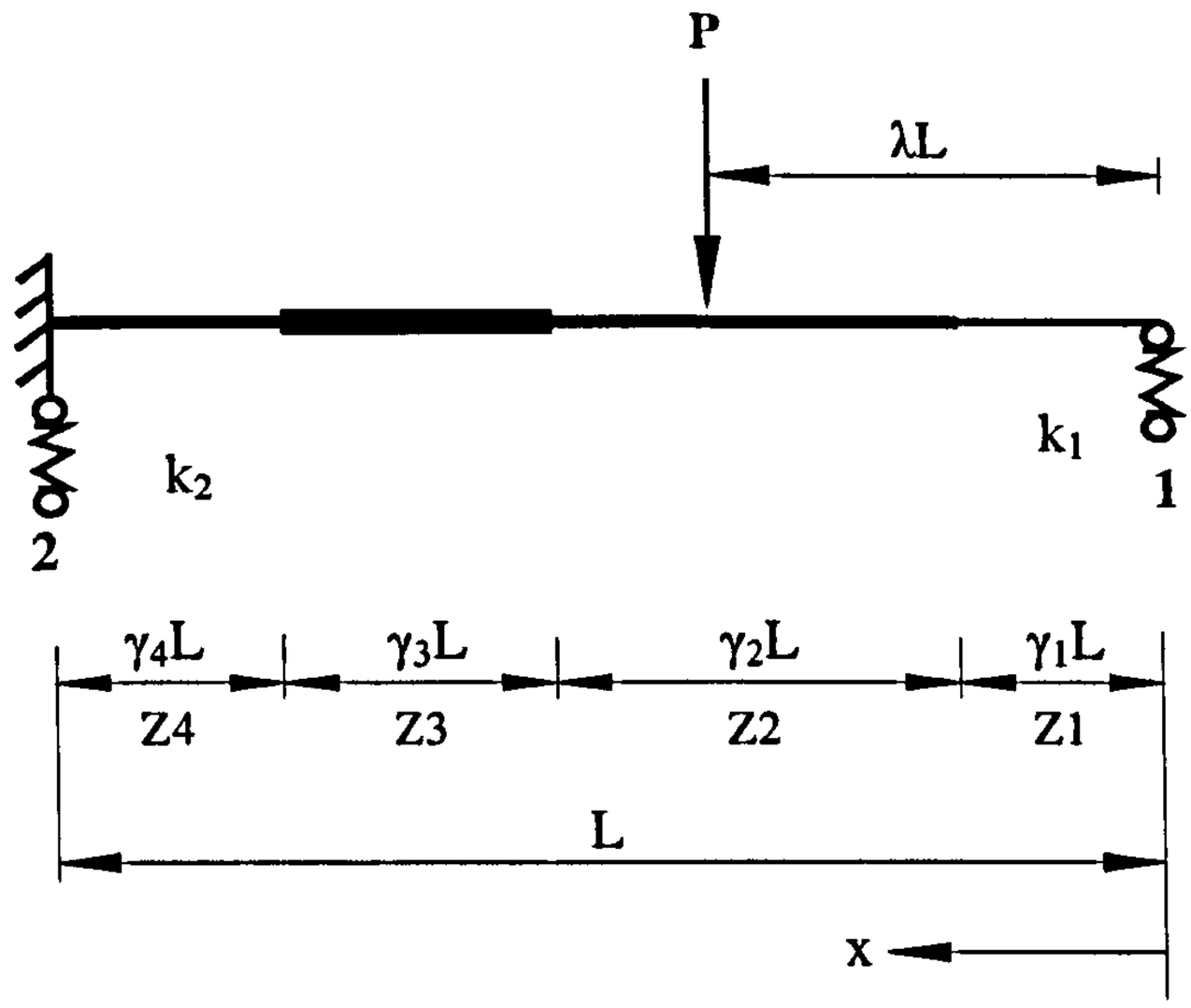

(a) Generalised beam model

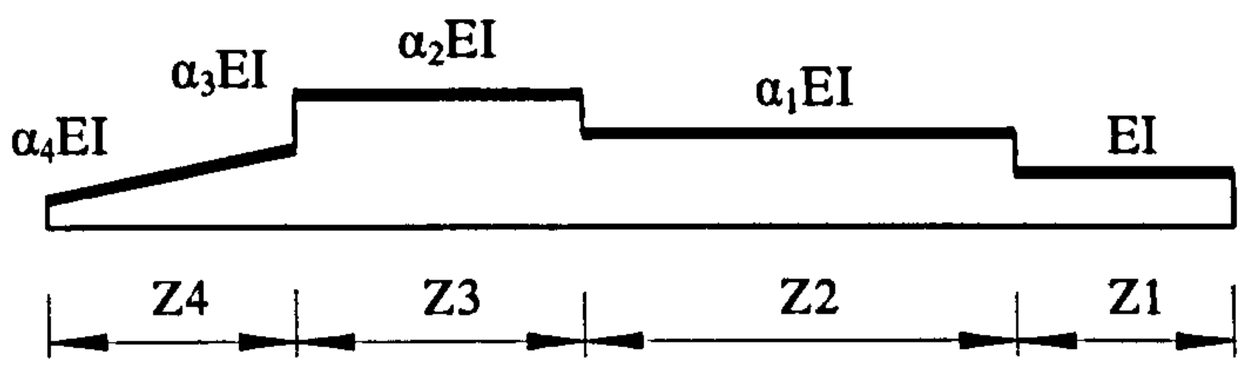

(b) Stiffness variation at ULS

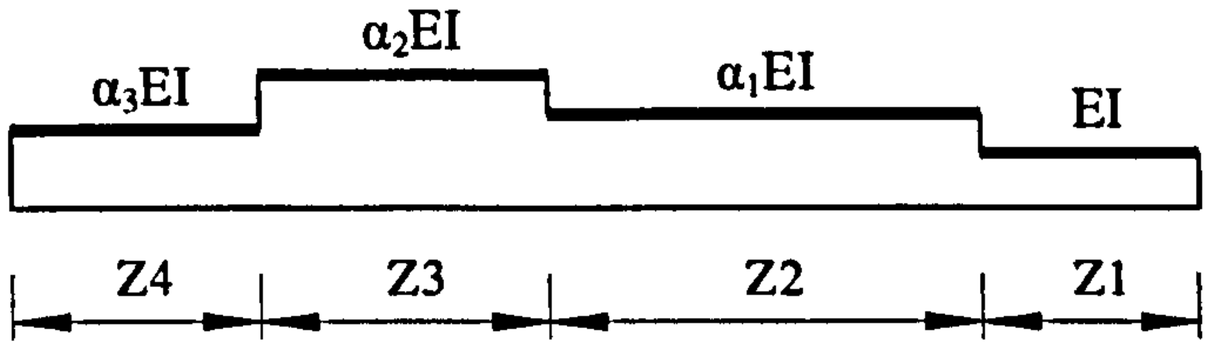

(c) Stiffness variation at SLS

Figure 3-3 - Modelling one span of a symmetric 2-span beam

There are three zones (Z1 to Z3) of constant stiffness (ratios 1, α_1 and α_2), the fourth zone (Z4) showing a linear drop in stiffness from α_3 to α_4 as discussed above. When $\alpha_3 = \alpha_4$, there is constant stiffness along Z4, causing the stiffness layout developed for the nonlinear regime to simplify to the SLS layout of Figure 3-3 (c).

3.2.1 Centre support section moment

Consider the beam shown in Figure 3-3 subject to distributed load w per unit length over the entire span. For this load and the stiffness variation of Figure 3-3 (b) for nonlinear behaviour, combined consideration of equilibrium, constitutive behaviour and boundary conditions (see Appendix 3A) leads to the moment at the centre support section as:

$$M_2 = C_w w L^2 \tag{3-2}$$

where the moment parameter C_w clearly reflects the effects of support-to-member stiffness *ratios* and the distribution of stiffness along the member as follows :

$$C_{WN} = \frac{1}{2} - \frac{\frac{1}{\beta_2} + \frac{1}{8}\left(\frac{1}{\alpha_1} - \frac{1}{\alpha_2}\right)\left(\Pi^4 - \gamma_1^4\right) + \frac{1}{8}\frac{1}{\alpha_2}\psi^4 + \frac{1}{6}\frac{1}{\varsigma}(1-\Psi^3) - \frac{1}{4}\frac{\xi}{\varsigma^2}(1-\Psi^2) + \frac{1}{2}\frac{\xi^2}{\varsigma^3}(1-\psi) - \frac{1}{2}\frac{\xi^3}{\varsigma^4}\ln\frac{\alpha_4}{\alpha_3}}{\frac{1}{\beta_1} + \frac{1}{\beta_2} + \frac{1}{3}\left(\frac{1}{\alpha_1} - \frac{1}{\alpha_2}\right)\left(\Pi^3 - \gamma_1^3\right) + \frac{1}{3}\frac{1}{\alpha_2}\Psi^3 + \frac{1}{2}\frac{1}{\varsigma}(1-\Psi^2) - \frac{\xi}{\varsigma^2}(1-\Psi) + \frac{\xi^2}{\varsigma^3}\ln\left(\frac{\alpha_4}{\alpha_3}\right)} \tag{3-3},$$

where $\Pi = \gamma_1 + \gamma_2$, $\Psi = \gamma_1 + \gamma_2 + \gamma_3$, $\xi = \alpha_3 - \frac{\alpha_4 - \alpha_3}{\gamma_4}\Psi$, and $\varsigma = \frac{\alpha_4 - \alpha_3}{\gamma_4}$.

If instead the stiffness distribution of Figure 3-3 (c) for linear behaviour applies when the span is subjected to the UDL, the following expression exists for C_w :

$$C_{WL} = \frac{1}{2} - \frac{\frac{1}{\beta_2} + \frac{1}{8}\left[\left(1 - \frac{1}{\alpha_1}\right)\gamma_1^4 + \left(\frac{1}{\alpha_1} - \frac{1}{\alpha_2}\right)\Pi^4 + \left(\frac{1}{\alpha_2} - \frac{1}{\alpha_3}\right)\Psi^4 + \frac{1}{\alpha_3}\right]}{\left(\frac{1}{\beta_1} + \frac{1}{\beta_2}\right) + \frac{1}{3}\left[\left(1 - \frac{1}{\alpha_1}\right)\gamma_1^3 + \left(\frac{1}{\alpha_1} - \frac{1}{\alpha_2}\right)\Pi^3 + \left(\frac{1}{\alpha_2} - \frac{1}{\alpha_3}\right)\Psi^3 + \frac{1}{\alpha_3}\right]} \tag{3-4}$$

A similar analysis for the beam under point load P applied at a distance λL from the outer support (Figure 3-3 (a)) gives the moment at the centre support as:

$$M_2 = C_p P L \tag{3-5}$$

where C_p is given in Equations (6) and (7) for the nonlinear and linear regimes, respectively.

$$C_{PN}=1-\lambda\frac{\frac{1}{\beta_2}+\frac{1}{3}\left(\frac{1}{\alpha_1}-\frac{1}{\alpha_2}\right)\Pi^3-\frac{1}{2}\lambda\left(\frac{1}{\alpha_1}-\frac{1}{\alpha_2}\right)\Pi^2-\frac{1}{2\alpha_2}\lambda\Psi^2+\frac{1}{6\alpha_1}\lambda^3+\frac{1}{3\alpha_2}\Psi^3+\frac{1}{\varsigma}\left(\frac{1}{2}-\gamma_4\lambda-\frac{1}{2}\Psi^2\right)-\frac{\xi}{\varsigma^2}\gamma_4+\frac{\xi}{\varsigma^2}\lambda\ln\frac{\alpha_4}{\alpha_3}+\frac{\varsigma^2}{\xi^3}\ln\frac{\alpha_4}{\alpha_3}}{\frac{1}{\beta_1}+\frac{1}{\beta_2}+\frac{1}{3}\left(\frac{1}{\alpha_1}-\frac{1}{\alpha_2}\right)\left(\Pi^3-\gamma_1^3\right)+\frac{1}{3\alpha_2}\Psi^3+\frac{1}{2\varsigma}(1-\Psi^2)-\frac{\xi}{\varsigma^2}(1-\Psi)+\frac{\xi^2}{\varsigma^3}\ln\left(\frac{\alpha_4}{\alpha_3}\right)} \quad (3\text{-}6)$$

$$C_{PL}=1-\lambda-\frac{\frac{1}{\beta_2}+\frac{1}{3}\left[\left(\frac{1}{\alpha_1}-\frac{1}{\alpha_2}\right)\Pi^3+\left(\frac{1}{\alpha_2}-\frac{1}{\alpha_3}\right)\Psi^3\right]-\frac{1}{2}\lambda\left[\left(\frac{1}{\alpha_1}-\frac{1}{\alpha_2}\right)\Pi^2+\left(\frac{1}{\alpha_2}-\frac{1}{\alpha_3}\right)\Psi^2\right]+\frac{1}{6\alpha_1}\lambda^3+\frac{1}{3\alpha_3}-\frac{1}{2\alpha_3}\lambda}{\frac{1}{\beta_1}+\frac{1}{\beta_2}+\frac{1}{3}\left[\left(1-\frac{1}{\alpha_1}\right)\gamma_1^3+\left(\frac{1}{\alpha_1}-\frac{1}{\alpha_2}\right)\Pi^3+\left(\frac{1}{\alpha_2}-\frac{1}{\alpha_3}\right)\Psi^3+\frac{1}{\alpha_3}\right]} \quad (3\text{-}7)$$

Equations (3-6) and (3-7) assume that the point load is applied somewhere within zone Z2 of Figure 3-3 (a), as location within this "middle" zone is likely to create a large moment at the middle support. In practice, *Cw* and *Cp* may be limited to be positive to avoid any uplift of the beam at the support.

Equations (3-3) to (3-7) may be checked to establish that they simplify to the expressions for beams of constant stiffness on rigid supports. This is done by assuming that $\alpha_1=\alpha_2=\alpha_3=\alpha_4$ and that $\beta_1=\beta_2=\infty$. In such cases, it is seen that the expressions simplify to $Cw=\frac{1}{8}$ and $Cp=\frac{1}{2}\lambda-\frac{1}{2}\lambda^3$. These are consistent with the results from basic structural analysis, so giving some confidence in the above expressions.

As discussed in Chapter 2, end peel and mid-span debonding are two of the major concerns with external bonding of FRP. End peel can be accommodated in the analysis by changing the relevant lengths of segments, and mid-span debonding by changing the stiffness parameters in relevant segments.

3.2.2 Deflection

When a moment curvature relationship is known, the virtual work principle can be used to calculate the deflection of structural members under any load:

$$\delta = \int_0^L m(x)\frac{M(x)}{EI(x)}dx \qquad (3\text{-}8)$$

where L = beam span; $EI(x)$ = section stiffness along the member; $m(x)$ = virtual moment, which can be determined using the expressions derived in the previous section; and $M(x)$ = real moment, which can be determined from the moments obtained using expressions from the previous section.

This approach is especially suited to structures where moment curvature relationships can be approximated as being linear, bilinear or tri-linear, as will be the case for steel- or FRP-plated RC sections (Sebastian 2002, 2005; Liu *et al.* 2006; Paththini and Burgoyne 2009), FRP-reinforced concrete sections (Razaqpur *et al.* 2000; CSA 2002), and FRP-plated steel sections (as will be illustrated in Chapter 4).

3.3 Verification study

A verification study of the above algebraic expressions was carried out using data from a test by El-Refaie *et al.* (2003b) on an FRP-plated 2-span continuous concrete beam and also test data from an experiment by Habeeb and Ashour (2008) on an FRP-reinforced 2-span continuous concrete beam.

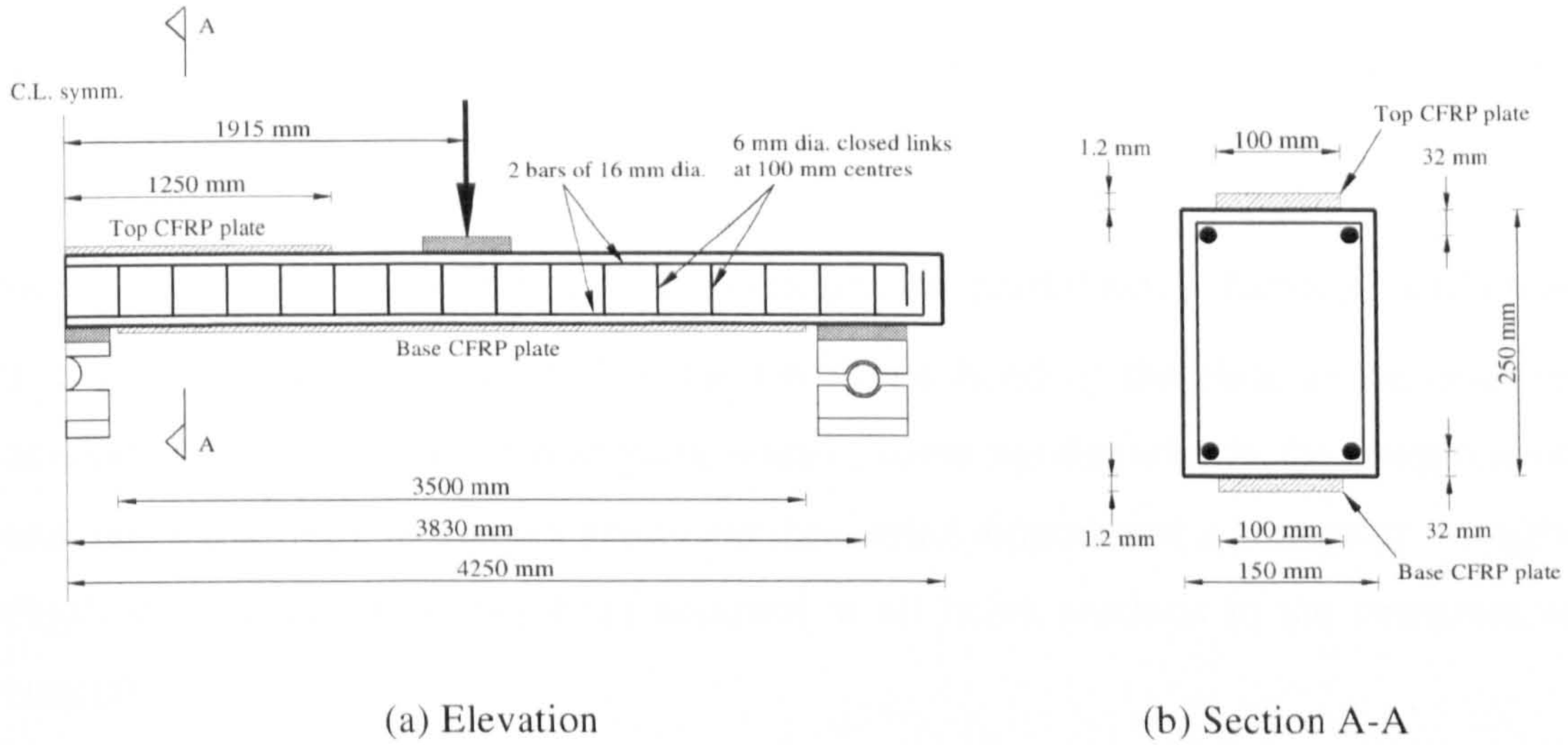

(a) Elevation (b) Section A-A

Figure 3-4 - Test details (E4 in El-Refaie *et al.* 2003b)

Concrete		Longitudinal bars		Vertical stirrups		CFRP	
f_{cu}	f_r	f_y	E_s	f_y	E_s	f_p	E_p
N/mm^2	N/mm^2	N/mm^2	kN/mm^2	N/mm^2	kN/mm^2	N/mm^2	kN/mm^2
46.1	4.4	520	201	308	201	2500	150

Table 3-1 - Material properties (El-Refaie *et al.* 2003b)

3.3.1 El-Refaie *et al.* (2003b)

Reinforced concrete beams strengthened with externally bonded carbon fibre reinforced polymer (CFRP) composites were tested by El-Refaie *et al.* (2003b). One of these beams, detailed in Figure 3-4 and material properties in Table 3-1, is now used to verify the present analysis.

The undeformed Young's modulus of the concrete (E_c) is estimated using the following expression from BS8110:

$$E_c = 5.5\sqrt{\frac{f_{cu}}{\gamma_m}} kN/mm^2 \tag{3-8}$$

where f_{cu} is the cube strength of the concrete and the partial safety factor γ_m is taken as 1 to reflect good quality control in the lab. Rigid bond of the plate to the adjacent concrete is assumed. In the post-yield regime, some nonlinearity in the compression concrete exists only in a small zone near the centre support and a triangular through-depth stress distribution has been assumed at all beam sections in the compression concrete.

There are effectively two zones for the beam as shown in Figure 3-5 (a), namely Z2 with base FRP plate and Z3 with top and base FRP plates. The stiffness variation during pre-yield behaviour is shown in Figure 3-5 (b). This is a simplified version of the one used in the theoretical analysis and is easily accommodated by taking $\gamma_1 = 0$ and $\alpha_2 = \alpha_3$.

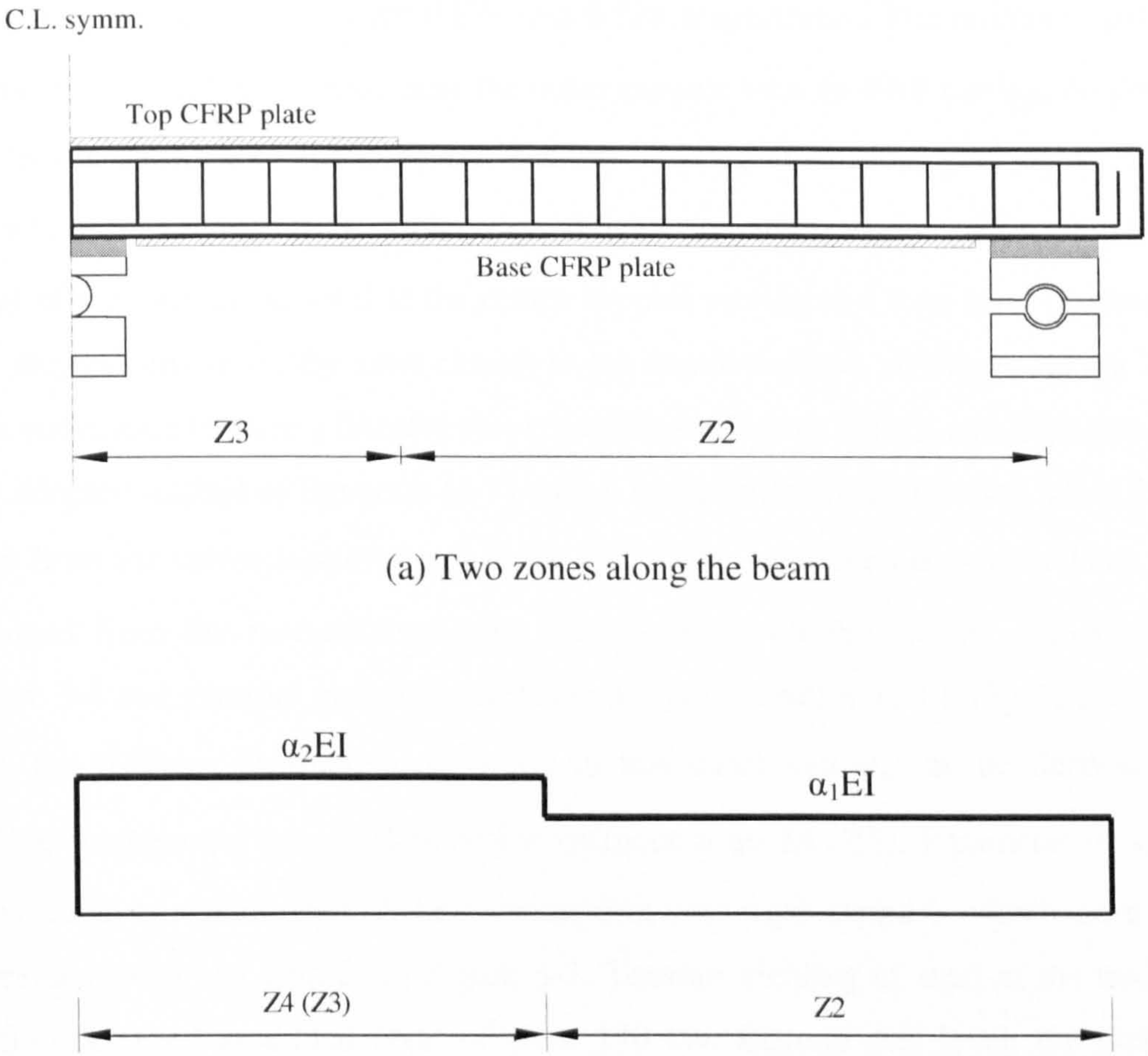

Figure 3-5 - Stiffness variation (E4 in El-Refaie *et al.* 2003b)

Length parameters γ_2 and γ_3 are 0.674 and 0.326 respectively. The reference stiffness is that of the (sag) RC section near the outer support with no FRP plating. Neglecting the tensile strength of the concrete, section bending stiffnesses give $\alpha_1 = 1.20$ and $\alpha_2 = 1.31$. The moments are then obtained using Equations (3-7) and (3-5) up till the onset of yielding in the steel at the centre support section at a load level of circa 140 kN. Beyond this level, the zone closest to the centre support, strictly speaking Z4, is then considered to have a linearly varying stiffness (Figure 3-5(c)) and Equation (3-6) was adopted instead of Equation (3-7) with a linear stiffness distribution taken for the zone from the centre support (α_4) to the end of the top plate ($\alpha_3 = \alpha_2$). Then α_4 is obtained from the moment-curvature relation based on the section dimensions of Figure 3-4 and material properties of Table 3-1 and Equation (3-8). Figure 3-6 shows how the stiffness parameters α_2 (= α_3 in this case) and α_4 can be derived from section moment-curvature relations for stiffness zone Z4 (Z3). Parameter α_1 can be obtained in a similar way. A key assumption was rigid supports which gave good agreement with test data as in Figure 3-7. Tension yielding of steel at the mid-span section occurred at a load level of circa 170 kN. Beyond this level, the predicted results depart from the experimental results. This is expected as yielding of the tension steel at the mid-span section is not accounted for in the analysis.

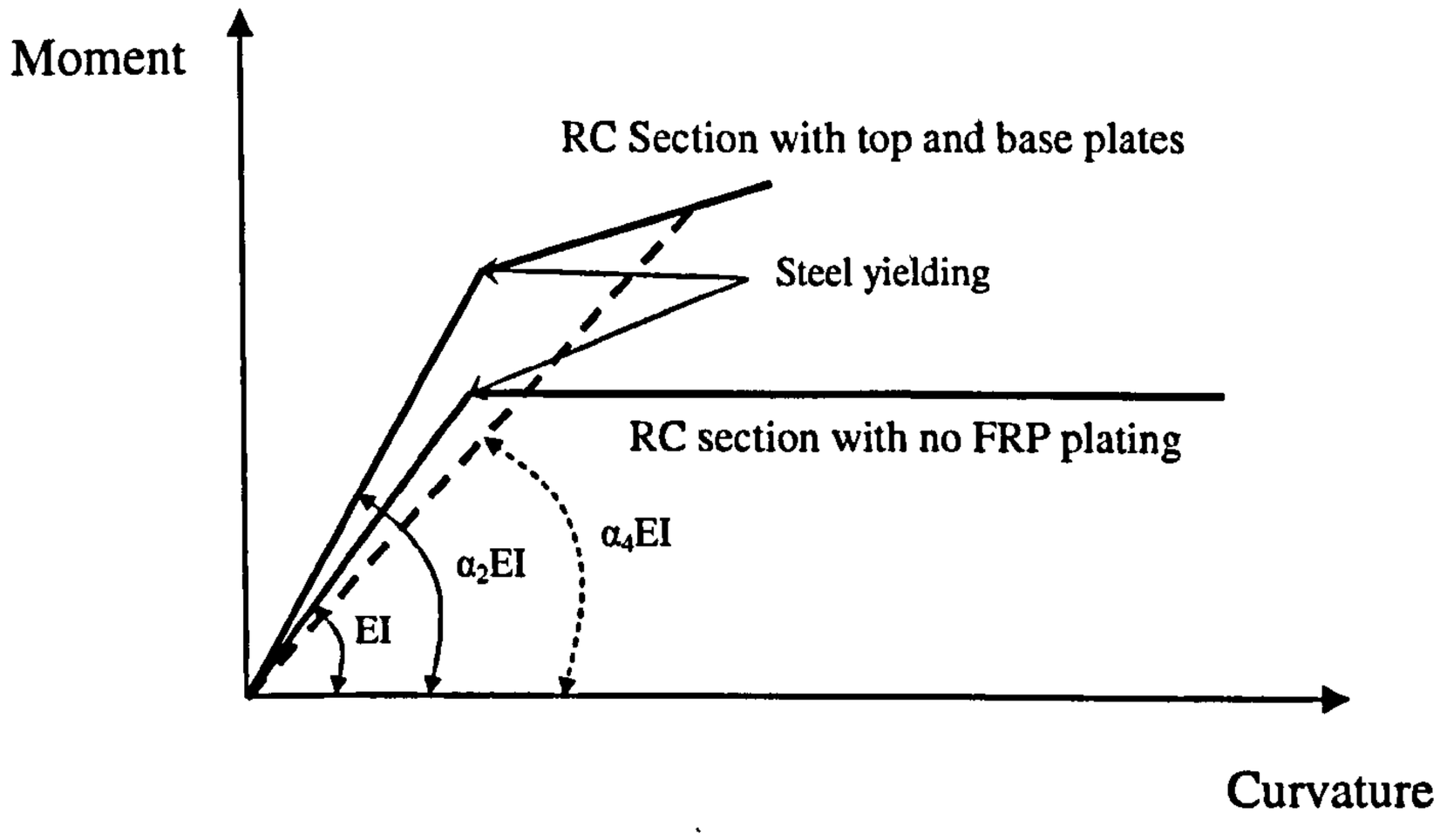

Figure 3-6 - Stiffness parameters from section moment-curvature relations

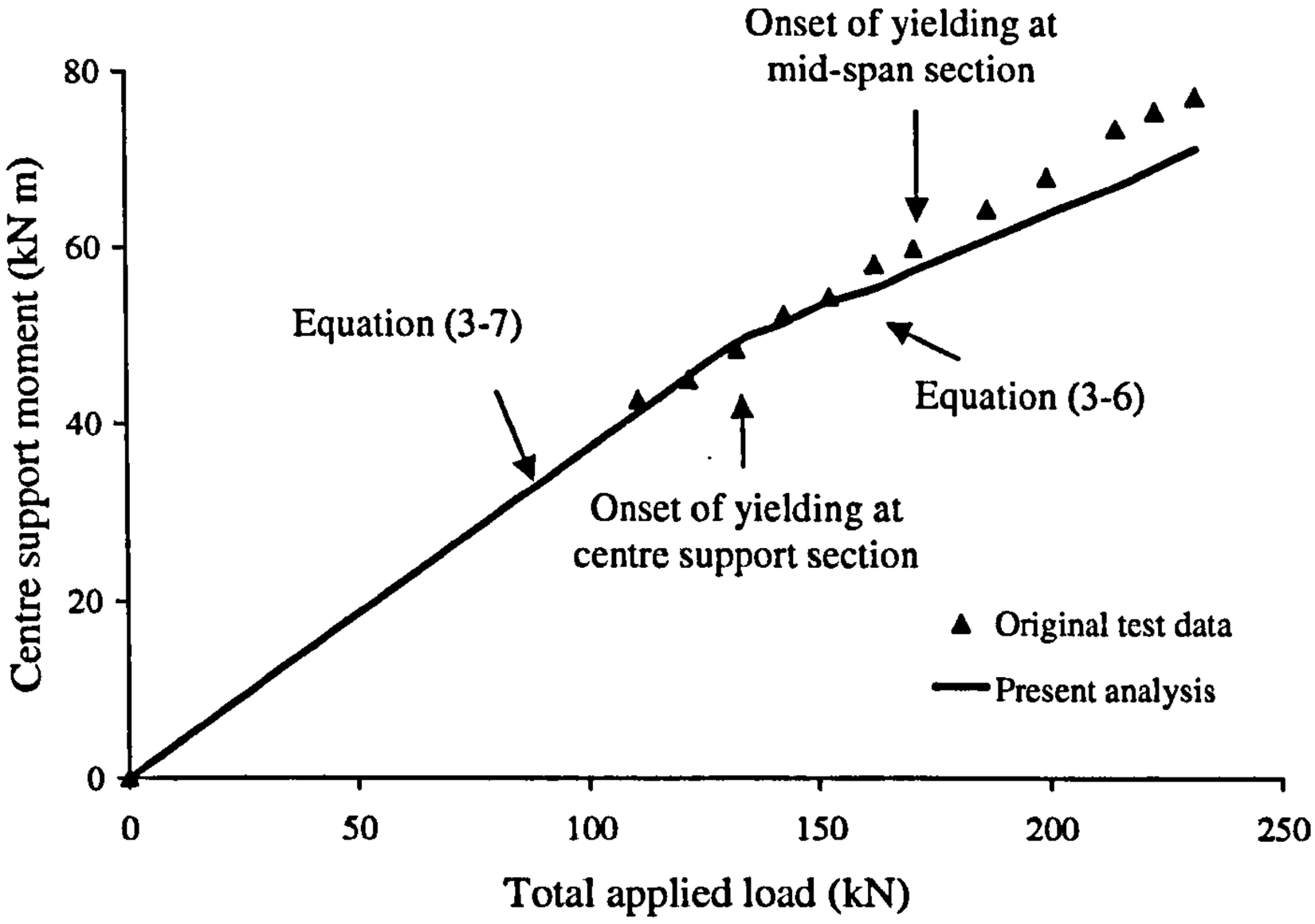

Figure 3-7 - Verification using El-Refaie *et al.* (2003b) test data

The close test-theory comparison (before the onset of yielding at mid-span section) of Figure 3-7 permits some confidence in the analysis. The possible effect of finite support stiffness was found to be insignificant in this particular case. This may be explained by the fact that the relatively low stiffness of the reference concrete beam may well have pushed the ratio of support stiffness to reference beam stiffness out of the sensitive zone, which will be discussed more in later sections.

Mid-span deflections were also evaluated and compared with the test data in Figure 3-8. It can be seen that the present analysis gives bigger prediction of the deflection at low load levels, which is expected as cracked section stiffness has been adopted. Close agreement has then been observed (up to the onset of yielding at mid-span section) between the test data and the results from the present analysis. The bigger disparity afterwards is attributed to the fact that the reduced stiffness at mid-span area caused by yielding of mid-span section was not considered in the current stiffness model. The reduced stiffness at mid-span section will inevitably lead to bigger mid-span deflections.

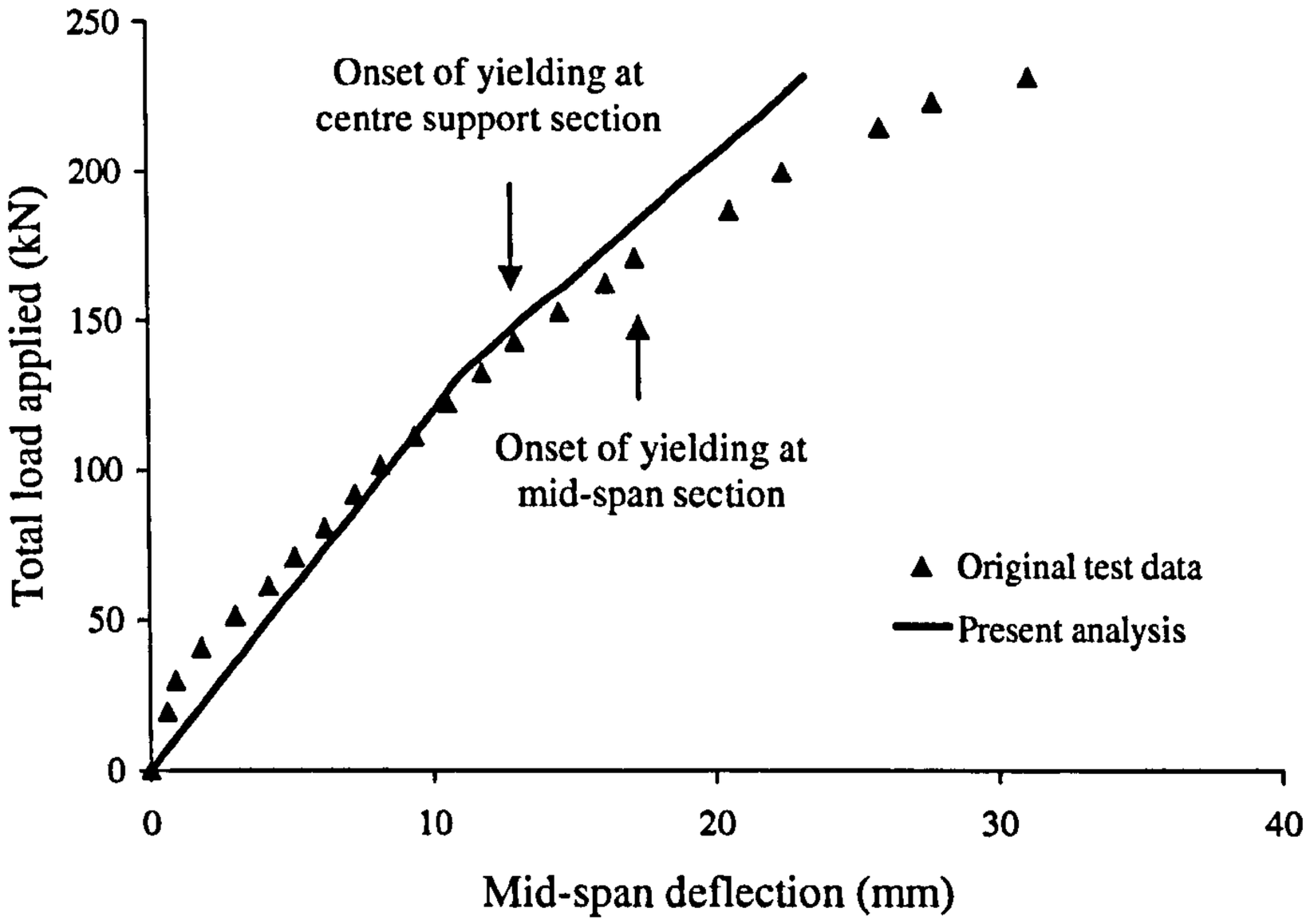

Figure 3-8 - Verification of deflections using El-Refaie *et al.* (2003b) test data

3.3.2 Habeeb and Ashour (2008)

The present analysis is equally applicable to FRP-reinforced concrete members. Habeeb and Ashour (2008) have tested three 2-span continuously supported concrete beams reinforced with GFRP bars. Specimen GcUO is used here as an example, the details of which are given in Figure 3-9 and Table 3-2. The lengths of the longitudinal reinforcing bars are not explicitly given in the paper and are taken here as running all the way along the beam span.

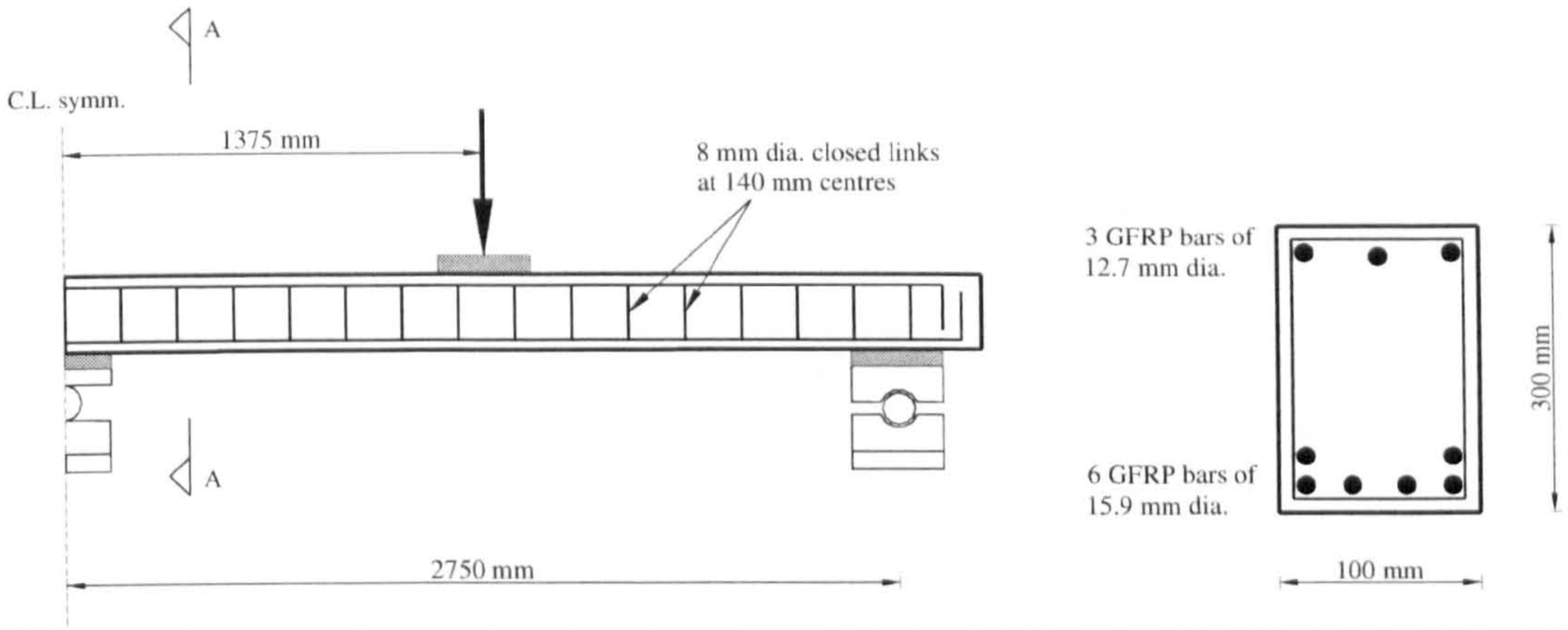

Figure 3-9 - Test details (GoUC in Habeeb and Ashour 2008)

Concrete compressive strength (N/mm^2)		Longitudinal GFRP bars			
		12.7 diameter bars		15.9 diameter bars	
f_c'	f_{cu}	E (kN/mm^2)	Ultimate strain	E (kN/mm^2)	Ultimate strain
29	35	44.2	0.015	38.7	0.018

Table 3-2 - Material properties (Habeeb and Ashour 2008)

The moment-curvature diagram of the GFRP reinforced concrete sections were calculated using the same procedure as set out in the previous section and shown in Figure 3-10. An average (constant) stiffness from best fitting was then used for the evaluation of the deflections as the nonlinearity of the concrete in compression has small effects on the section stiffness. Therefore, in the present analysis, the beam is taken as being of constant stiffness ($\alpha_1 = \alpha_2 = \alpha_3 = 1$) along its entire length up to ultimate load.

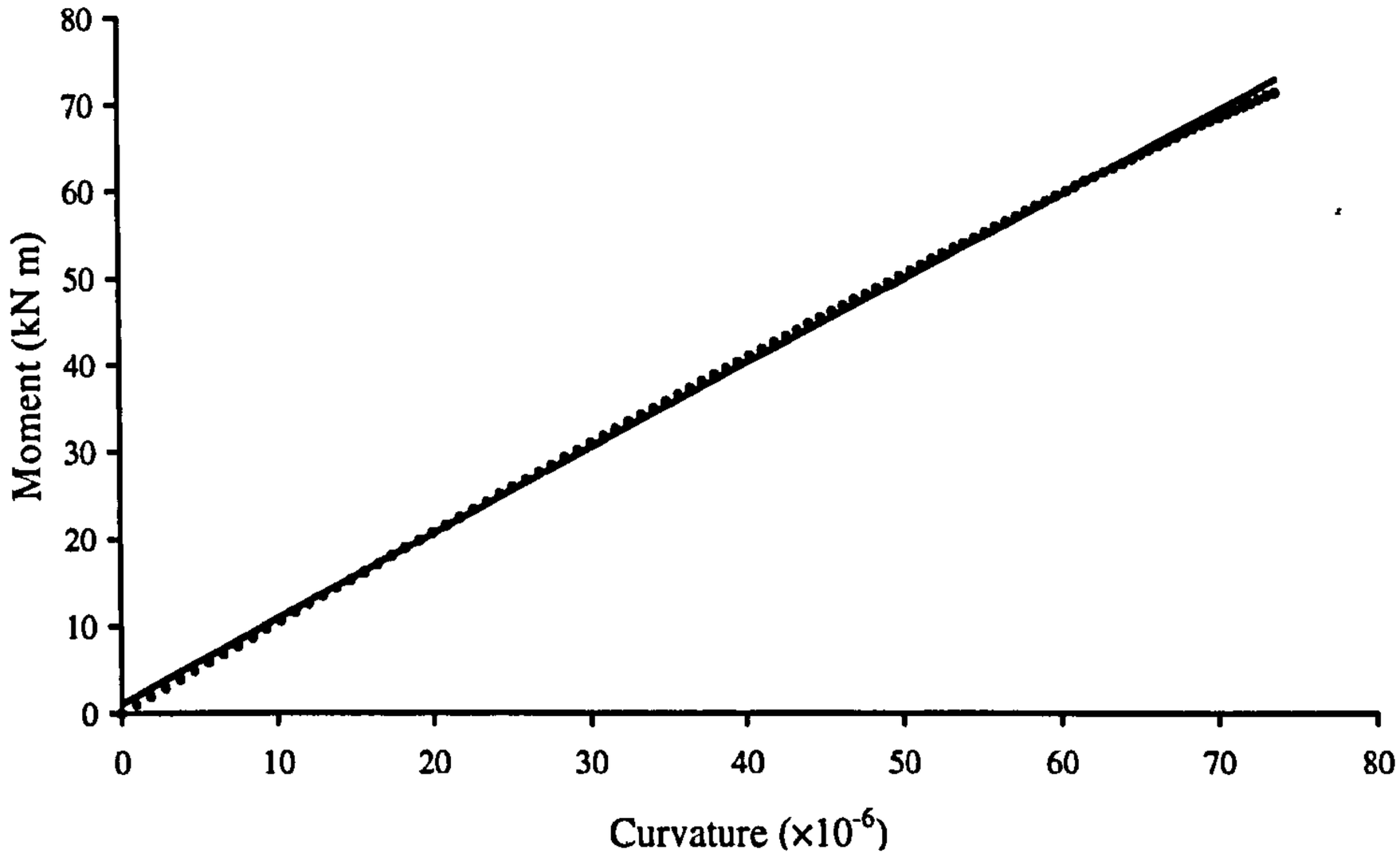

Figure 3-10 - Moment-curvature relations (GoUC in Habeeb and Ashour 2008)

The results are shown in Figure 3-11 together with the test data and the data calculated using ACI equation using mid-span properties and the modified equation by Habeeb and Ashour (2008). Considering that it excluded the uncracked section stiffness at low load levels and used the average stiffness from a best fitting of the moment curvature plots, the present analysis gives good prediction of deflections. The model by Habeeb and Ashour (2008) gives the best results but then, their modification of the ACI equation has been made on calibration of the very test data. As explained in Habeeb and Ashour (2008), the underestimation of deflections at higher loads is believed to be largely due to the increasing over-support crack widths.

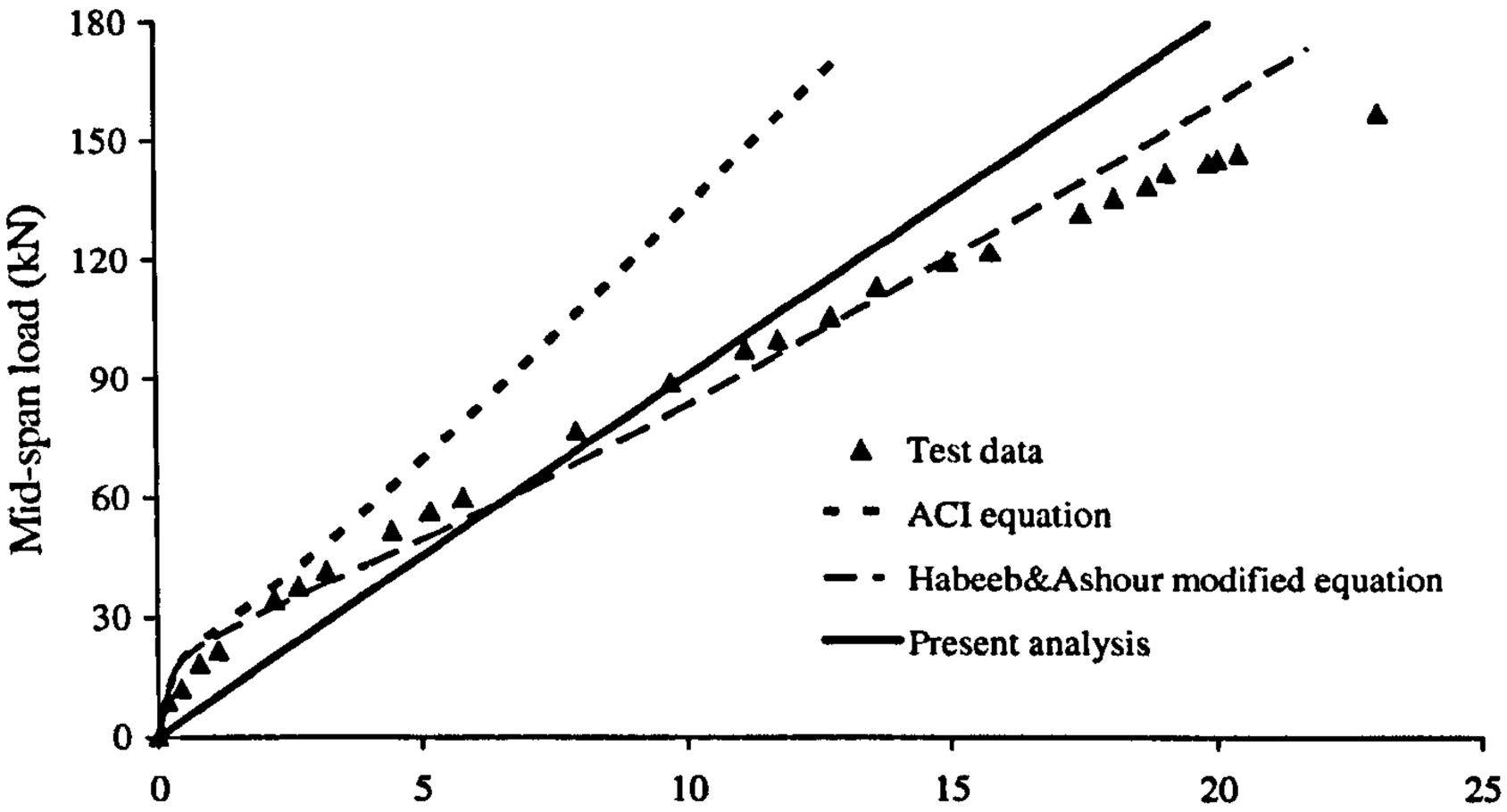

Figure 3-11 - Verification using Habeeb and Ashour (2008) test data

3.4 Parametric study

A parametric study is presented here to investigate the effects of different variables on the moments at the centre support section. The FRP-plated 2-span continuous steel beam tested in the Structures Lab at Bristol (specimen B1 in Chapter 4) is taken as the reference beam. The dimensions and loading details are shown in Figure 3-12. The material properties are given in Table 3-3. Rigid FRP-to-steel bond is assumed in evaluating the bending stiffnesses of the composite sections. The support stiffnesses were evaluated from the deflections of and loads at the supports measured by dial gauges and load cells respectively, the details of which will be given in Chapter 4. The key parameters are shown in Table 3-4. One of the parameters was varied each time with all other values constant unless otherwise stated. The parameters varied in this study include the support-to-member stiffness ratios, the relative section flexural stiffnesses of different segments of the beam, the relative lengths of the different stiffness zones along the span, the linear stiffness variation (defined by α_3 and α_4) and the location of the point load.

Steel		Adhesive		CFRP
f_y	E_s	f_t	E_a	E_p
N/mm^2	kN/mm^2	N/mm^2	kN/mm^2	kN/mm^2
300	196	32	10	135.5

Table 3-3 - Material properties of the reference beam

λ	γ_1	γ_2	γ_3	γ_4	α_1	α_2	α_3	β_1	β_2
0.5	0.095	0.571	0.286	0.048	1.18	1.438	1.21	57.3	56.9

Table 3-4 - Key parameters in the algebraic expression

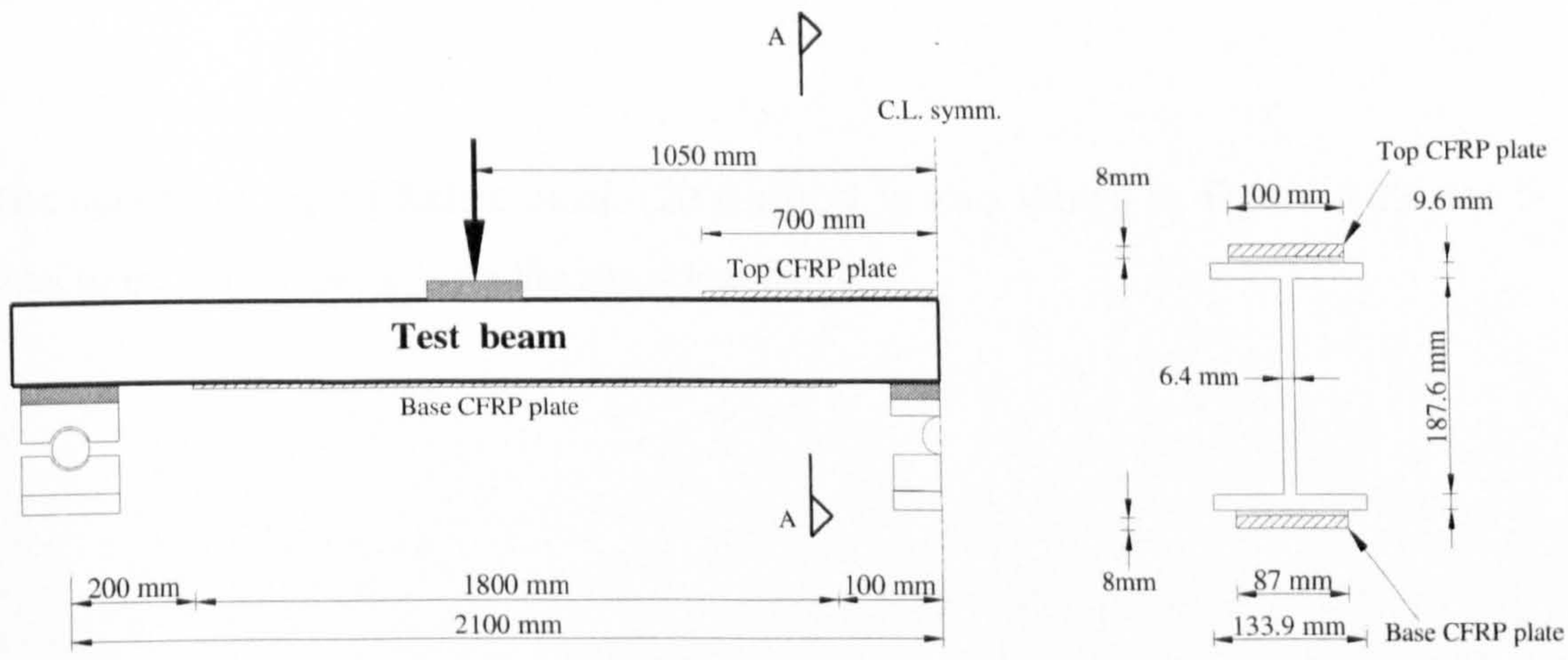

(a) Geometric dimensions (b) Section A-A

Figure 3-12 - Dimensions and loading details of the reference beam

For a typical FRP-plated beam (Figure 3-1), the stiffness of the doubly reinforced section is not independent of those of the sections with only hogging or sagging reinforcement, even though the theoretical analysis could accommodate any stiffness profile along an indeterminate span. Due to limited data available in the literature, an empirical approach is adopted in an attempt to establish a correlation between these stiffnesses for this parametric study.

The FRP-plated steel beam in Figure 3-12 is taken as the reference beam. Assuming the same reinforcement for hogging and sagging (i.e. $\alpha_1 = \alpha_3$ in Figure 3-3) and rigid FRP-to-steel bond, the stiffness parameters α_1 and α_2 are evaluated for the FRP plate thicknesses varying from 4-32 mm with an increment of 2 mm. Curve fitting (Figure 3-13) is then used leading to a quadratic expression relating α_1 and α_2 as follows:

$$\alpha_2 = 1.7\alpha_1^2 - 1.53\alpha_1 + 0.843 \tag{3-9}$$

An extension of this expression is suggested for different hogging and sagging reinforcements as:

$$\alpha_2 = 1.7\alpha_1\alpha_3 - 1.53\frac{(\alpha_1 + \alpha_3)}{2} + 0.843 \tag{3-10}$$

The data from the El-Refaie et *al.* (2003b) test is also shown in Figure 3-13 and is seen to be not far away from the empirical result.

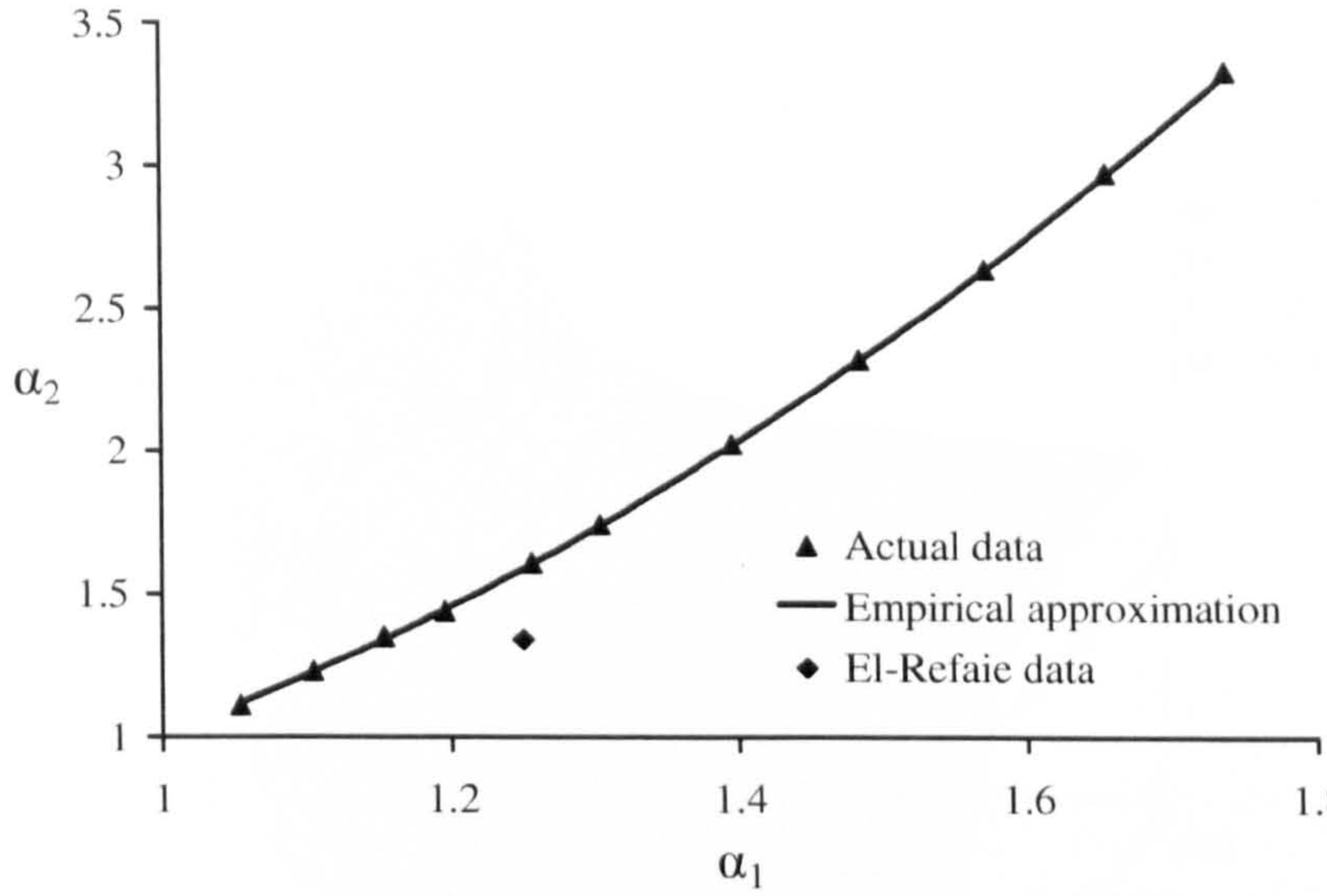

Figure 3-13 - Correlation between stiffnesses of different segments

3.4.1 Effects of support-to-member stiffness ratios

Recall that β_1 and β_2 are the stiffness multipliers for the end and central supports respectively in Equation (3-1). Moment parameters C_p and C_w were evaluated for varying support stiffnesses. The effects of varying support stiffnesses are shown in Figure 3-14. All other properties are as given in Table 3-4.

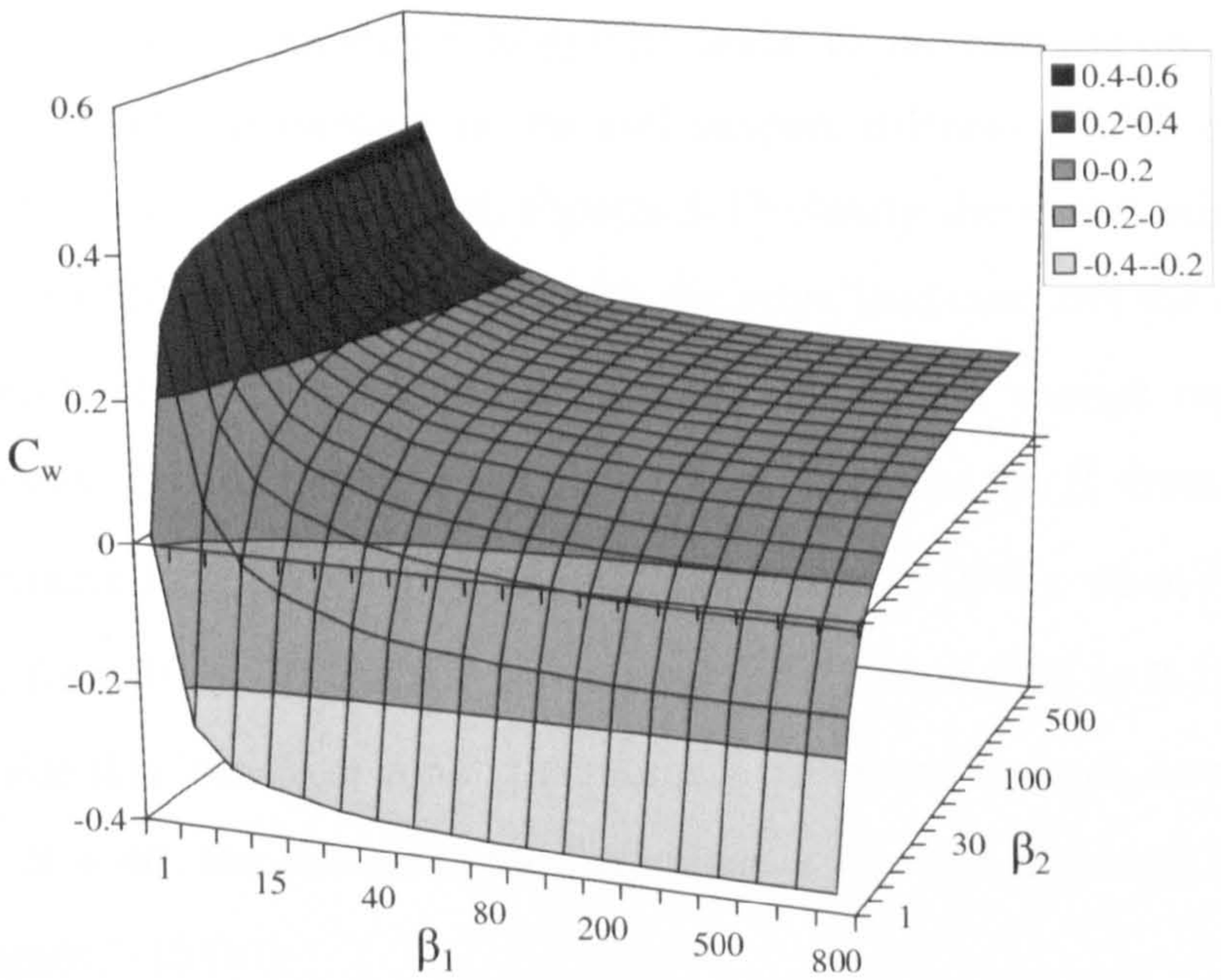

(a) Distributed load

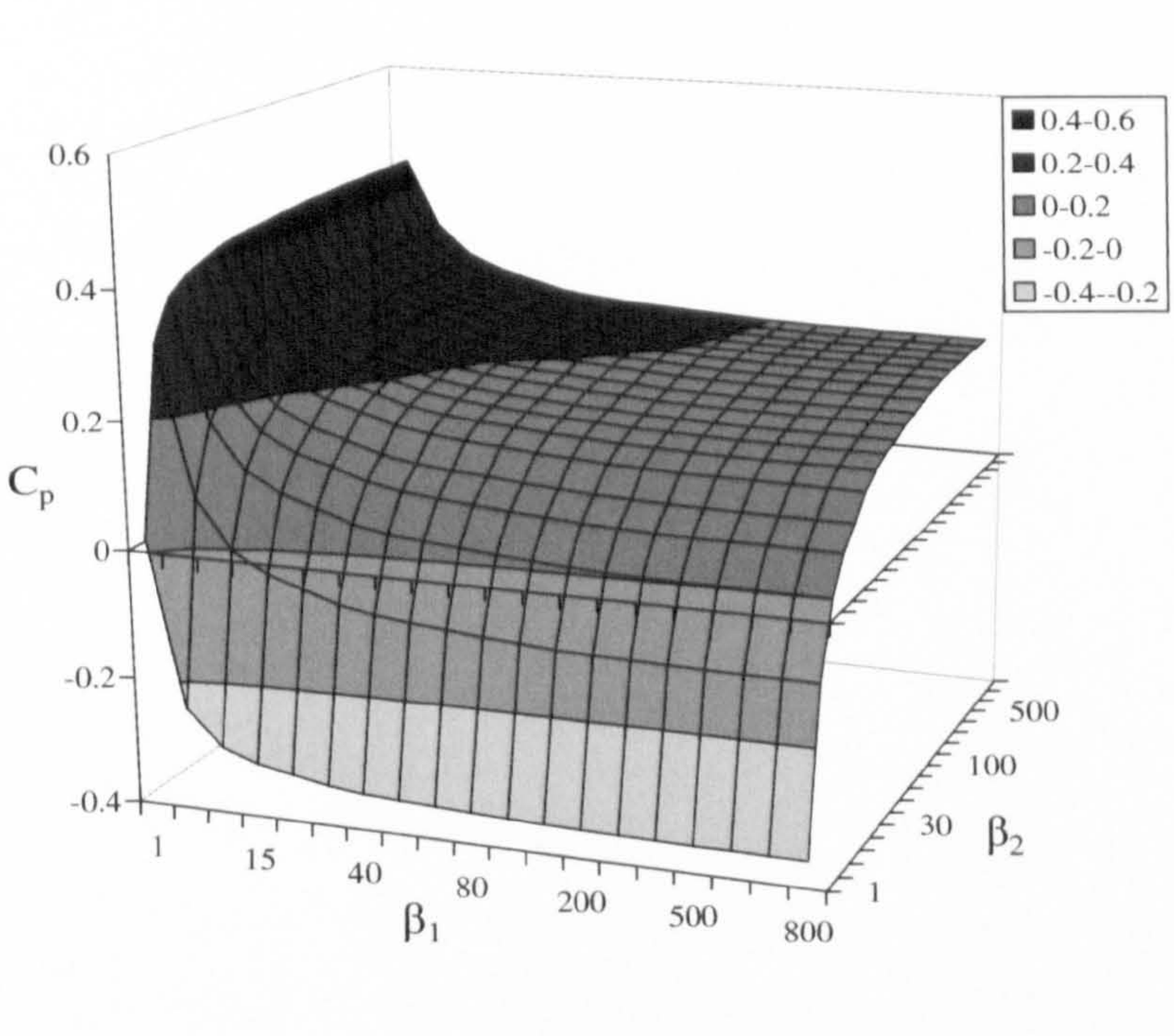

(b) Point load

Figure 3-14 - Effects of support stiffness

As can be seen in Figure 3-14 (a) and (b), in both cases, an increase in the centre support stiffness (which encourages hogging) leads to an increase in the centre support moment, while an increase in the end support stiffness (which encourages sagging) tends to decrease the moment. Figures 3-15 clearly shows the existence of a 'sensitive zone' (0-60) for both β_1 and β_2 with the point load case and the distributed load case respectively, within which the moment parameters change rapidly with support stiffnesses. For example, when $\beta_2 = 40$, an increase in β_1 from 10 to 30 results in a decrease in C_P from 0.24 to 0.17 (a decrease of 29%); when $\beta_1 = 40$, an increase in β_2 from 10 to 30 leads to an increase in C_P from 0.03 to 0.15 (a 5-fold increase). Outside this 'sensitive zone', the moment parameter changes slowly (Figure 3-15 (a)). For $\beta_1 = 40$, the change in the parameter is 7% with a change in β_2 from 100 to 300 (Figure 3-15 (b)).

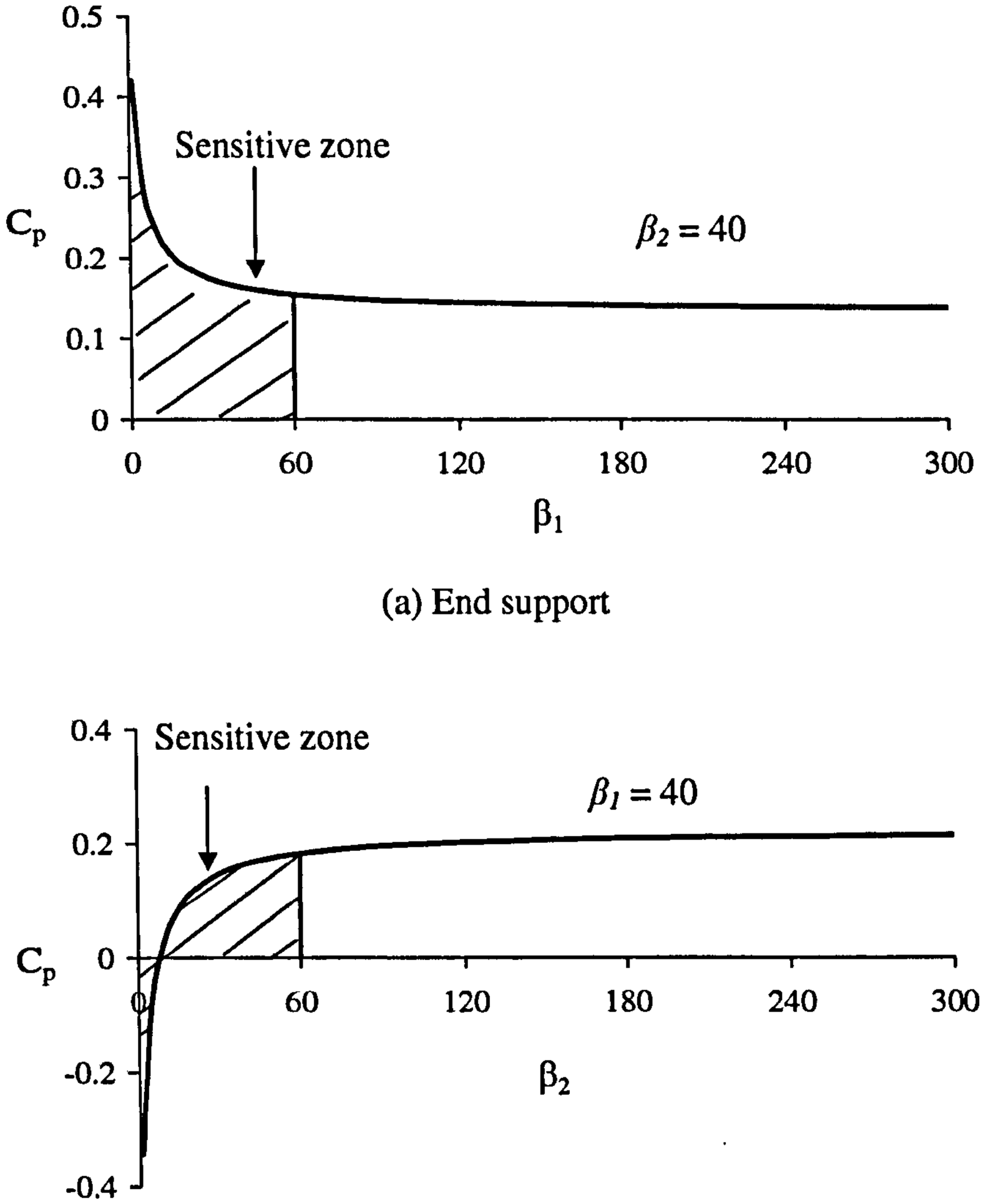

Figure 3-15 - Sensitive zones for support stiffnesses with point load case

The same trend can be seen with the distributed load case (Figure 3-16). This is significantly important for tests in the lab and also for bridges in practice where support stiffness is controlled by vertical straining of the elastomeric bearing pads, by different ground conditions for each support, and by the fact that the forces are different for each support. For the specimens tested by the present authors, the experimental data suggest that the equivalent stiffness of the test beam is within this 'sensitive zone'. This will be discussed more in Chapter 4.

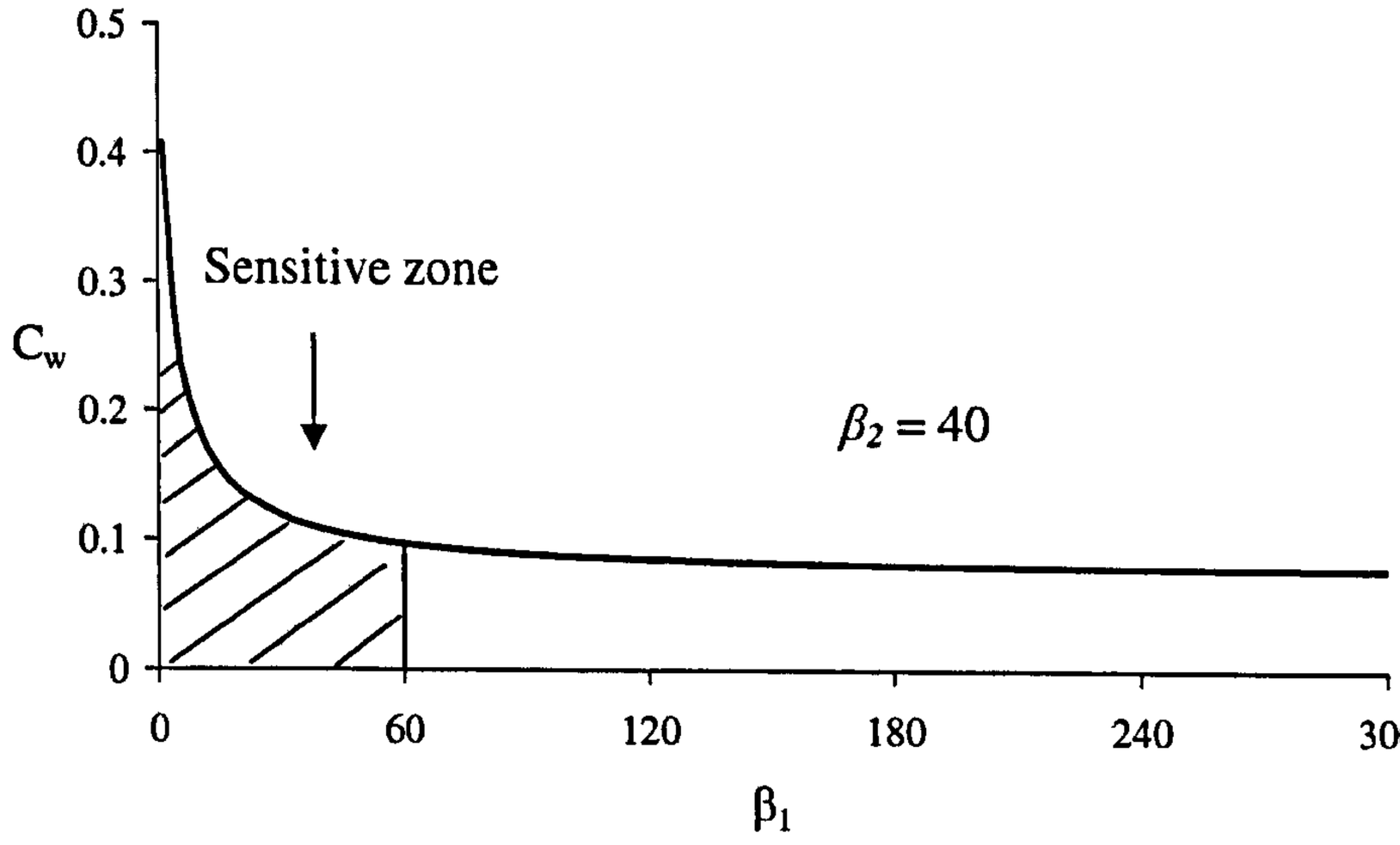

(a) End support

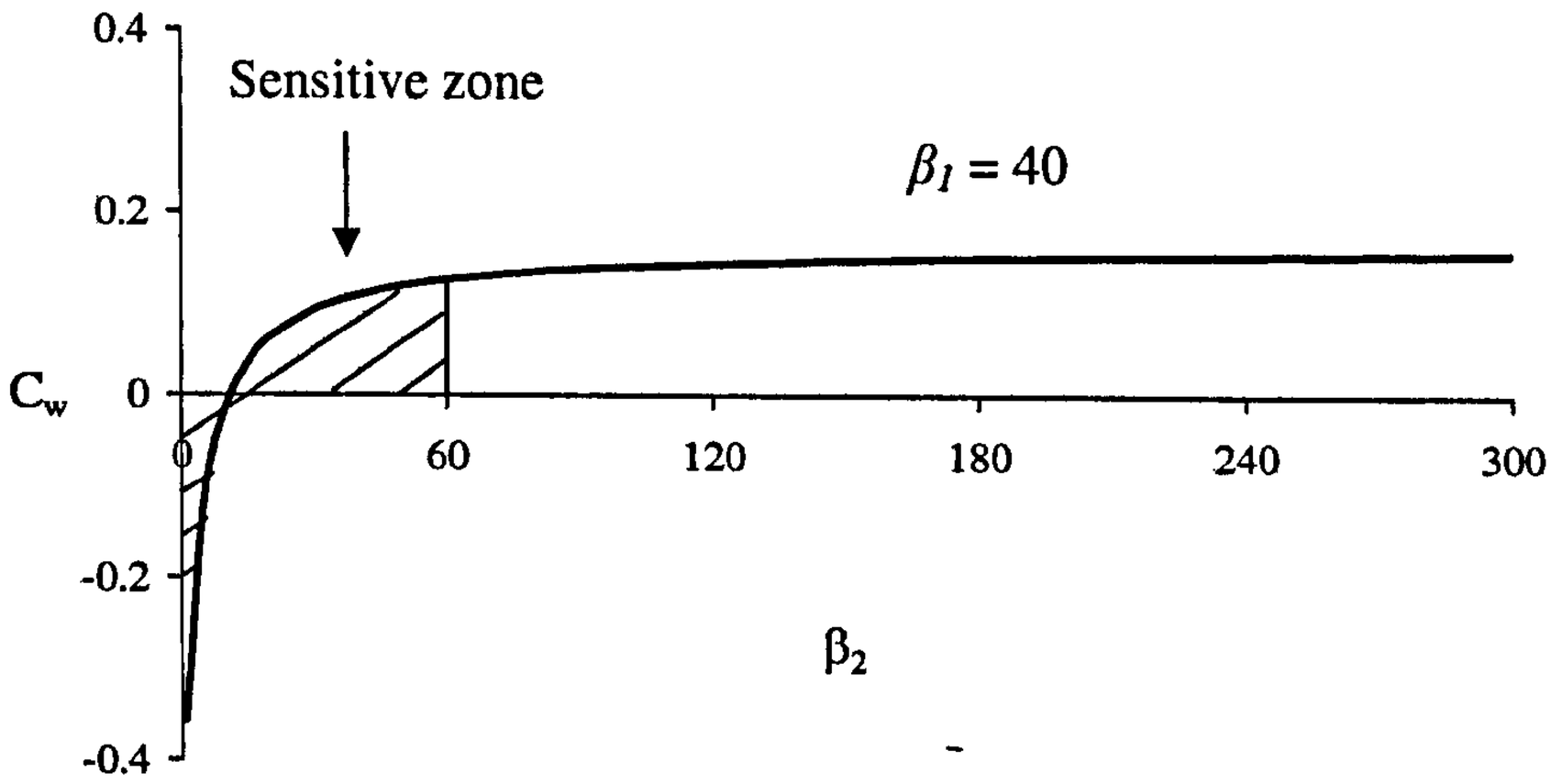

(b) Centre support

Figure 3-16 - Sensitive zones for support stiffnesses with distributed load case

Self equilibrating moments expressed relative to the rigid support moment are evaluated using Equation (3-11) and the results are shown in Figure 3-17.

$$\zeta = \frac{M_{flexible} - M_{rigid}}{M_{rigid}} = \frac{C_{flexible} - C_{rigid}}{C_{rigid}} \qquad (3\text{-}11)$$

where M_{rigid} is the moment at the centre support section with rigid supports and $M_{flexible}$ is the moment at the centre support section with flexible supports. C_{rigid} and $C_{flexible}$ are the corresponding moment parameters, which can be obtained from Equations (3-4) and (3-7) for distributed and point load cases, respectively. The data used to produce the plots in Figure 3-17 are given in Appendix 3B.

The self-equilibrating moment can be very significant in some cases noting that for $\zeta = 1$, the self-equilibrating moment is as high as the moment evaluated with rigid supports. As noted in Section 3.2.1, however, the moment parameters should be limited to be positive in practice to avoid any uplift of the beam at the support. There is a line on which the self-equilibrating moment is zero, which means that for certain support stiffness combinations, the moment at the centre support section is constant when the load is applied at this particular point (λ = 0.5 in this particular case). This will be discussed more in later sections.

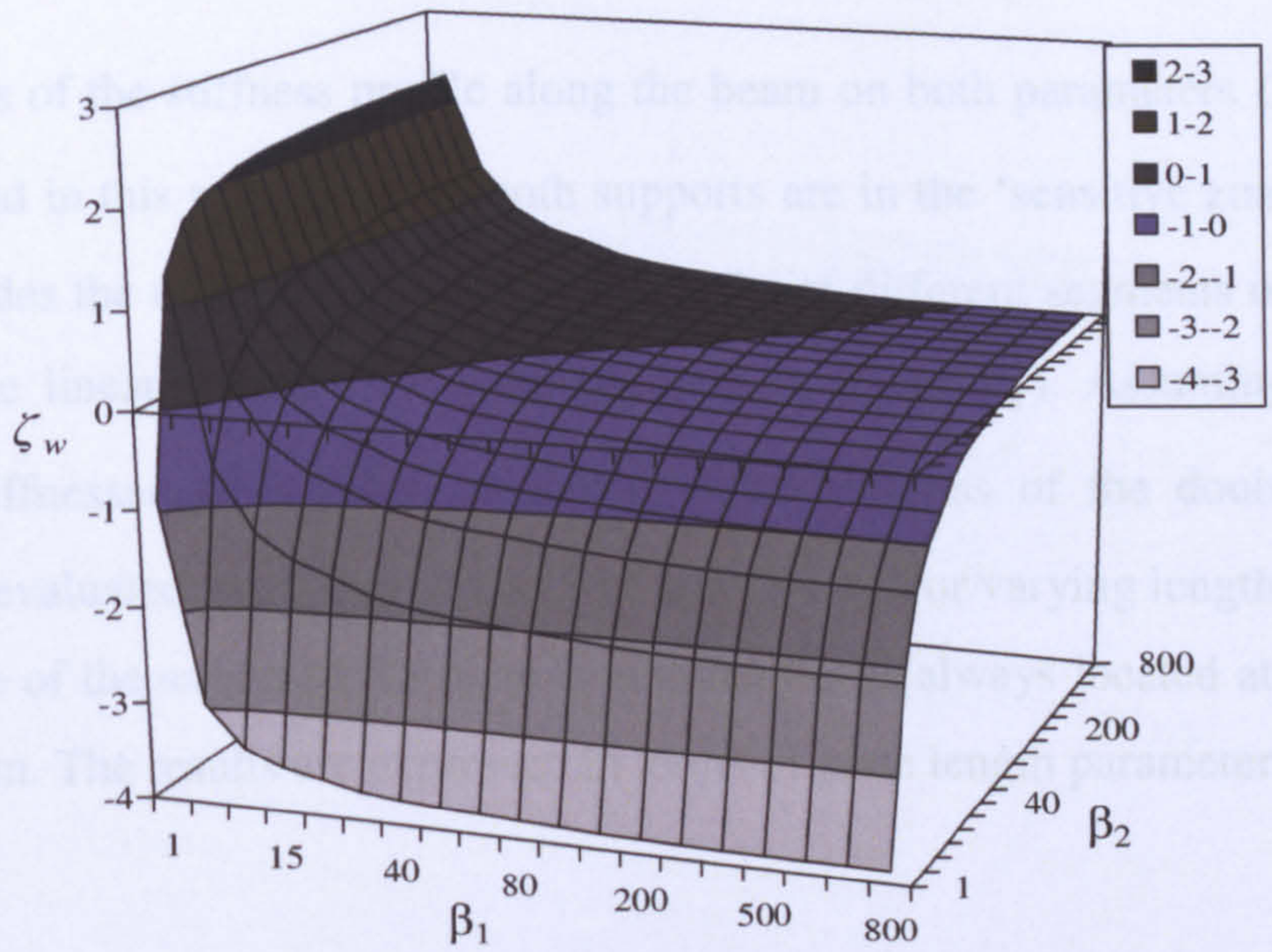

(a) Distributed load

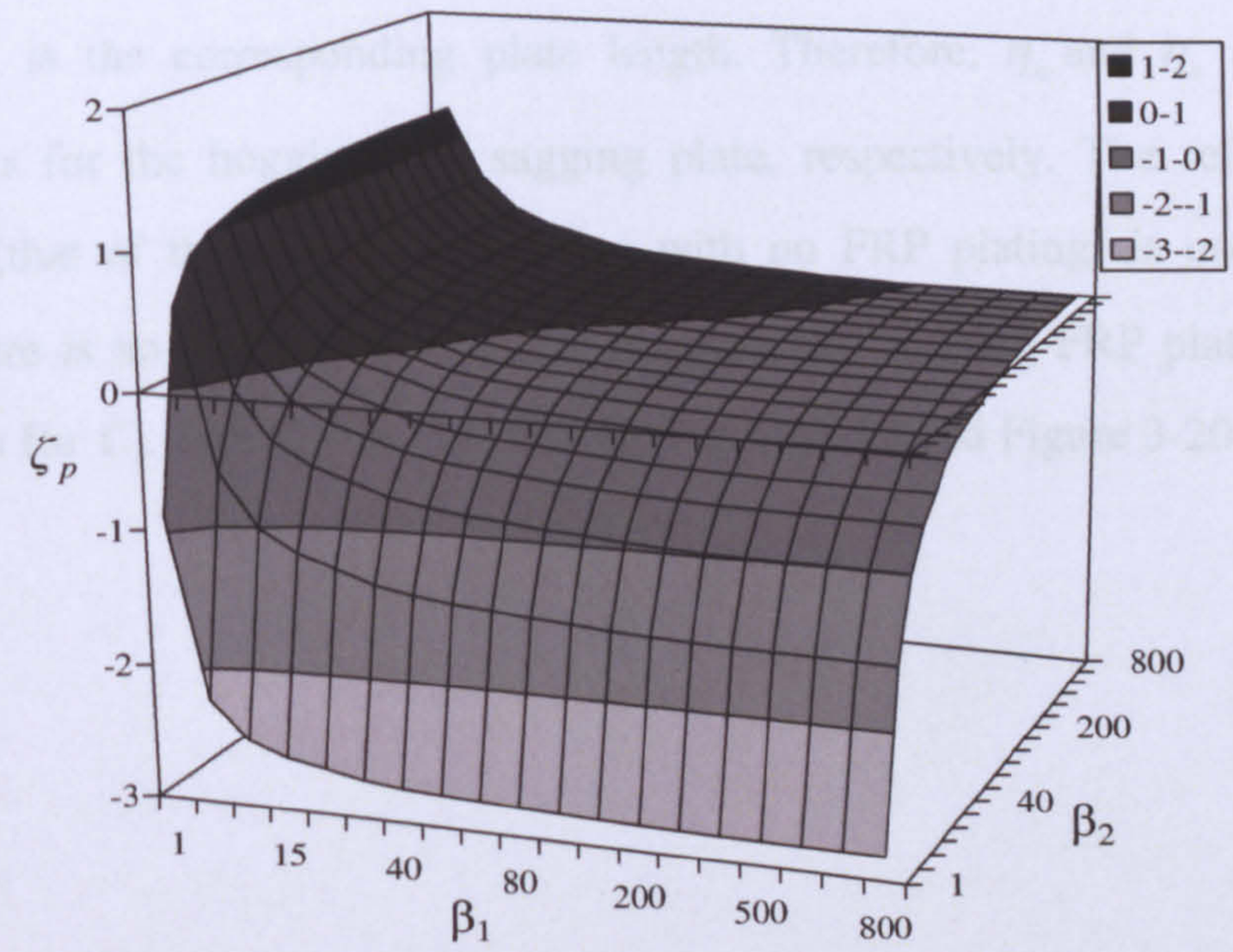

(b) Point load

Figure 3-17 - Self-equilibrating moments

3.4.2 Effects of the stiffness profile along the beam

The effects of the stiffness profile along the beam on both parameters C_w and C_P are investigated in this section where both supports are in the 'sensitive zone' ($\beta_1 = 40$). This includes the relative stiffnesses and lengths of different segments of the beam as well as the linear stiffness variation (defined by α_3 and α_4). Assuming supports of similar stiffnesses, β_2 is taken as half β_1. The stiffness of the doubly reinforced section is evaluated using Equations (3-9) and (3-10). For varying lengths of the plate, the middle of the sagging FRP plate is assumed to be always located at the mid span of the beam. The results are expressed in terms of plate length parameters defined as:

$$\eta = \frac{L_p}{L} \qquad (3\text{-}12),$$

where L_p is the corresponding plate length. Therefore, η_h and η_s are the length parameters for the hogging and sagging plate, respectively. The reference section stiffness (that of the steel section alone with no FRP plating) is used (i.e. $\alpha_2 = 1$) where there is no overlap between the hogging and sagging FRP plates. The results are shown for C_P and C_w in Figure 3-18, Figure 3-19 and Figure 3-20.

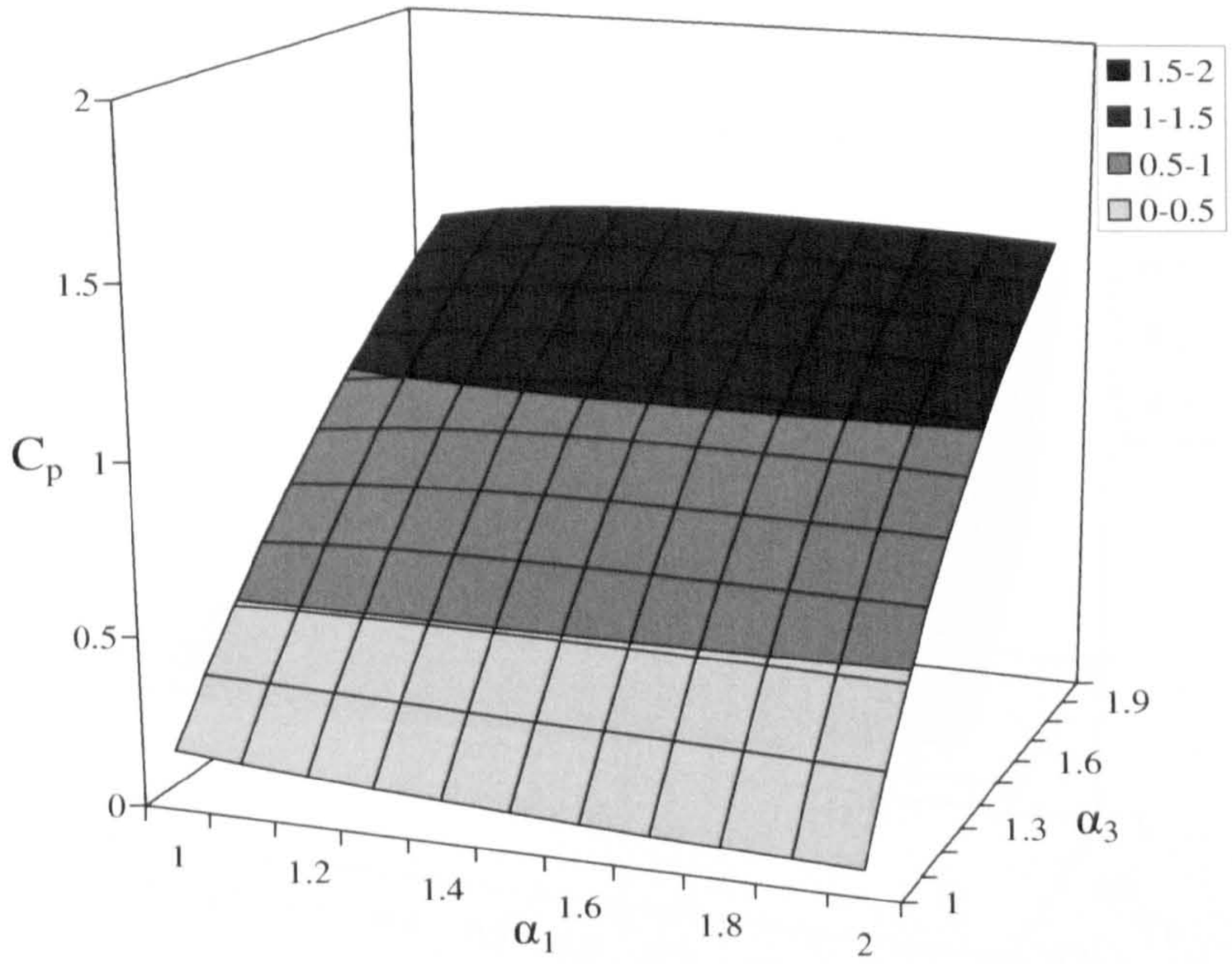

(a) Point load

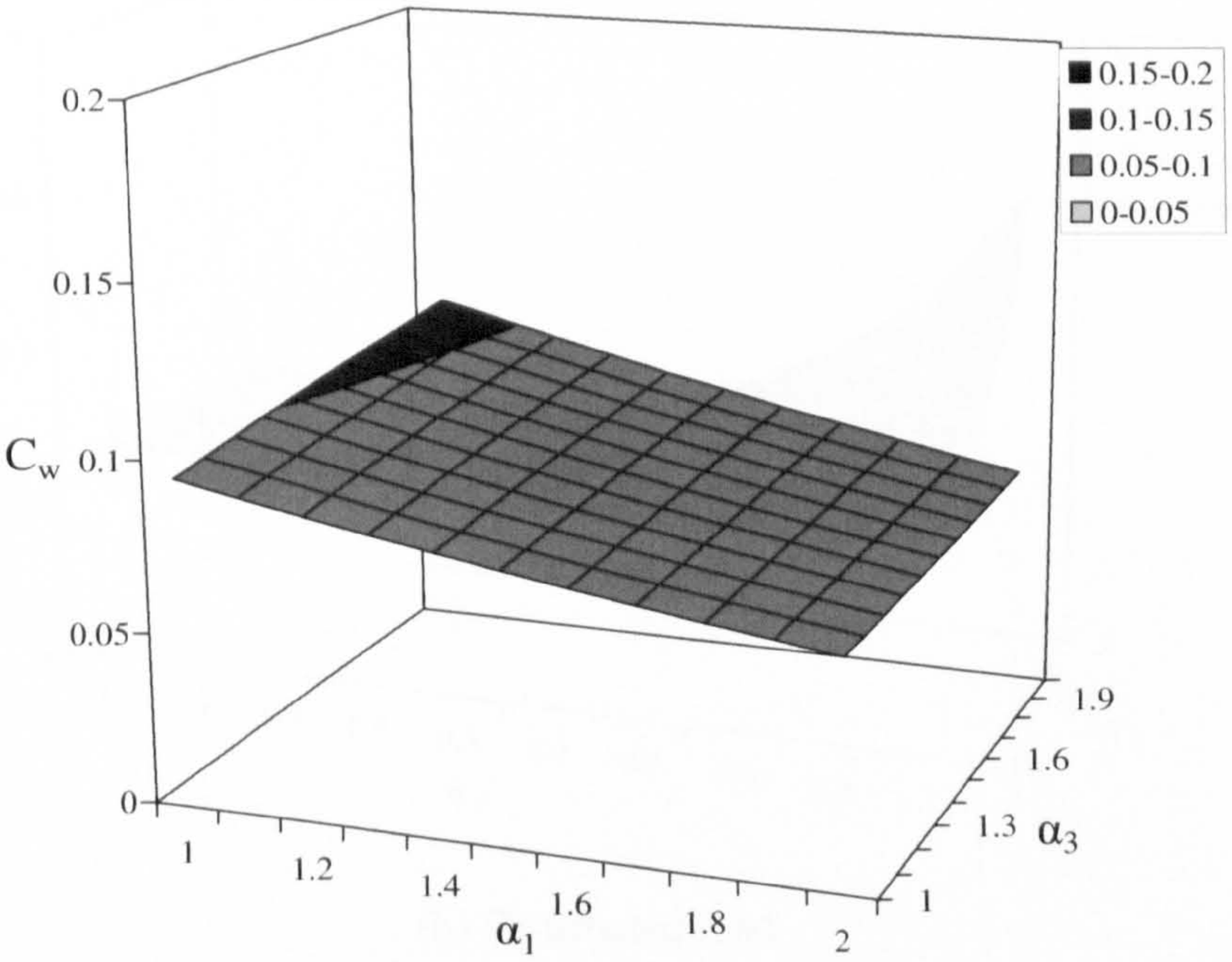

(b) Distributed load

Figure 3-18 - Effects of segment stiffnesses

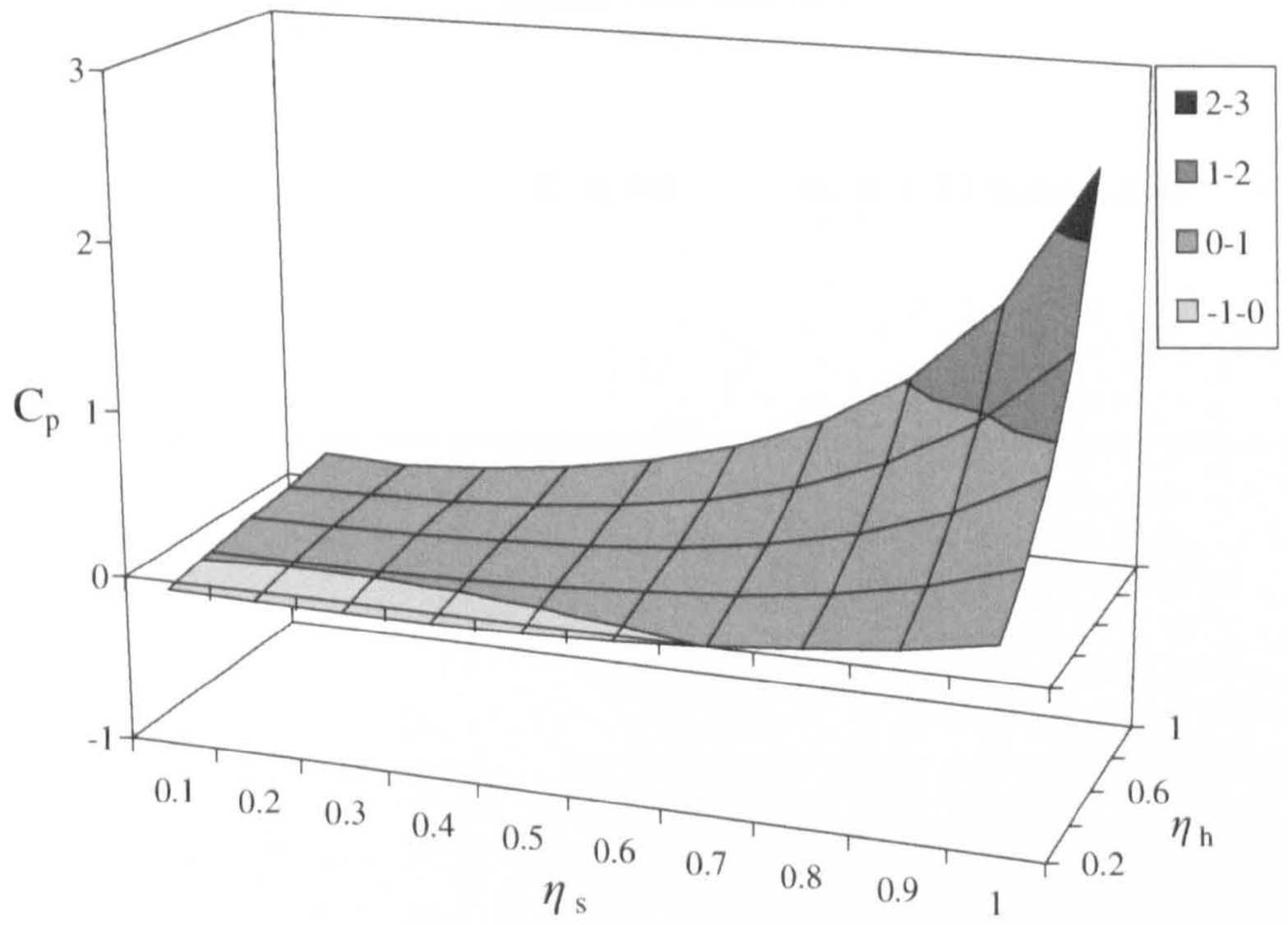

(a) Point load

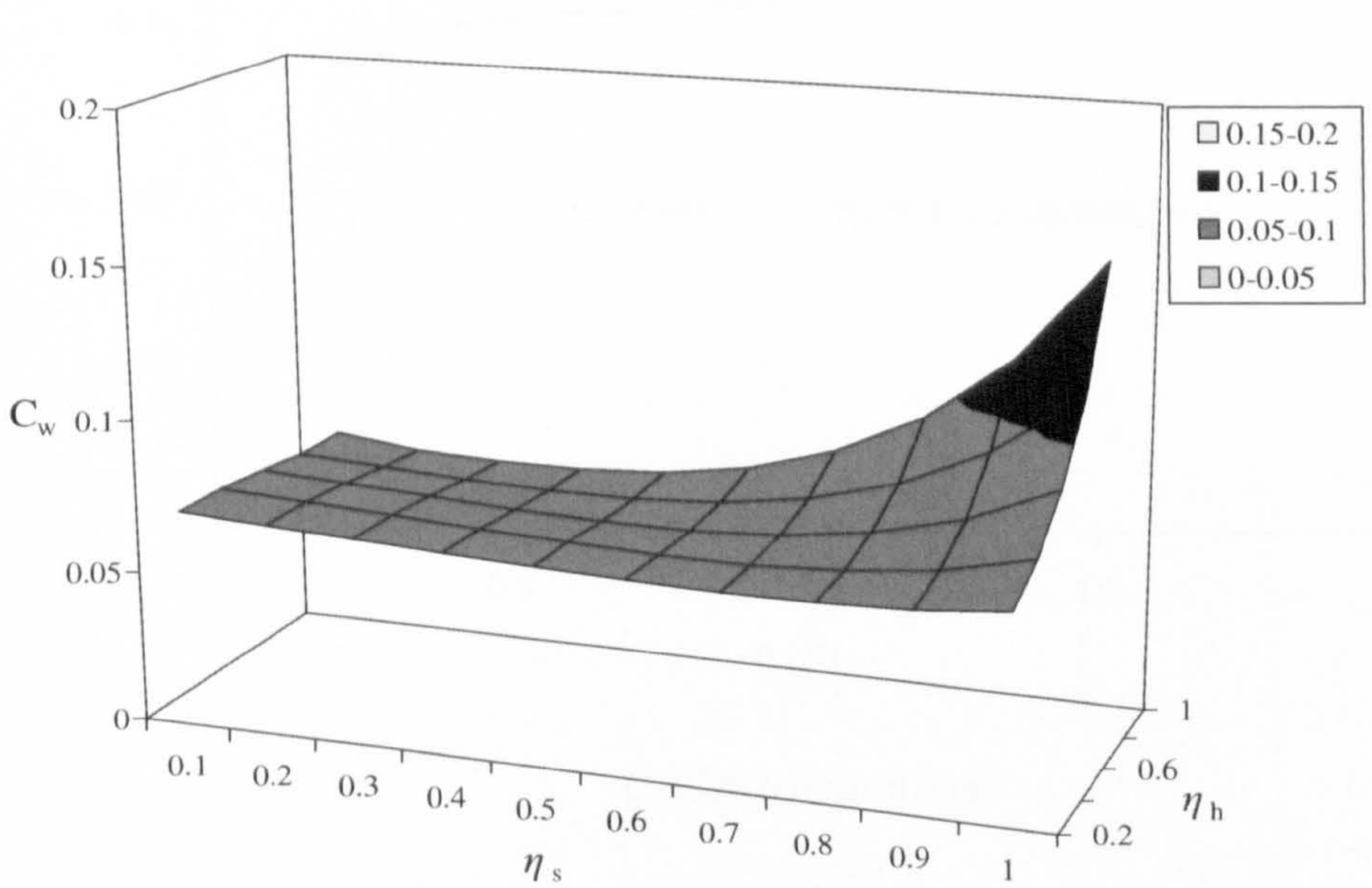

(b) Distributed load

Figure 3-19 - Effects of segment lengths

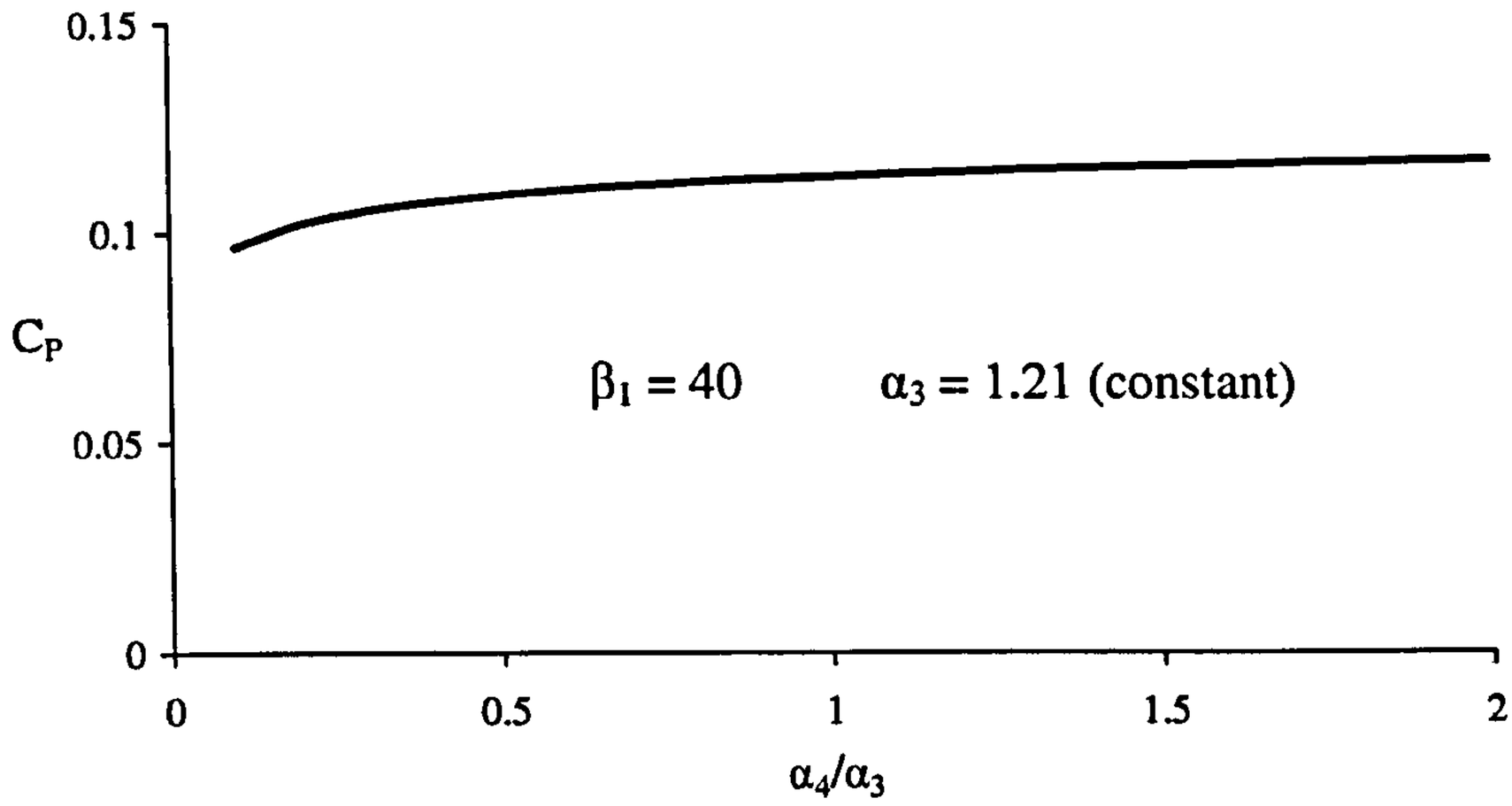

(a) Point load

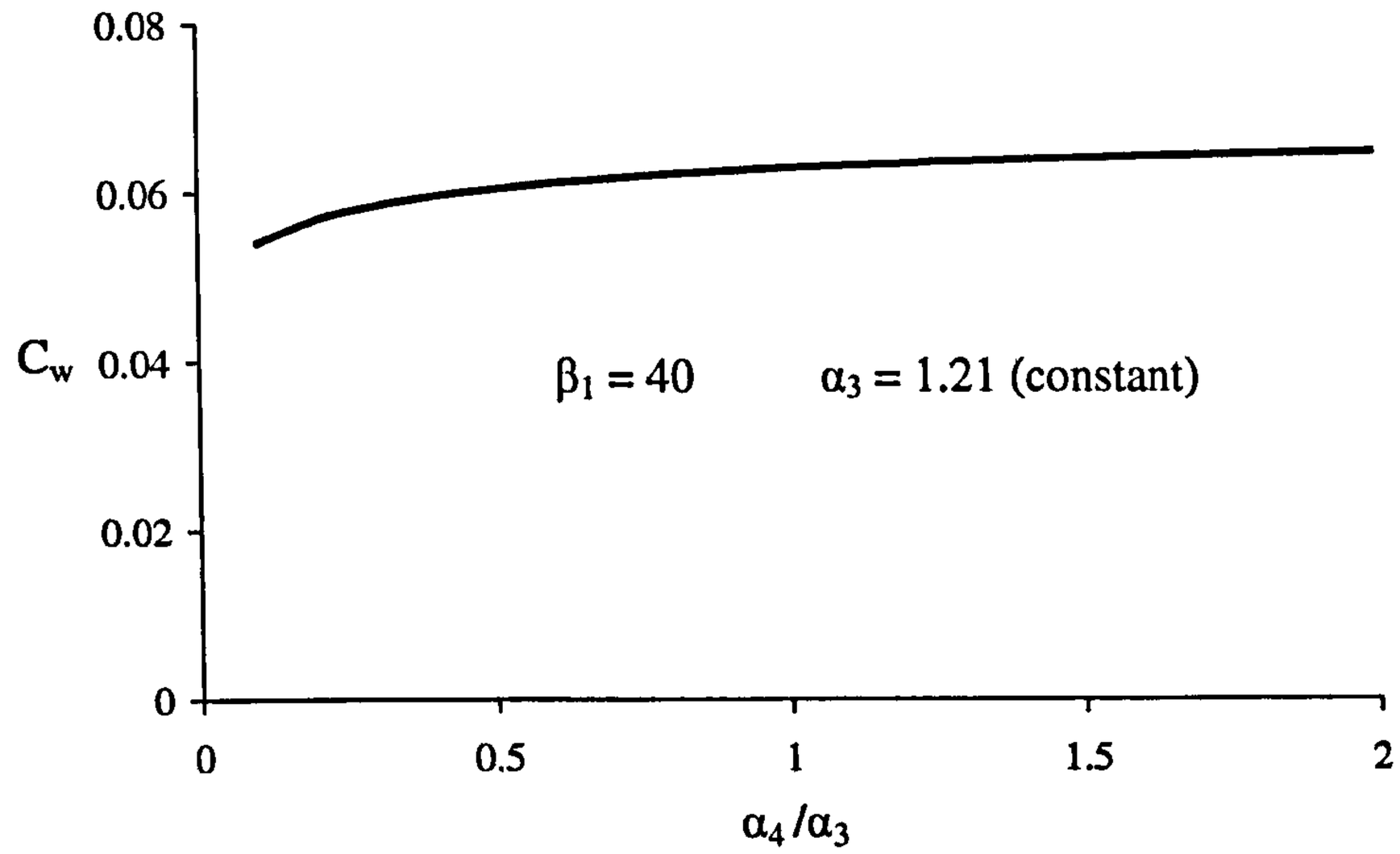

(b) Distributed load

Figure 3-20 - Linear stiffness variation in Z4

The moment parameter C_P decreases slowly when α_1 increases, and increases rapidly with an increase in α_3, as can be seen from Figure 3-18 (a). For distributed load, the

change is more gradual in both cases as can be seen in Figure 3-18 (b). Figure 3-19 shows that there are slight increases in both C_p and C_w with an increase of γ_2, while an increase in γ_4 leads to more rapid increases. This indicates that the length and stiffness of the hogging FRP plate have more significant influence on the moment distribution along the beam than those of the sagging FRP plates for the point load case. When under distributed load, the length of the hogging plate is the more important factor while the stiffness has much less influence than compared with point load case. It can also be seen from Figure 3-20 that both the moment parameters C_p and C_w decrease gradually with a decrease in α_4. This is expected as the centre support section takes on less proportion of the moment after yielding occurs.

3.4.3 Effect of the position of the point load

The effects of the position of the point load on the moment parameter C_p are investigated in this section for the following four support stiffness cases: rigid support ($\beta_1 = \infty$), both supports outside of the 'sensitive zone' ($\beta_1 = 400$), one support in the 'sensitive zone' ($\beta_1 = 80$), then both supports in the 'sensitive zone' ($\beta_1 = 40$). β_2 is taken as half β_1 in all analyses. All the remaining parameters are kept constant as set out in Table 3-4. The results are shown in Figure 3-21 (a).

It is interesting to see that a point exists where the moment at the centre support section is constant regardless of the actual support stiffnesses. A further check reveals that $R_2 = \frac{1}{2} R_1$ at this point. Recall that β_2 is taken as half β_1 for this study. The point is where the support settlement is the same for both supports, i.e. no differential settlement, and therefore the self-equilibrating moment is zero. This is a rather general scenario. For a beam with given support siffness ratio ($\beta_2 / \beta_1 = \mu =$ constant) (Figure 3-21 (b)), there always exists such a point and the location of this point is dependent on the stiffness profile along the beam and the stiffness ratio μ. On one side of this point closer to the centre support, the self-equilibrating moment increases the moment at centre support section; on the other side of the point, it reduces the moment at centre support section. The self-equilibrating moment increases with a decrease in the support stiffness, as illustrated in Section 3.1.

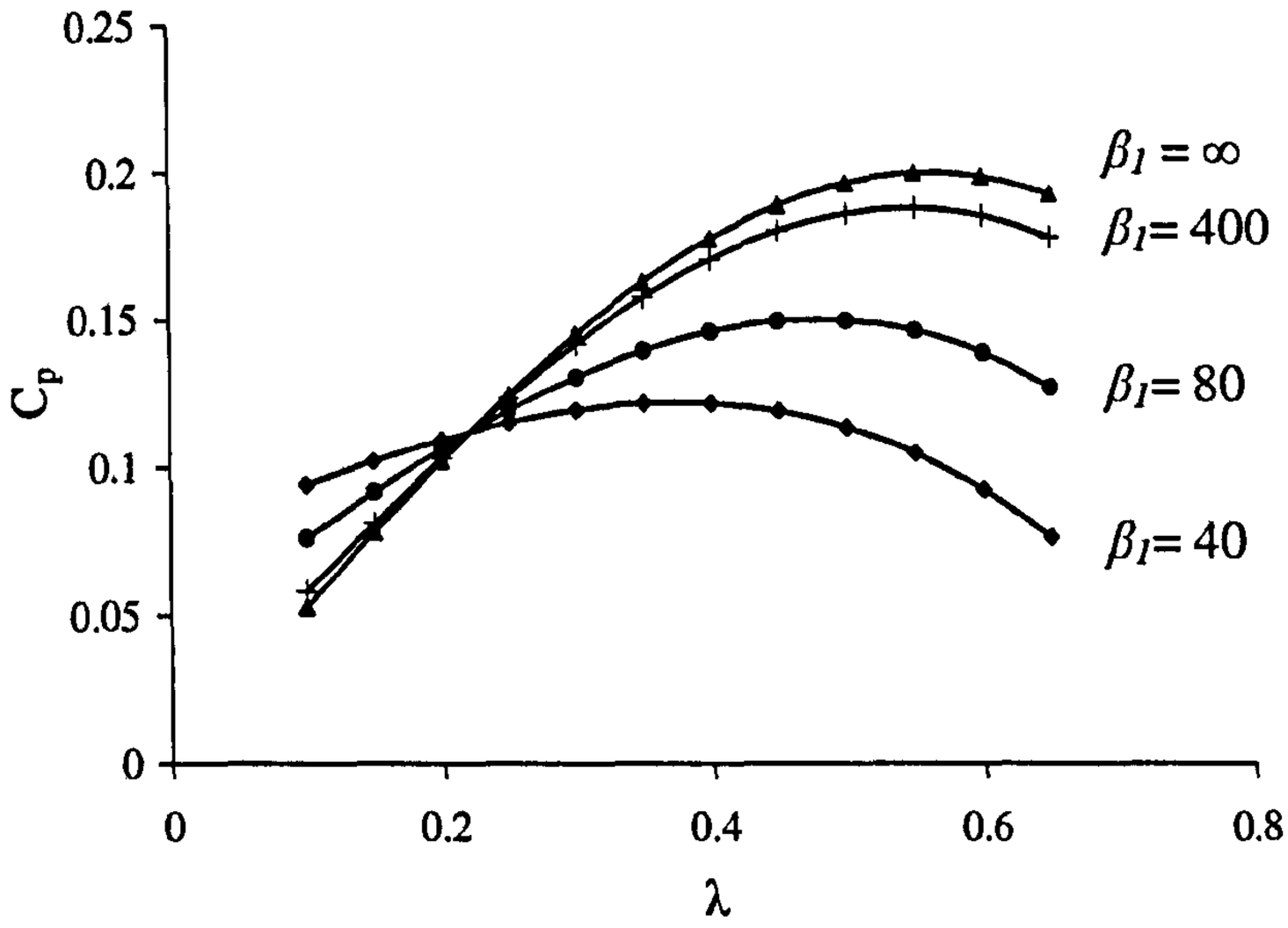

(a) Effects of the position of the point load

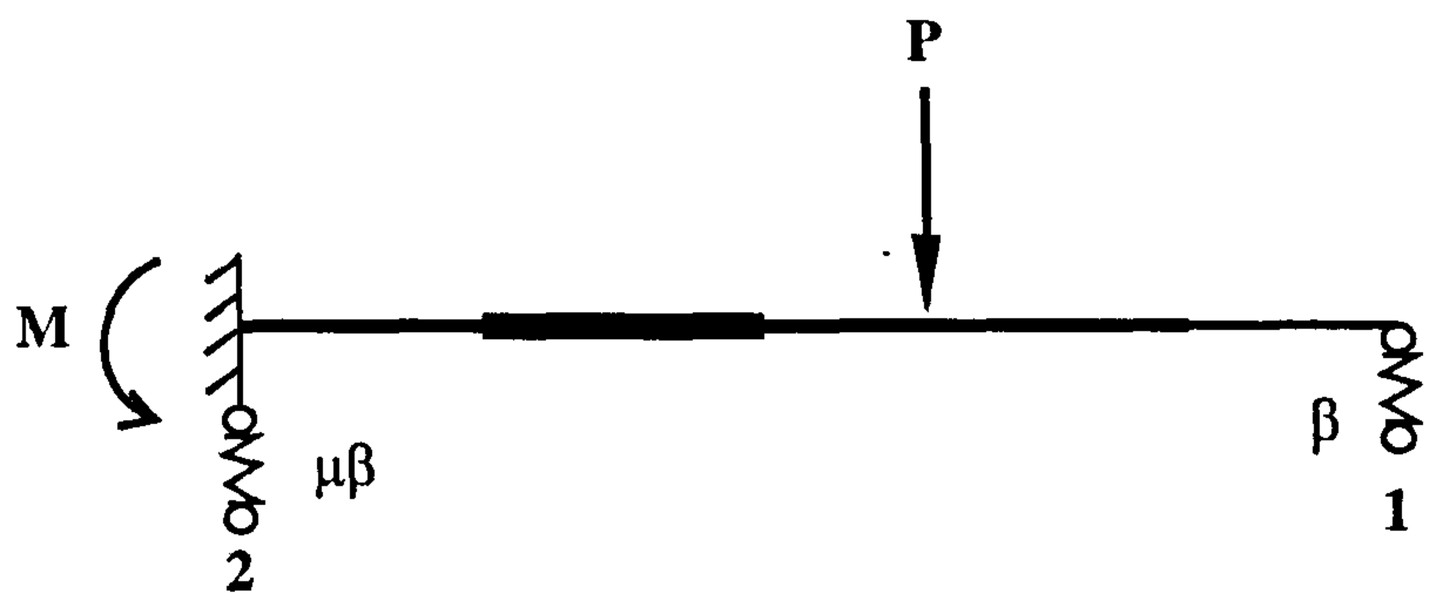

(b) Generalised beam

Figure 3-21 - Effects of the position of the point load

3.5 Estimation of support stiffnesses

In the previous section, the existence of 'sensitive zone' has been identified for support stiffnesses that may give rise to significant self-equilibrating moments. Support stiffnesses could be determined by measuring the support settlements and corresponding support reactions. This may either need special design of equipment in a lab environment, as is the case for test set-up in Chapter 4, or not be possible at all for bridges in practice. In this section, a simple method based on deflections of the structure is proposed to estimate the support stiffnesses.

Deflections (AA'') at any point A (Figure 3-22) along the span of a structure comprise two parts: (a) deflections due to the support settlements (AA'); and (b) deflections due to load action (A'A''). The support settlements (δ_1, δ_2) can be determined if deflections due to support settlements are known for at least two points (A and B in Figure 3-22) along the span. The total deflections (AA'') can be easily measured, so if the deflections due to load action are known (A'A''), deflections due to support settlements (AA') can be obtained. As the deflections due to load action (A'A'') also depend on the support settlements, an iterative process may have to be used:

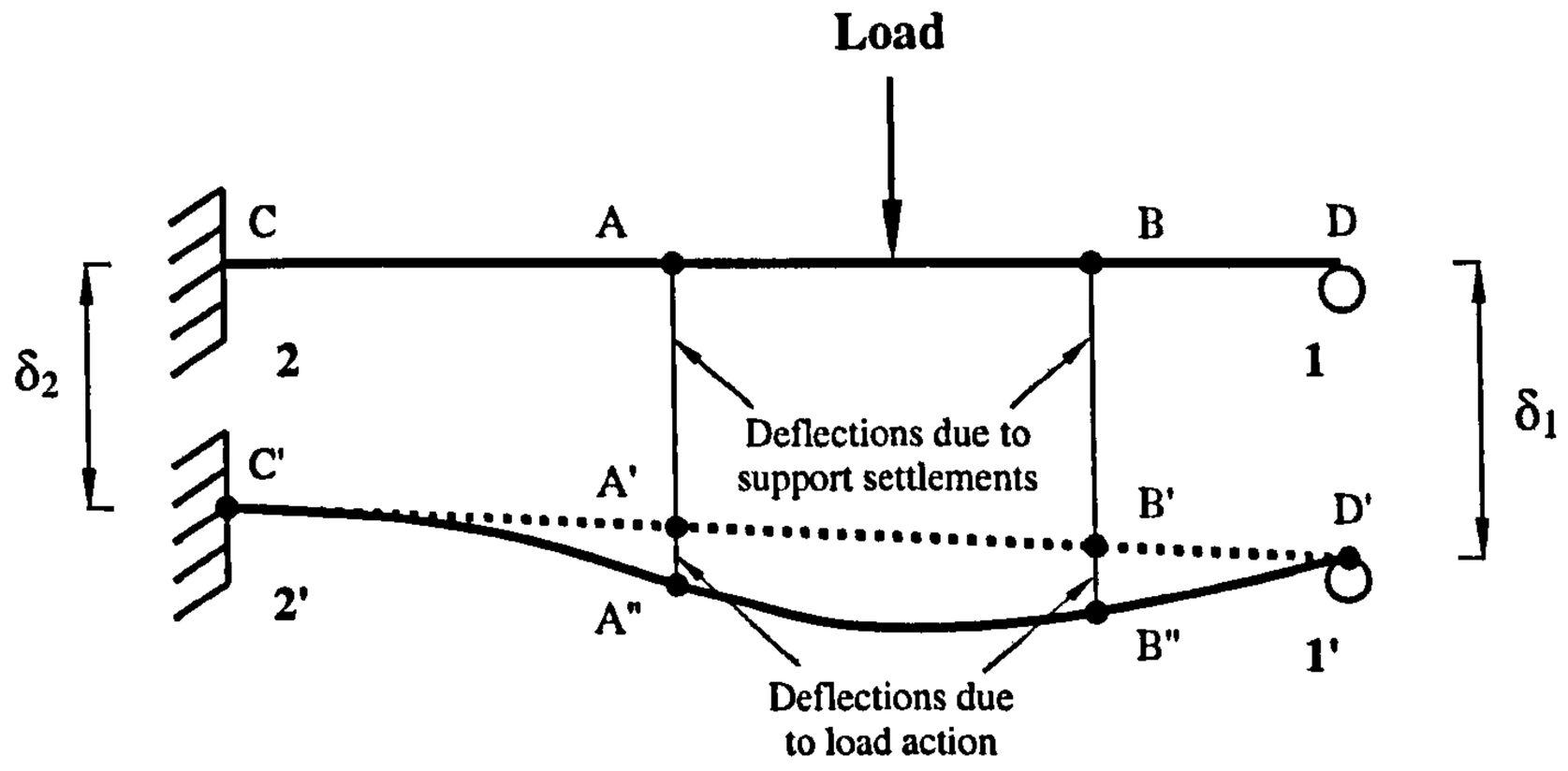

Figure 3-22 - Deflections of a structure

- Initially, analyses are carried out assuming rigid supports to give the deflections at points A and B due to load action; support reactions are also obtained;
- By subtracting the deflections due to load action from the measured (which is also total) deflections, the deflections due to support settlements are obtained for points A and B. The support settlements (δ_1, δ_2) can be then determined through interpolation.
- From the support settlements and the support reactions, support stiffnesses can be determined. Unless the support stiffnesses give deflections that are consistent with the measured deflections, this updated support stiffnesses should be modified by repeating the analysis.
- The process continues until convergence is attained.

The proposed approach is based on the assumption of linear beam stiffness variation so that the difference in calculated and measured deflections is solely attributed to the support settlements. It is worth noting that any departure from the approximated linear stiffness variation along the spans of the beam will also lead to changes in both the calculated and measured deflections. These effects are not accommodated in the proposed approach.

This approach will be used to estimate the support stiffnesses of 2-span continuous beams in Chapter 4 and verified with support stiffnesses obtained from measuring the support settlements and corresponding support reactions.

3.6 Conclusions and further applications

Closed-form nonlinear algebraic expressions have been presented for prediction of total (including self-equilibrating) moments due to differential settlement between supports of 2-span continuous structures for both distributed and point load cases. Based on the work principle, deflections were also obtained. The analysis has been verified via limited test data and then used to construct 3D plots showing how the moments depend on the support-to-member stiffness *ratios* and on the distribution of stiffness along the member. A quadratic expression from curve fitting was used to relate the stiffnesses of the doubly reinforced sections to those of the singly reinforced

sections. A simple method based on deflections was proposed to estimate the support stiffnesses. The following conclusions can be drawn from the results:

- A 'sensitive zone' ($\beta = 0-60$) exists for support stiffnesses where particular care should be taken for test set-up in the lab and also for bridges in practice.
- For beams subject to point load, both the length and the stiffness of the segment nearest the centre support have a significant effect on the moment distribution along the span.
- End peel and mid-span debonding can be accommodated in the analysis by changing the relevant lengths of segments and by changing the stiffness parameters in relevant segments, respectively.
- Linear variation along the segment nearest to the centre support (Z4) was assumed for the ULS analysis. Change in section stiffness at the centre support leads to a gradual change in the centre support moment.
- For a beam of given stiffness profile subjected to a point load with constant support stiffness ratio, a point exists along the beam where there is no self-equilibrating moment. On the one side of the point closer to the centre support, the self-equilibrating moment increases the moment at the centre support section; on the other side of the point, it decreases the moment at the centre support section.
- The use of effective support stiffnesses gives good prediction of self-equilibrating moments developed due to differential settlement under both ultimate and service loads. A deflection-based approach has been proposed to estimate the support stiffnesses.

The analysis was conducted on 2-span symmetric beams; however, the same principles can be applied for the analysis of non-symmetric beams by introducing an extra rotational spring and combining the equations for each span of the beam. Also, the expressions for the point load case assume that the point load is applied within the 'middle' zone (zone Z2 in Figure 3-3) of the beam. For cases where the load is applied in other zones, the expressions in this Chapter may not be directly applicable, although similar procedures to those given in Appendix 3A can be followed to attain expressions for the particular case in consideration.

In the following chapter, tests performed on FRP-plated 2-span continuous steel beam will be reported. The analyses presented in this chapter will be applied to obtain the

total moments which will be compared with the test results. The deflection-based method will be used to estimate the support stiffnesses and verified with those obtain by measuring the support settlements and the corresponding support reactions.

Appendix 3A

Derivation of Moment Parameter Equations

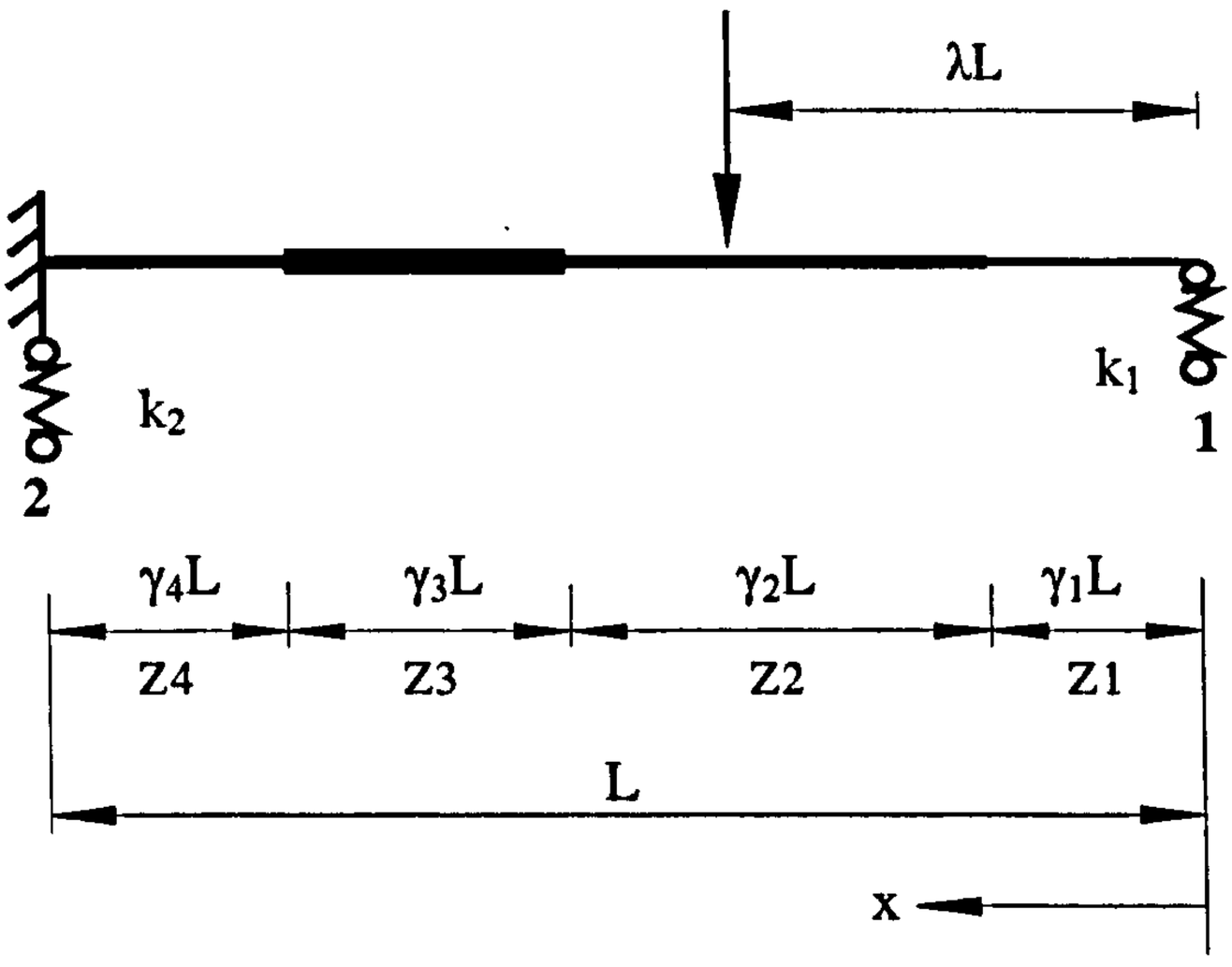

(a) Generalised beam model

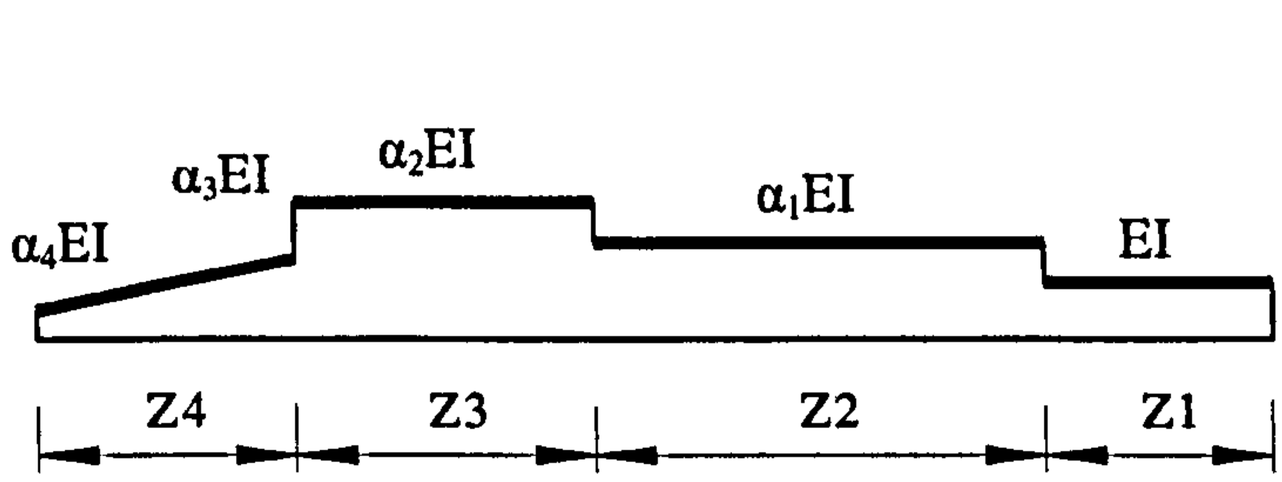

(b) Stiffness variation at ULS

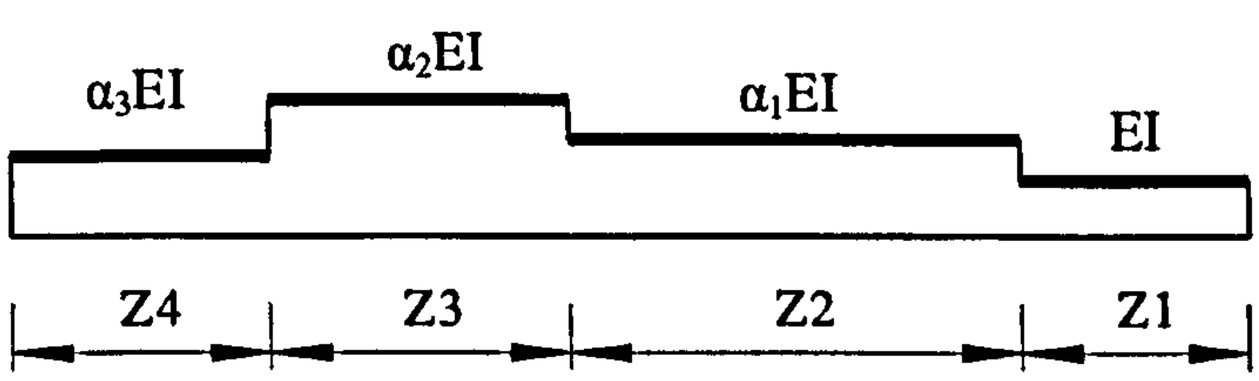

(c) Stiffness variation at SLS

Figure 3A-1 - Generalised model of a symmetric 2-span beam

3A.1 Linear stiffness regime

The stiffness profile for the linear regime is shown in Figure3A-1(c).

3A.1.1 Distributed load case

The force in the spring 1, R_1, is taken as the redundant force. Then, by considering the equilibrium of the entire beam, the other two reactions, M_2 and R_2 can be expressed in terms of R_1:

$$R_2 = wL - R_1 \qquad M_2 = \frac{wL^2}{2} - R_1 L \qquad \text{(3A-1 a, b)}$$

The bending moment M at distance x from the pin-end can be expressed in terms of load and redundant reaction:

$$M = R_1 x - \frac{wx^2}{2} \qquad \text{(3A-2)}$$

The second-order differential equations of the deflection curve for different segments are as follows:

$$\text{Segment 1: } -EIv'' = M = R_1 x - \frac{wx^2}{2} \ (0 \le x \le \gamma_1 L) \qquad \text{(3A-3)}$$

$$\text{Segment 2: } -\alpha_1 EIv'' = M = R_1 x - \frac{wx^2}{2} \ (\gamma_1 L \le x \le \Pi L) \qquad \text{(3A-4)}$$

$$\text{Segment 3: } -\alpha_2 EIv'' = M = R_1 x - \frac{wx^2}{2} \ (\Pi L \le x \le \Psi L) \qquad \text{(3A-5)}$$

$$\text{Segment 4: } -\alpha_3 EIv'' = M = R_1 x - \frac{wx^2}{2} \ (\Psi L \le x \le L) \qquad \text{(3A-6)}$$

After two successive integrations, the following equations for the slopes and deflections of the beam can be obtained:

$$\text{Segment 1: } -EIv' = \frac{R_1 x^2}{2} - \frac{wx^3}{6} + C_1 \qquad \text{(3A-7)}$$

$$-EIv = \frac{R_1 x^3}{6} - \frac{wx^4}{24} + C_1 x + C_2 \ (0 \le x \le \gamma_1 L) \qquad \text{(3A-8)}$$

Segment 2: $$-\alpha_1 EIv' = \frac{R_1 x^2}{2} - \frac{wx^3}{6} + C_3 \qquad \text{(3A-9)}$$

$$-\alpha_1 EIv = \frac{R_1 x^3}{6} - \frac{wx^4}{24} + C_3 x + C_4 \ (\gamma_1 L \le x \le \Pi L) \qquad \text{(3A-10)}$$

Segment 3: $$-\alpha_2 EIv' = \frac{R_1 x^2}{2} - \frac{wx^3}{6} + C_5 \qquad \text{(3A-11)}$$

$$-\alpha_2 EIv = \frac{R_1 x^3}{6} - \frac{wx^4}{24} + C_5 x + C_6 \ (\Pi L \le x \le \Psi L) \qquad \text{(3A-12)}$$

Segment 4: $$-\alpha_3 EIv' = \frac{R_1 x^2}{2} - \frac{wx^3}{6} + C_7 \qquad \text{(3A-13)}$$

$$-\alpha_3 EIv = \frac{R_1 x^3}{6} - \frac{wx^4}{24} + C_7 x + C_8 \ (\Psi L \le x \le L) \qquad \text{(3A-14)}$$

Boundary conditions

The continuity conditions give:

$$v_L\Big|_{x=\gamma_1 L} = v_R\Big|_{x=\gamma_1 L} \ ; \ v'_L\Big|_{x=\gamma_1 L} = v'_R\Big|_{x=\gamma_1 L} \qquad \text{(3A-15 a b)}$$

$$v_L\Big|_{x=(\gamma_1+\gamma_2)L} = v_R\Big|_{x=(\gamma_1+\gamma_2)L} \ ; \ v'_L\Big|_{x=(\gamma_1+\gamma_2)L} = v'_R\Big|_{x=(\gamma_1+\gamma_2)L} \qquad \text{(3A-16 a, b)}$$

$$v_L\Big|_{x=(\gamma_1+\gamma_2+\gamma_3)L} = v_R\Big|_{x=(\gamma_1+\gamma_2+\gamma_3)L} \ ; \ v'_L\Big|_{x=(\gamma_1+\gamma_2+\gamma_3)L} = v'_R\Big|_{x=(\gamma_1+\gamma_2+\gamma_3)L} \qquad \text{(3A-17 a, b)}$$

The boundary conditions are:

$$v(0) = \frac{R_B}{k_1} \qquad \text{(3A-18)}$$

$$v\Big|_{x=L} = \frac{wL - R_B}{k_2} \ ; \ \frac{dv}{dx}\Big|_{x=L} = 0 \qquad \text{(3A-19 a, b)}$$

Substitute the continuity and boundary equations (3A-15) to (3A-19) into equations (3A-3) to (3A-14), an expression for M_2 is obtained

$$M_2 = C_{wL} wL^2 \qquad \text{(3A-20)}$$

where C_w is a moment parameter given as:

$$C_{WL}=\frac{1}{2}-\frac{\frac{1}{\beta_2}+\frac{1}{8}\left[\left(1-\frac{1}{\alpha_1}\right)\gamma_1^4+\left(\frac{1}{\alpha_1}-\frac{1}{\alpha_2}\right)\Pi^4+\left(\frac{1}{\alpha_2}-\frac{1}{\alpha_3}\right)\Psi^4+\frac{1}{\alpha_3}\right]}{\left(\frac{1}{\beta_1}+\frac{1}{\beta_2}\right)+\frac{1}{3}\left[\left(1-\frac{1}{\alpha_1}\right)\gamma_1^3+\left(\frac{1}{\alpha_1}-\frac{1}{\alpha_2}\right)\Pi^3+\left(\frac{1}{\alpha_2}-\frac{1}{\alpha_3}\right)\Psi^3+\frac{1}{\alpha_3}\right]} \quad \text{(3A-21)}$$

3A1.2 Point load case

The force in the spring 1, R_1, is taken as the redundant force. Then, by considering the equilibrium of the entire beam, the other two reactions, M_2 and R_2 can be expressed in terms of R_1:

$$R_2 = P - R_1 \qquad M_2 = P(1-\lambda)L - R_1 L \quad \text{(3A-22 a, b)}$$

The bending moment M at distance x from the pin-end can be expressed in terms of load and redundant reaction:

$$M = R_1 x \ (x \le \lambda L) \quad \text{(3A-23)}$$

$$M = R_1 x - P(x-\lambda L) \ (\lambda L \le x \le L) \quad \text{(3A-24)}$$

Take $\Pi = \gamma_1 + \gamma_2$ and $\Psi = \gamma_1 + \gamma_2 + \gamma_3$, and the second-order differential equations of the deflection curve for different segments are as follows:

Segment 1: $-EIv'' = M = R_1 x \ (0 \le x \le \gamma_1 L)$ (3A-25)

Segment 2: $-\alpha_1 EIv'' = M = R_1 x \ (\gamma_1 L \le x \le \lambda L)$ (3A-26)

$$-\alpha_1 EIv'' = M = R_1 x - P(x-\lambda L) \ (\lambda L \le x \le \Pi L) \quad \text{(3-A27)}$$

Segment 3: $-\alpha_2 EIv'' = M = R_1 x - P(x-\lambda L) \ (\Pi L \le x \le \Psi L)$ (3A-28)

Segment 4: $-\alpha_3 EIv'' = M = R_1 x - P(x-\lambda L) \ (\Psi L \le x \le L)$ (3A-29)

After two successive integrations, the following equations for the slopes and deflections of the beam can be obtained:

Segment 1: $-EIv' = \frac{R_1 x^2}{2} + C_1$ (3A-30)

$$-EIv = \frac{R_1 x^3}{6} + C_1 x + C_2 \quad (0 \le x \le \gamma_1 L) \quad \text{(3A-31)}$$

Segment 2: $-\alpha_1 EIv' = \frac{R_1 x^2}{2} + C_3$ (3A-32)

$$-\alpha_1 EIv = \frac{R_1 x^3}{6} + C_3 x + C_4 \ (\gamma_1 L \le x \le \lambda L) \quad \text{(3A-33)}$$

$$-\alpha_1 EIv' = \frac{R_1 x^2}{2} - \frac{Px^2}{2} + \lambda PLx + C_5 \quad \text{(3-A34)}$$

$$-\alpha_1 EIv = \frac{R_1 x^3}{6} - \frac{Px^3}{6} + \frac{\lambda PLx^2}{2} + C_5 x + C_6 \ (\lambda L \le x \le \Pi L) \quad \text{(3A-35)}$$

Segment 3: $-\alpha_2 EIv' = \frac{R_1 x^2}{2} - \frac{Px^2}{2} + \lambda PLx + C_7$ (3A-36)

$$-\alpha_2 EIv = \frac{R_1 x^3}{6} - \frac{Px^3}{6} + \frac{\lambda PLx^2}{2} + C_7 x + C_8 \ (\Pi L \le x \le \Psi L) \quad \text{(3A-37)}$$

Segment 4: $-\alpha_3 EIv' = \frac{R_1 x^2}{2} - \frac{Px^2}{2} + \lambda PLx + C_9$ (3A-38)

$$-\alpha_3 EIv = \frac{R_1 x^3}{6} - \frac{Px^3}{6} + \frac{\lambda PLx^2}{2} + C_9 x + C_{10} \ (\Psi L \le x \le L) \quad \text{(3A-39)}$$

Boundary conditions

The continuity conditions give:

$$v_L\big|_{x=\gamma_1 L} = v_R\big|_{x=\gamma_1 L} \ ; \ v'_L\big|_{x=\gamma_1 L} = v'_R\big|_{x=\gamma_1 L} \quad \text{(3A-40 a, b)}$$

$$v_L\big|_{x=\lambda L} = v_R\big|_{x=\lambda L} \ ; \ v'_L\big|_{x=\lambda L} = v'_R\big|_{x=\lambda L} \quad \text{(3A-41 a, b)}$$

$$v_L\big|_{x=(\gamma_1+\gamma_2)L} = v_R\big|_{x=(\gamma_1+\gamma_2)L} \ ; \ v'_L\big|_{x=(\gamma_1+\gamma_2)L} = v'_R\big|_{x=(\gamma_1+\gamma_2)L} \quad \text{(3A-42 a, b)}$$

$$v_L\big|_{x=(\gamma_1+\gamma_2+\gamma_3)L} = v_R\big|_{x=(\gamma_1+\gamma_2+\gamma_3)L} \ ; \ v'_L\big|_{x=(\gamma_1+\gamma_2+\gamma_3)L} = v'_R\big|_{x=(\gamma_1+\gamma_2+\gamma_3)L} \quad \text{(3A-43 a, b)}$$

The boundary conditions are:

$$v(0) = \frac{R_1}{k_1} \quad \text{(3-A44)}$$

$$v\Big|_{x=L} = \frac{P - R_1}{k_2} \ ; \ \frac{dv}{dx}\Big|_{x=L} = 0 \quad \text{(3A-45 a, b)}$$

where $k_1 = \beta_1 \frac{EI}{L^3}$ and $k_2 = \beta_2 \frac{EI}{L^3}$.

Substitute the continuity and boundary equations (3A-40) to (3A-45) into equations (3A-25) and (3A-39), an expression for M_2 is obtained:

$$M_2 = C_{PL} PL \tag{3A-46}$$

where C_P is a moment parameter given as:

$$C_{WL} = \frac{1}{2} - \frac{\frac{1}{\beta_2} + \frac{1}{8}\left[\left(1-\frac{1}{\alpha_1}\right)\gamma_1^4 + \left(\frac{1}{\alpha_1}-\frac{1}{\alpha_2}\right)\Pi^4 + \left(\frac{1}{\alpha_2}-\frac{1}{\alpha_3}\right)\Psi^4 + \frac{1}{\alpha_3}\right]}{\left(\frac{1}{\beta_1}+\frac{1}{\beta_2}\right) + \frac{1}{3}\left[\left(1-\frac{1}{\alpha_1}\right)\gamma_1^3 + \left(\frac{1}{\alpha_1}-\frac{1}{\alpha_2}\right)\Pi^3 + \left(\frac{1}{\alpha_2}-\frac{1}{\alpha_3}\right)\Psi^3 + \frac{1}{\alpha_3}\right]} \tag{3A-47}$$

3A.2 Nonlinear stiffness regime

Assume linear variation along segment 4, the stiffness profiles is shown in Figure 3A-1(b). The stiffness parameter of any section a distance x from the pin-end can be expressed as:

$$\alpha_x = \xi + \varsigma \frac{x}{L} \quad (\Psi L \le x \le L) \tag{3A-48}$$

where $\xi = \alpha_3 - \frac{\alpha_4 - \alpha_3}{\gamma_4}\Psi$, and $\varsigma = \frac{\alpha_4 - \alpha_3}{\gamma_4}$.

Following the same solution procedure as in the previous section, the moment parameters can be obtained for both point load and distributed load cases and they are given as:

$$C_{WN} = \frac{1}{2} - \frac{\frac{1}{\beta_2} + \frac{1}{8}\left(\frac{1}{\alpha_1}-\frac{1}{\alpha_2}\right)\left(\Pi^4 - \gamma_1^4\right) + \frac{1}{8}\frac{1}{\alpha_2}\psi^4 + \frac{1}{6}\frac{1}{\varsigma}(1-\Psi^3) - \frac{1}{4}\frac{\xi}{\varsigma^2}(1-\Psi^2) + \frac{1}{2}\frac{\xi^2}{\varsigma^3}(1-\psi) - \frac{1}{2}\frac{\xi^3}{\varsigma^4}\ln\frac{\alpha_4}{\alpha_3}}{\frac{1}{\beta_1}+\frac{1}{\beta_2} + \frac{1}{3}\left(\frac{1}{\alpha_1}-\frac{1}{\alpha_2}\right)\left(\Pi^3 - \gamma_1^3\right) + \frac{1}{3}\frac{1}{\alpha_2}\Psi^3 + \frac{1}{2}\frac{1}{\varsigma}(1-\Psi^2) - \frac{\xi}{\varsigma^2}(1-\Psi) + \frac{\xi^2}{\varsigma^3}\ln\left(\frac{\alpha_4}{\alpha_3}\right)} \tag{3A-49}$$

$$C_{PN}=1-\lambda-\frac{\frac{1}{\beta_2}+\frac{1}{3}\left(\frac{1}{\alpha_1}-\frac{1}{\alpha_2}\right)\Pi^3-\frac{1}{2}\lambda\left(\frac{1}{\alpha_1}-\frac{1}{\alpha_2}\right)\Pi^2-\frac{1}{2}\frac{1}{\alpha_2}\lambda\Psi^2+\frac{1}{6}\frac{1}{\alpha_1}\lambda^3+\frac{1}{3}\frac{1}{\alpha_2}\Psi^3+\frac{1}{\varsigma}(\frac{1}{2}-\gamma_4\lambda-\frac{1}{2}\Psi^2)-\frac{\xi}{\varsigma^2}\gamma_4+\frac{\xi}{\varsigma^2}\lambda\ln\frac{\alpha_4}{\alpha_3}+\frac{\varsigma^2}{\xi^3}\ln\frac{\alpha_4}{\alpha_3}}{\frac{1}{\beta_1}+\frac{1}{\beta_2}+\frac{1}{3}\left(\frac{1}{\alpha_1}-\frac{1}{\alpha_2}\right)(\Pi^3-\gamma_1^3)+\frac{1}{3}\frac{1}{\alpha_2}\Psi^3+\frac{1}{2}\frac{1}{\varsigma}(1-\Psi^2)-\frac{\xi}{\varsigma^2}(1-\Psi)+\frac{\xi^2}{\varsigma^3}\ln(\frac{\alpha_4}{\alpha_3})}$$

(3A-50)

Appendix 3B

Supplementary Data on the Self-Equilibrating Moment Parameters

---

Based on the information given in Table 3-4, the moment parameters C_w and C_p were evaluated for various support stiffness combinations using Equations (3-4) and (3-7) for distributed and point load cases, respectively. The results are given in Table 3B-1. Using Equation (3-11), the corresponding self-equilibrating moment parameters were then evaluated. The results are given in Table 3B-2.

C_w		β_1														
		5	10	20	30	40	50	60	80	100	150	200	300	400	600	800
β_2	1	-0.253	-0.308	-0.340	-0.350	-0.356	-0.359	-0.362	-0.364	-0.366	-0.368	-0.370	-0.371	-0.371	-0.372	-0.372
	5	0.050	-0.031	-0.084	-0.104	-0.115	-0.121	-0.126	-0.131	-0.135	-0.139	-0.141	-0.144	-0.145	-0.146	-0.147
	10	0.150	0.072	0.019	-0.002	-0.013	-0.019	-0.024	-0.030	-0.034	-0.039	-0.041	-0.044	-0.045	-0.046	-0.047
	15	0.191	0.118	0.066	0.046	0.035	0.028	0.023	0.017	0.013	0.008	0.006	0.003	0.002	0.001	0.000
	20	0.214	0.143	0.093	0.073	0.062	0.055	0.050	0.044	0.041	0.036	0.033	0.031	0.030	0.028	0.028
	30	0.239	0.171	0.122	0.103	0.092	0.085	0.081	0.075	0.071	0.066	0.064	0.061	0.060	0.059	0.058
	40	0.252	0.186	0.138	0.119	0.108	0.102	0.097	0.091	0.088	0.083	0.081	0.078	0.077	0.076	0.075
	50	0.260	0.195	0.148	0.129	0.118	0.112	0.107	0.102	0.098	0.093	0.091	0.088	0.087	0.086	0.085
	60	0.265	0.202	0.155	0.136	0.125	0.119	0.115	0.109	0.105	0.101	0.098	0.096	0.094	0.093	0.093
	80	0.272	0.210	0.163	0.145	0.134	0.128	0.124	0.118	0.115	0.110	0.107	0.105	0.104	0.102	0.102
	100	0.276	0.214	0.169	0.150	0.140	0.134	0.129	0.124	0.120	0.115	0.113	0.111	0.109	0.108	0.108
	150	0.282	0.221	0.176	0.158	0.147	0.141	0.137	0.131	0.128	0.123	0.121	0.118	0.117	0.116	0.115
	200	0.285	0.224	0.180	0.161	0.151	0.145	0.141	0.135	0.132	0.127	0.125	0.122	0.121	0.120	0.119
	300	0.288	0.228	0.183	0.165	0.155	0.149	0.145	0.139	0.136	0.131	0.129	0.126	0.125	0.124	0.123
	400	0.289	0.230	0.185	0.167	0.157	0.151	0.147	0.141	0.138	0.133	0.131	0.128	0.127	0.126	0.125
	500	0.290	0.231	0.186	0.168	0.158	0.152	0.148	0.142	0.139	0.134	0.132	0.130	0.128	0.127	0.127
	600	0.290	0.231	0.187	0.169	0.159	0.153	0.149	0.143	0.140	0.135	0.133	0.130	0.129	0.128	0.127
	700	0.291	0.232	0.188	0.169	0.160	0.153	0.149	0.144	0.140	0.136	0.133	0.131	0.130	0.129	0.128
	800	0.291	0.232	0.188	0.170	0.160	0.154	0.150	0.144	0.141	0.136	0.134	0.131	0.130	0.129	0.128

(a) Distributed load

C_p		β_1														
		5	10	20	30	40	50	60	80	100	150	200	300	400	600	800
β_2	1	-0.241	-0.296	-0.327	-0.337	-0.343	-0.346	-0.348	-0.351	-0.353	-0.355	-0.356	-0.357	-0.358	-0.358	-0.359
	5	0.076	-0.001	-0.050	-0.069	-0.079	-0.085	-0.090	-0.095	-0.098	-0.102	-0.105	-0.107	-0.108	-0.109	-0.110
	10	0.180	0.110	0.061	0.042	0.032	0.026	0.022	0.016	0.013	0.008	0.006	0.004	0.003	0.001	0.001
	15	0.224	0.158	0.112	0.094	0.084	0.078	0.073	0.068	0.065	0.060	0.058	0.056	0.055	0.053	0.053
	20	0.248	0.185	0.141	0.123	0.113	0.107	0.103	0.098	0.095	0.091	0.088	0.086	0.085	0.084	0.083
	30	0.274	0.215	0.173	0.156	0.146	0.141	0.137	0.132	0.128	0.124	0.122	0.120	0.119	0.118	0.117
	40	0.287	0.231	0.190	0.173	0.164	0.158	0.155	0.150	0.147	0.142	0.140	0.138	0.137	0.136	0.136
	50	0.296	0.241	0.200	0.184	0.175	0.170	0.166	0.161	0.158	0.154	0.152	0.150	0.149	0.148	0.147
	60	0.301	0.247	0.208	0.192	0.183	0.177	0.174	0.169	0.166	0.162	0.160	0.158	0.157	0.156	0.155
	80	0.308	0.256	0.217	0.201	0.193	0.187	0.184	0.179	0.176	0.172	0.170	0.168	0.167	0.166	0.165
	100	0.313	0.261	0.223	0.207	0.199	0.193	0.190	0.185	0.182	0.178	0.176	0.174	0.173	0.172	0.172
	150	0.319	0.268	0.231	0.215	0.207	0.202	0.198	0.193	0.191	0.187	0.185	0.183	0.182	0.181	0.180
	200	0.322	0.272	0.235	0.219	0.211	0.206	0.202	0.198	0.195	0.191	0.189	0.187	0.186	0.185	0.185
	300	0.325	0.275	0.239	0.224	0.215	0.210	0.207	0.202	0.199	0.195	0.194	0.192	0.191	0.190	0.189
	400	0.326	0.277	0.241	0.226	0.217	0.212	0.209	0.204	0.201	0.198	0.196	0.194	0.193	0.192	0.191
	500	0.327	0.278	0.242	0.227	0.219	0.214	0.210	0.206	0.203	0.199	0.197	0.195	0.194	0.193	0.193
	600	0.328	0.279	0.243	0.228	0.220	0.215	0.211	0.206	0.204	0.200	0.198	0.196	0.195	0.194	0.194
	700	0.328	0.280	0.243	0.228	0.220	0.215	0.212	0.207	0.204	0.201	0.199	0.197	0.196	0.195	0.194
	800	0.328	0.280	0.244	0.229	0.221	0.216	0.212	0.208	0.205	0.201	0.199	0.197	0.196	0.195	0.195

(b) Point load

Table 3B-1 - Moment parameters

ζ_w		β_1														
		5	10	20	30	40	50	60	80	100	150	200	300	400	600	800
β_2	1	-2.950	-3.379	-3.618	-3.702	-3.745	-3.771	-3.788	-3.810	-3.823	-3.841	-3.850	-3.859	-3.863	-3.868	-3.870
	5	-0.613	-1.241	-1.648	-1.803	-1.884	-1.934	-1.968	-2.011	-2.038	-2.073	-2.091	-2.109	-2.118	-2.128	-2.132
	10	0.155	-0.442	-0.852	-1.012	-1.097	-1.150	-1.186	-1.232	-1.261	-1.299	-1.318	-1.338	-1.347	-1.357	-1.362
	15	0.477	-0.091	-0.490	-0.648	-0.733	-0.786	-0.822	-0.868	-0.897	-0.935	-0.954	-0.974	-0.984	-0.994	-0.999
	20	0.653	0.106	-0.284	-0.439	-0.523	-0.576	-0.611	-0.657	-0.685	-0.724	-0.743	-0.763	-0.772	-0.782	-0.787
	30	0.842	0.321	-0.057	-0.209	-0.291	-0.342	-0.378	-0.423	-0.450	-0.488	-0.507	-0.527	-0.536	-0.546	-0.551
	40	0.942	0.435	0.065	-0.084	-0.165	-0.216	-0.251	-0.295	-0.323	-0.360	-0.379	-0.398	-0.408	-0.418	-0.423
	50	1.003	0.506	0.142	-0.006	-0.086	-0.137	-0.171	-0.215	-0.243	-0.280	-0.298	-0.317	-0.327	-0.337	-0.342
	60	1.045	0.554	0.194	0.047	-0.032	-0.082	-0.117	-0.161	-0.188	-0.224	-0.243	-0.262	-0.272	-0.281	-0.286
	80	1.098	0.616	0.261	0.116	0.037	-0.013	-0.046	-0.090	-0.117	-0.153	-0.172	-0.191	-0.200	-0.210	-0.215
	100	1.130	0.654	0.301	0.158	0.079	0.030	-0.003	-0.047	-0.073	-0.110	-0.128	-0.147	-0.156	-0.166	-0.171
	150	1.173	0.705	0.357	0.215	0.137	0.089	0.055	0.012	-0.014	-0.050	-0.068	-0.087	-0.096	-0.106	-0.111
	200	1.195	0.731	0.385	0.244	0.167	0.118	0.085	0.042	0.016	-0.020	-0.038	-0.057	-0.066	-0.075	-0.080
	300	1.217	0.757	0.414	0.273	0.197	0.148	0.115	0.073	0.047	0.011	-0.007	-0.026	-0.035	-0.044	-0.049
	400	1.228	0.770	0.428	0.288	0.212	0.164	0.130	0.088	0.062	0.026	0.008	-0.010	-0.019	-0.029	-0.033
	500	1.235	0.778	0.437	0.297	0.221	0.173	0.140	0.097	0.071	0.036	0.018	-0.001	-0.010	-0.019	-0.024
	600	1.240	0.783	0.443	0.303	0.227	0.179	0.146	0.103	0.077	0.042	0.024	0.006	-0.004	-0.013	-0.018
	700	1.243	0.787	0.447	0.307	0.231	0.183	0.150	0.108	0.082	0.046	0.028	0.010	0.001	-0.009	-0.013
	800	1.245	0.790	0.450	0.310	0.234	0.186	0.154	0.111	0.085	0.050	0.032	0.013	0.004	-0.005	-0.010

$C_{w,\ rigid} = 0.130$

(a) Distributed load

ζ_p		β_1														
		5	10	20	30	40	50	60	80	100	150	200	300	400	600	800
β_2	1	-2.227	-2.505	-2.661	-2.715	-2.743	-2.760	-2.771	-2.785	-2.794	-2.805	-2.811	-2.817	-2.820	-2.823	-2.824
	5	-0.613	-1.003	-1.256	-1.352	-1.403	-1.434	-1.455	-1.482	-1.498	-1.521	-1.532	-1.543	-1.549	-1.554	-1.557
	10	-0.083	-0.442	-0.688	-0.785	-0.836	-0.868	-0.890	-0.918	-0.935	-0.958	-0.969	-0.981	-0.987	-0.993	-0.996
	15	0.139	-0.195	-0.431	-0.524	-0.574	-0.605	-0.627	-0.654	-0.671	-0.693	-0.705	-0.716	-0.722	-0.728	-0.731
	20	0.262	-0.057	-0.284	-0.374	-0.423	-0.453	-0.474	-0.501	-0.517	-0.540	-0.551	-0.562	-0.568	-0.574	-0.577
	30	0.392	0.094	-0.122	-0.209	-0.256	-0.285	-0.305	-0.331	-0.347	-0.368	-0.379	-0.391	-0.396	-0.402	-0.405
	40	0.461	0.174	-0.035	-0.119	-0.165	-0.194	-0.214	-0.239	-0.254	-0.275	-0.286	-0.297	-0.302	-0.308	-0.311
	50	0.503	0.224	0.020	-0.063	-0.108	-0.137	-0.156	-0.181	-0.196	-0.217	-0.227	-0.238	-0.244	-0.249	-0.252
	60	0.532	0.258	0.057	-0.025	-0.070	-0.097	-0.117	-0.141	-0.156	-0.177	-0.187	-0.198	-0.203	-0.208	-0.211
	80	0.568	0.301	0.104	0.024	-0.020	-0.047	-0.066	-0.090	-0.105	-0.125	-0.135	-0.146	-0.151	-0.156	-0.159
	100	0.591	0.328	0.133	0.054	0.011	-0.016	-0.035	-0.059	-0.073	-0.093	-0.104	-0.114	-0.119	-0.124	-0.127
	150	0.621	0.364	0.173	0.095	0.053	0.026	0.008	-0.016	-0.030	-0.050	-0.060	-0.070	-0.076	-0.081	-0.083
	200	0.636	0.382	0.193	0.116	0.074	0.047	0.029	0.006	-0.009	-0.028	-0.038	-0.048	-0.053	-0.058	-0.061
	300	0.651	0.400	0.214	0.137	0.095	0.069	0.051	0.028	0.014	-0.006	-0.016	-0.026	-0.031	-0.036	-0.038
	400	0.659	0.410	0.224	0.148	0.106	0.080	0.062	0.039	0.025	0.005	-0.004	-0.014	-0.019	-0.024	-0.027
	500	0.663	0.415	0.230	0.154	0.113	0.087	0.069	0.046	0.032	0.012	0.002	-0.008	-0.013	-0.018	-0.020
	600	0.666	0.419	0.234	0.158	0.117	0.091	0.073	0.050	0.036	0.017	0.007	-0.003	-0.008	-0.013	-0.016
	700	0.669	0.422	0.237	0.161	0.120	0.094	0.076	0.053	0.039	0.020	0.010	0.000	-0.005	-0.010	-0.012
	800	0.670	0.424	0.239	0.164	0.122	0.097	0.079	0.056	0.042	0.022	0.013	0.003	-0.002	-0.007	-0.010

$C_{p,\ rigid} = 0.197$

(b) Point load

Table 3B-2 - Self-equilibrating moment parameters

Chapter 4

Tests on FRP-Plated Continuous Steel Beams

4.1 Introduction

In Chapter 2 it was identified that research to date into statically indeterminate (especially metallic) structures is limited, while in the Chapter 3 an analytical study was carried out to investigate the behaviour of 2-span continuous beams at both the serviceability and ultimate limit states. Chapter 3 specifically focused on the important effects in indeterminate spans of self-equilibrating moments due to support settlements and of stiffness variations along the spans.

The present chapter builds on Chapter 3 by presenting the results of tests performed in this PhD study on FRP-plated 2-span continuous steel beams. The following ideas have been employed to obtain the results discussed henceforth:

- Use of sufficient load cells and dial gauges to permit equilibrium and symmetry checks, and to quantify support stiffnesses so that self-equilibrating moments in the indeterminate spans due to differential settlement can be assessed ;
- Different FRP plate layouts to vary the stiffness profiles between specimens;
- Use of instrumentation layouts which enable equivalent moment-curvature characteristics of the plated sections to be quantified and compared with those from rigid bond analysis (used in the analytical study);
- Strain gauges employed at both outer and inner surfaces of the FRP plates in some specimens, to allow the effects on the interfacial bond stresses of using only outer surface strains (which is customary) to be studied;
- The novel approach of using adhesive bonding to connect steel stiffeners to the webs of the steel beams.

In the remainder of this chapter, the scientific considerations which underpinned the tests are presented. The details of the test set-up are then given, after which the test results are discussed. The inferences on structural behaviour as drawn from these test results are put forward and finally conclusions are drawn on the work presented in this chapter. The results are presented in terms of beam failure behaviour, stiffnesses of FRP-plated steel sections, interfacial adhesive stresses, support settlements, moment distribution and load-deflection behaviour. These results will be referred to in subsequent chapters.

4.2 Scientific Considerations in Design of Tests

4.2.1 Use of 2-span continuous beams

Most of the investigations so far on statically indeterminate specimens have entailed 2-span continuous symmetric beams. This looks set to continue in the lab. Also, 2-span bridges are common in the practice. Therefore, the tests presented in this chapter (and also the analyses of the previous chapter) are conducted on 2-span continuous symmetric beams. FRP plates of different thicknesses are applied at various positions to give more insight into the potential effects these might have on the overall structural behaviour of the strengthened beam. The details of the test setup will be given in Section 4.3.

4.2.2 Consideration of self-equilibrating moments

One unique feature of statically indeterminate structures is that self-equilibrating moments develop from causes such as differential settlement, thermal gradients and plasticity-inducing load histories, which depend not only on the loading but also on the stiffness profile of the structural system (including supports and the member). In Chapter 3, self-equilibrating moments due to differential settlement and their effects on the moment diagram along the member have been analytically studied. In the present chapter, these effects are experimentally investigated. Dial gauges and load cells were used to measure the support deflections and the support reactions,

respectively, as will be shown later. The support stiffnesses can then be obtained for the uses illustrated in Chapter 3.

4.2.3 Buckling in thin-walled metallic structural components

In addition to the debonding failures commonly found in FRP-plated RC structures, buckling is also a major concern for thin-walled metallic members. Conventionally, steel stiffeners are welded onto the web and the flanges to prevent local buckling. Sayed-Ahmed (2006) numerically investigated the potential use of FRP strips on compression webs to delay the onset of local buckling. Several strengthening techniques using CFRP were reported by Zhao *et al.* (2006) to have led to significantly improved web buckling behaviour of rectangular hollow sections.

In the present experiments where I-section steel beams were used, the novel approach of adhesive bonding has been employed to attach the steel stiffeners to the test beam in an attempt to inhibit local buckling. The process (to be shown later in this chapter) is simple and does not require special equipment or skills. The main advantage of the technique, however, probably lies in the fact that it avoids welding and therefore heating, which is particularly important where strain gauges were needed at the section of stiffening (such as the tests described in this chapter). Also, in practice, heating is detrimental to the material properties of, for example, wrought iron girders, or to the bonding strength where there are already FRP plates adhesively bonded. Furthermore, its ease of application means that the technique may potentially be attractive for use in temporary structures.

Caution should be exercised, however, to ensure that adhesives can be used in the temperature range that a real structure might be exposed to. As an example, steel is highly conductive and the heat from natural sunshine (and other causes) can be transferred very quickly to the adhesive and cause it to soften if it exceeds its glass transition temperature (American Concrete Society 2008; Concrete Society 2004).

4.2.4 Axial strain in the CFRP plates

Significant strain variation through the CFRP plate thickness may exist due to the high thickness and/or local bending of the plates. It is the *average* through-thickness strain which should be used for the evaluation of interfacial shear stresses (Sebastian

2001; Sebastian and Luke 2007). The potential errors in shear bond stresses based on strains measured from only *one* surface of the plate has been noted in Kim (2003) for FRP-plated RC members. This average strain could be measured by either applying strain gauges at the mid-thicknesses of the plates or at both the bonded and exposed surfaces of the plates, which has not been commonly done even for determinate beams (where this issue also applies). In the present tests, the second approach (gauges on both bonded and exposed plate surfaces) was adopted in an attempt to investigate the potential effects of using exposed surface strain only (which is often the case) on the average shear bond stresses at the steel/FRP interface. This strain measurement system also allowed normal interfacial stresses to be determined.

4.2.5 Bond between FRP and substrate material

The analytical overestimation of interfacial bond stresses due to the assumption of rigid bond between the FRP plate and the substrate has been well documented in the literature (Sebastian 2001; Backy *et al.* 2007; Elsayed *et al.* 2007) and various bond slip models have been proposed to study the bond behaviour of the FRP-strengthened members (Monti *et al.* 2003; Dai *et al.* 2005; Lu *et al.* 2005). A study by Sebastian (2005) involving comparison of rigid bond and bond-slip shear stresses shows that the conservatism of rigid bond predictions is a function of load, member and spread of yield. Rigid bond is usually assumed in the section analysis of FRP-plated beams, mainly due to its ease of implementation. The potential effects of this assumption on the plated-section stiffness, however, have not been reported in the literature. In the present study, strain gauges were distributed through the depths of the FRP-plated sections and applied on both the steel and FRP at different heights, in an attempt to check how closely the rigid bond assumption is justified and so determine whether the equivalent moment-curvature characteristics obtained from rigid bond analysis are valid.

4.2.6 Symmetry and load equilibrium

Symmetry is one of the key assumptions in most of the experimental investigations and the corresponding analyses so far reported in the literature. This has been often checked by comparing deflections at each mid-span during post-test interpretation of

data (El-Refaie *et al.* 2003) (and supposedly during the test for monitoring purposes, although not mentioned). In the present tests, three load cells were employed (see later in this chapter) to explicitly check the equilibrium between the applied load and the support reactions and to check how closely the assumption of symmetry was justified.

4.3 Experimental set-up

4.3.1 Key details

Four 2-span continuous I-section steel beams with adhesively bonded carbon fibre-reinforced polymer (CFRP) plates (an example is shown in Figure 4-1) were tested. Details of the specimens, named B1 to B4, are given in Figure 4-2. The relevant member and material properties are as follows:

- Each beam was of two equal spans of 2.1 m;
- All I-section steel members were 203×133×30 Universal Beams;
- Young's modulus and yield stress for the steel were 196 kN/mm^2 and 300 N/mm^2, respectively (obtained from testing on steel coupons as will be discussed below);
- Young's modulus for the CFRP was 135.5 kN/mm^2 for B1, B3, B4 and base CFRP plate on B2, and 127.4 kN/mm^2 for top CFRP plate on B2 (obtained from testing on appropriate coupons);
- Plates of various widths and lengths were applied at different positions of the beam (See Figure 4-2 for the details) to provide different stiffness profiles along the specimens;
- The plates were terminated at different positions relative to zero-moment section to investigate any debonding behaviour of the plates both in tension and in compression;
- In specimen B2, composite plate thicknesses of 4 mm and 1.5 mm were used for the base and top plates, respectively;

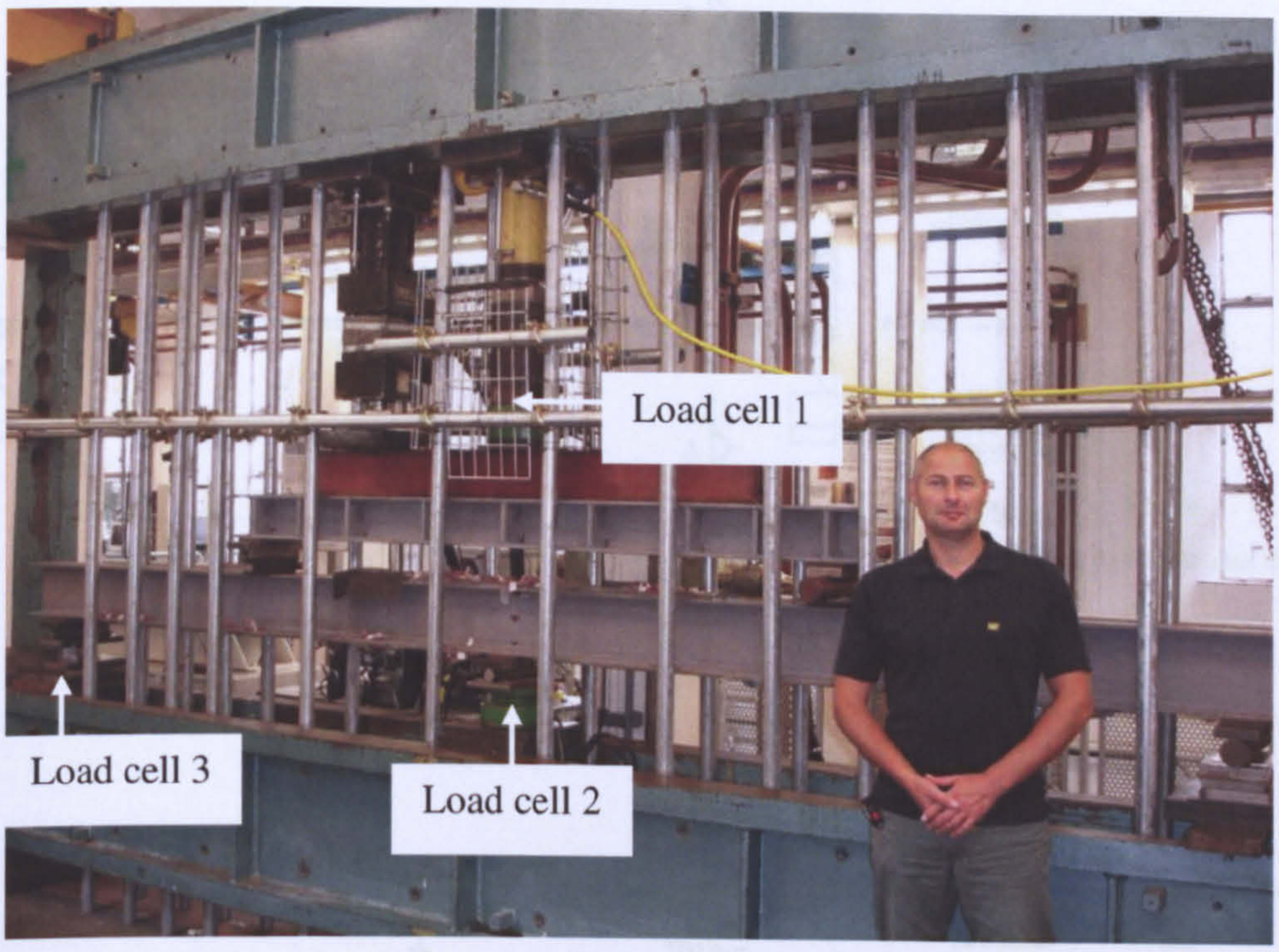

Figure 4-1 - FRP-plated 2-span continuous steel beam tested in this PhD study

- The multilayer plates used in specimens B1, B3 and B4 were fabricated by bonding composite plates of 4 mm thick to each other with 0.5 mm thick adhesive layers (the thickness of the adhesive layer between plates are ignored in the analyses of the test results);
- MBT Mbrace Adhesive HT 65 was used to bond the CFRP plates to the steel. The manufacturer's quoted Young's modulus and tensile strength for this adhesive were 10 kN/mm^2 and 32 N/mm^2, respectively;
- An adhesive layer of target thickness 4 mm was employed between plate and beam in all specimens;
- For specimens B2 – B4, steel stiffening plates of 12 mm thickness and 50 mm width were adhesively bonded to the web and both flanges (Figure 4-2) on both sides of the beam;

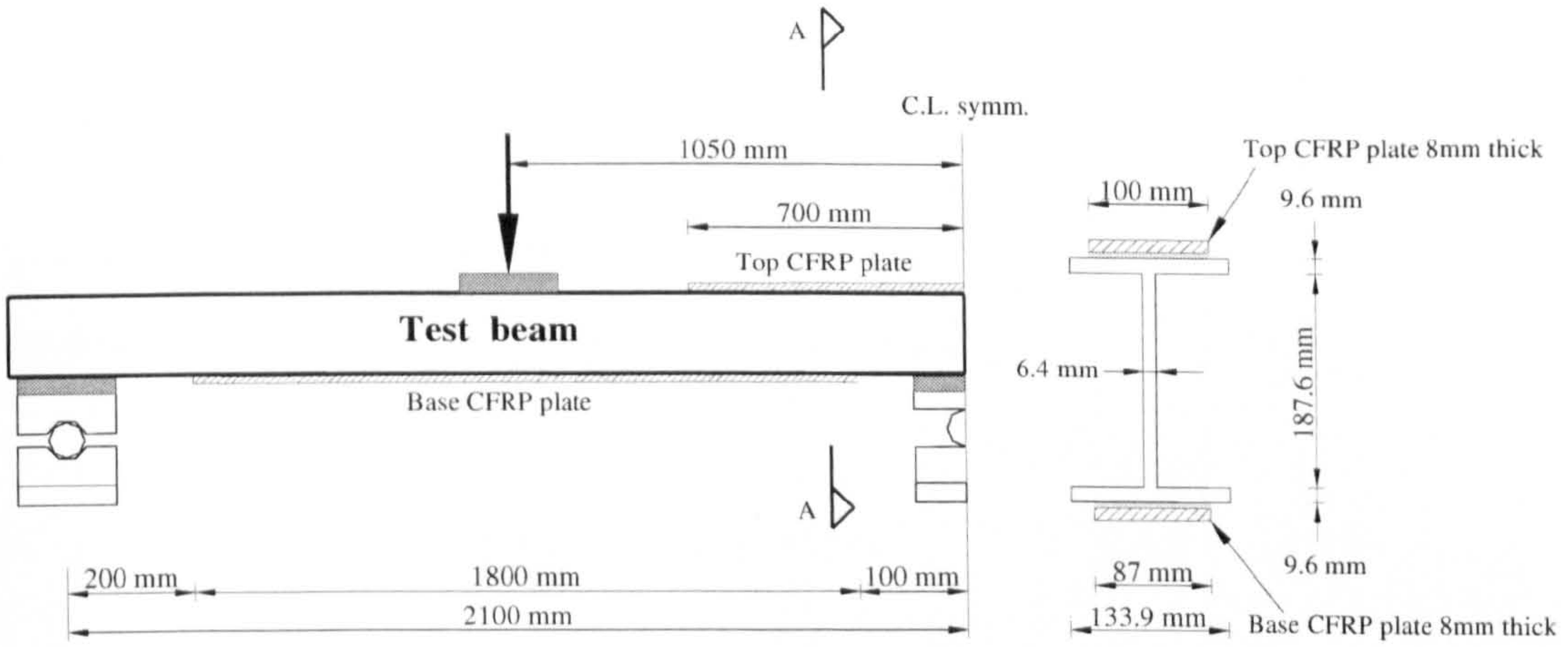

(a) Specimen B1

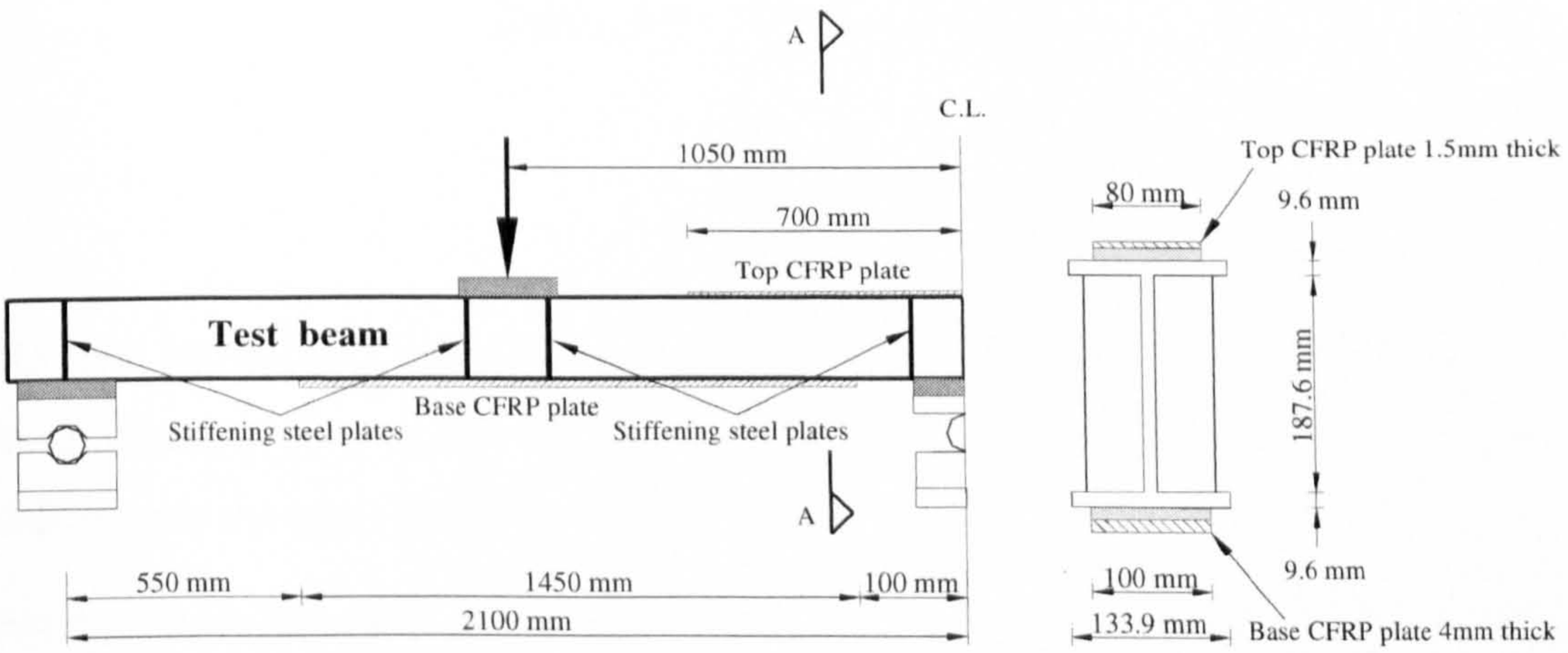

(b) Specimen B2

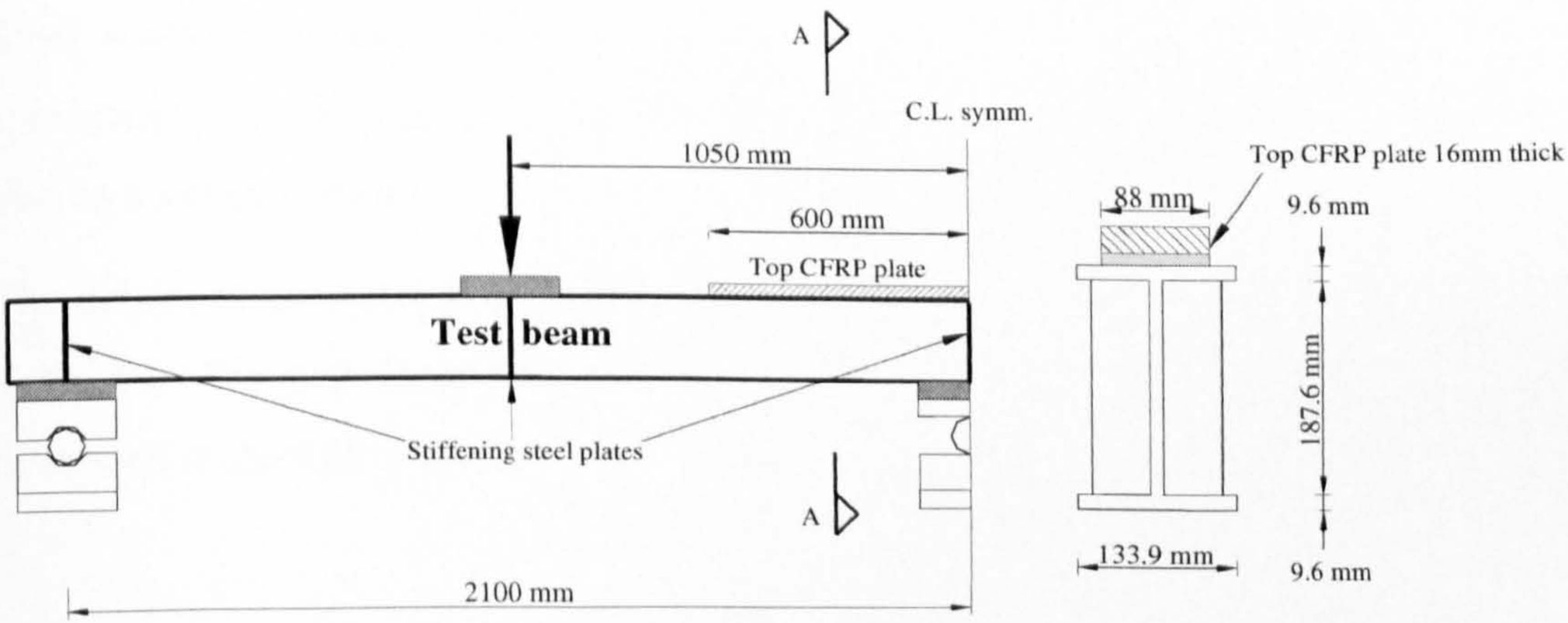

(c) Specimen B3

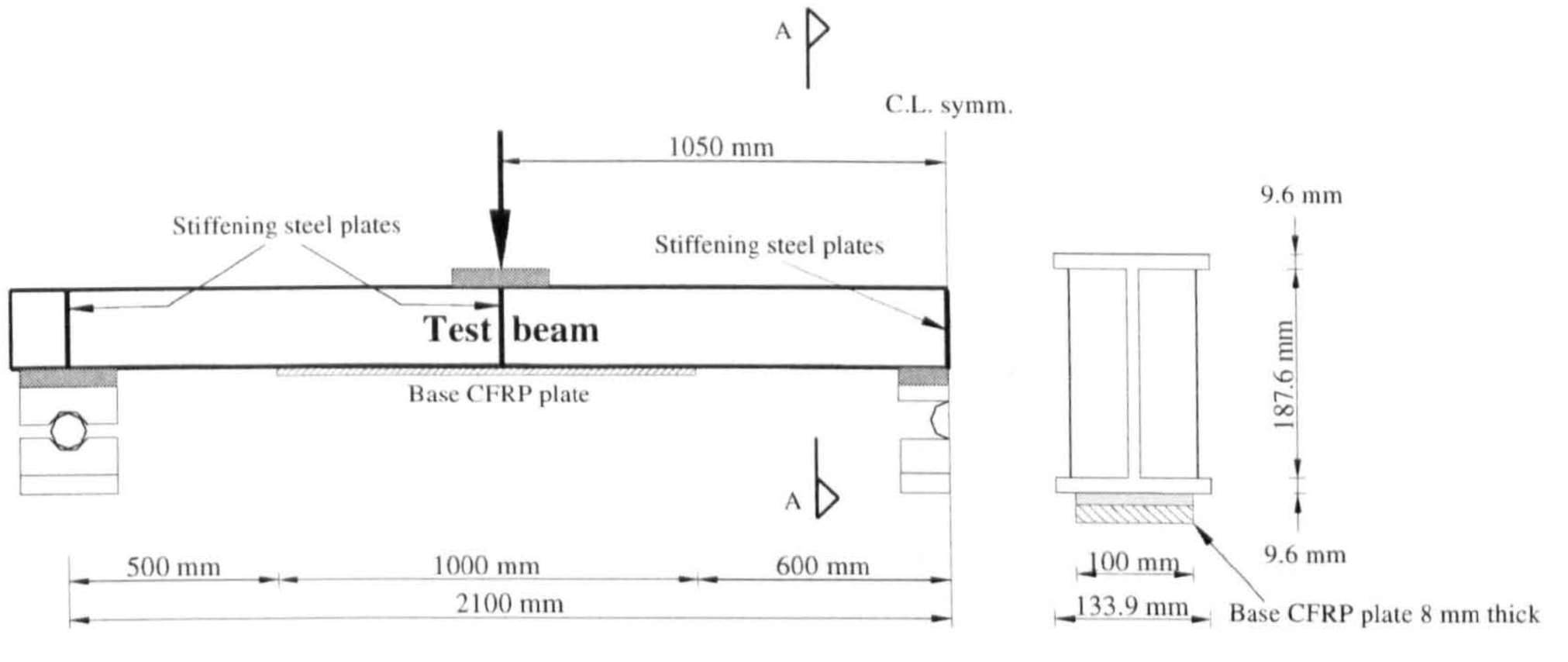

(d) Specimen B4

Figure 4-2 - Specimen details

- No steel stiffening plates were applied to specimen B1, so that this specimen could have been used as a control to assess the efficiency of adhesive bonding of steel plate stiffeners to the other beam specimens;
- For specimen B2, steel stiffening plates were applied directly under the load within the right span and at a beam depth either side of the load position within the left span to allow the application of strain gauges at the left mid-span section;
- Steel scaffolding poles were placed along both sides of (but not attached to) all specimens – see Figure 4-1 – to inhibit lateral torsional buckling of the beams and also as a safety feature.

The details of the specimens are summarized in Table 4-1 and material properties in Table 4-2. The steel material properties were obtained from coupon testing as will be discussed in the following section.

Specimen notation	Top CFRP plate			Base CFRP plates		
	Length	Width	Thickness	Length	Width	Thickness
	mm	Mm	mm	mm	mm	mm
B1	1400	100	8	1800	87	8
B2	1400	80	1.5	1450	100	4
B3	1200	88	16	N/A		
B4	N/A			1000	100	8

Table 4-1 - Details of test specimens

Steel		Adhesive		CFRP			
				Top plate on B2		Remainder	
E_s	f_y	E_a	f_t	E_p	ε_u	E_p	ε_u
kN/mm^2	N/mm^2	kN/mm^2	N/mm^2	N/mm^2	$\times 10^{-6}$	N/mm^2	$\times 10^{-6}$
196	300	10	32	127.4	13000	135.5	N/A

Table 4-2 - Material properties

4.3.2 Steel material behaviour

Steel is commonly taken as an elastic-perfectly plastic material. In practice, steels may deviate from this behaviour (Sebastian 2006a). Four coupons were tested, two from the flange and two from the web. All coupons were taken from the low moment area of specimen B3, so that no yield occurred there prior to testing of the coupons. The coupons were loaded in uniaxial tension. The results are shown for strain levels up to *circa* 5000 με (just over the maximum strain in the steel observed in the tests) in Figure 4-3.

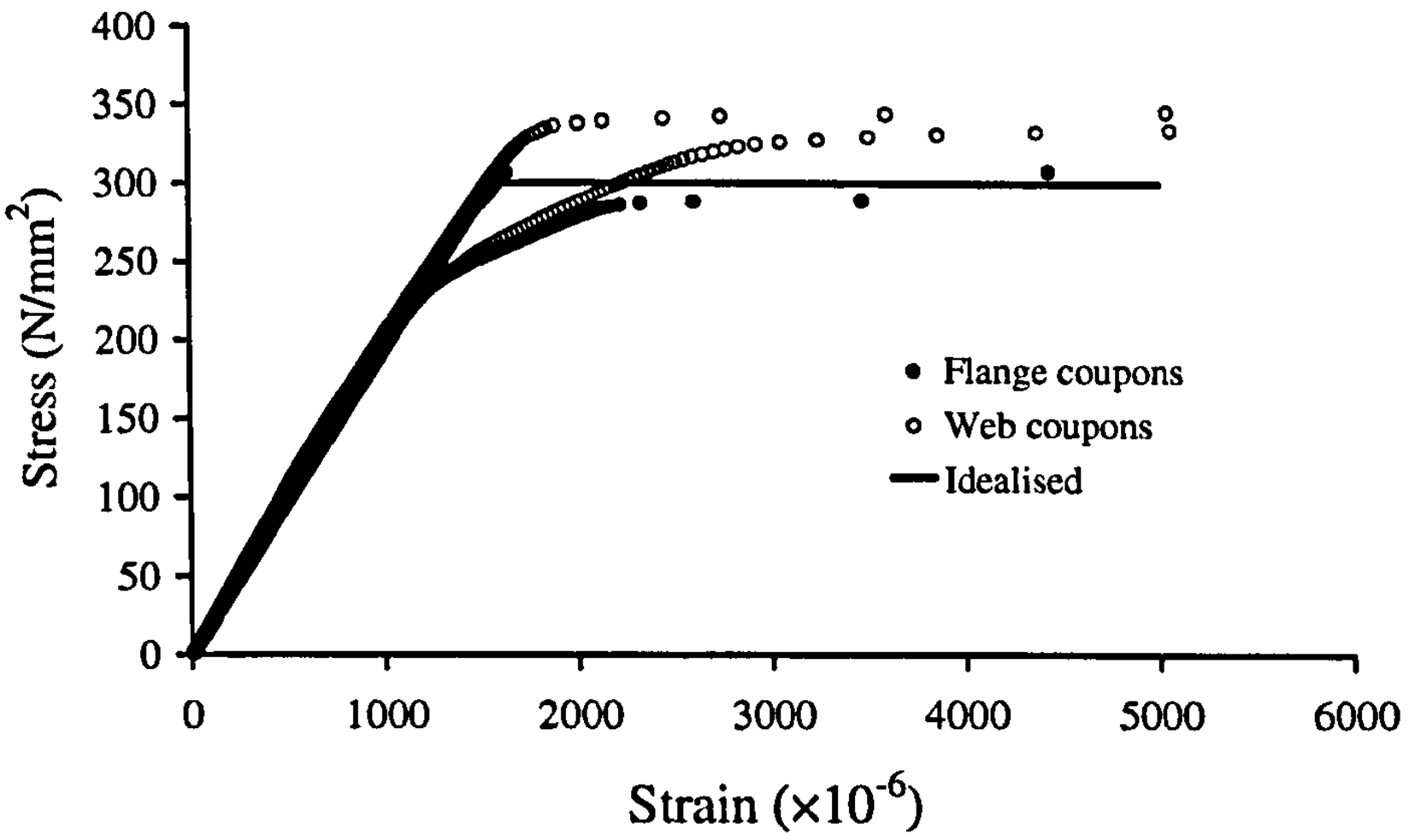

Figure 4-3 - Stress-strain characteristics of steel

It can be seen that the steel initially shows a well-pronounced linear elastic behaviour. There was variation in yield stress between the flange and web coupons and also between the two flange coupons as well as between the two web coupons. Idealised elastic-perfectly plastic stress-strain relations that give good fit of the coupon test data were taken and used for the analyses of the test results. An average yield stress was taken from the two flange coupons (rather than from the four total coupons for the modulus of elasticity) to account for the bigger effect that the flanges – relative to the webs – have on the section moment resistance compared to the web.

4.3.3 CFRP plate and stiffening steel plate bonding

All CFRP plates were pultruded. The steel flanges were grit blasted followed by use of a high-pressure air line to remove residual loose particles. For the top plates of specimens B1 and B2 and the base plate of specimens B2 and B3, bonding of the CFRP plates was undertaken in the Structures Lab at the University of Bristol. The steel flanges were sanded to remove the rust until the shiny metal surface was revealed. Scratches were deliberately made on the surfaces in an attempt to provide better bonding before the surface was finally degreased with acetone.

The bonding process is shown in Figure 4-4. A two-part (resin and hardener) epoxy adhesive (Figure 4-4 (b)) was used for bonding. Stiff, light aluminium strips were used between the longitudinal edges of the CFRP plates and those of each flange of the steel beam to control the locations of the plates across the widths of these flanges (Figure 4-4 (a)). Slots were hand-filed along the strips to allow wires from strain gauges attached to the plates to come through. Adhesive was applied to the cleaned, bonding faces of both the beam and the FRP plate (Figure 4-4 (c)). After placing the plates against the beams with the wet adhesive in between (Figure 4-4 (d)), gentle pressure was applied using weights along the outer surfaces of the plates to squeeze out air bubbles and to further control the adhesive thickness (Figure 4-4 (e)). The adhesive was left to cure for at least 5 days (Figure 4-4 (f), full cure from supplier's technical data sheets) before testing. In practice, installation procedures (covering surface preparations, application of resin, installation of FRP and curing) are in place to ensure bond quality. However, perfect bond is very difficult if at all possible to achieve.

For specimens B2-B4, a novel process based on use of adhesive was used to connect the stiffening steel plates to the steel beam. Beam surfaces where the stiffening plates were to be placed were sanded to remove the rust and then degreased with acetone. The process is shown in Figure 4-5. Strain gauges were placed on the beam and then covered with flexible rubber pads for protection (Figure 4-5 (a)). Adhesive (the same as that used for CFRP plate bonding) was placed on all three bonding faces of the stiffening plates and also on the surfaces of the beam where contact was to be made (Figure 4-5 (b)). The plates were positioned and adjusted wherever necessary (Figure 4-5 (c)). The beam was then left for at least 5 days to cure (Figure 4-5 (d)). The process is simple and does not require special equipment.

(a) (b)

(c) (d)

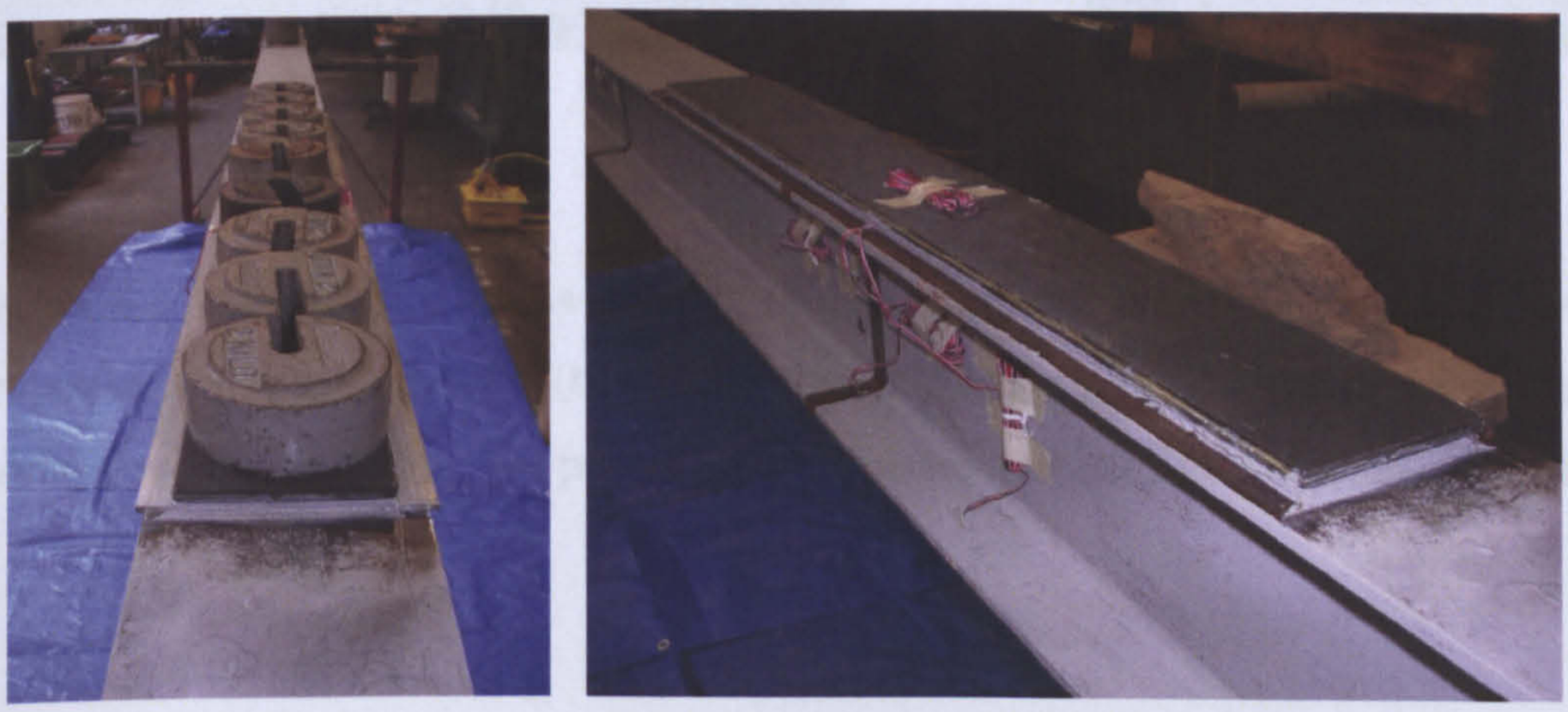

(e) (f)

Figure 4-4 - Bonding of CFRP plate to steel beam: (a) Positioning aluminium strips; (b) Adhesive components; (c) Applying adhesive; (d) Placing the plate; (e) Weights on plate to apply pressure during curing; and (f) Bonded plate after curing and removal of the aluminium strips

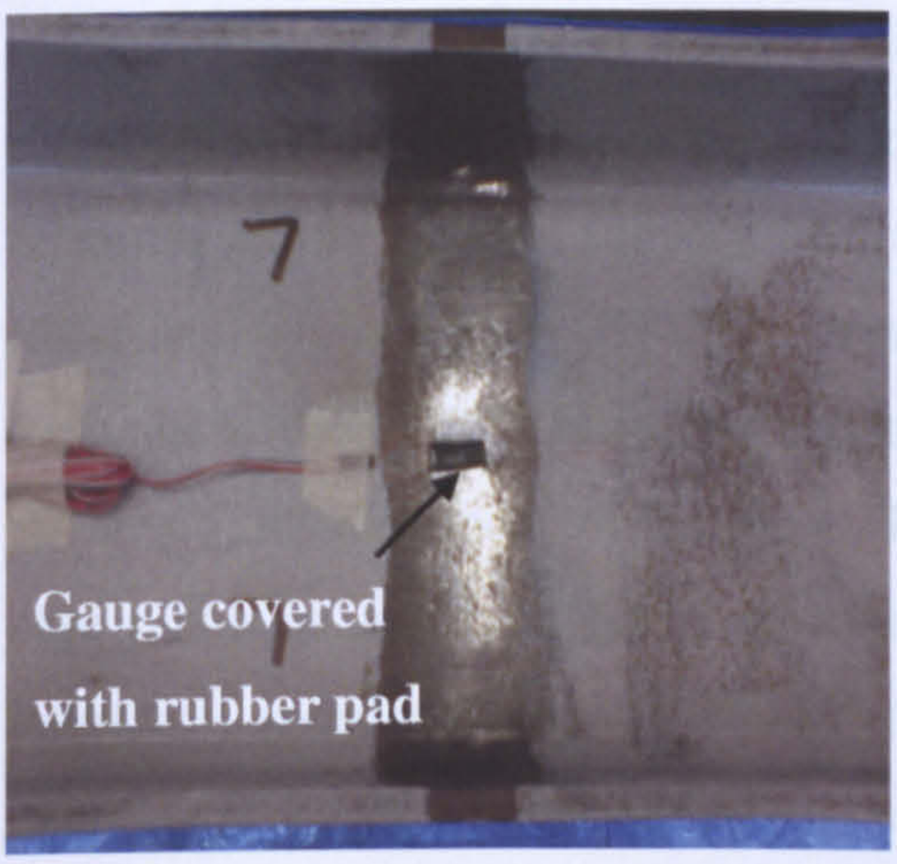

(a)

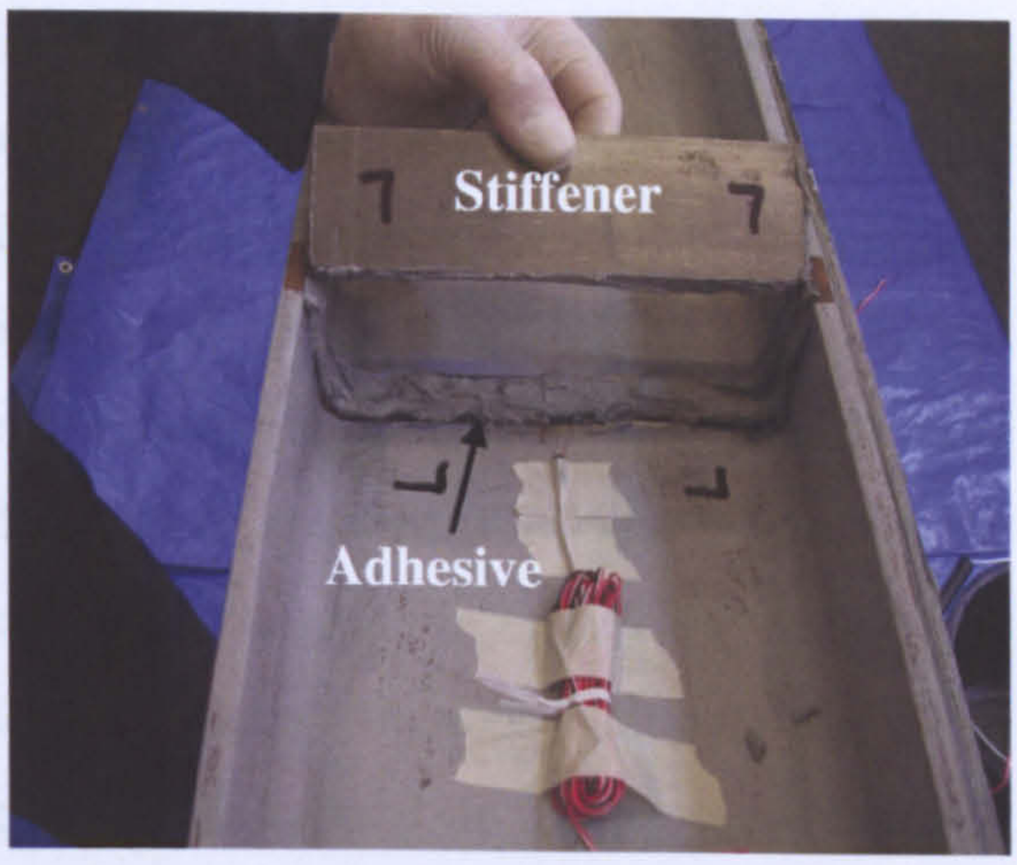

(b)

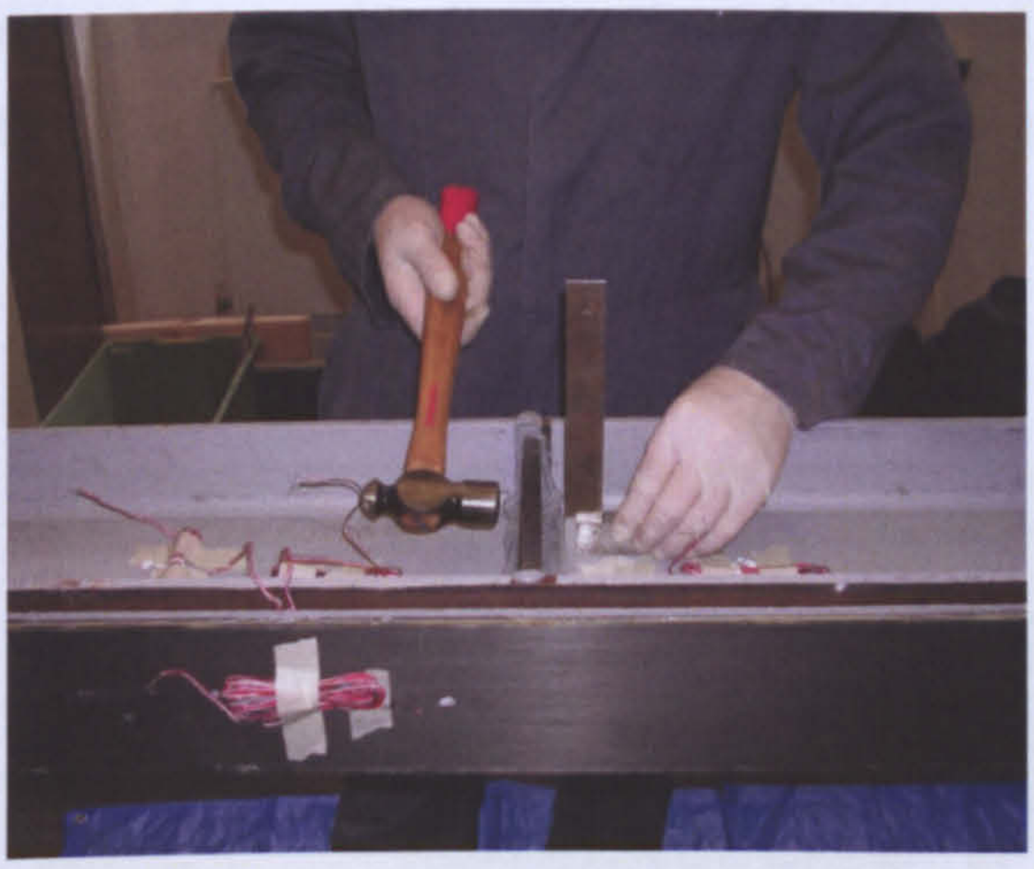

(c)

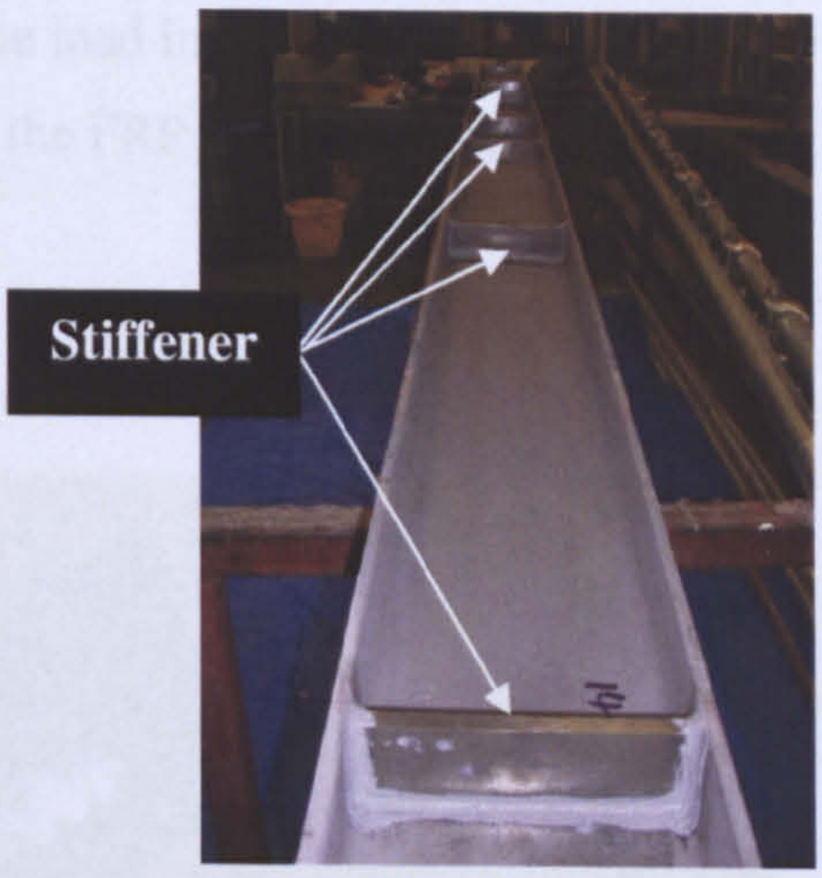

(d)

Figure 4-5 - Bonding process for stiffening steel plates: (a) Surface cleaning and protection for strain gauges; (b) Fitting steel stiffening plates onto previously laid adhesive; (c) Adjusting the position of the plate; and (d) Final stiffener layout

4.3.4 Instrumentation and loading of specimens

An hydraulic jack, controlled via a manually operated pump was used to load the beam. Loads were applied at mid-span sections through a spreader beam. High strength rubber pads – which may have significantly influenced support stiffness – were used to spread the load and inhibit local buckling of the steel member around the

loads. At one end, specially made up split rollers (Figure 4-6) were used to provide a pin support. Load cells were used to measure the total load applied along with the reactions at the centre support and at one end support (Figure 4-1). Electrical resistance strain gauges (ERSGs) were attached to the steel sections and to the surfaces of the CFRP plates to measure strains. Strain gauges were applied at both inner and outer surfaces of the top CFRP plates of specimens B1 and B2 and of the base plates of specimen B4 in an attempt to investigate the effects on the average interfacial shear stresses of the plate thickness and/or potential local bending of the plate. Dial gauges were placed on top of each support to measure the support settlements (Figure 4-7). The instrumentation details are given in Figure 4-8. Load cells, ERSGs and potentiometers/LVDTs were all connected to data loggers and recorded automatically at each load increment. The load increments were informed by the observed peak strain at the external surface of the FRP plate during the test.

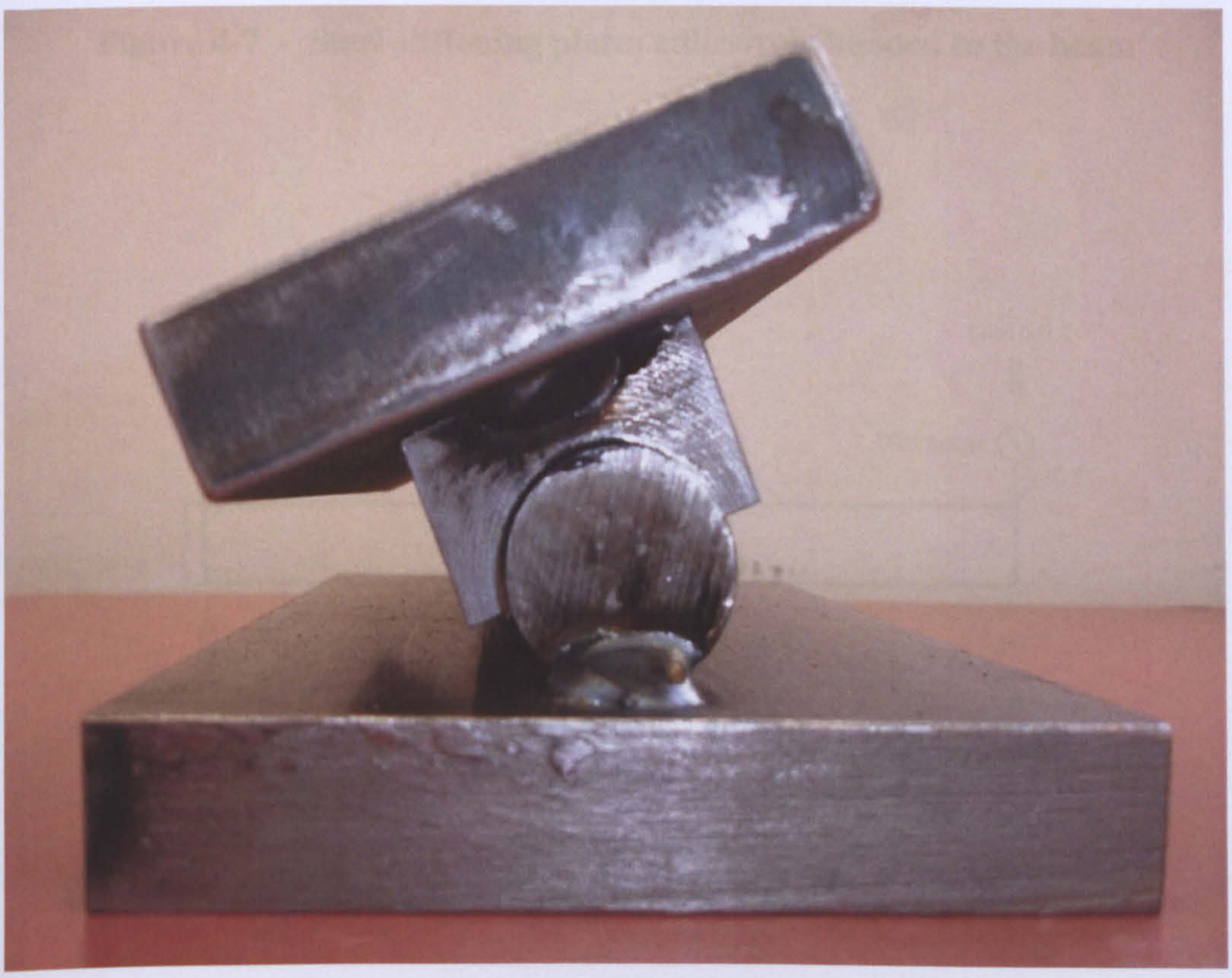

Figure 4-6 - Split rollers

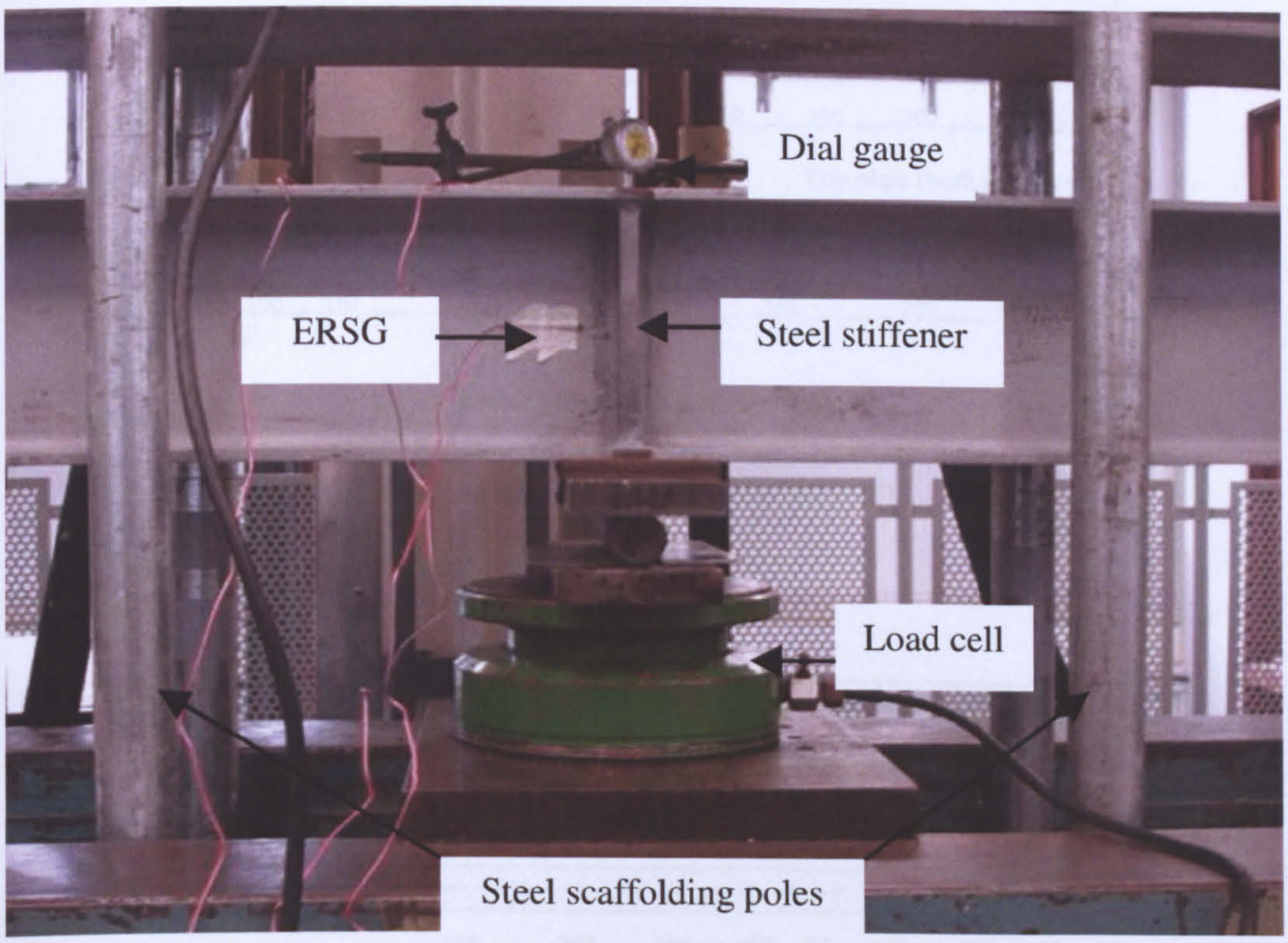

Figure 4-7 - Steel stiffening plates adhesively bonded to the beam

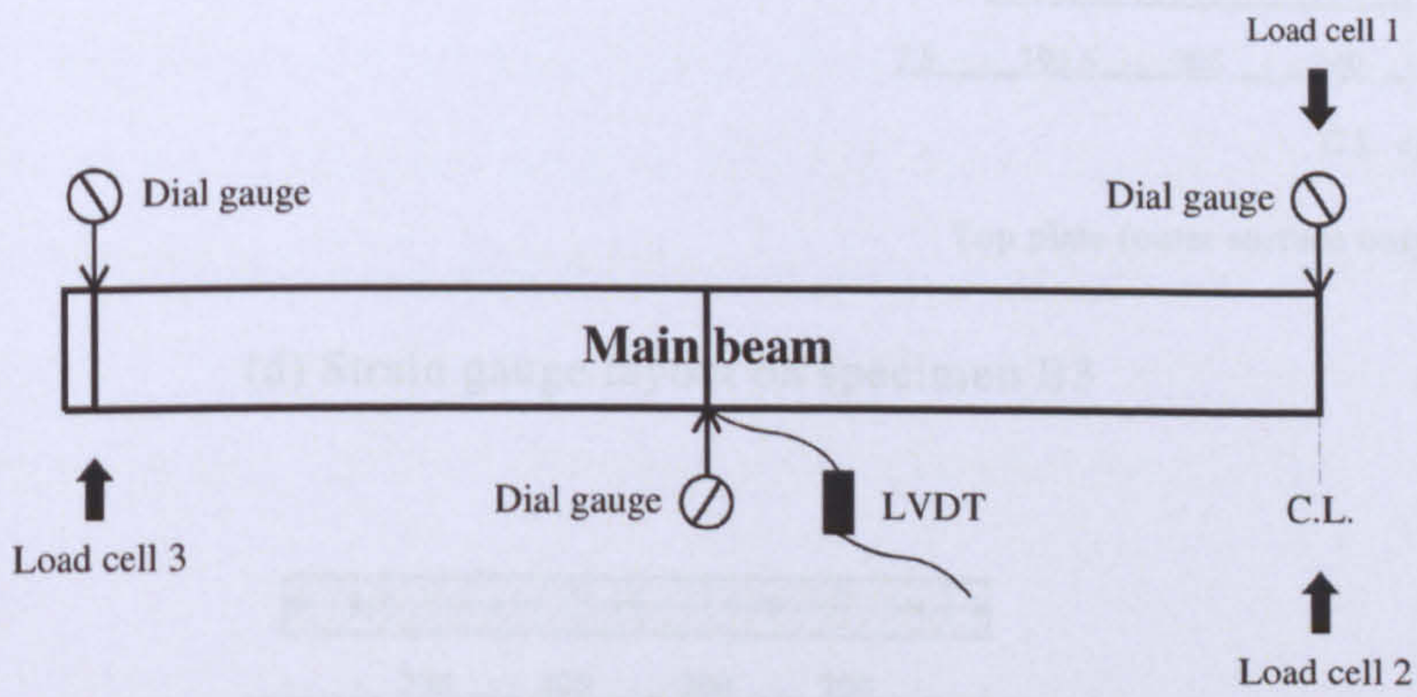

(a) All specimens

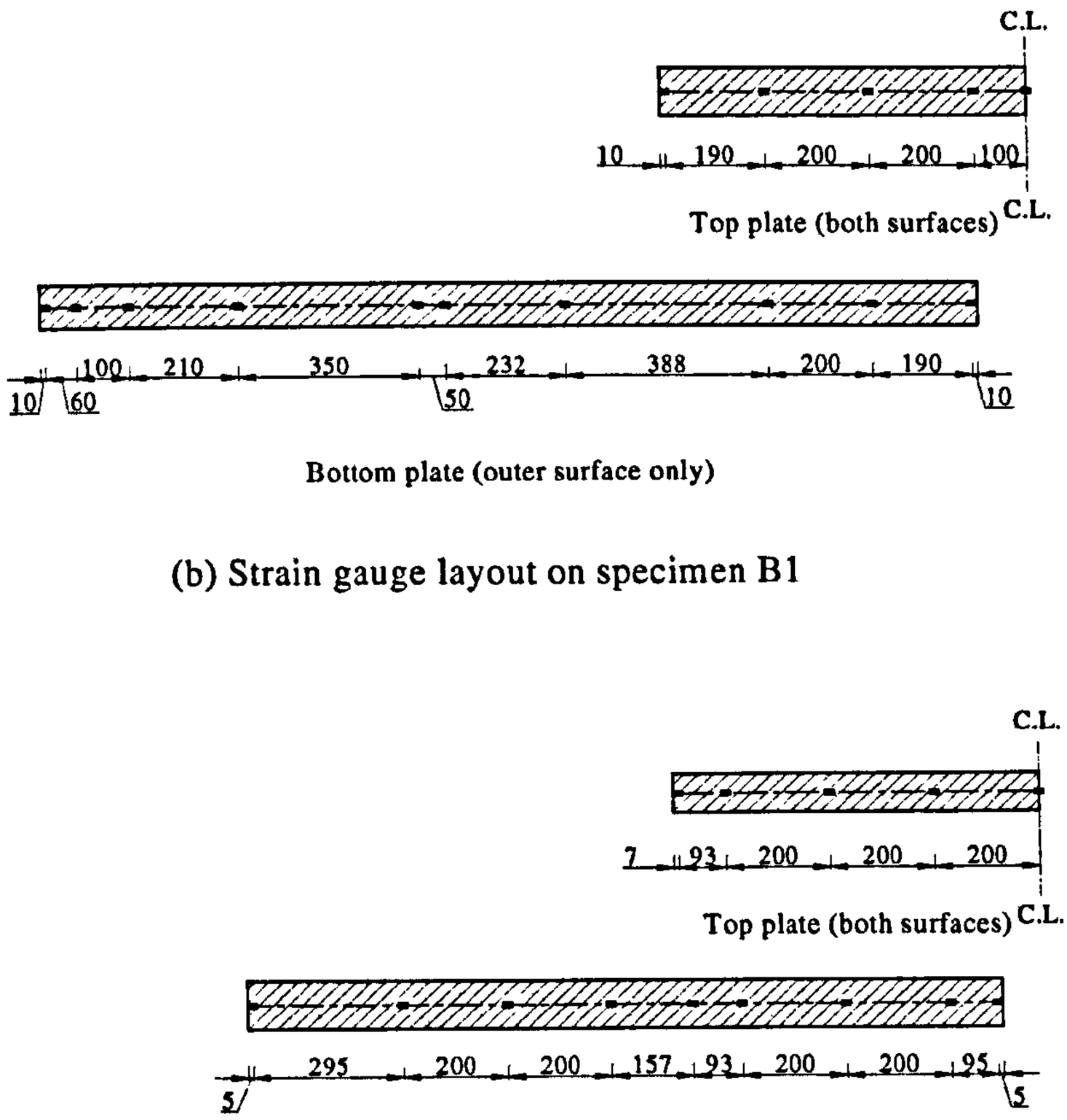

(b) Strain gauge layout on specimen B1

(c) Strain gauge layout on specimen B2

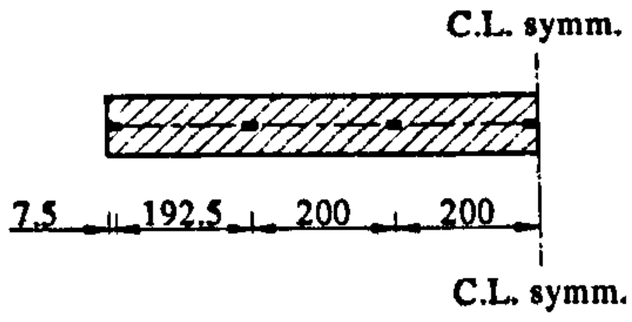

(d) Strain gauge layout on specimen B3

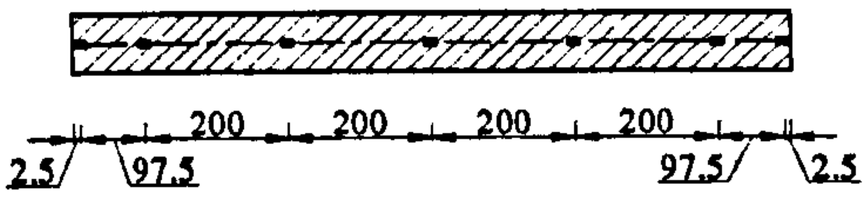

(e) Strain gauge layout on specimen B4

Figure 4-8 - Instrumentation details

4.4 Test results

Failure of the tested beams was judged to occur when the beam under testing could not carry increased load. In the case of specimen B3, the test had to stop when the capacity of load cell 1 that was used to record the total applied load (Figures 4-1 and 4-8 (a)) was reached. At that stage, the applied load was released and no further data were recorded.

In what follows, the general failure behaviours and the relative failure loads for the specimens are first discussed after which load equilibrium is checked using readings from the three load cells. The recorded instrumentation data are then presented and discussed. The analytical model proposed in Chapter 3 is also used to predict the moment distribution along the span and the results are compared with the test data.

4.4.1 Failure modes

Two different failure modes were observed in the tests – loss of stability caused by local buckling and brittle plate separation failure. Brief descriptions of the failure modes of the four specimens together with the failure loads are summarised in Table 4-3 and are further discussed below.

Beams B1 and B2 both failed by lateral torsional buckling. Local buckling initiated at the supports and also at the sections where loads were applied. Shown in Figure 4-9 is specimen B1 at a total applied load of 333 kN. Some end peel at the FRP/adhesive interface of both base CFRP plates from the steel beam was observed symmetrically about the centre support. Figure 4-10 shows this end peel for one plate. This is discussed again in later sections. No debonding was observed in B2.

Beam	Failure load (kN)	Failure behaviour
B1	333	Loss of stability caused by local buckling; entire beam twisted; some end peel at the plate/adhesive interface near compression end of plate in latter stages
B2	388	Loss of stability caused by local buckling; entire beam twisted and both spans leaned against scaffolding on opposite sides of beam
B3	453	Test stopped due to load cell reaching capacity; no buckling or debonding observed
B4	411	Brittle separation of plates from beam; carried significantly greater load after separation

Table 4-3 - Summary of failure behaviours

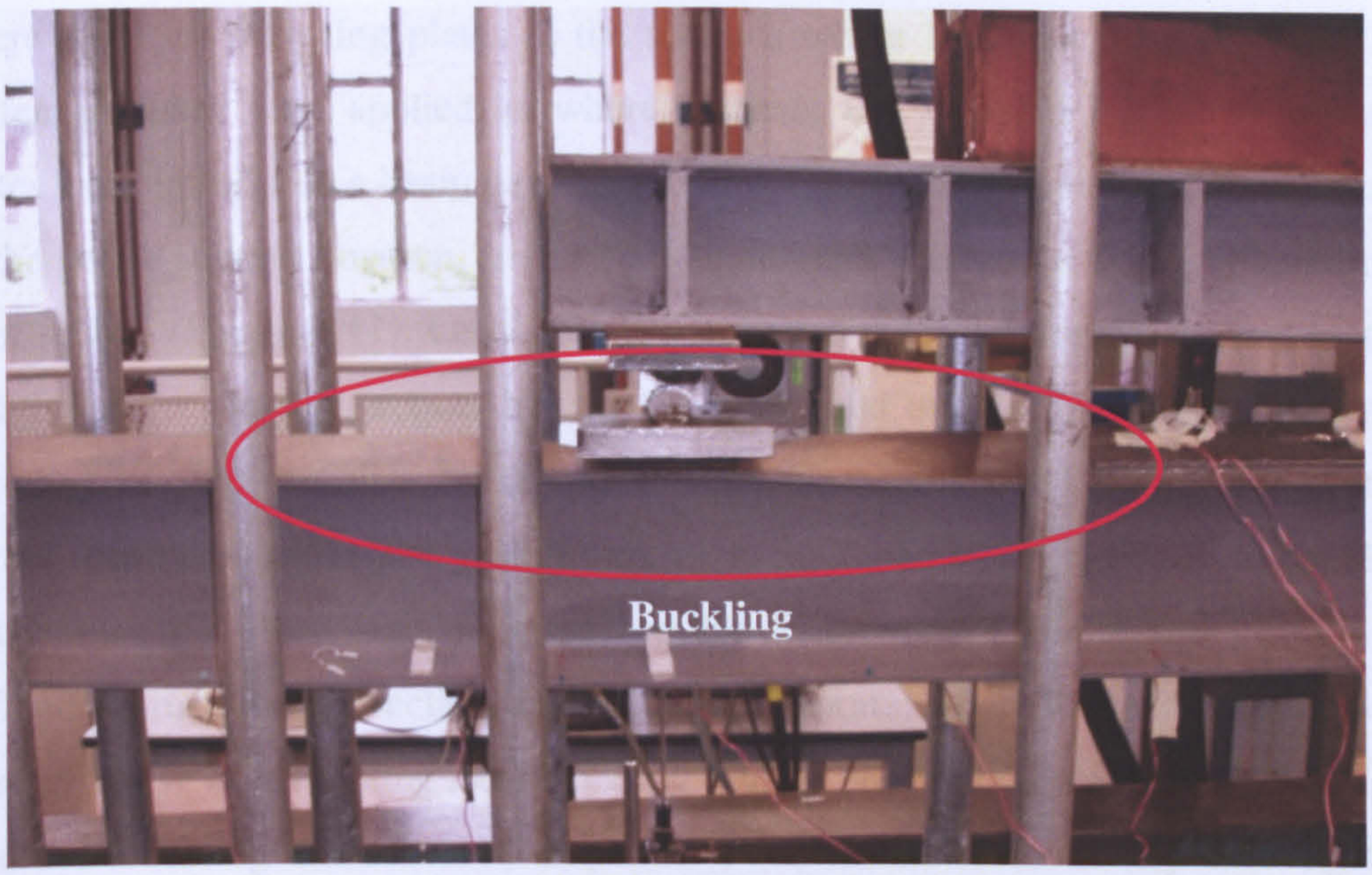

Figure 4-9 - B1 buckling at 333 kN total applied load

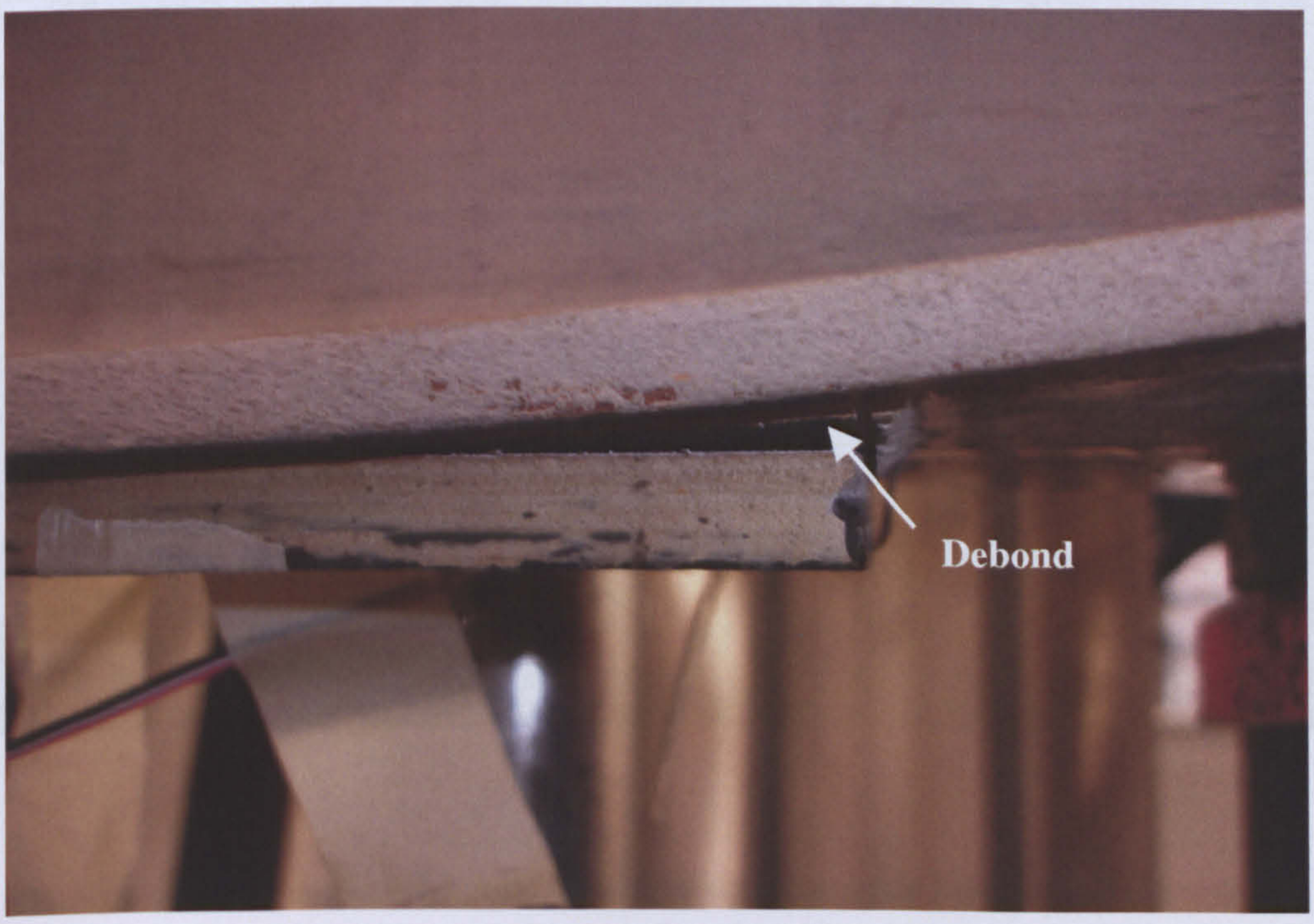

Figure 4-10 - End peel in B1 at 333 kN total applied load

There were no stiffening plates at the sections where local buckling occurred. No stiffening plates were applied anywhere in beam B1. In beam B2, stiffening steel plates were introduced a beam depth each side of the left hand mid-span position and of the centre support position, and directly underneath the load at the right hand mid-span section (Figure 4-11). Local buckling occurred at the left hand mid-span section and the centre support section, but not the right hand mid-span section as shown in Figure 4-12. The fact that thinner plates were used for B2 at both top and bottom flanges compared to B1 and yet B2 took more load than B1, suggests local buckling could leave the steel beam more susceptible to premature failure and placing the stiffeners directly at the section (including the supports) where load was applied were more effective in preventing local buckling. This is confirmed in testing of B3 and B4, where no buckling was observed. In practice, concrete slabs commonly used together with steel beams would normally help provide buckling restraint.

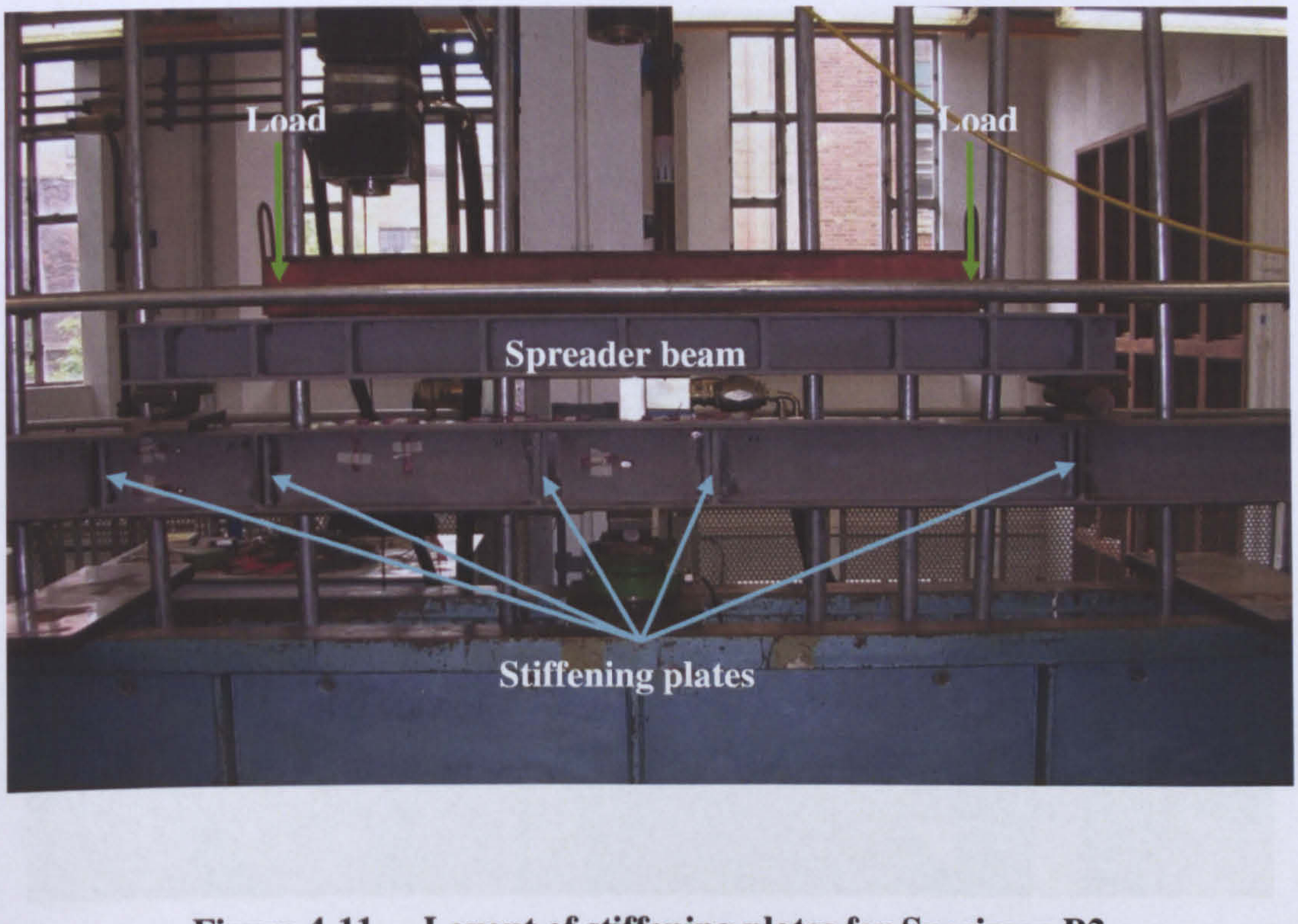

Figure 4-11 - Layout of stiffening plates for Specimen B2

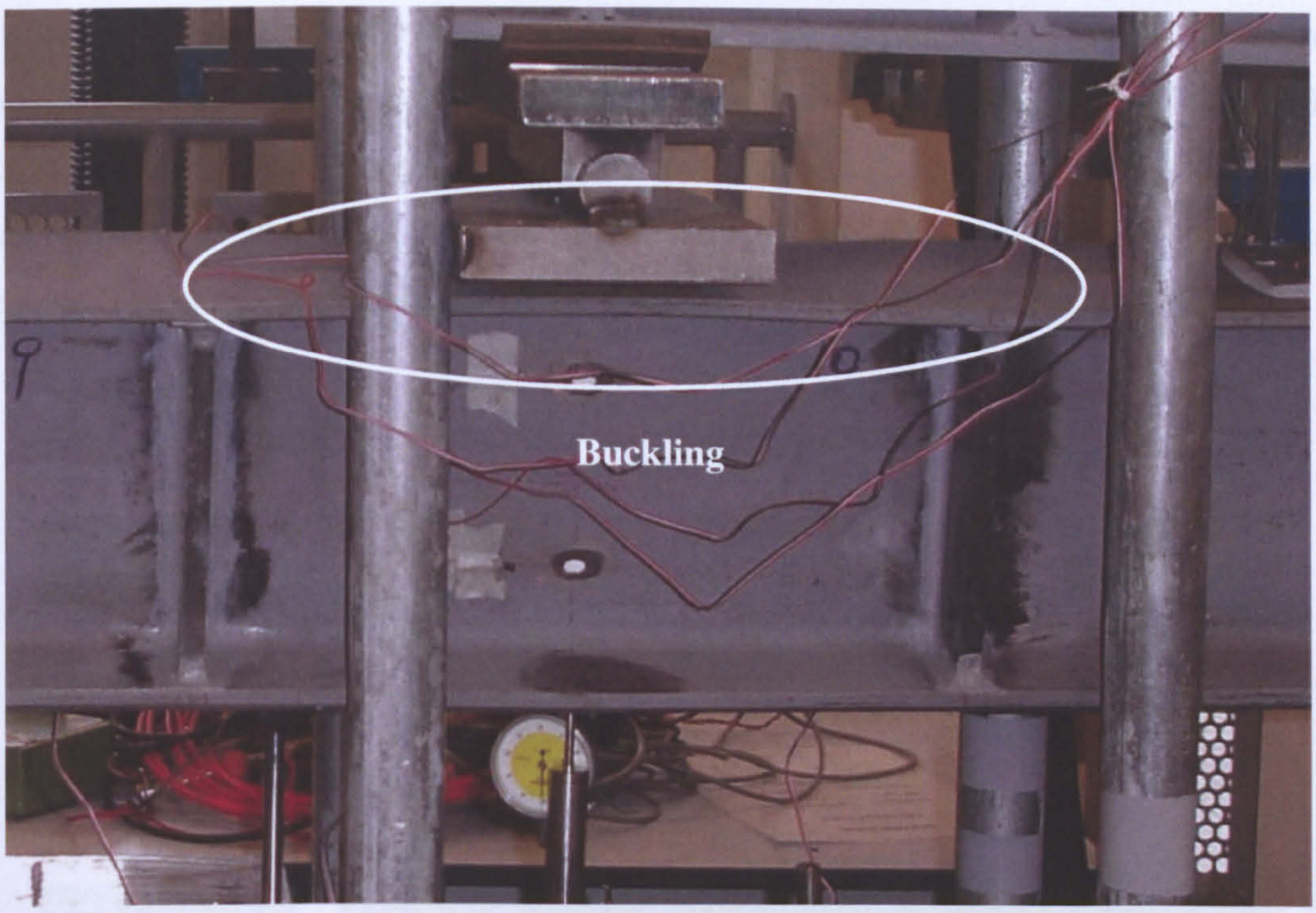

(a)

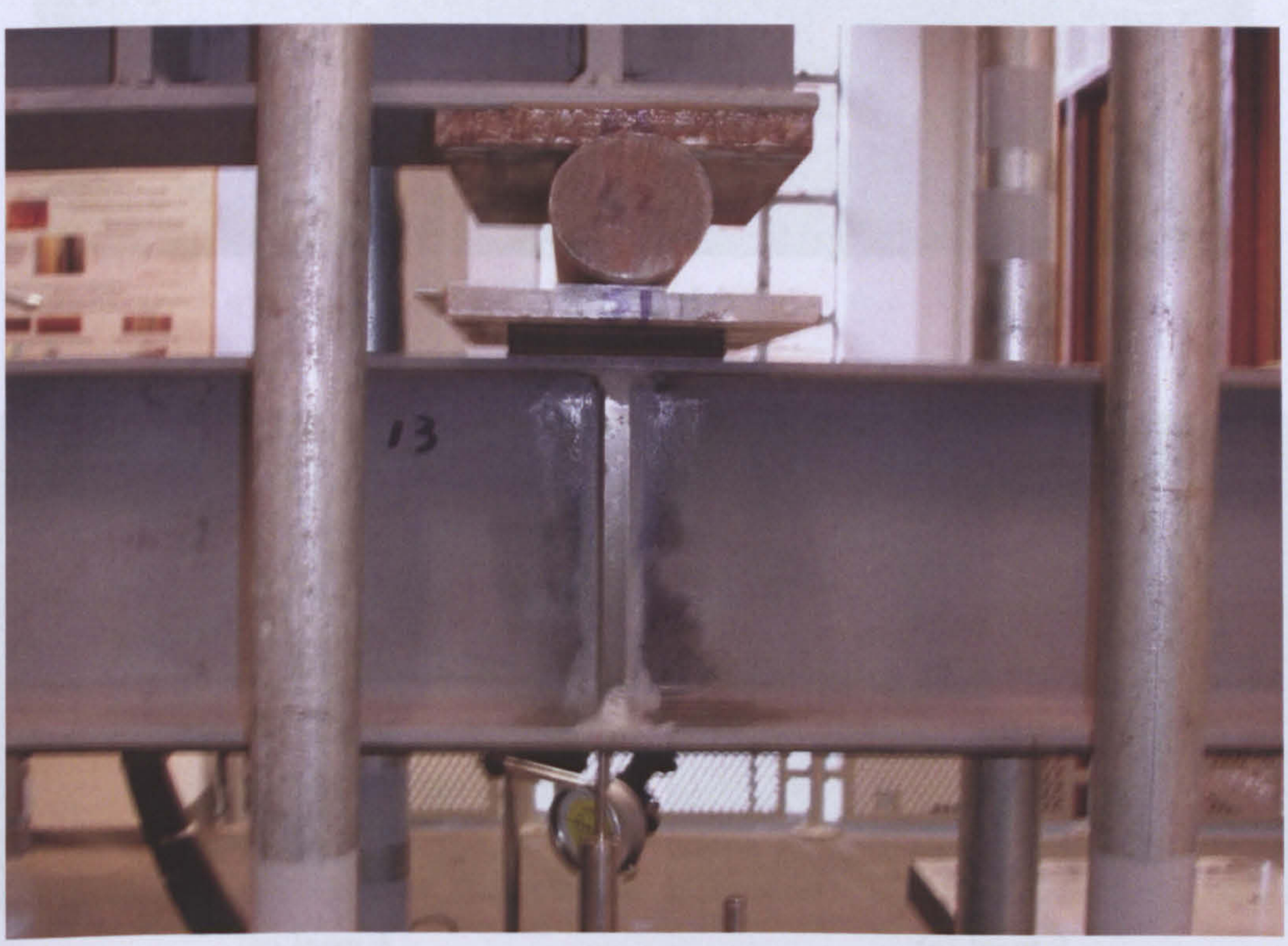

(b)

Figure 4-12 - Layouts of steel stiffening plates at B2: (a) Left hand span and (b) Right hand span

In beam B4, sudden separation occurred first at the left hand span at 277 kN total applied load and then at the right hand span at 315 kN total applied load. Within each span, separation was at the steel/adhesive interface and started at the end of the plate nearer the outer support of the span (Figure 4-13). Bond defects are believed to be the cause. The beam went on to take more load and failed at 411 kN total applied load.

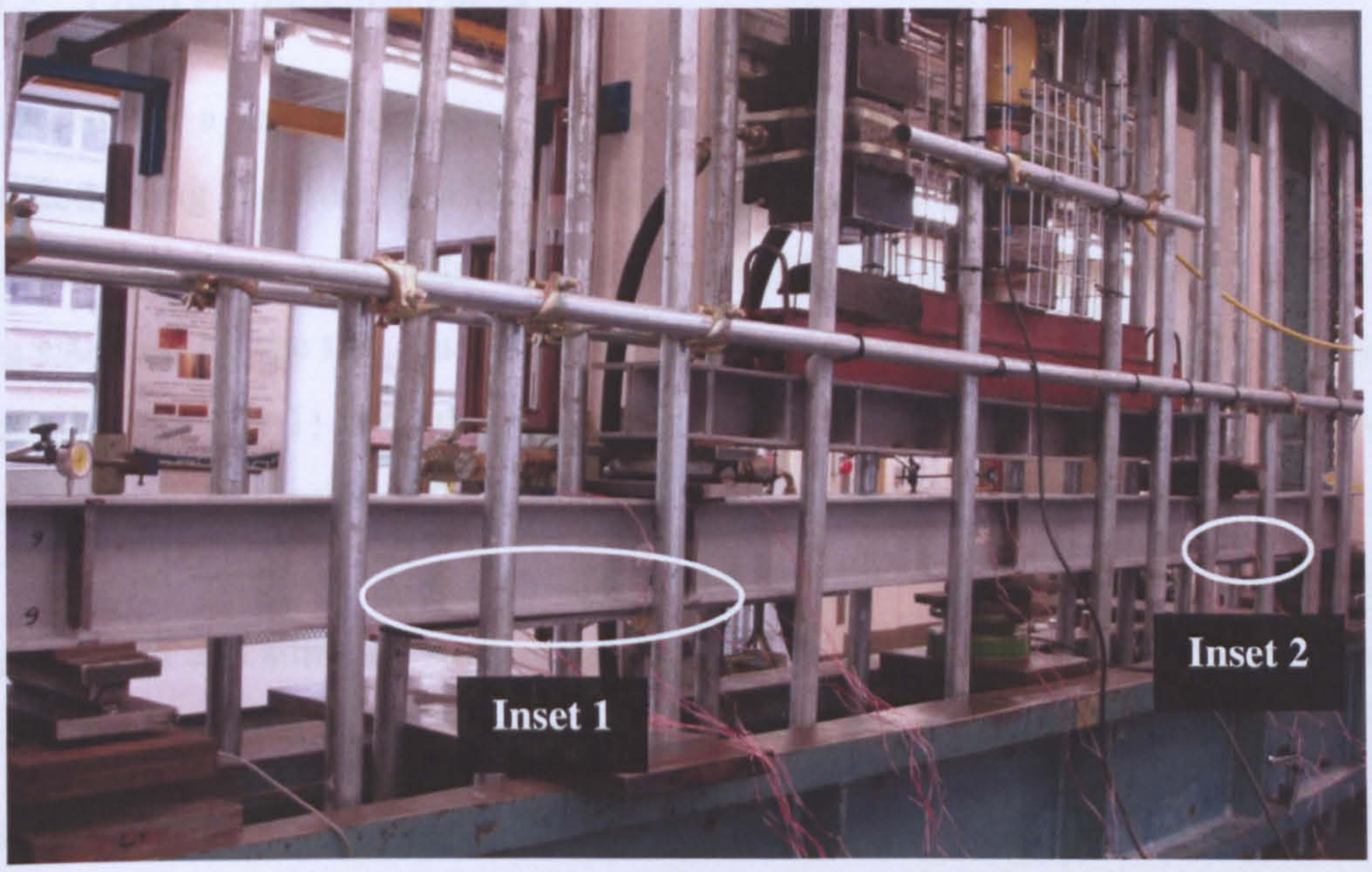

(a) Overview

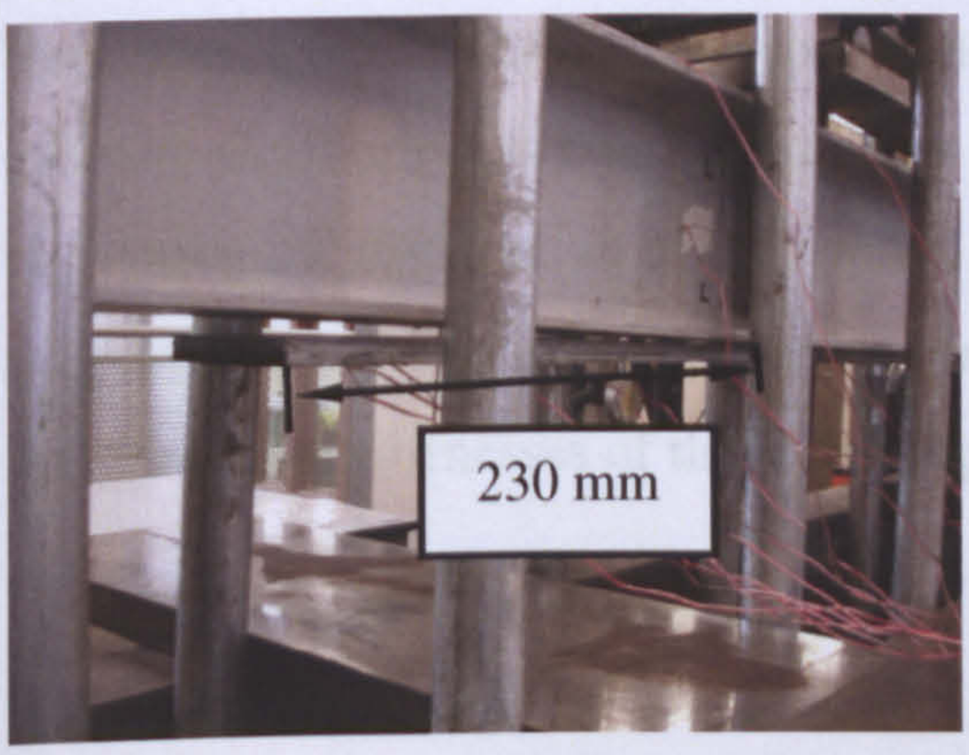

(b) Inset 1

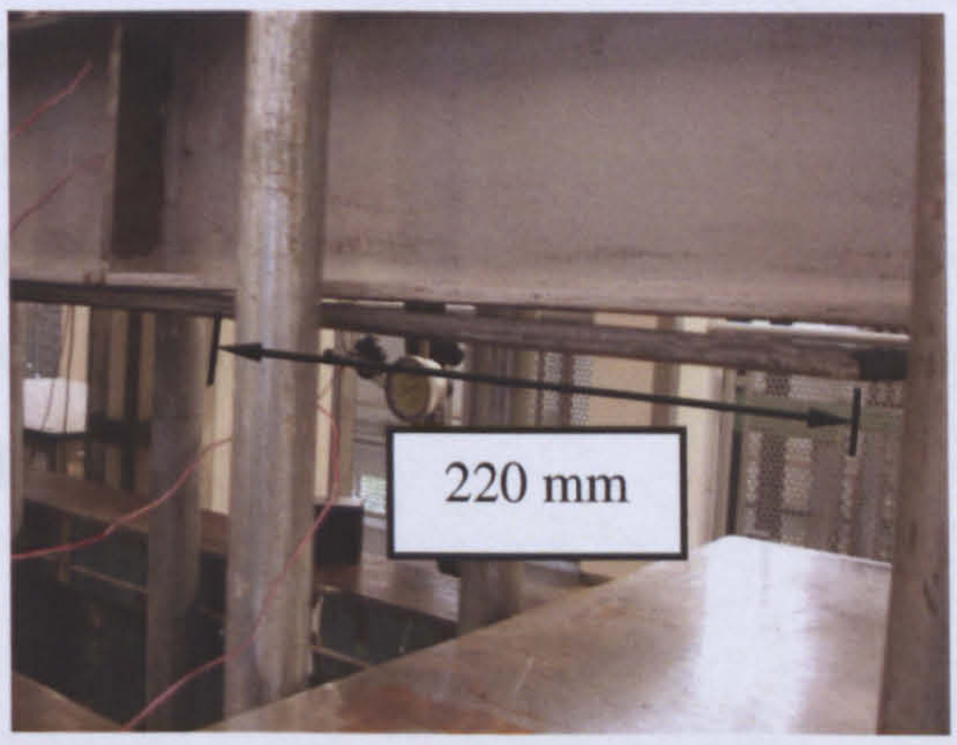

(c) Inset 2

Figure 4-13 - Separation of CFRP plate from the steel beam in specimen B4

Debonding occurred at either the FRP/adhesive interface (specimen B1) or the adhesive/steel interface (specimen B4), indicating that the weakest connection in FRP strengthened steel members can be the interface in contrast to the concrete cover in FRP strengthened RC members. This is mainly attributed to the superior failure properties of steel over concrete. Surface preparation also plays an important role in this finding.

4.4.2 Load equilibrium check

Symmetry is a key assumption in the interpretation of the test results. This may be checked using the mid-span deflections. In addition, equilibrium must be satisfied. To that end, three load cells were used to explicitly check how closely equilibrium was satisfied by the test data. The check was conducted by comparing the total load applied (load cell 1) with the support reactions from load cells 2 and 3 summed as (load cell 2 + load cell 3 × 2); symmetry being implied by equating the reaction forces at both end supports. The resulting variation, for each test, of quotient between applied load and summed support reactions is shown in Figures 4-14. The loads from load cell readings at each load step are given for all specimens in Appendix 4B.

A nearly constant ratio close to 1 (0.96-0.97) in all tests suggests that equilibrium was satisfied by the results. Small differences between load cell calibrations – and not between vertical stiffnesses of the end supports – may have caused the slight disparities from 1. The end supports cannot be culpable for the following reason. If moment equilibrium is considered about the central support it is found that, owing to the symmetric distribution of the applied loads within the two spans about that central support, the two end support reactions must be equal to each other independently of the settlement stiffnesses of those end supports.

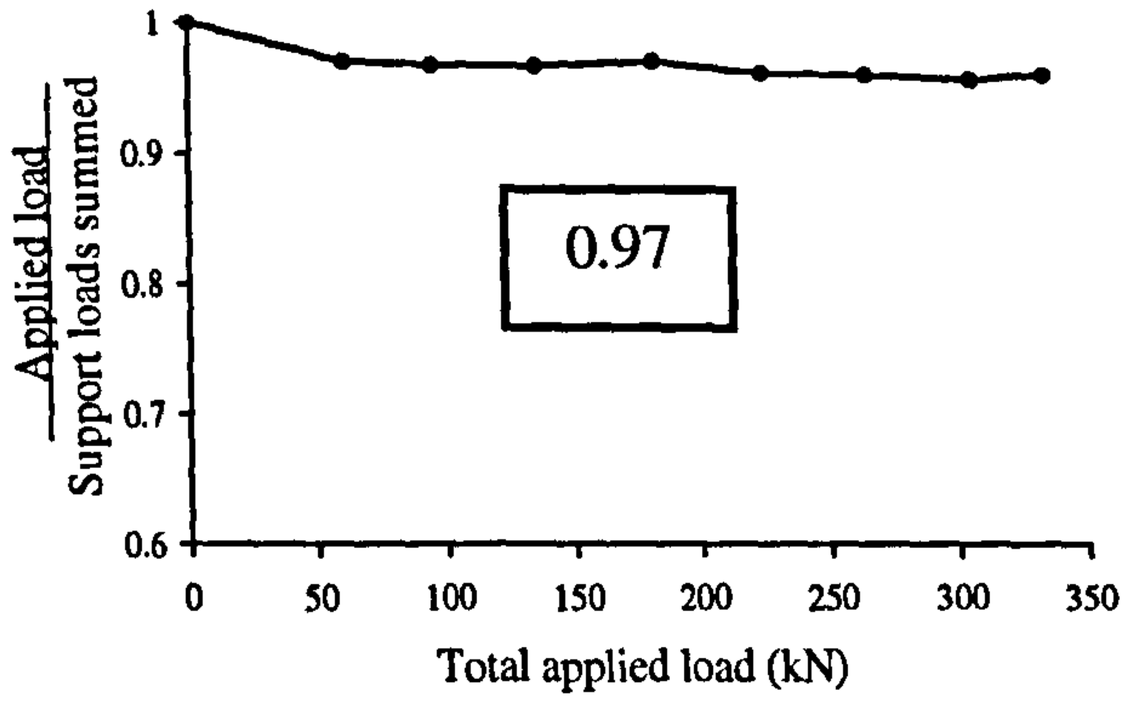

(a) B1

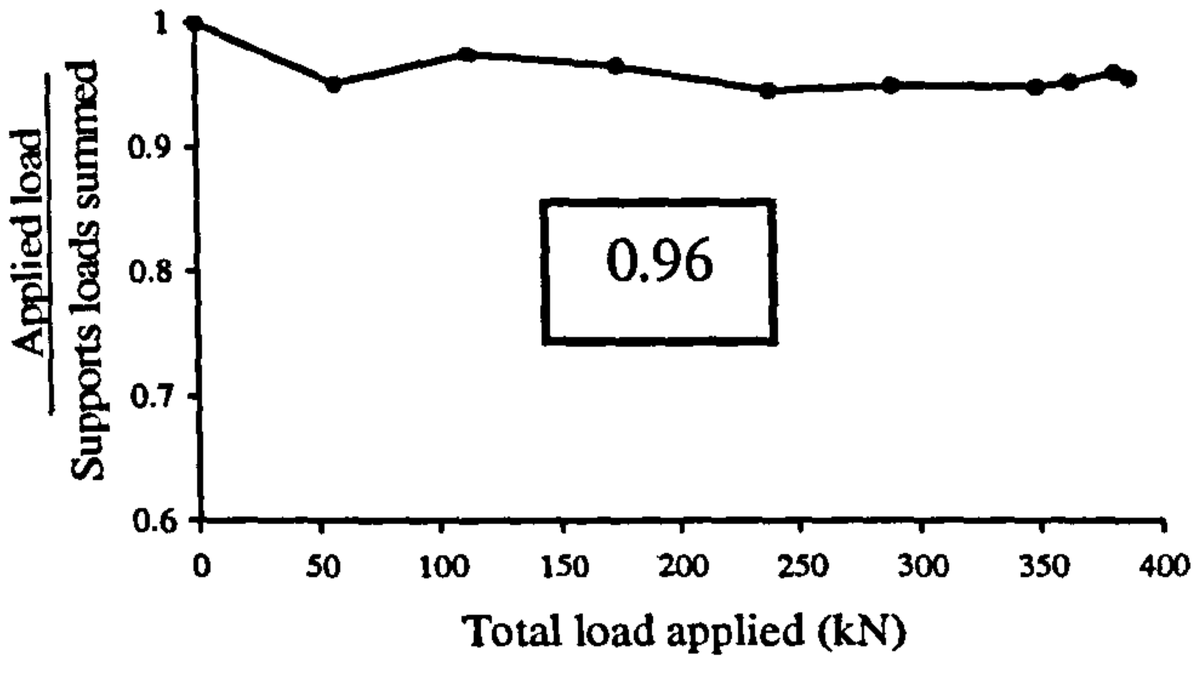

(b) B2

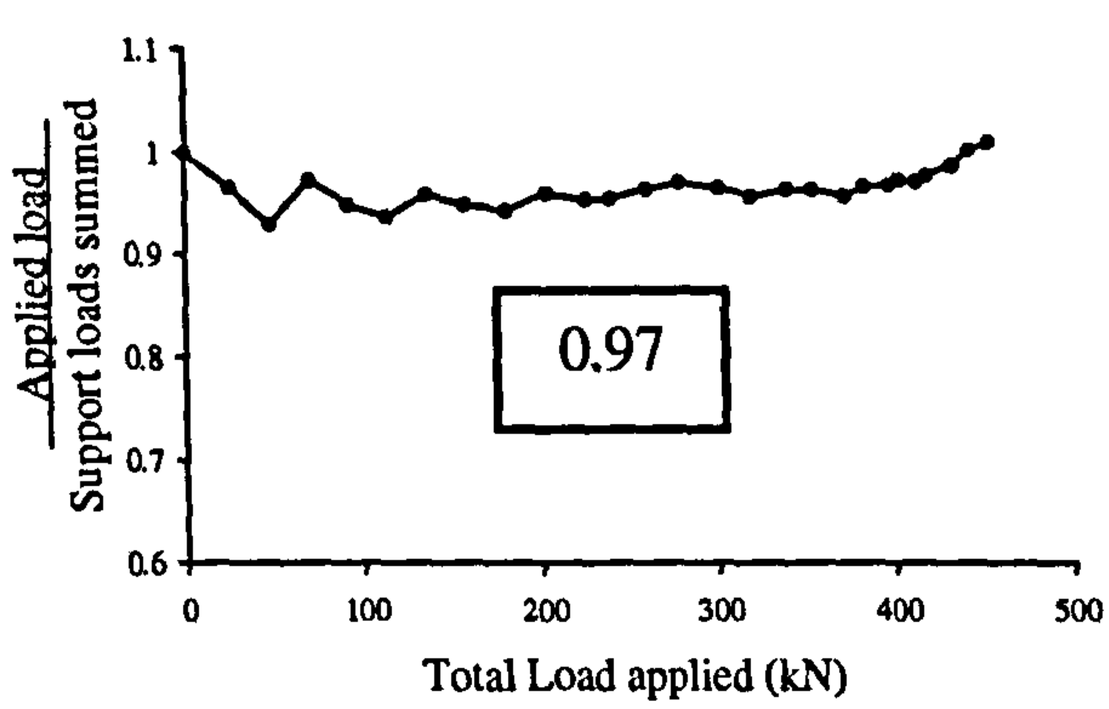

(c) B3

(d) B4

Figure 4-14 - Load equilibrium check for specimens B1 – B4

4.4.3 Strain distributions along the FPR plates

Figure 4-15 shows, for beam B1 at the failure load of 333 kN, longitudinal strain profiles along the inner and outer surfaces of the top CFRP plate, and along the outer surface of the base CFRP plate. The base plate's outer surface strain tends to zero at the ends. The strain profile (including the peak at the load location) for the base plate follows the moment diagram along the member. A similar trend can be seen with the outer surface strain along the top plate. The inner surface strain for the top plate, however, is not zero at the plate's end, as can be seen in Figure 4-15. This suggests local bending of this plate near its curtailment. Using the moment diagram deduced from the load cell readings (Figure 4-16), the point of contraflexure is located *circa* 1615 mm from the end support. This correlates well with that deduced from the point where all three strains are zero in Figure 4-15. The maximum strain at the outer surface of the base plate is bigger than that of the top plate. Noting that similar plates were used at the top and the base, this suggests a bigger moment at the mid-span sections relative to the moment over the central support, which is confirmed in the moment diagram shown in Figure 4-16.

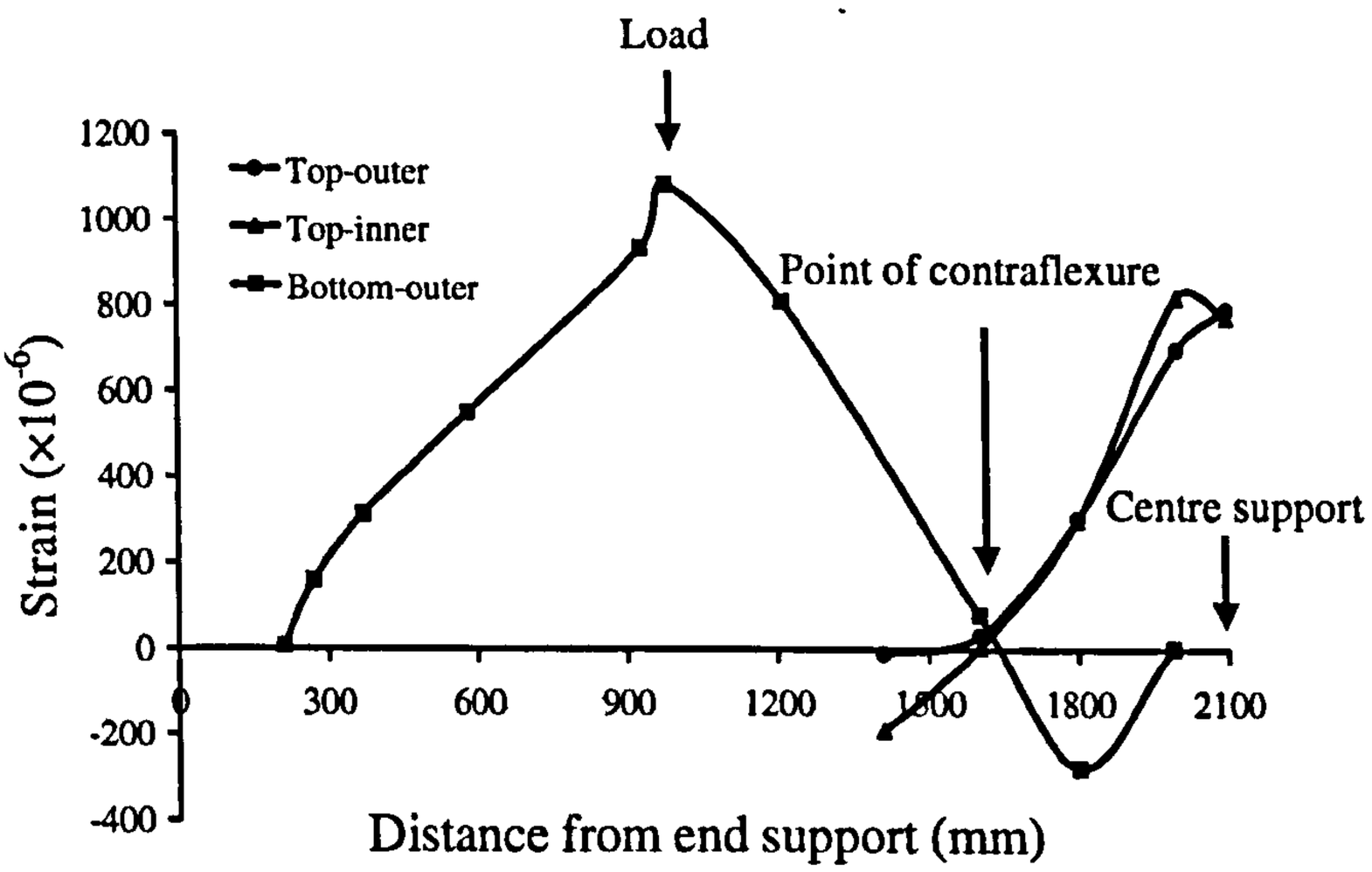

Figure 4-15 - Strains (tensile +ve) along FRP plates (B1) at 333 kN load

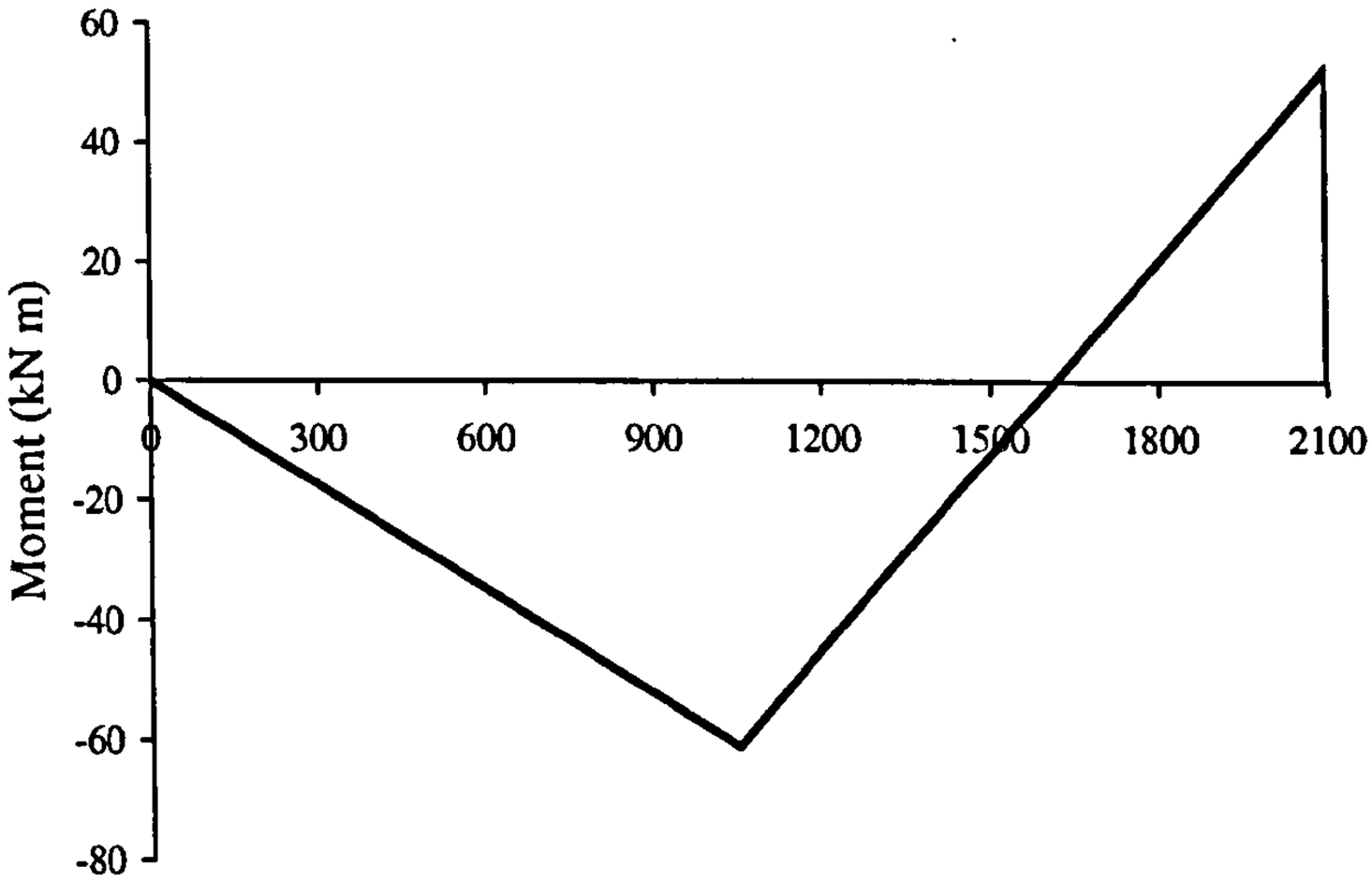

Figure 4-16 - Moment diagram for B1 at 333 kN load (from load cell readings)

A feature of FRP-strengthening of an indeterminate member is that the FRP plate may be subject to compression if it extends beyond any points of contraflexure. The further beyond the point of contraflexure the plate extends, the higher are the compressive strains. This can cause buckling of the CFRP fibres. Also, any offsets of plate curtailment from nearby contraflexure can lead to high bond stresses and consequent brittle end peel of the plate from the beam. Both these effects have been confirmed in the present tests. Figure 4-15 clearly shows that significant compressive strains developed in the top and base plates on opposite sides of contraflexure. The peak compressive measured strain in the base plate corresponds to a compressive stress of almost 40 N/mm^2. Also, note that the base plate's curtailment is further away from contraflexure than the top plate's. Thus, given that the plates are similar, higher end bond stresses may be expected for the base plate. This probably explains the observation stated earlier that end peel was noted for the *base* plates but not for the top ones.

Similar trends can be seen with B2 as shown in Figure 4-17. There is little difference between the strains at the inner and outer surfaces of the top plate apart from very near the end. Noting that the plate is much thinner (1.5 mm) thick compared with that for specimen B1 (8 mm), this suggests that local bending and/through thickness

variations are insignificant for the thin plate. This can also be seen from the interfacial bond stress variations as will be discussed later. Again, the location of the point of contraflexure correlates well with the moment diagram obtained from load cell readings (Figure 4-18).

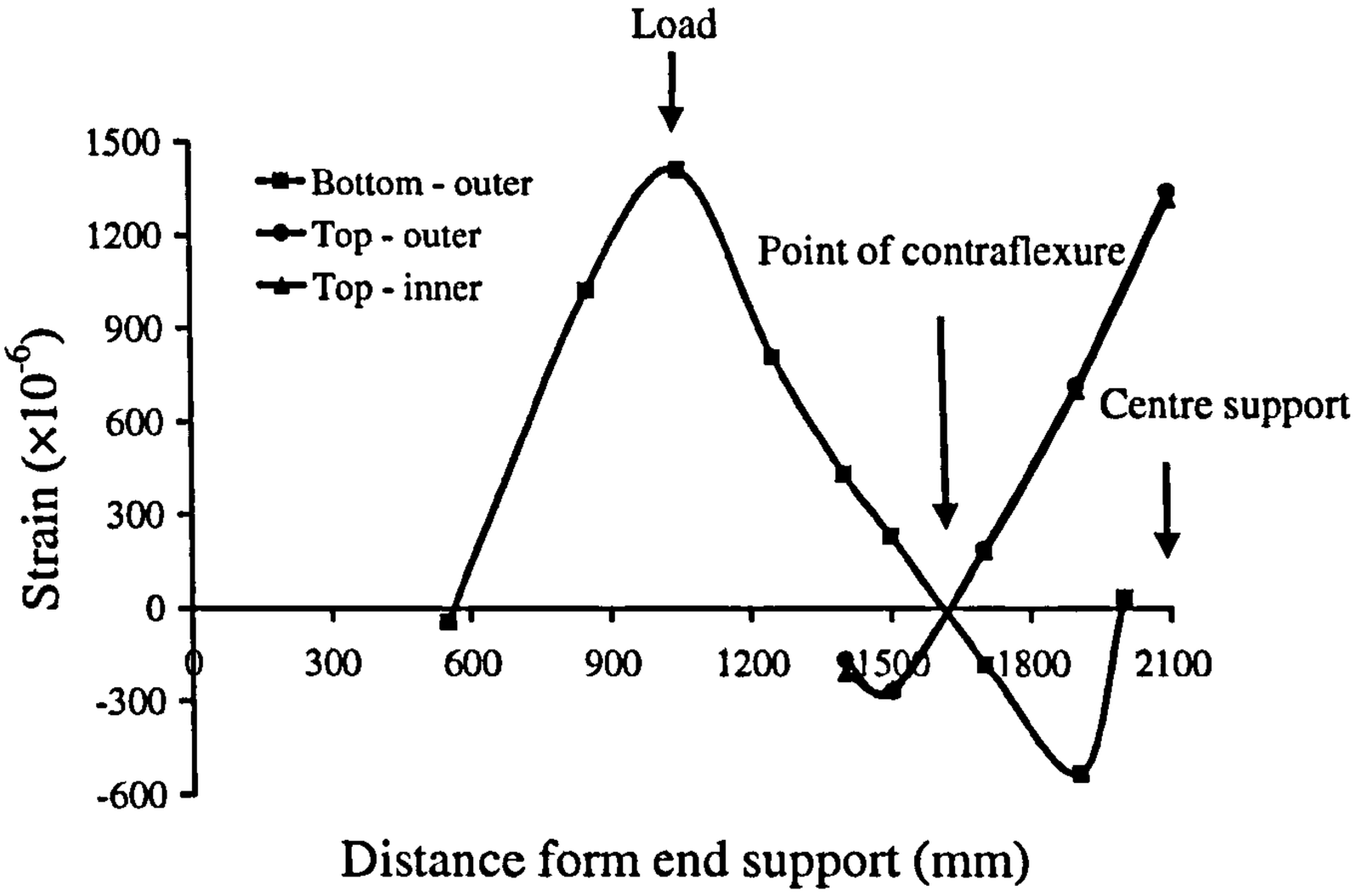

Figure 4-17 - Strain distribution along FRP surfaces (B2) at 388 kN load

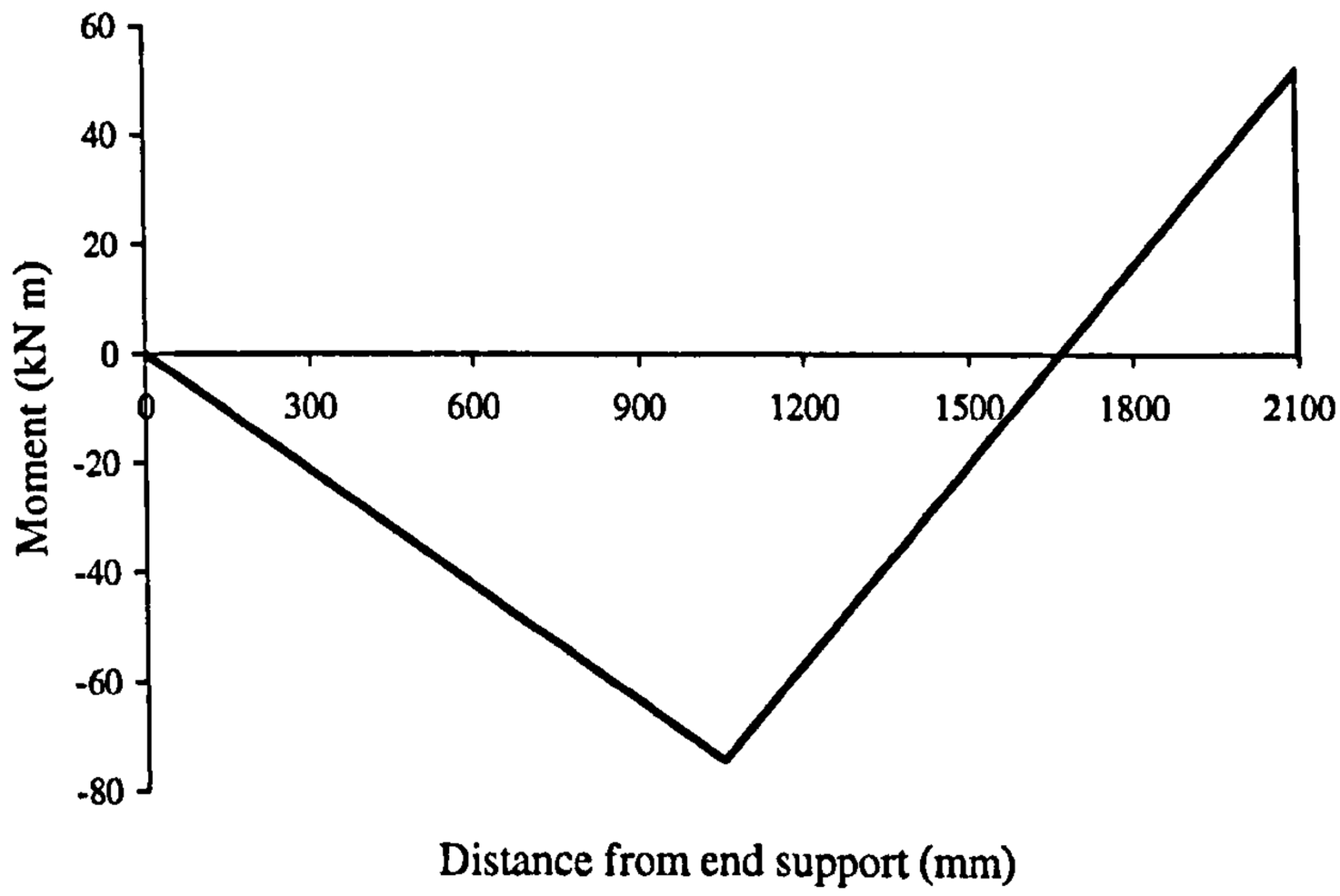

Figure 4-18 - Moment diagram for B2 at 388 kN load (from load cell readings)

In specimen B3, only a top plate (of 16 mm thickness) was applied over the centre support region. Strain gauges were applied symmetrically about the centre support section all the way along the outer surface of the plate. This has enabled a check on symmetry (see Figure 4-19). The symmetric strain distribution about the centre support section indicates that the symmetry assumption is satisfied by the strains.

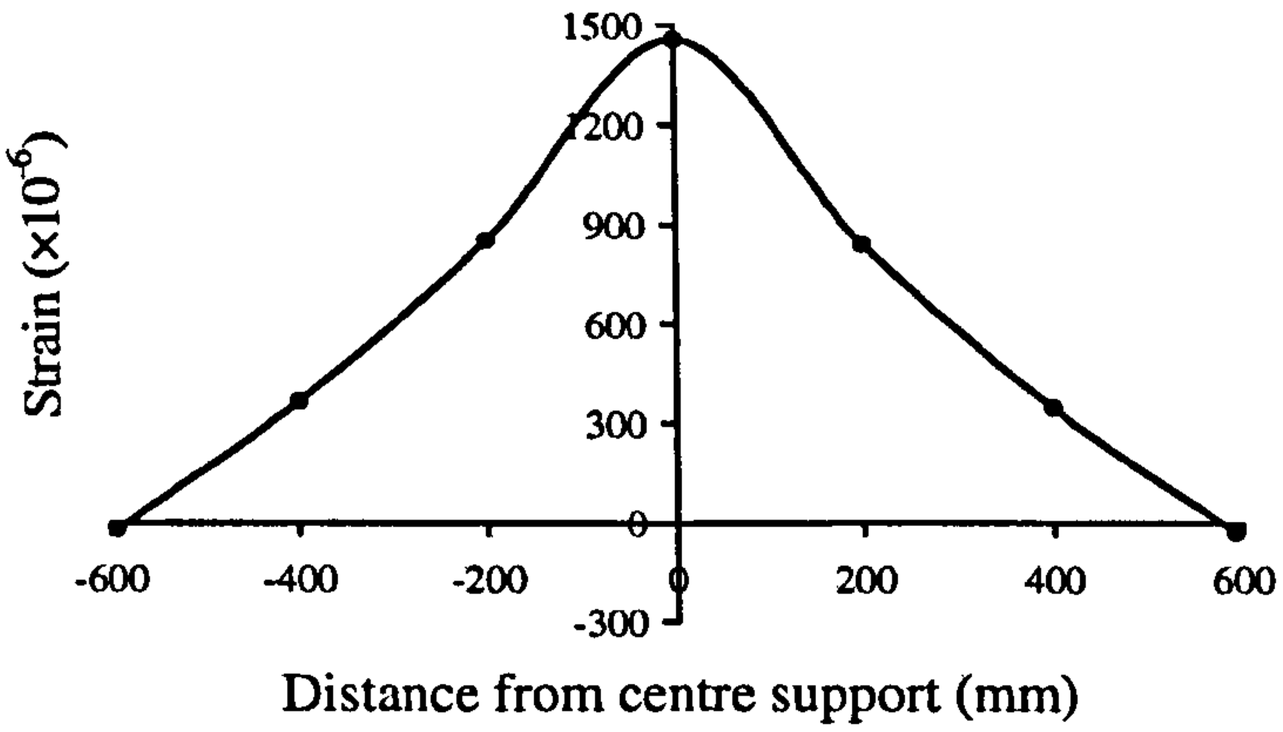

Figure 4-19 - Strain distribution along FRP surfaces (B3) at 453 kN load

For specimen B4, Figure 4-20 shows the strain distribution along the left hand span plate surfaces at 247 kN total applied load before the soffit CFRP plate separated suddenly from the steel beam. The point of contraflexure evaluated from the moment diagram indicates that the plate was within the sag moment zone, but from the strain distribution there was clearly some local bending near both ends of the plate – the outer surface was in compression and the inner surface in tension. Noting that strain gauges were normally placed a short distance (5-7 mm) away from the end of the plate and that the strain distribution is just before debonding occurred, this might suggest that there was substantial local bending occurring as the plate 'tried' to bend away from the steel beam (Figure 4-21). Recall that separation occurred over 230 mm distance from the plate end close to the end support. There might also be some slip (although not visually observed) gradually building up as the inner surface strains change in a somewhat irregular manner.

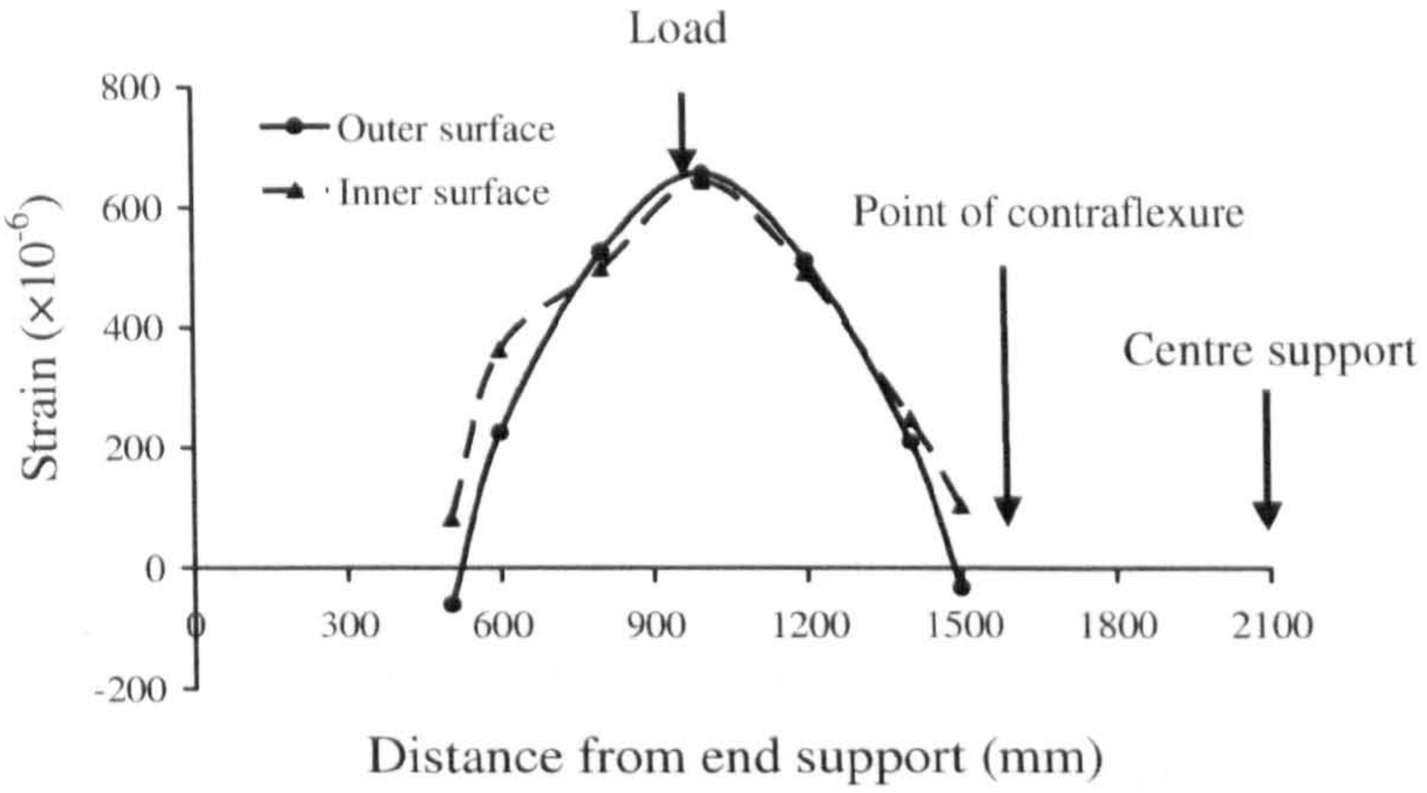

Figure 4-20 - Strain distribution along FRP surfaces (B4) at 247 kN load

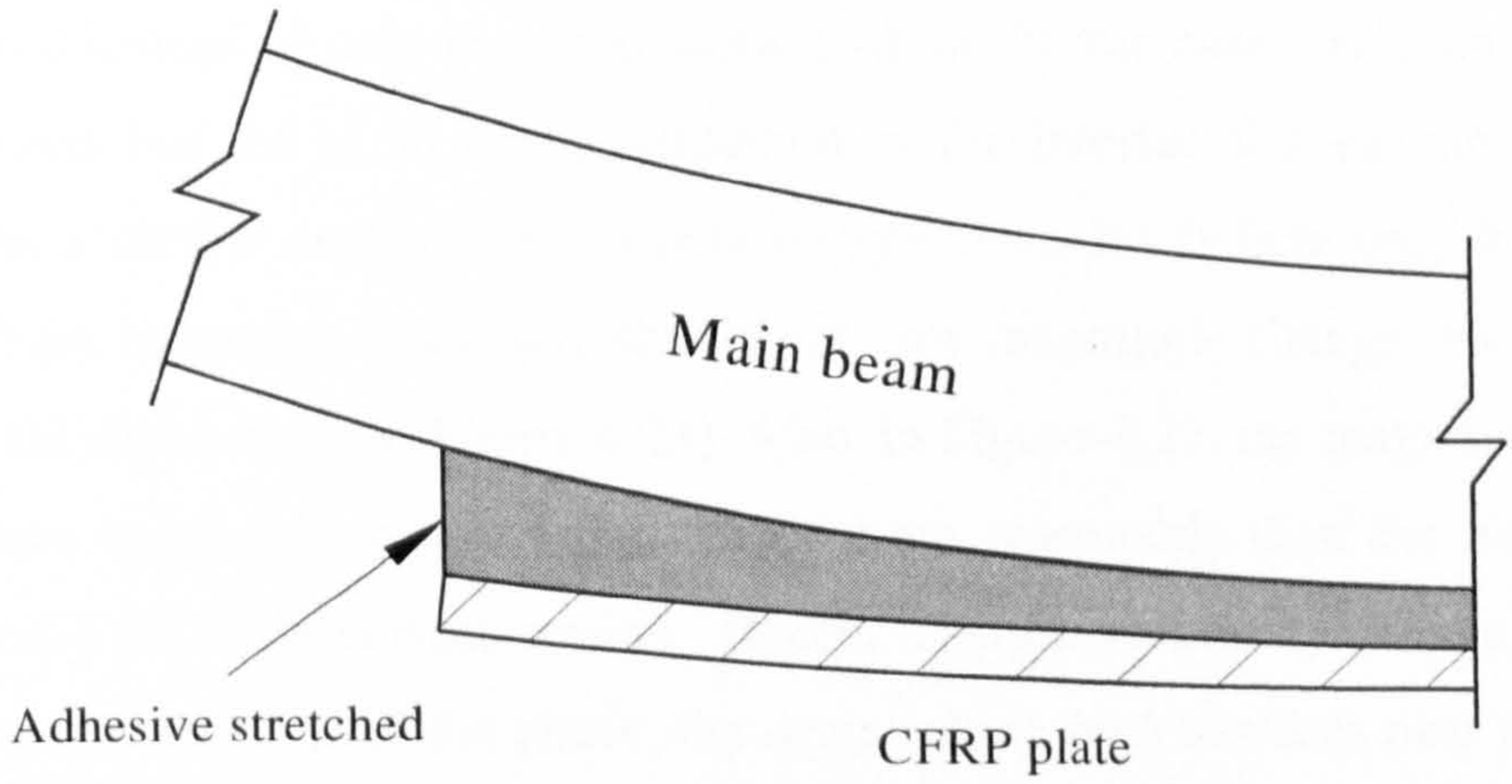

Figure 4-21 - Mechanism of development of vertical stresses in adhesive near plate ends

4.4.4 Average interfacial shear stresses

For a plate bonded to a main beam, the average interfacial shear stress at the bonded surface of the plate between two locations distance Δx apart along the plate can be estimated using the following equation:

$$\tau_a = E_p t_p \frac{\Delta \varepsilon_p}{\Delta x} \tag{4-1}$$

where τ_a is the average shear stress; E_p is Young's modulus of the plate material; t_p is the thickness of the plate and $\Delta\varepsilon_p$ is the difference in longitudinal strain between the two locations along the plate. The deviation of the equation is given in Appendix 4-1.

Using Equation (4-1) as a base, two cases were considered for the top plate to investigate the effects, on the shear bond stresses, of local bending and/or high plate thickness, namely: (1) using outer surface strain readings only; and (2) using the *average* of the outer and inner surface strain readings. Figure 4-22 shows for specimen B1 the average shear stress profile along the plate for each case. The assumption is made that strains (along both inner and outer surfaces) at the plate's ends are zero. It is clear that the strain variation through the thickness of the plate leads to a large difference in the deduced shear stresses near the plate's end. Near the left end, the shear stress changes from 1.2 N/mm^2 to 11 N/mm^2 when the average FRP strain is used instead of only the outer surface strain. In this case, using only surface strain readings has led to an under-estimation of the interfacial shear stresses. The results from a similar analysis of test data for specimen B4 (where only base plates were used) for these two cases have shown not only magnitude change, but also *sign* change in the shear stresses (Figure 4-23). Also, in Figure 4-23, the magnitudes of the bond stresses based on average strains seem more reasonable than the high values based on only the outer surface strains. Hence, to more accurately deduce the shear bond stress near the ends of the plates, the strains along *both* surfaces near the plates' ends need to be taken into account.

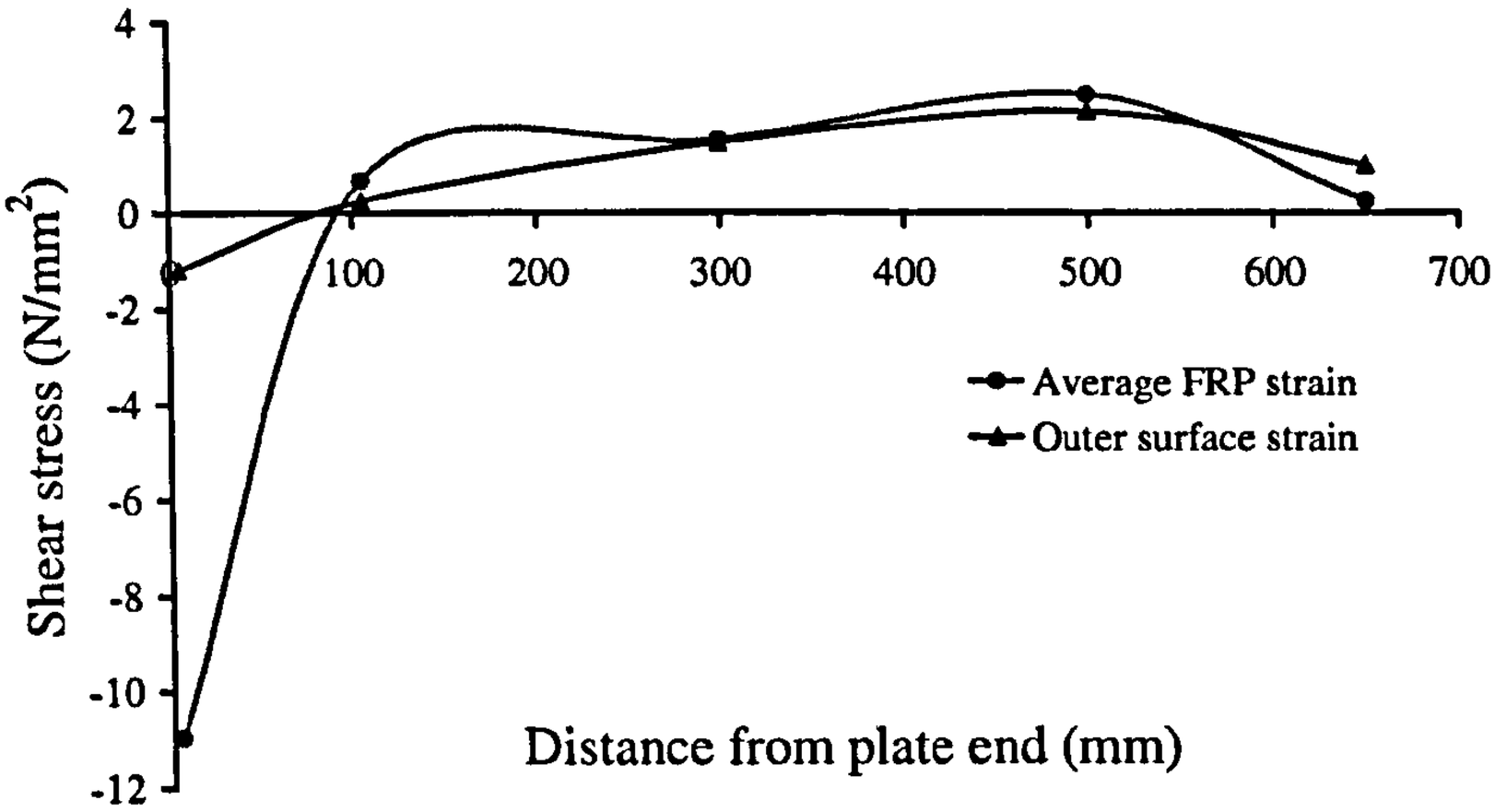

Figure 4-22 - Shear bond stress for top plate (B1) at 333 kN load

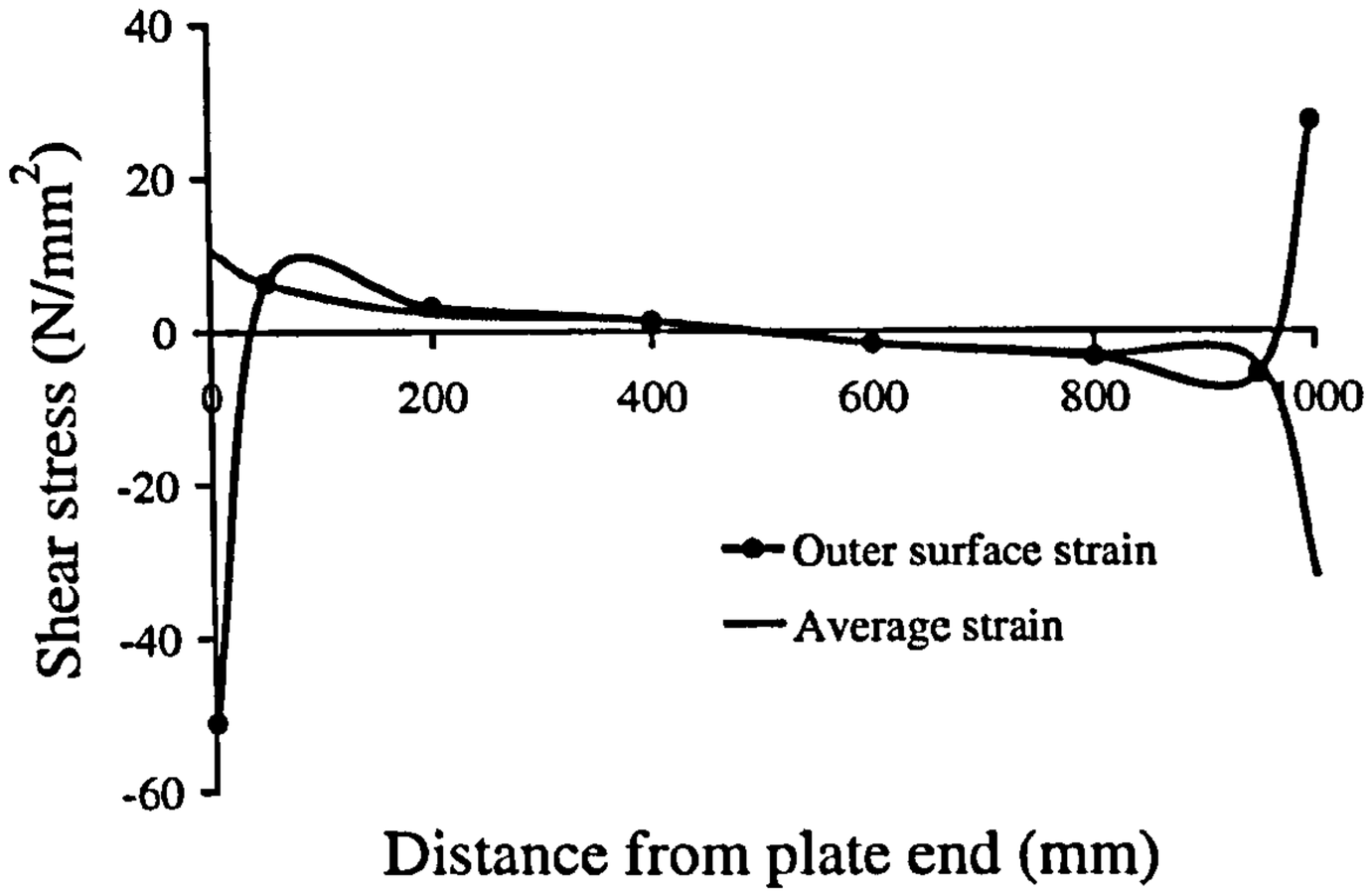

Figure 4-23 - Shear bond stress for top plate (B4) at 247 kN load

Similar analyses for specimen B2 where a thinner plate (1.5 mm thick) was used have shown little difference in shear stresses between the two cases as can be seen in Figure 4-24.

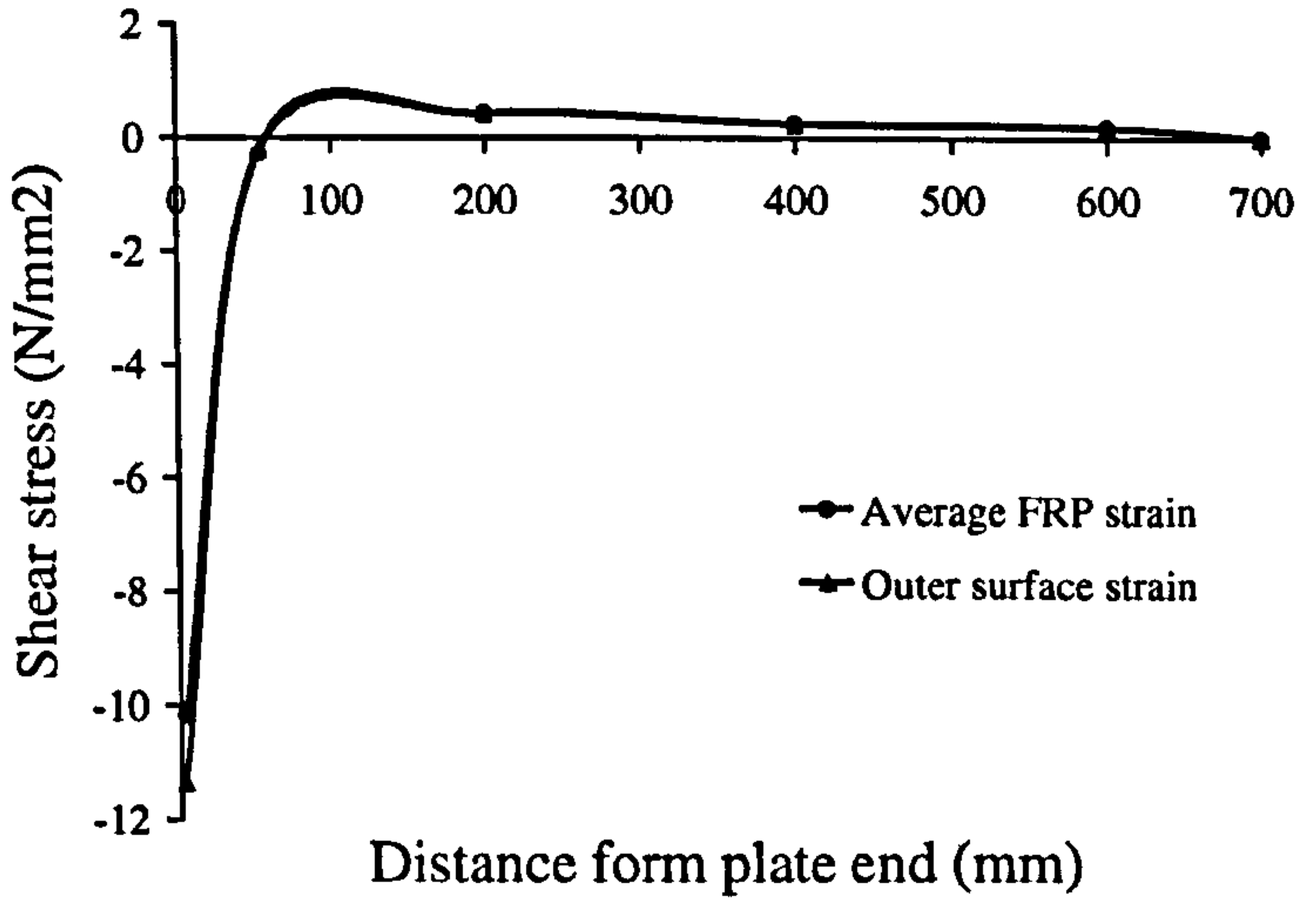

Figure 4-24 - Shear bond stress for top plate (B2) at 388 kN load

Shown in Figure 4-25 is the shear stress profile at the adhesive-plate interface for specimen B3. As strain gauges were only applied along the outer surface of the plate, potential effects of the through-thickness strain variation cannot be considered here. Significantly different 'actual' shear stresses could be expected as a much thicker plate (16 mm) was used. However, these peak shear stresses can be reasonably assumed to be supported in the FRP-steel connection through adhesive as shear stress of as high as 16 N/mm^2 in the adhesive has been reported for FRP-concrete connection in Bizindavyi and Neale (1999).

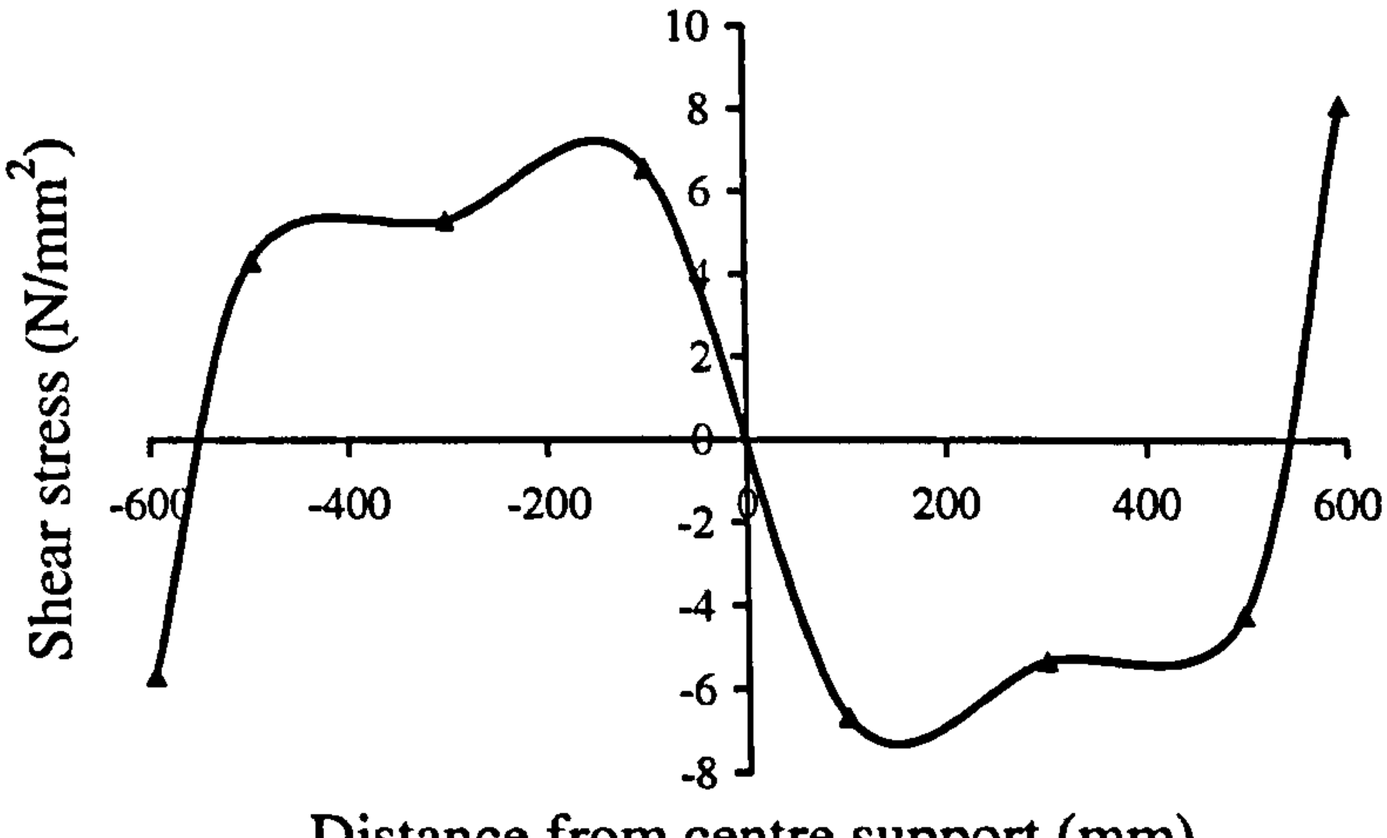

Figure 4-25 - Shear bond stress for top plate (B3) at 453 kN load

Figure 4-26 shows for specimen B1 the average shear stress profile along the base CFRP plate (strains from only the outer surface were available for this plate). After a small value near the end of the plate, the shear stress reaches a peak value at about 40 mm from the plate's end. The shear stress profile follows the slope of the strain distribution and changes sign near where load was applied. This somewhat approximates the shear force variation along the member. The shear stress also changes sign towards the plate's end near the centre support and is close to zero at the end. This is due to the fact that the strain gauge nearest to the centre support is located where the plate has peeled off. The sudden increase in shear stress at a distance of 840 mm from the plate end (Figure 4-26) is due to the kink in the strain distribution in Figure 4-15. The shear bond stress distribution along the base plate for specimen B2 (Figure 4-27) generally follows the same trend. A much bigger shear stress was shown near the plate end closer to the end support. Two causes might account for this. Firstly, the cut-off point (close to the end support) is further away from the end support for specimen B2 compared to specimen B1. Secondly, the potential underestimation of the shear stresses using outer surface strain readings would have been smaller for specimen B2 as a thinner plate (4 mm) was used compared with the 8 mm thick plate in specimen B1.

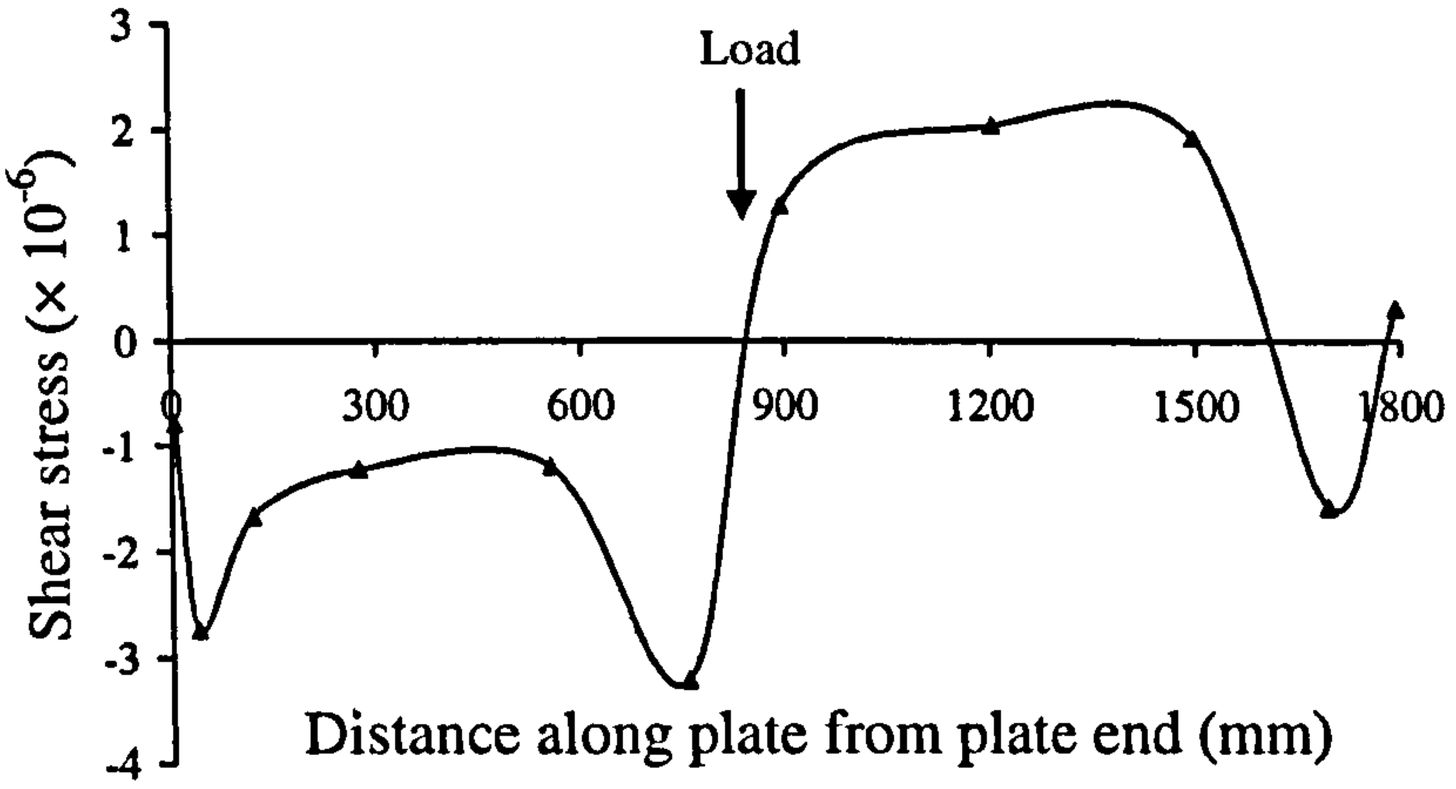

Figure 4-26 - Shear stress for base plate (B1) at 333 kN load

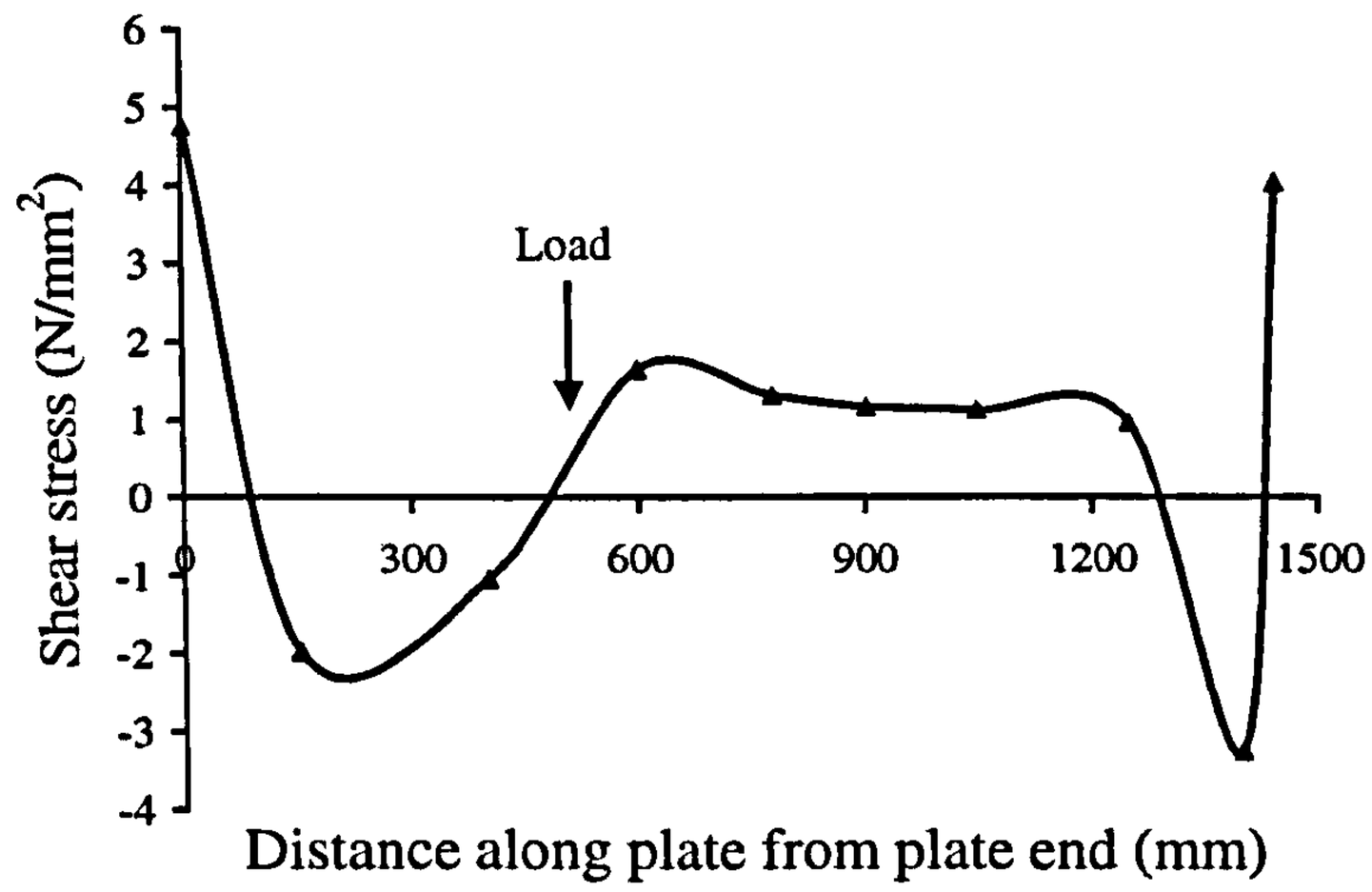

Figure 4-27 - Shear stress for base plate (B2) at 388 kN load

There were not sufficient strain gauges on the plate's surfaces near the ends, so the actual shear stress variations along the plates (including the peak shear stress near the plates' ends) were not determined accurately. However, while the effect on the shear bond stresses of this through-thickness strain variation in the FRP plate remains to be explored further, using outer surface strain readings only may lead to incorrect estimation of the shear stresses, especially for thick plates.

4.4.5 Average interfacial normal stresses

For plates where strain gauges were applied at both outer and inner surfaces, normal stress may also be estimated once the average shear stresses were evaluated using the following equation:

$$\sigma_a = -\frac{E_p t_p^3}{12}\frac{\Delta\left(\frac{\Delta\phi_p}{\Delta x}\right)}{\Delta x} + \frac{t_p}{2}\frac{\Delta\tau_a}{\Delta x} \tag{4-2}$$

where Δx is the distance between the adjacent strain gauges; ϕ_p is the local curvature of the CFRP plate and can be expressed as:

$$\phi_p = \frac{\varepsilon_o - \varepsilon_i}{t_p} \tag{4-3}$$

where ε_o and ε_i are outer and inner surface strains of the CFRP plate, respectively. The derivation of the equation is also given in Appendix 4-1.

The results together with those for the average shear stresses are shown for specimens B1, B2 and B4 in Figures 4-28, 4-29 and 4-30, respectively. Normal stresses peak near the plates' ends and there is a change of sign in normal stresses some distance further away from the plates' ends in all cases. The normal stresses then level up to a value close to zero towards the middle of the plates. This somewhat agrees with the general predictions of normal stresses in FRP-plated beams (Smith and Teng 2001, Yang *et al.* 2004). Although subject to a lower load compared to specimen B1 and B2, specimen B4 has a bigger peak normal stress value near the plate ends. This is due to a combination of the bigger distance away from the outer support (zero moment section) of the plate's adjacent end and bigger contribution of change in shear stresses. The average peak normal stress at the plate's end close to the outer support – from which end brittle separation initiated – is bigger than that near the end close to the centre support.

Again, there were not sufficient strain gauges on the plate's surfaces near the ends, so the actual normal stress variation in the adhesive (including the peak shear stress near the plate's end) could not have been determined more accurately. Nonetheless, this provides a viable means for interfacial normal stresses to be determined.

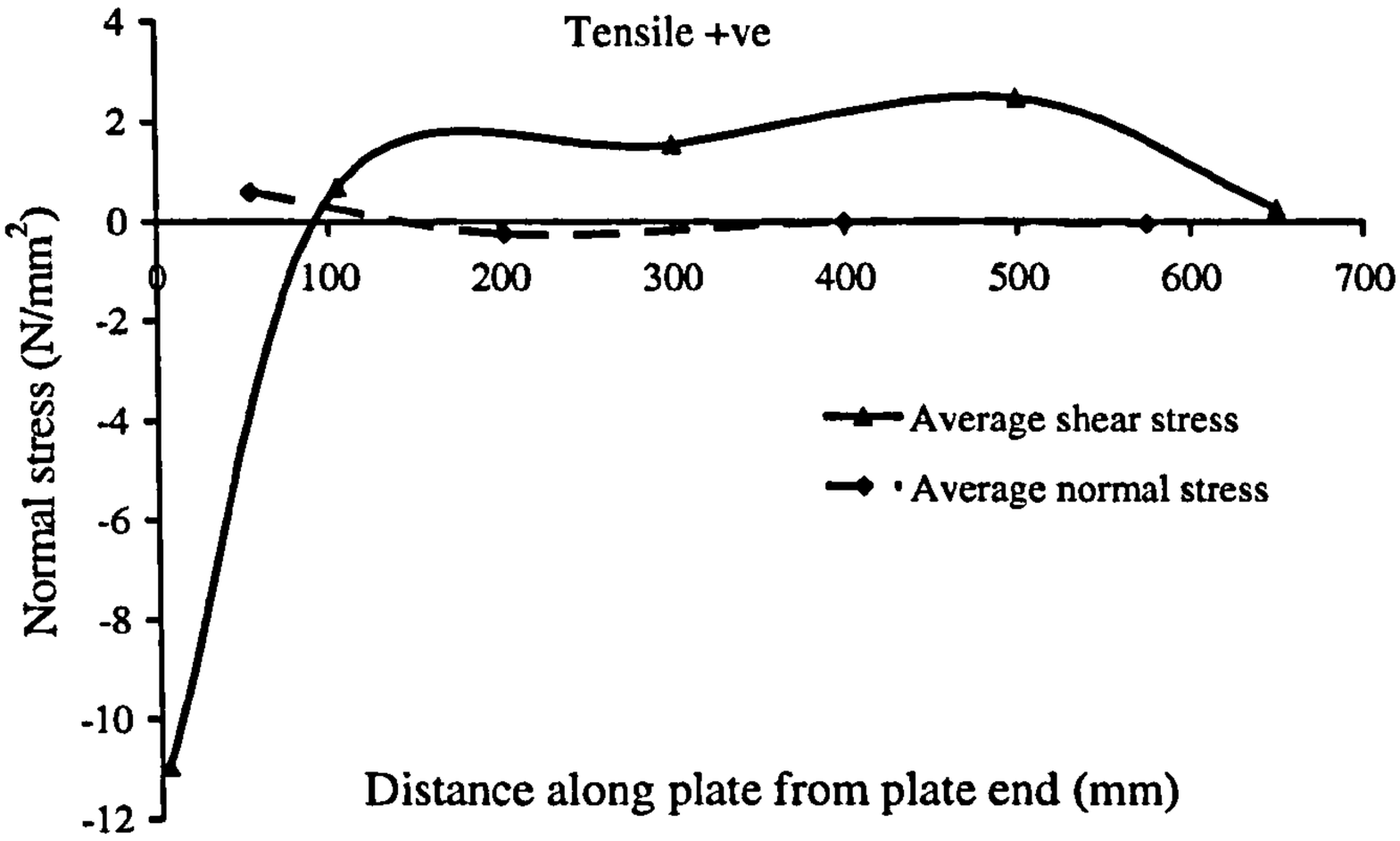

Figure 4-28 - Normal bond stress along base plate (B1) at 333 kN load

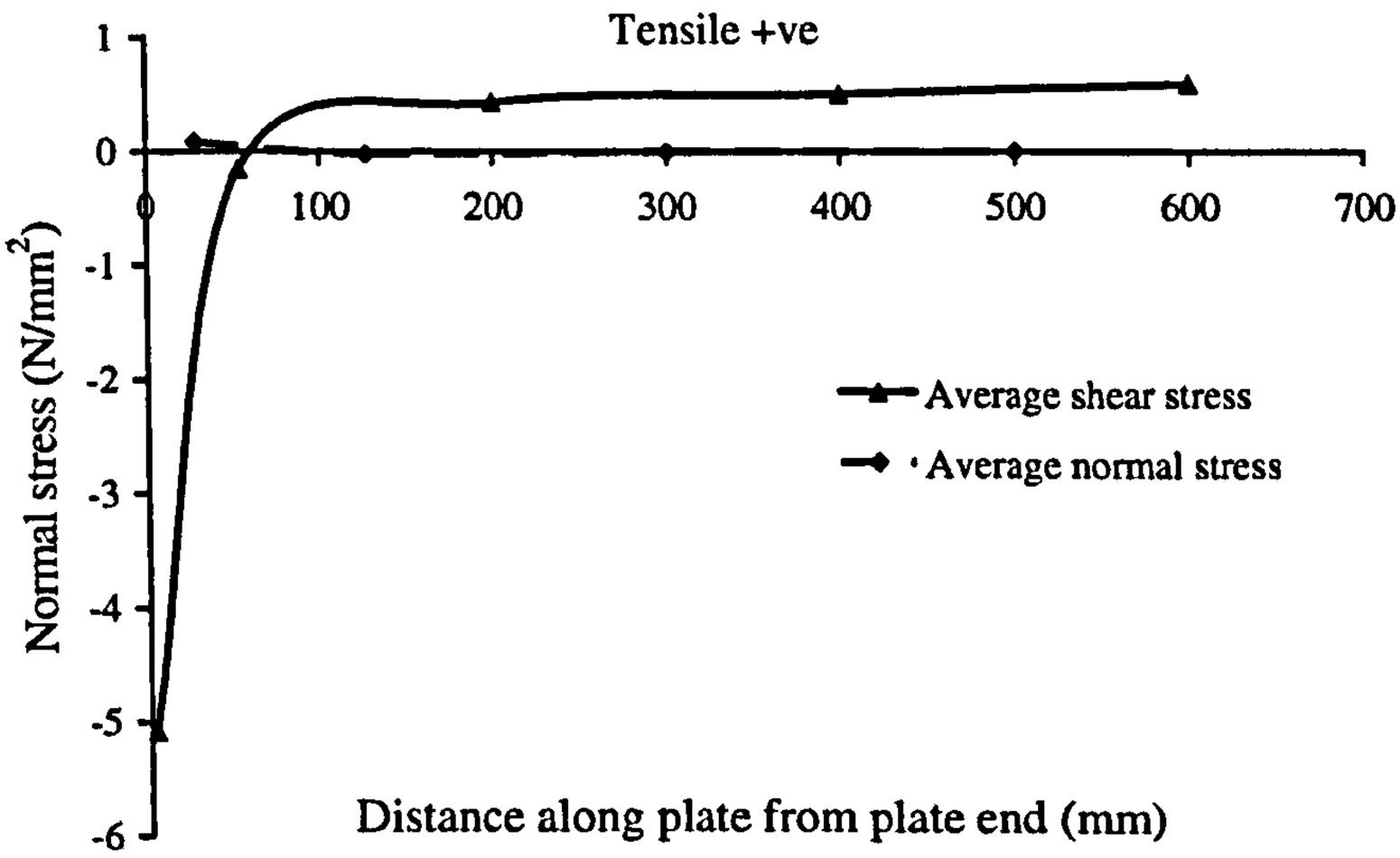

Figure 4-29 - Normal bond stress along top plate (B2) at 388 kN load

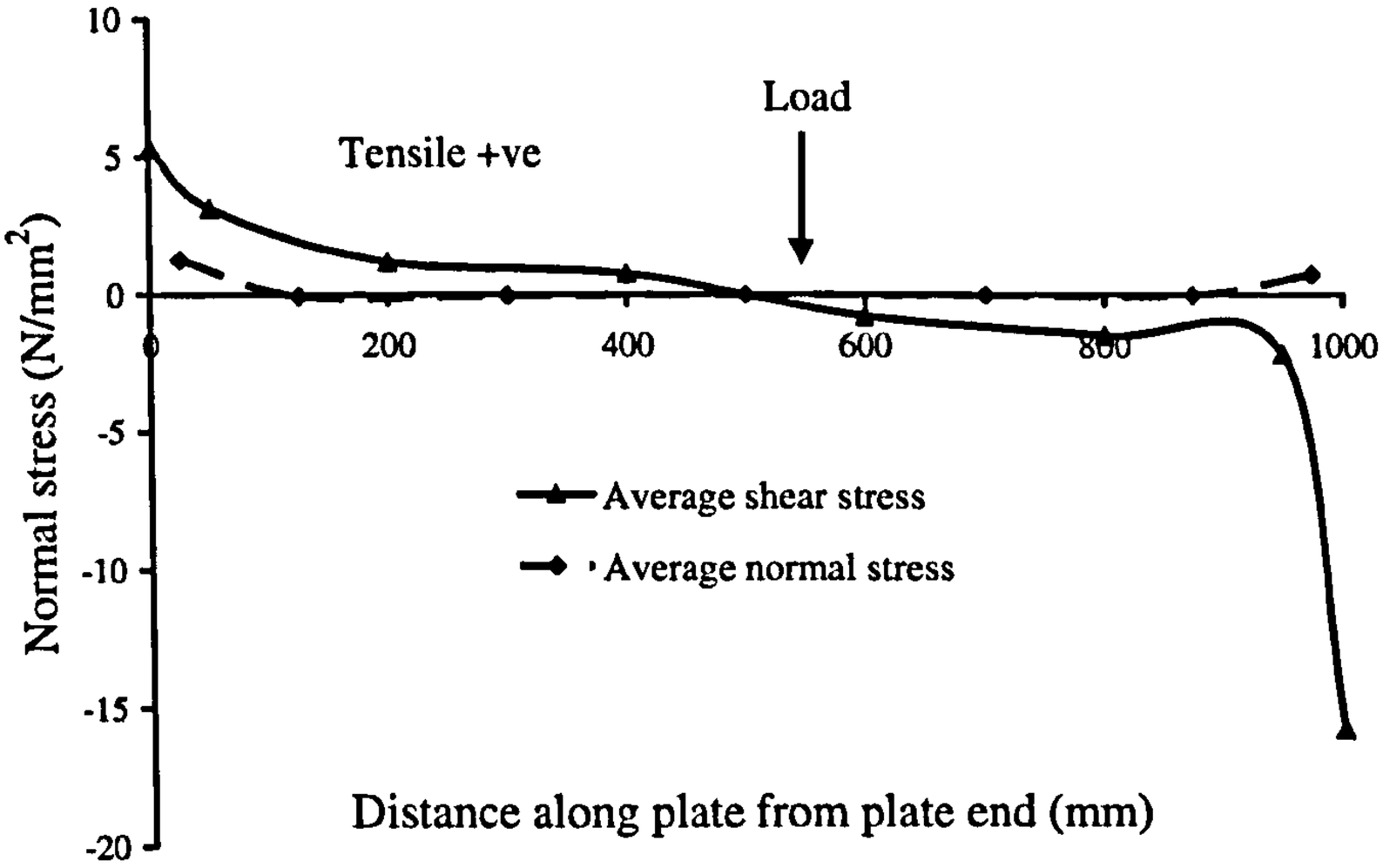

Figure 4-30 - Normal bond stress along base plate (B4) at 247 kN load

4.4.6 Moment-curvature characteristics

Strain readings from through the depths of the unplated steel sections (2 different levels on the steel beam) enabled the evaluation of section curvatures, which were combined with the section moments deduced from the load cells. In both specimens B3 and B4, a sudden jump was noted in the strain readings at the outer surfaces of the flanges – at the mid-span section for B3 and at both the centre support and mid-span sections for B4 – before the idealised yielding strain of the steel (1530με) was reached. A check on the moment diagrams deduced from the load cell readings (see Figure 4-31) shows that the moments at these sections are below the moment at which yielding is supposed to occur. As the load was applied at a relatively constant rate during testing, this sudden jump in strain might have suggested the onset of yielding in the steel. The low strain level at which yielding occurred suggests that there might be substantial residual stresses in the steel. This residual stress was not observed in testing the steel coupons. One possible cause that might have accounted for this is that any potential residual stresses might have been released during cutting the coupons from the beam.

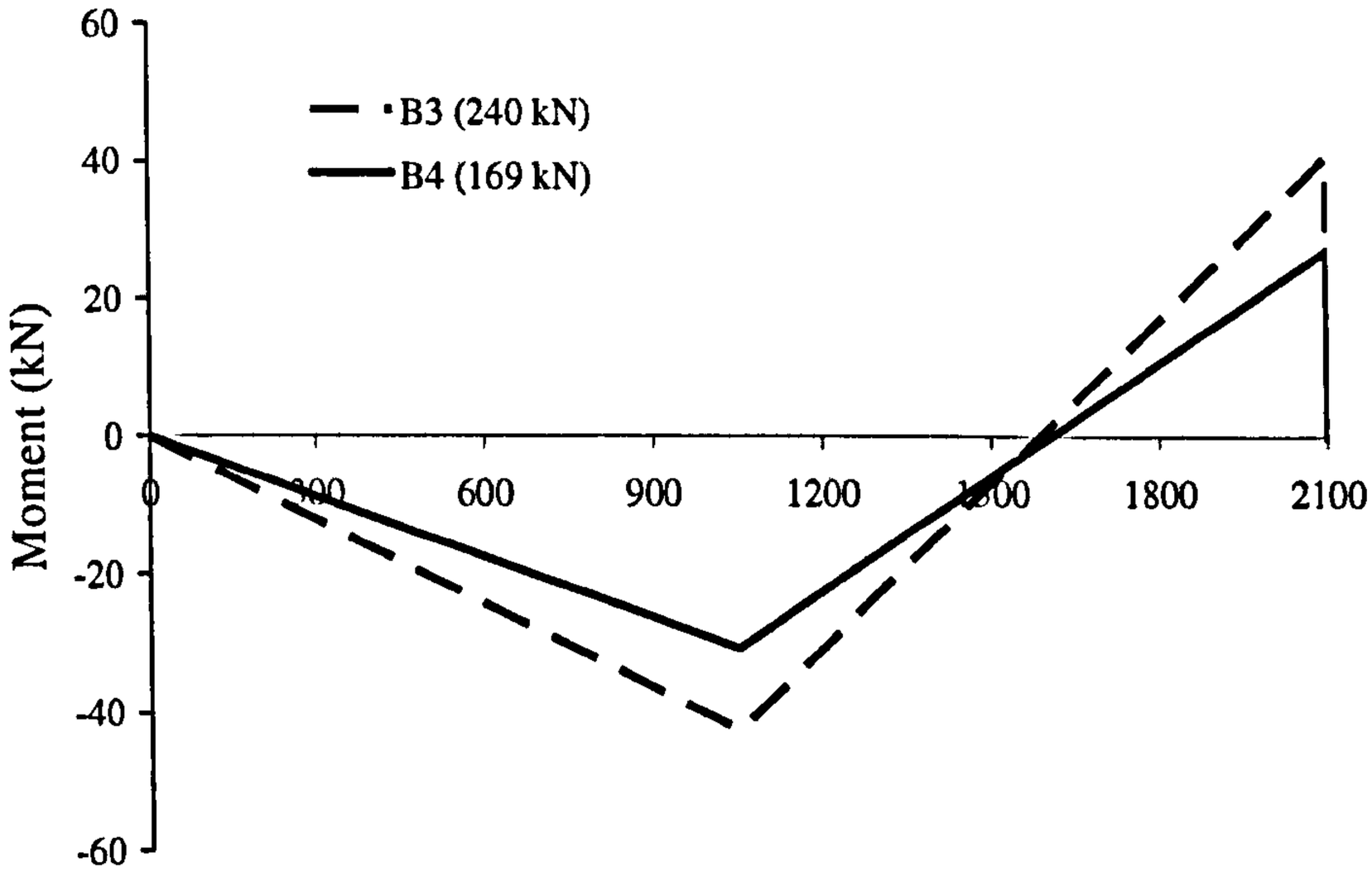

Figure 4-31 - Moment diagrams (deduced from load cell readings)

Residual stresses are not uniformly distributed in the steel (BS 5950-1:2000) and may be idealised as being linearly distributed (European Convention for Constructional Steelwork 1984). Shown in Figure 4-32 are typical residual stress patterns and their effects on the through-depth stress distribution (before yielding). It can be seen that linear strain distribution across the depth of the section, which is commonly assumed for section analysis of the beams, does not hold true in the existence of residual stresses so strictly speaking, the concept of moment-curvature relations is not valid.

However, if an 'equivalent curvature' can be assumed, then the 'real-moment (that derived from the actual stress distribution) –equivalent-curvature' relations can be determined. An example is shown in Figure 4-33 for the steel section of the test beams assuming the peak residual stress 70.5 MPa (European Convention for Constructional Steelwork 1984). The 'real moment' data start from the point where there is only one level of zero strain in the section (which is then taken as the neutral axis for deriving the section moments).

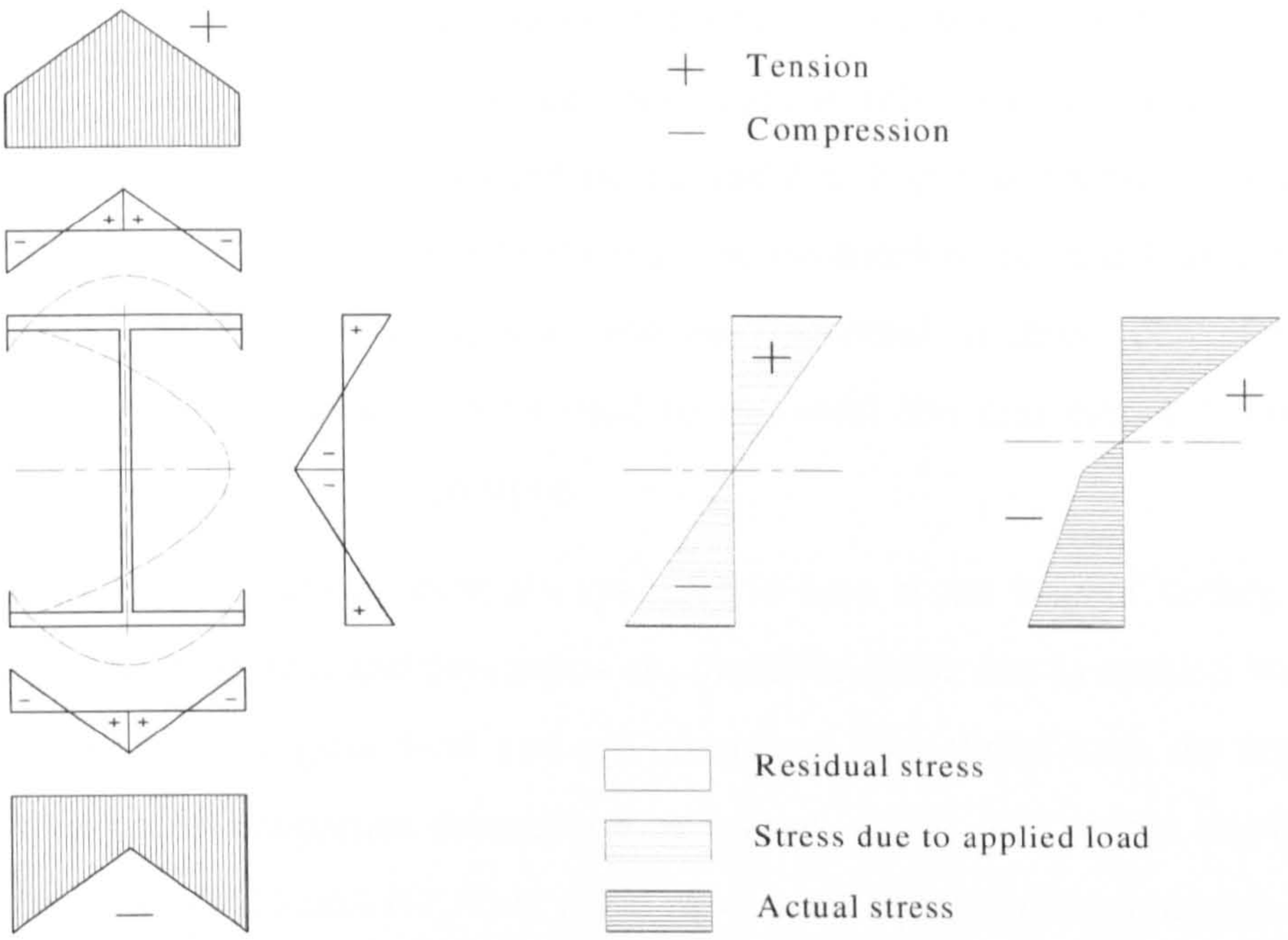

Figure 4-32 - Typical residual stress patterns and actual stress distribution through the depth of rolled steel I-section (European Convention for Constructional Steelwork 1984)

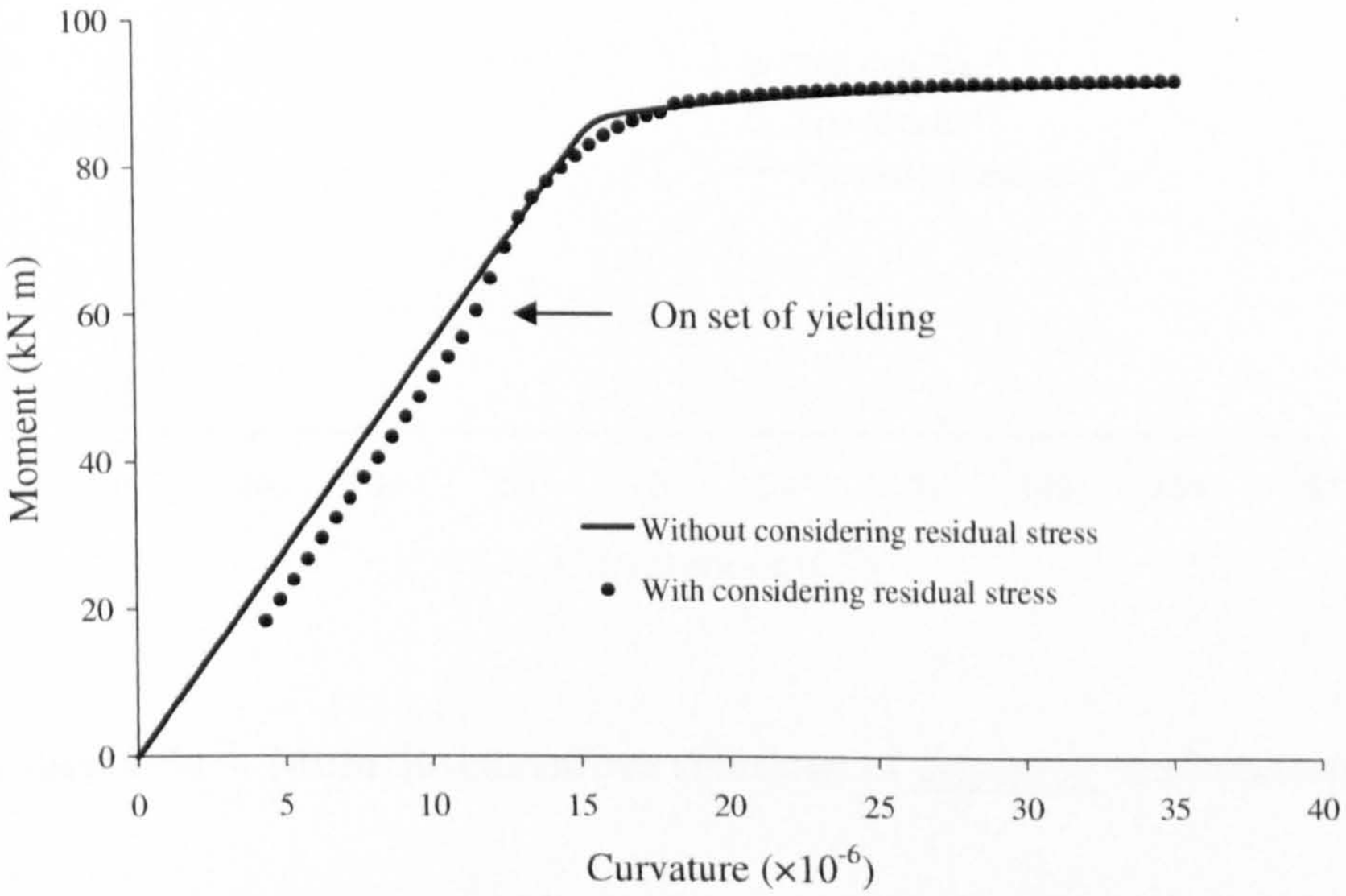

Figure 4-33 - Moment-curvature relations for steel section

It can be seen that although the existence of residual stresses changes the actual stress distribution of the section, they do not significantly affect section moment, particularly after the onset of yielding in the section. It can therefore be reasonably assumed that when the 'equivalent curvature' is assumed to be equal to that due to applied load, the moment-curvature relations obtained without considering the existence of residual stresses can be used to represent the real-moment-equivalent-curvature characteristics of the sections.

As the strain gauge readings were always reset to zero at the start of testing, the so-obtained section moments and curvatures are therefore those due to applied loads. The results are shown in Figure 4-34 and are compared with those from the theoretical analysis using steel properties determined in Section 4.3.2. The results show a good correlation for both B3 and B4. This gives more confidence for the analysis of FRP-plated sections.

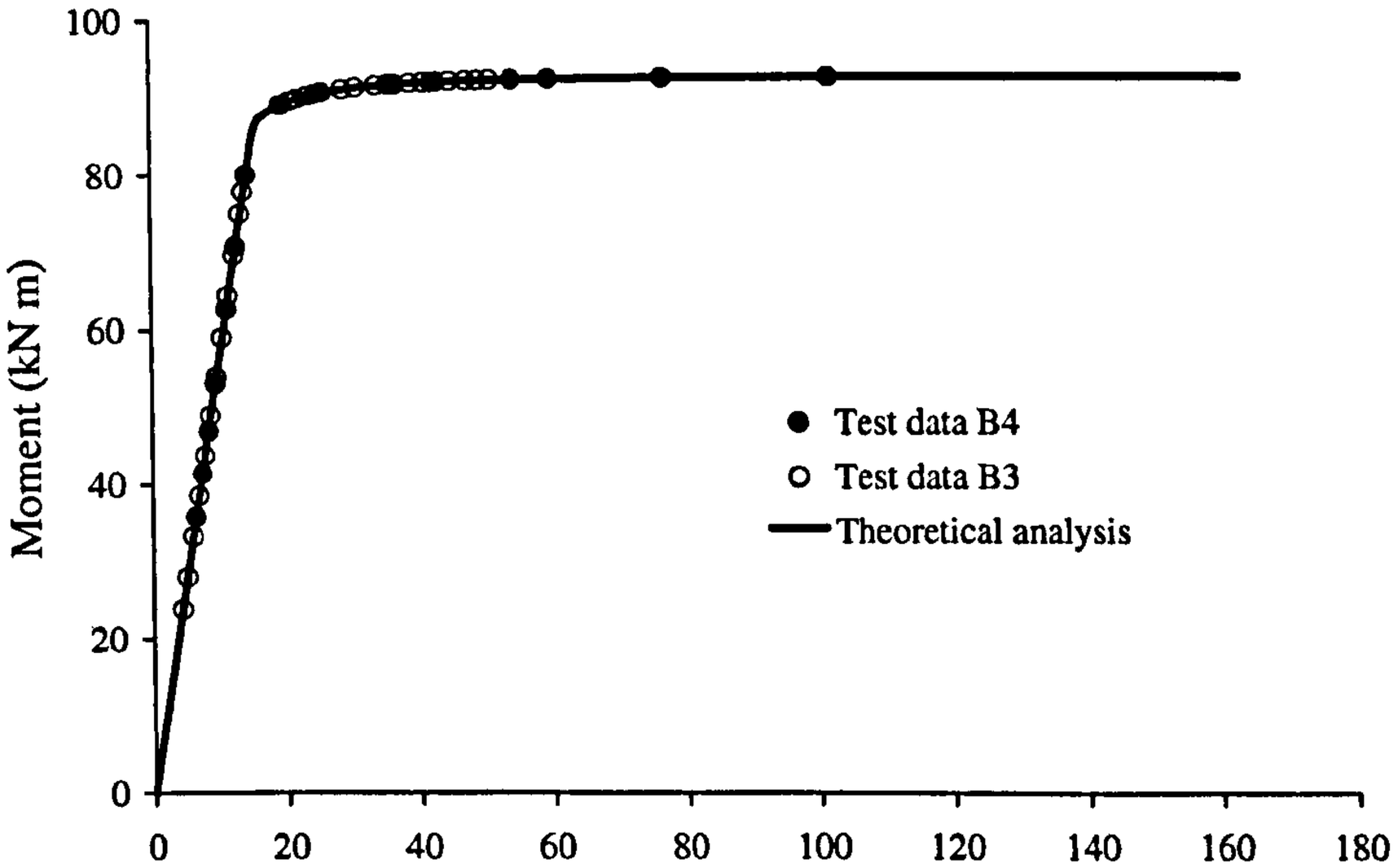

Figure 4-34 - Moment-curvature relations of unplated steel sections

The moment-curvature relations of the FRP-plated steel sections were also evaluated from the strain readings across the depths of the plated sections (2 different levels on the steel beam, and outer and inner surfaces of the CFRP plate). The (local) curvature of the steel section is used as the curvature of the plated section in the interpretation of the test data and the potential effects of the residual strains are ignored. Where no strain gauges were applied at the inner surface of the CFRP plate, strain is assumed to be constant through the thickness of the plate and the CFRP plate outer surface strain readings were used. The results are shown in Figure 4-35. All theoretical analyses stopped just before yielding started in the plated steel flange.

It can be seen that rigid bond analysis gives good prediction of the section stiffness for FRP-plated steel sections for plate thickness up to 8 mm. The offset of the test data for specimen B4 from the theoretical analysis is believed to be due to the existence of residual stress distribution. Using only the outer surface strains did not lead to much overestimation of the section stiffness for the 4 mm thick FRP-plated section and the test value is somewhat smaller than that from the rigid bond analysis when yielding occurred. For the 16 mm thick FRP-plated section, however, the test data shows bigger section stiffness. The through thickness strain variation across the FRP plate is cited as a possible cause as assuming a constant strain equal to that at the outer surface of the FRP plate (therefore the maximum) through its thickness will lead to an overestimation of the stiffness of the plated section.

The general good agreement between the test results and those from the rigid bond analysis has given confidence in the theoretical analysis proposed in Chapter 3 using the rigid bond assumption. In what follows, support stiffnesses are first evaluated after which theoretical analyses as proposed in Chapter 3 have been carried out to predict the moments in the beams over the centre supports for specimens B1-B4. The member stiffnesses were obtained from the moment-curvature relations from rigid bond analyses.

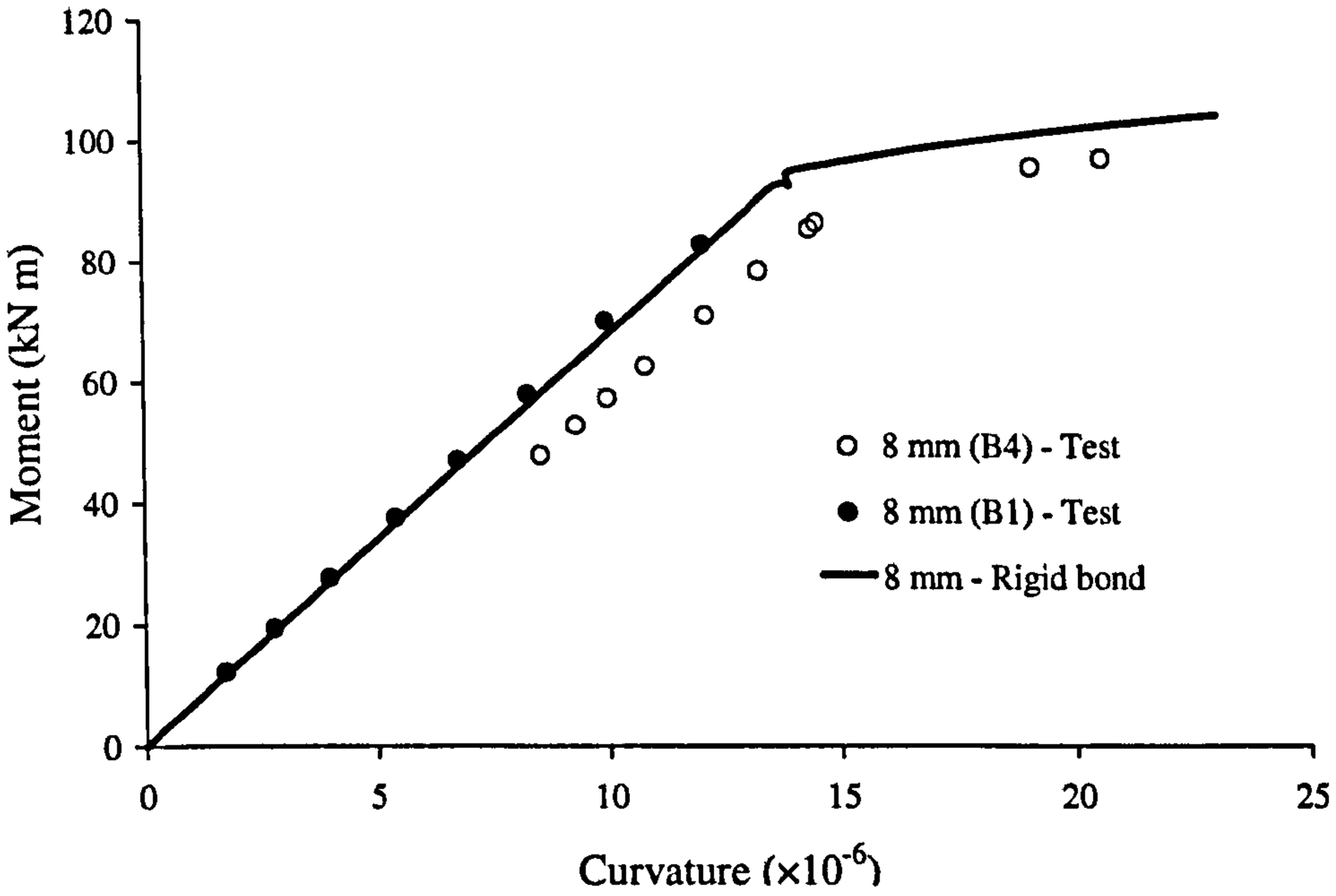

(a) Strain readings from both outer and inner surfaces of CFRP plates

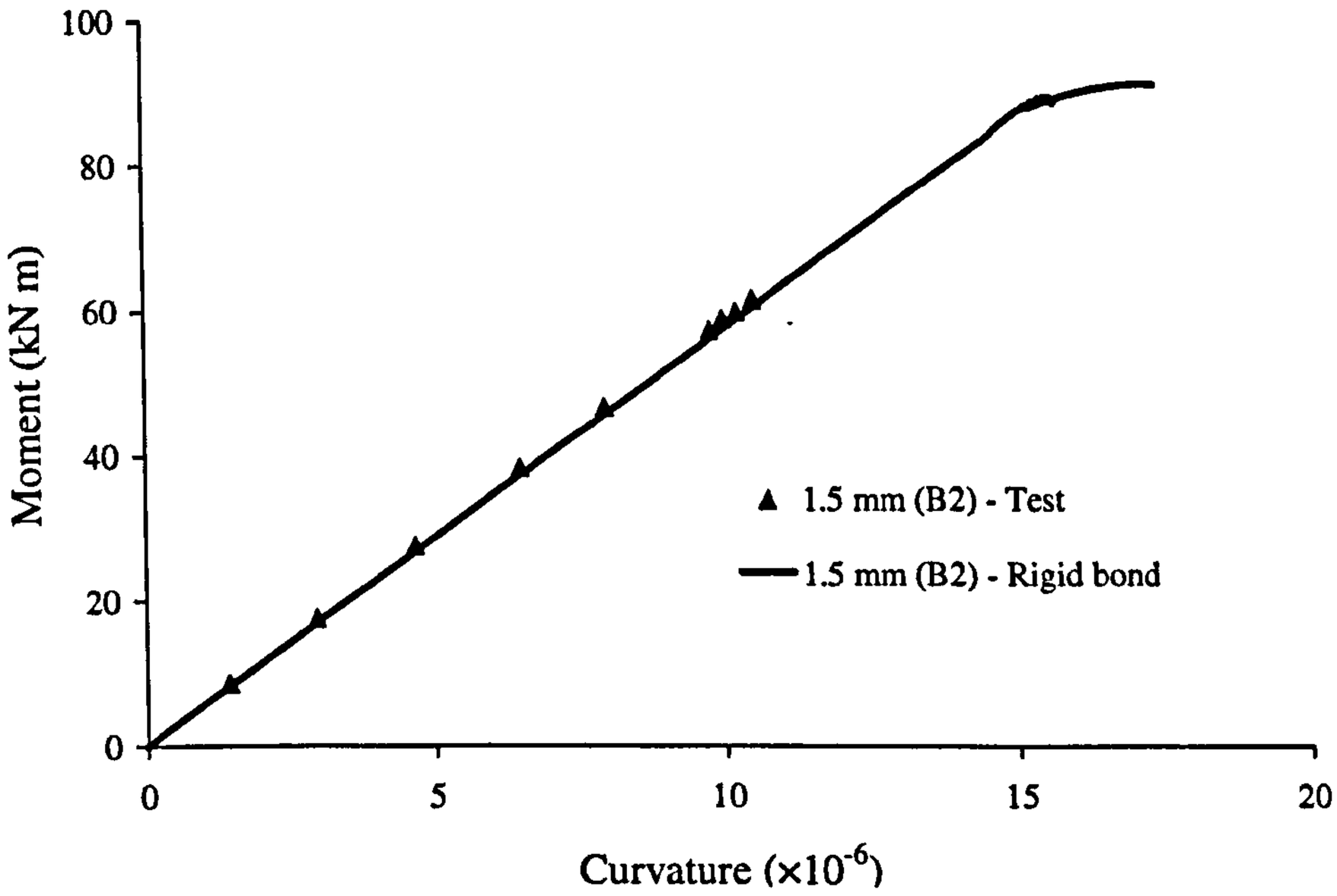

(b) Strain readings from both outer and inner surfaces of CFRP plates

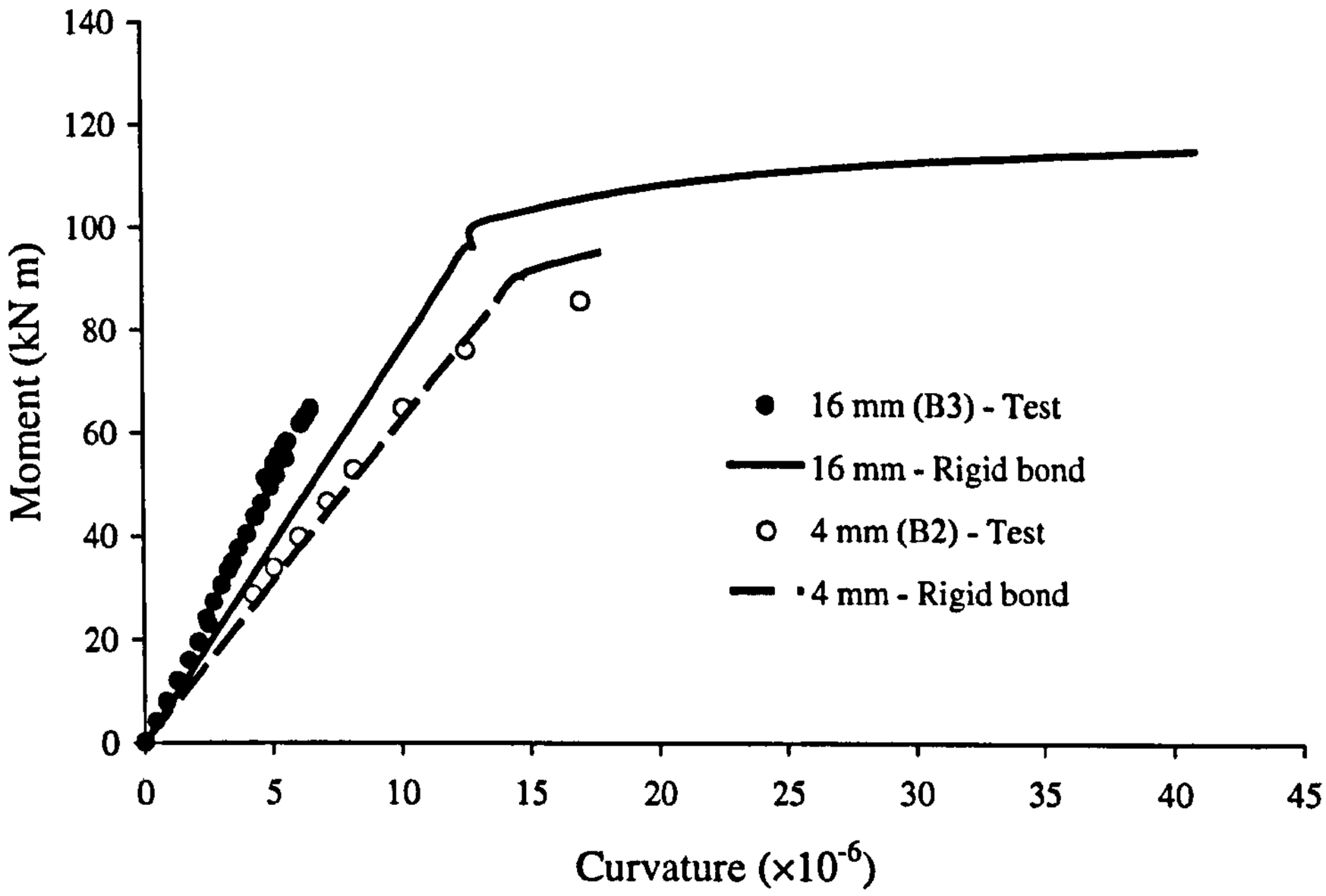

(c) Strain readings from only outer surfaces of CFRP plates

Figure 4-35 - Moment-curvature relations of CFRP-plated steel sections

4.4.7 Support stiffnesses

The effective support stiffness (the quotient of load and deflection at the support) was defined in Chapter 3 as follows:

$$k = \frac{R}{\delta} = \beta \frac{EI}{L^3} \tag{4-4}$$

The use of load cells and dial gauges at the supports (e.g. Figure 4-36, note the rubber pad which influences support stiffness) has enabled the effective support stiffnesses and therefore the support stiffness parameters β to be determined. The effective support stiffnesses could also be estimated using the deflection based approach described in Chapter 3. The support settlements were directly measured so no interpolation was required in this case. The results are shown in Figure 4-37 for

specimens B1-B4. The end support deformations are the average of deformations of the left- and right-span outer supports.

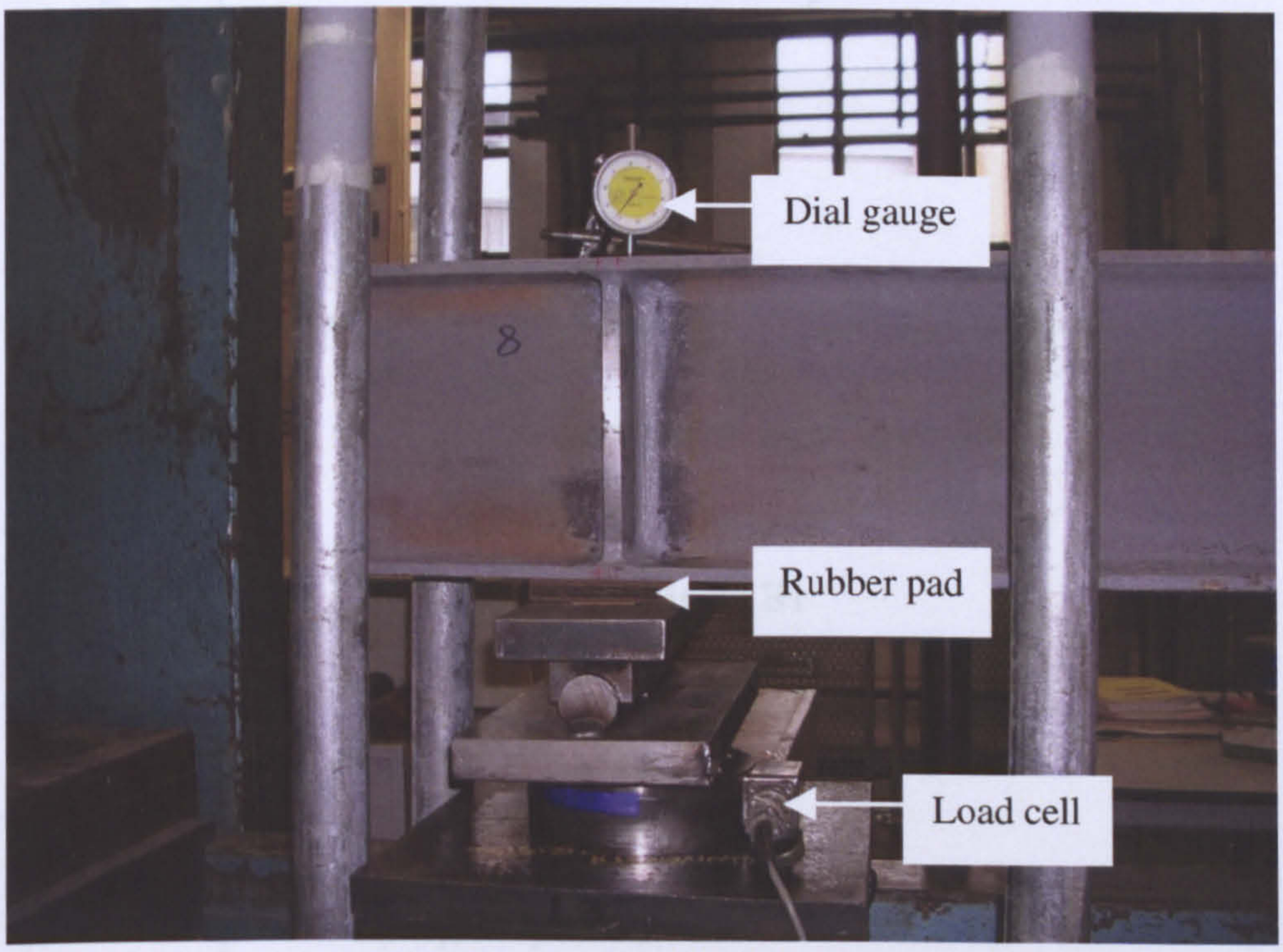

Figure 4-36 - Instrumentation set-up at outer support

From Figure 4-37, the deformation-based approach generally gives fairly good prediction of the support stiffnesses. However, when the support stiffness parameters were evaluated using linear support reaction-deformation relations that give good fit of each set of data (the results are summarised in Table 4-4), it can be seen that the support stiffnesses in most cases are near the edge of or just outside the 'sensitive zone' (0-60) as identified in Chapter 3, so particular care should be taken as a slight change in support stiffness parameters may cause a significant change in the centre support moment. In the following sections, the results from test data are used to determine the centre support moments.

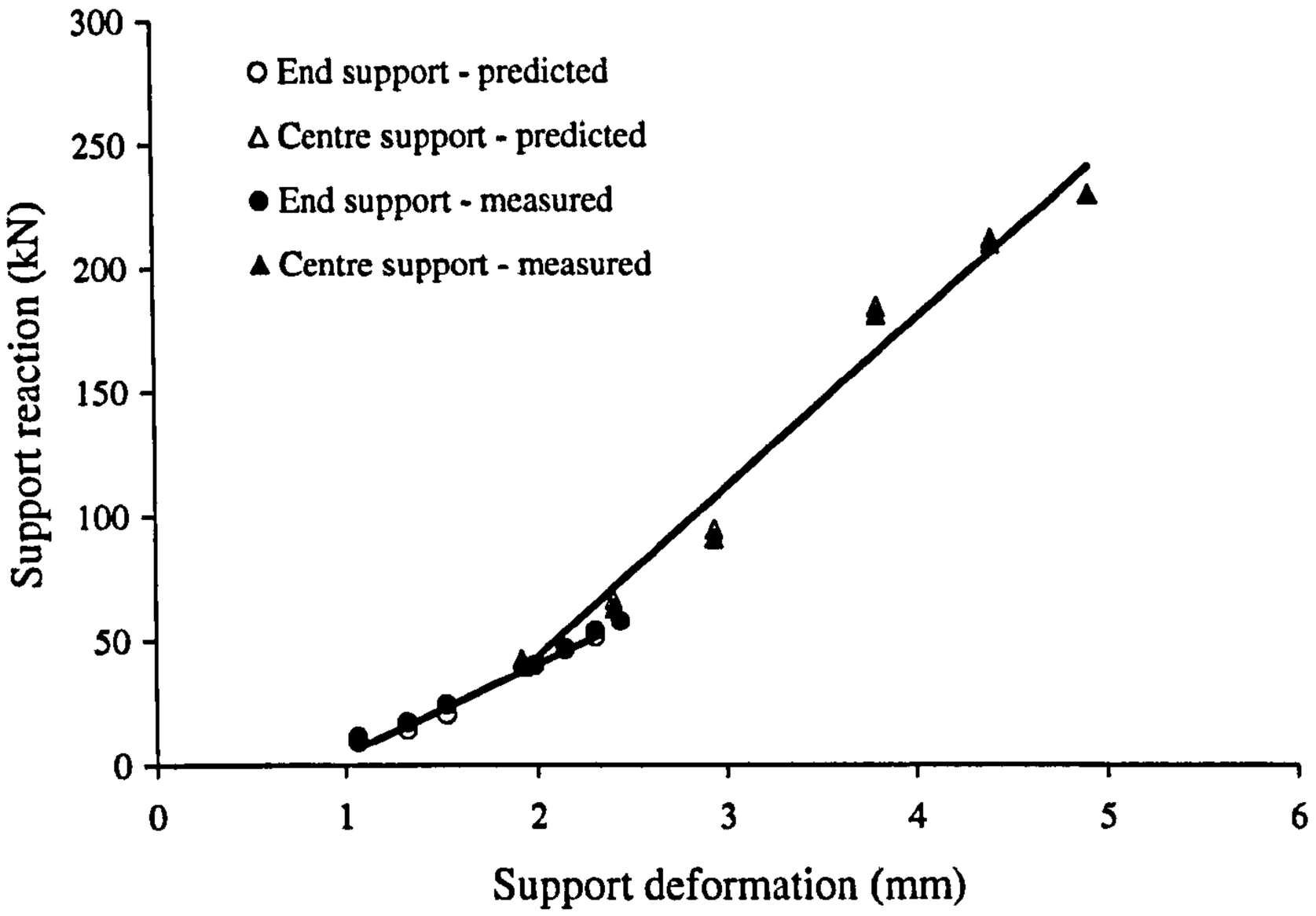

(a) Specimen B1

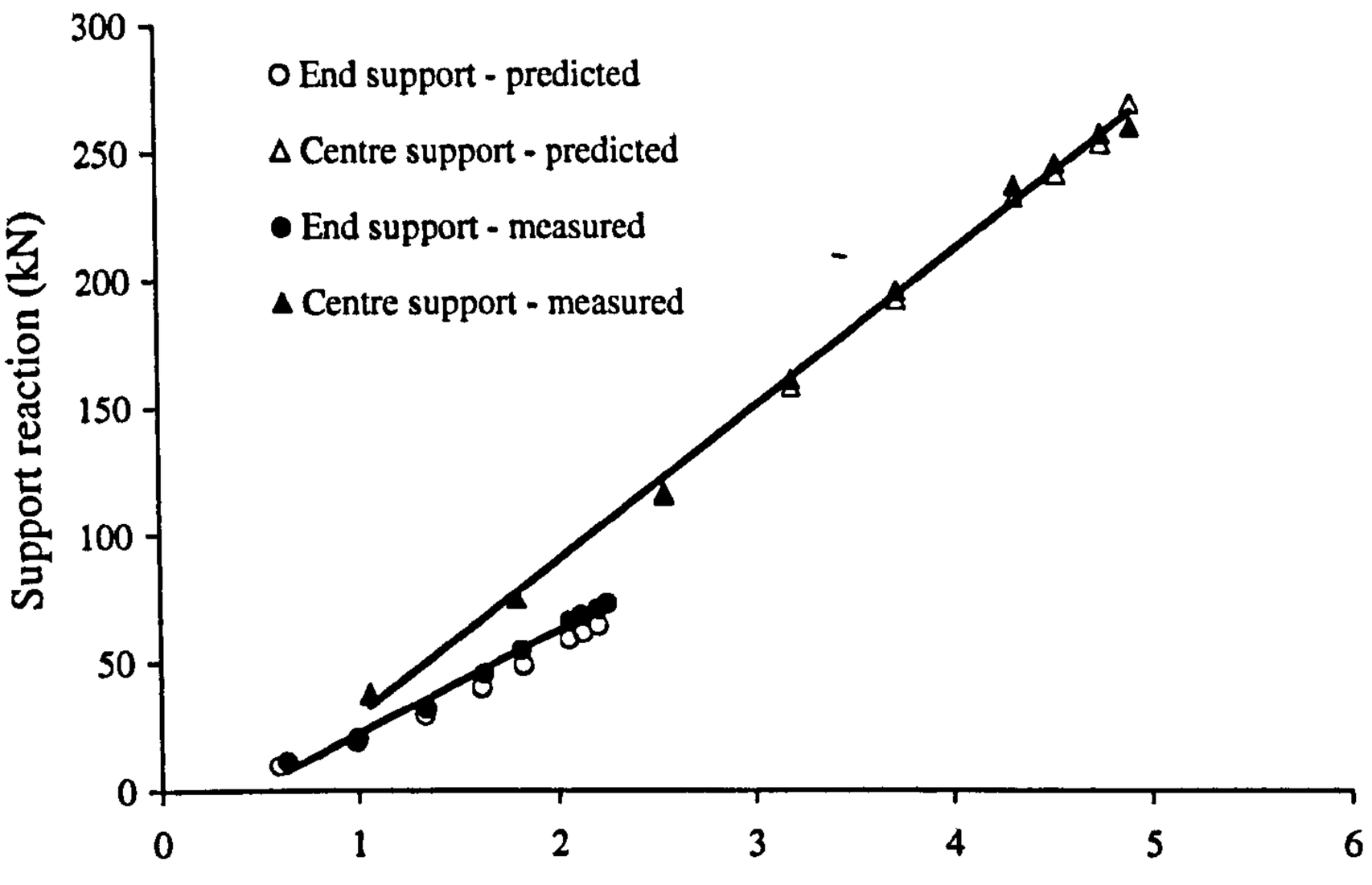

(b) Specimen B2

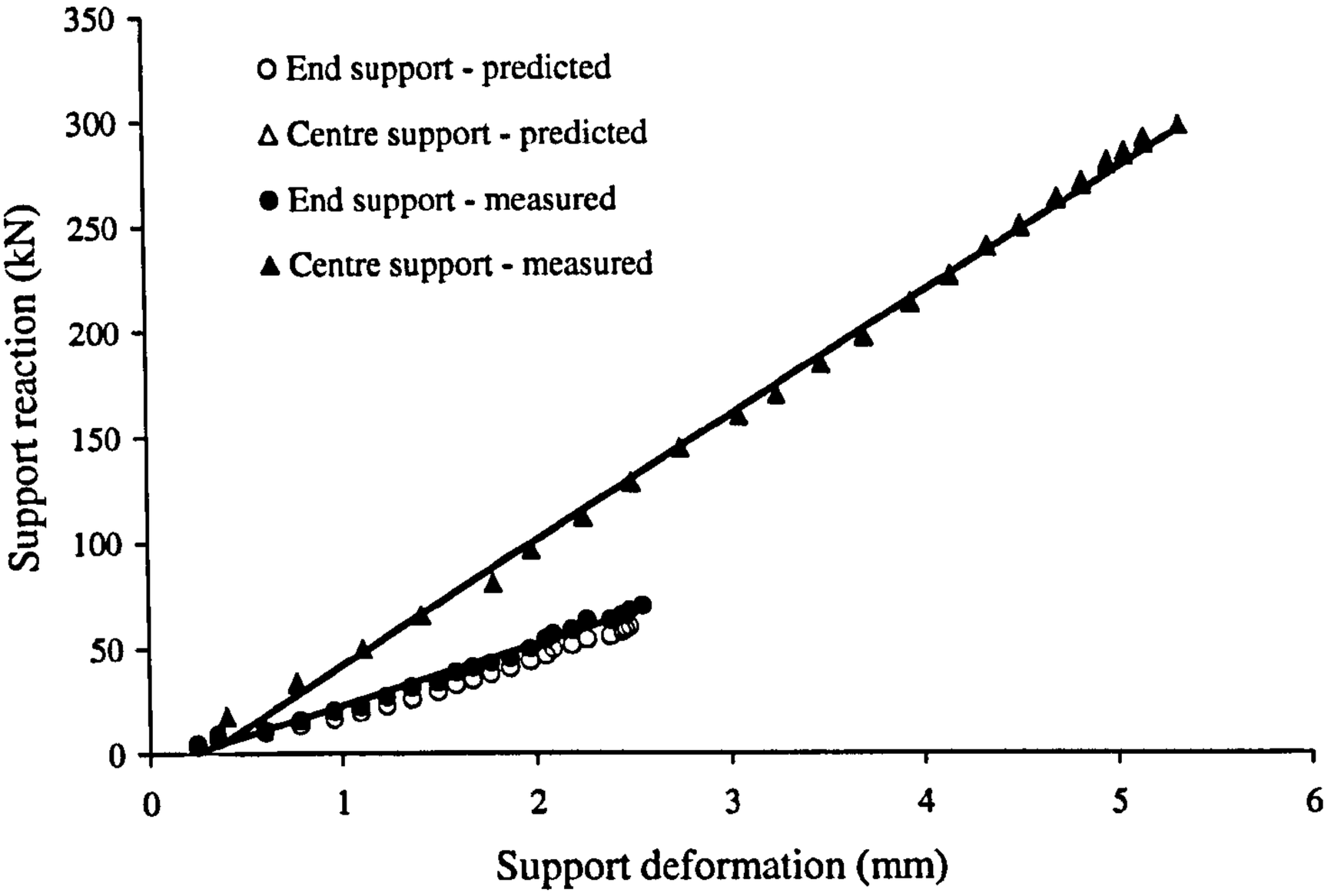

(c) Specimen B3

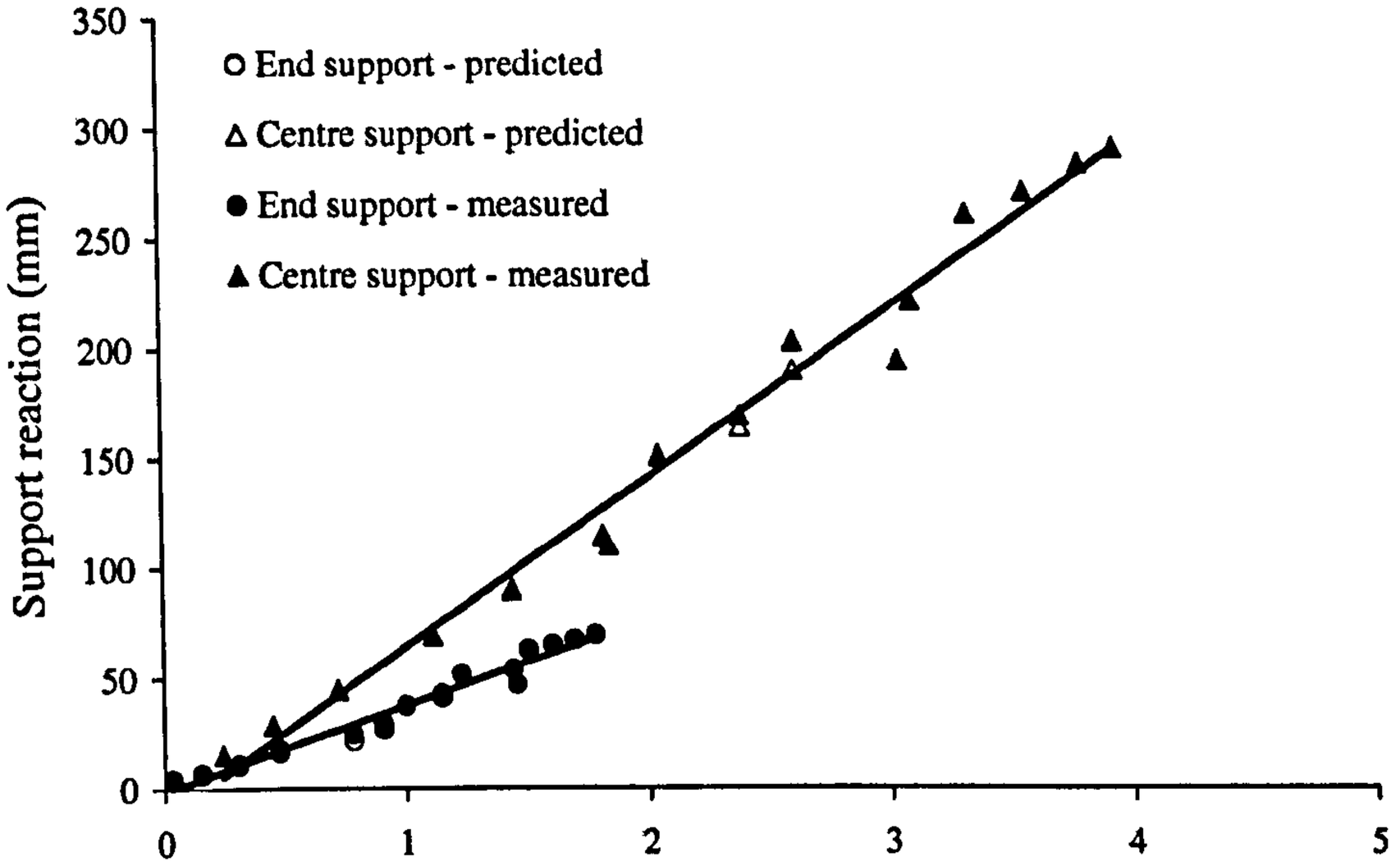

(d) Specimen B4

Figure 4-37 - Effective support stiffnesses

	End support (β_1)		Centre support (β_2)	
	Measured	Predicted	Measured	Predicted
B1	57.3	57.9	56.9	55.1
B2	65.1	57.4	49.6	47.7
B3	47.9	41.8	48.8	45.6
B4	64.2	59.2	62.8	59.1

Table 4-4 - Support stiffness parameters

4.4.8 Centre support moments

In this section, the centre support moments deduced from the load cell readings are presented and compared with those calculated using the theoretical models proposed in Chapter 3. In the theoretical analyses, the material properties and support stiffness parameters from the previous sections in this chapter were used. The moment-curvature relations from rigid bond analyses were used to obtain the stiffnesses of the plated-steel sections. The key parameters are summarized in Table 4-5. Two cases were considered: (a) flexible supports, where support stiffnesses are considered; and (b) rigid supports, where supports were taken as being rigid and any support deformations were ignored. The results are shown in Figure 4-38.

	γ_1	γ_2	γ_3	γ_4	α_1	α_2	α_3	β_1	β_2
B1	0.095	0.571	0.286	0.048	1.18	1.44	1.21	57.3	56.9
B2	0.262	0.405	0.286	0.048	1.11	1.15	1.03	65.1	49.6
B3	0	0.714	0	0.286	1	1.36		47.9	48.8
B4									
Pre-debond	0.238	0.476	0	0.286	1.21	1		64.2	62.8
Post-debond	0.345	0.369	0	0.286	1.21	1		64.2	62.8

Table 4-5 - Key parameters for theoretical analysis

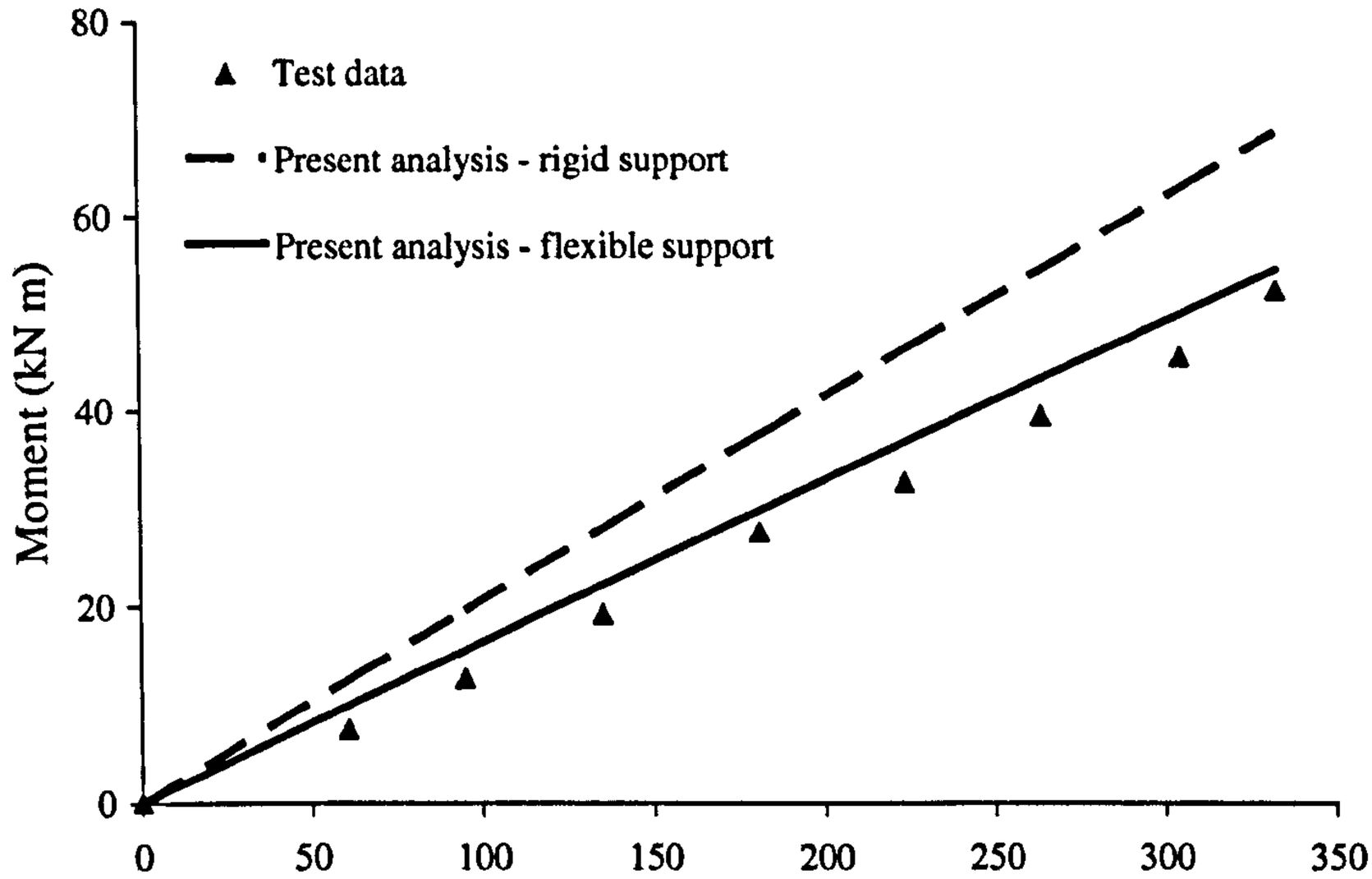

(a) Specimen B1

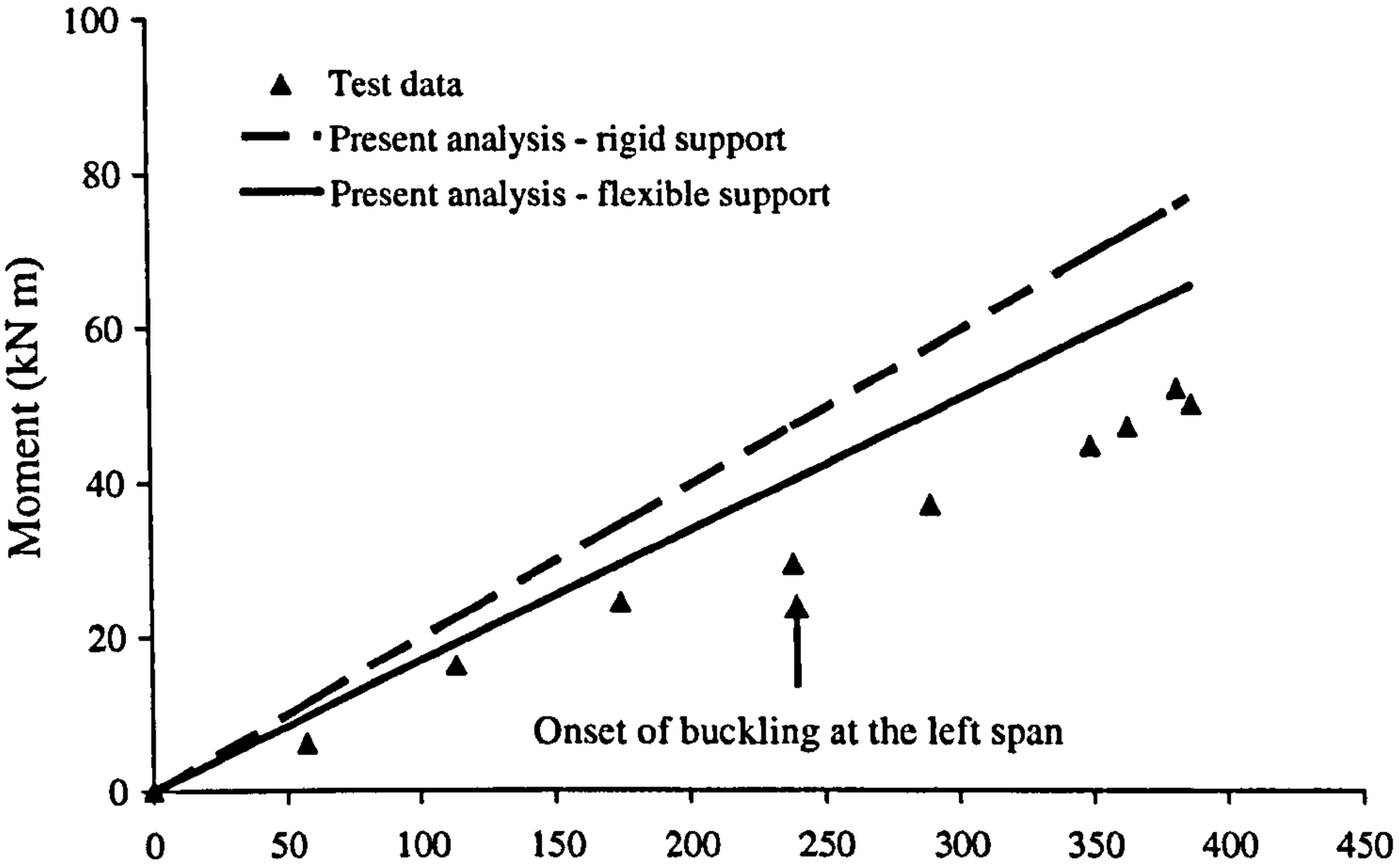

(b) Specimen B2

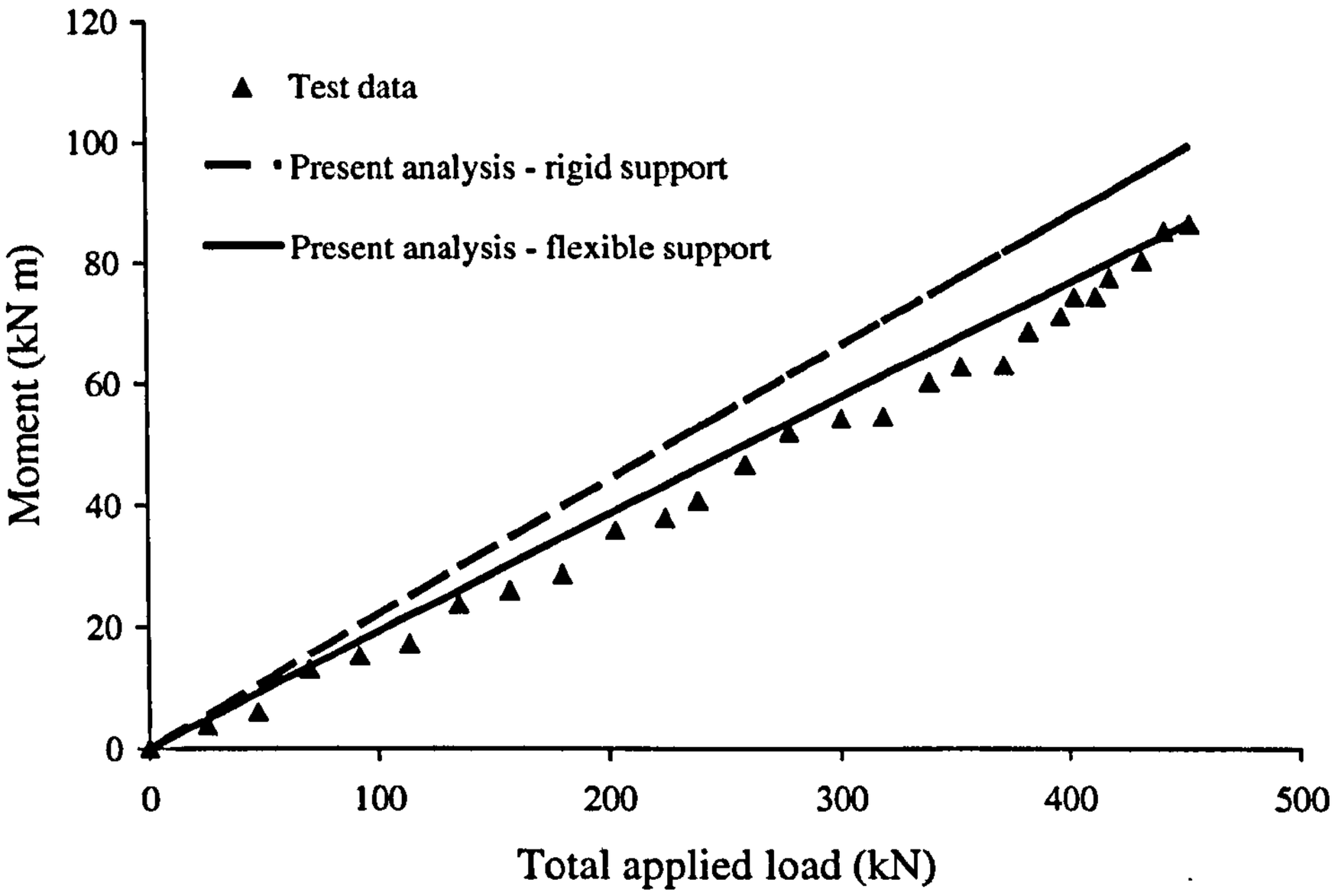

(c) Specimen B3

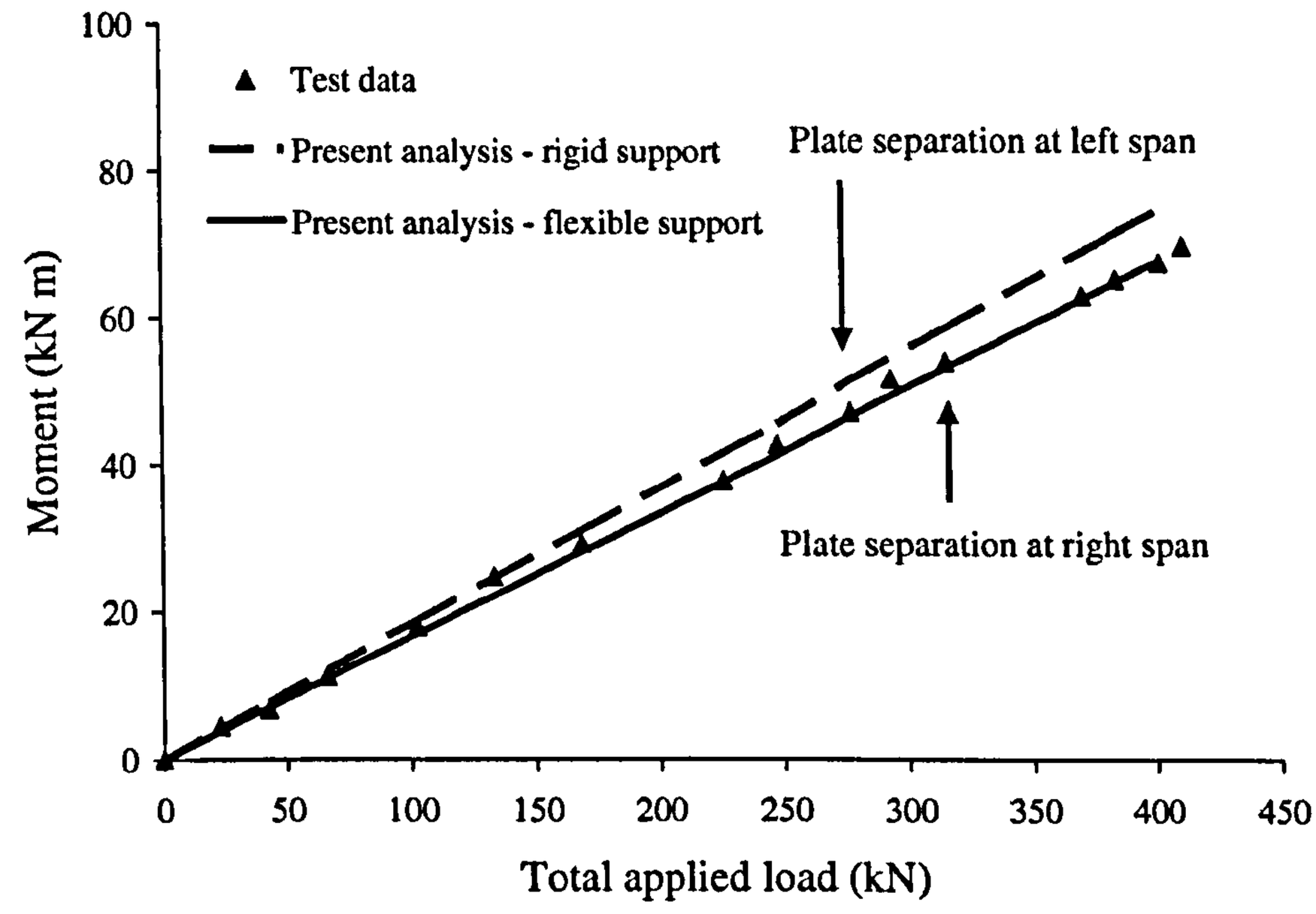

(d) Specimen B4

Figure 4- 38 - Centre support moments

It can be seen that considering the support stiffnesses generally gives better prediction of the centre support moments. Ignoring the support stiffnesses would have led to bigger estimation of the centre support section moments, particularly for specimens B1 – B3. The effects of the support stiffnesses were less pronounced for specimen B4. A check of support stiffness reveals that the support stiffnesses were out of the 'sensitive zone' (0-60) defined in Chapter 3. There is a large overestimation for specimen B2, particularly at later stages of loading. From Section 4.4.1, bucking occurred at the left span but not at the right span of specimen B2. This will have led to a lower stiffness of the left mid-span section compared to that of the right mid-span section. In turn, this asymmetric stiffness distribution may well have led to a complex redistribution of moments within the beam.

Shown in Figure 4-39 are the moment diagrams for specimens B1 – B3 at their respective maximum loads and also for specimen B4 at the maximum load before separation. The effects of support settlements on the moment over the central support are significant, particularly for specimens B1, B2 and B3. The rigid support assumption leads to over-estimation of this moment by 30.9, 51.9, 15.0 and 11.4% for specimens B1 – B4, respectively. By contrast, when the experimentally-deduced support stiffnesses and the beam's stiffness profile are used in the theoretical approach of Chapter 3, the resulting predicted moment over the central support is only 4.0%, 0.3%, and 0.9% different from the test values for specimens B1, B3 and B4, respectively. The bigger disparity for specimen B1 may be attributed to potential effects on the stiffness profile of the occurrence of buckling over the entire specimen. An over-estimation of 20.7% was noted for specimen B2. Again, the asymmetry due to buckling within the left (but not the right) span is a possible cause.

Relative to the flexible supports, rigid supports also shift the point of conraflexure along the span (*circa* 108 mm for specimen B1). This is important when the FRP plates are being curtailed at the points of contraflexure in order to prevent end peel or to ensure that the plate is extended a certain distance beyond the point of contraflexure to provide sufficient anchorage (as discussed in Chapter 2). In these cases, the shift of the points of contraflxure due to support settlements has to be considered and properly accounted for in the design of FRP strengthening schemes.

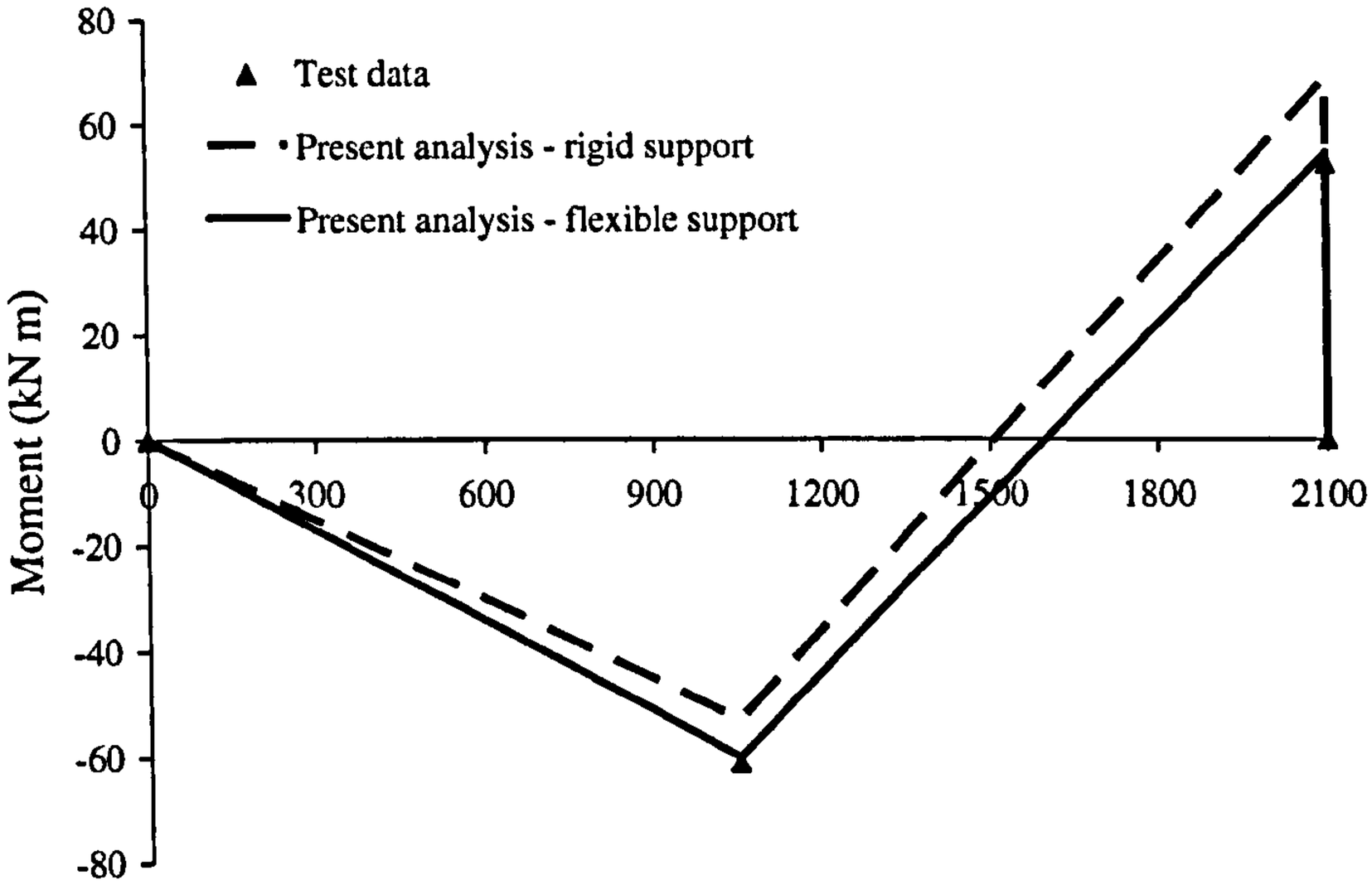

Distance from end support (mm)

(a) Specimen B1

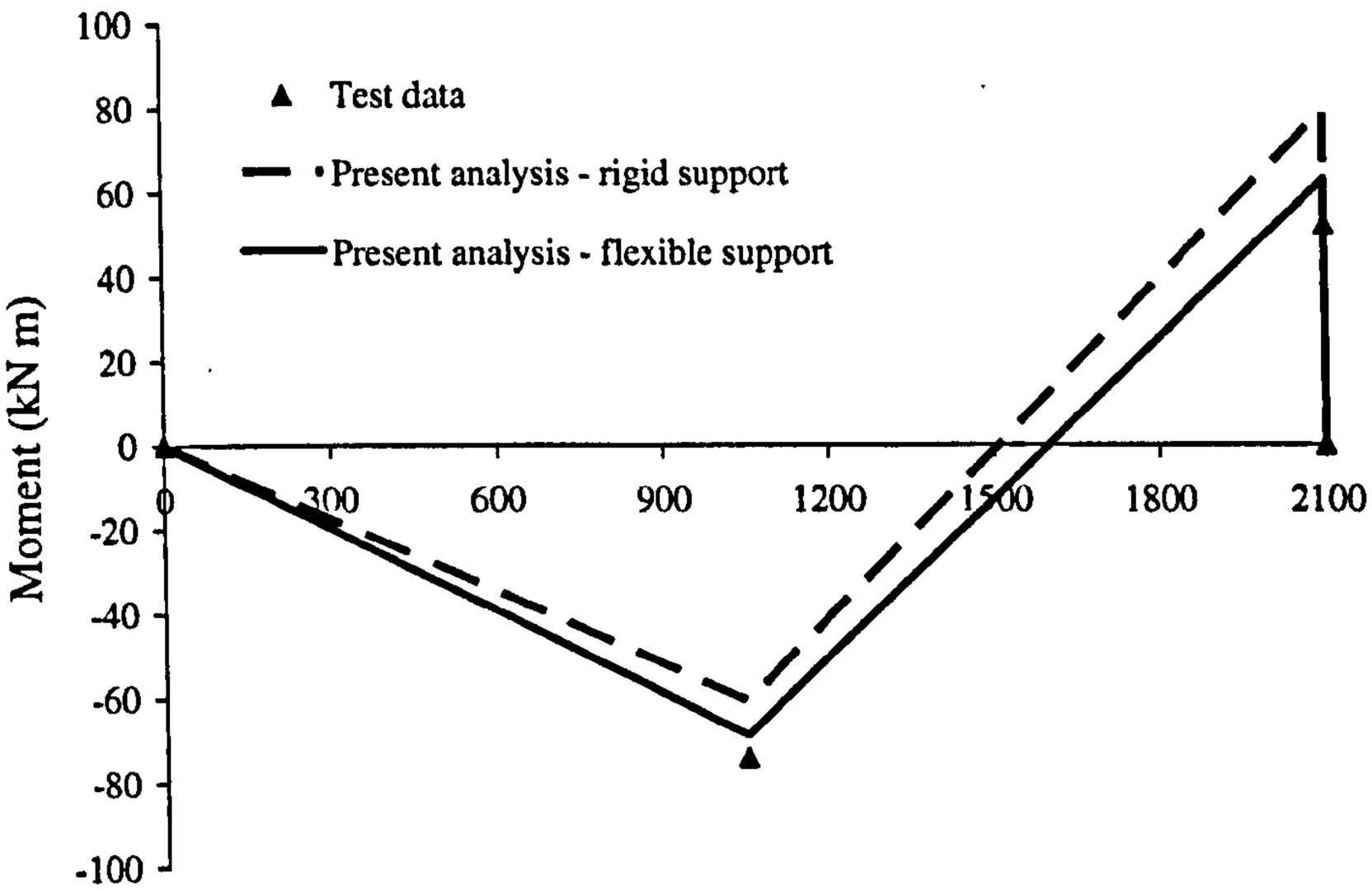

Distance from end support (mm)

(b) Specimen B2

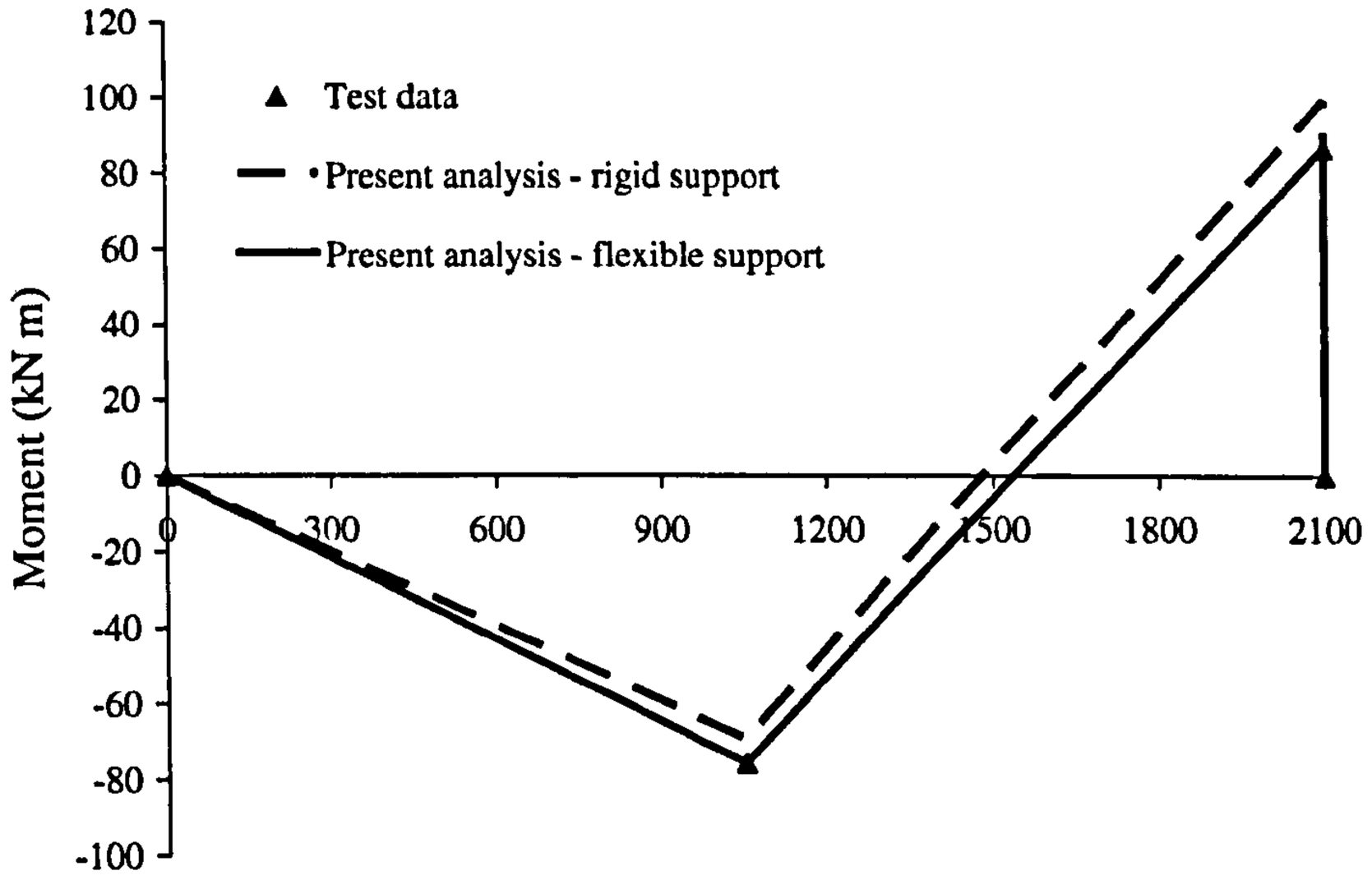

(c)Specimen B3

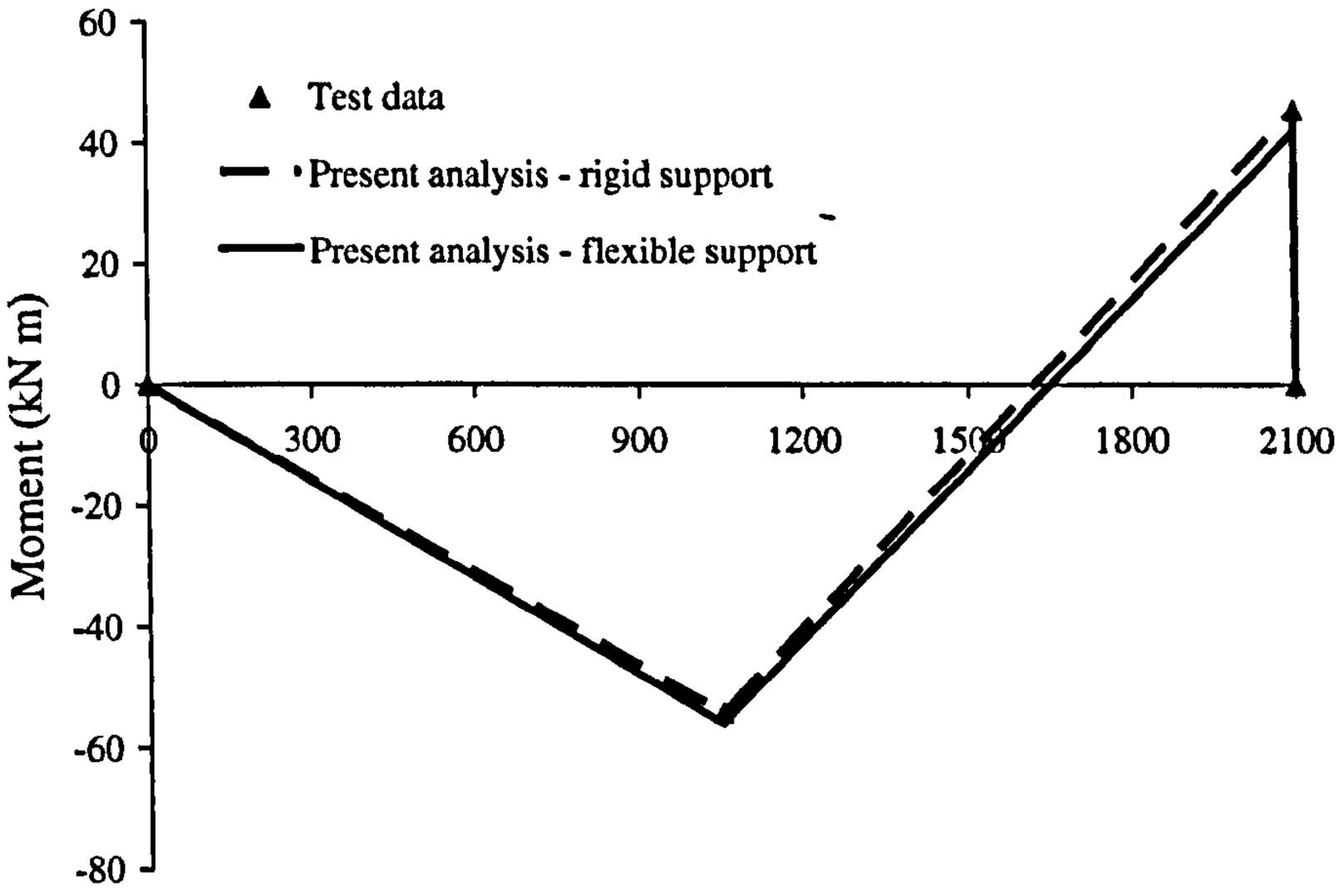

(d) Specimen B4

Figure 4-39 - Moment diagrams along the left span

4.5 Conclusions

Four 2-span CFRP-plated steel beam specimens have been fabricated and tested. As one of the novel tests of its kind, the main aspects of investigation include those related to FRP plated thin-walled metallic structures such as buckling, plate debonding, interfacial strain and (average) interfacial bond stresses along the FRP plates, and also issues related to structural indeterminacy such as support deformations, stiffness variations along the member, and migration of point of contraflexure. The main parameters varied between specimens include layout of plates and plate thicknesses. Strain gauges were applied at both the outer and inner surfaces of the FRP plates to investigate the effects of thickness of and/or local bending in these plates on interfacial stresses. It also enabled the investigation to establish how closely the rigid bond assumption is justified in evaluating CFRP plated-steel section stiffnesses. The novel approach of adhesively bonding the steel stiffeners to the test beams was taken to try and inhibit local buckling.

From the physical observations made and data collected and processed during and after these experiments, the following points may be made :

- Two specimens failed by loss of stability induced by local buckling. Plate debonding also occurred where there was a combination of thick plates, big offsets between the plate end and the nearest point of contraflexure, and bond defects. Some debonding was observed at the compression end of specimen B1 and sudden separation occurred with specimen B4. In both cases, debonding occurred at the interfaces (steel/adhesive interface for B4 and adhesive/plate interface for B1) in contrast to common failure in the concrete cover in FRP strengthened reinforced concrete beams. Specimen B3 did not fail when the capacity of one load cell was reached.

- The novel use of adhesive bonding to attach the steel stiffeners to the test beam worked efficiently. This technique is an alternative to welding and allows for safe application of strain gauging at the section of stiffening.

- There were significant differences in strain readings between the outer and inner surfaces of the plates near the plates' ends, especially for thick plates, which implies that through thickness variation and/or local bending, are important in the evaluation of the average shear bond stresses. Indeed, from the shear bond stress distribution, it

can be seen that using outer surface strains only (which is common in the research environment) could lead to unreasonable prediction of interfacial shear stresses.

- There is significant variation in material properties of the steel. However, the idealised elastic-perfectly plastic characteristic commonly taken for steel has shown to be satisfactory. Residual stresses may also be present in the steel although of course they were not observed in testing of the steel coupons.

- The existence of residual stresses changes the stress distribution across the steel sections. However, if an equivalent curvature can be assumed to be equal to that due to the applied load, then the moment-curvature relations derived without considering the existence of residual stresses can be used to represent the moment-curvature characteristics of the steel section.

- Section stiffnesses obtained from the strain distribution across plated sections were compared with results from rigid bond analyses. The generally good comparison for various plate thicknesses ranging 1.5 to 16 mm suggests that rigid bond analyses can be reliably used to calculate section stiffness.

- Differential settlement must be properly accounted for in the analyses of statically indeterminate members. The use of effective support stiffnesses gives good prediction of the centre support moments and, consequently, of the moment diagrams along the span.

- Support stiffnesses can be estimated using the method described in Chapter 3. The estimated results compared well with those obtained from the measured data. However, as the support stiffnesses in most cases are within or close to the 'sensitive zone' (0-60) as defined in Chapter 3, care should be taken in evaluating the centre support moment.

The theoretical analysis in Chapter 3 and the experimental work in this Chapter have been conducted on 2-span continuous steel members. The following two chapters will focus on the analysis and design of more general ductility-deficient indeterminate structures. In chapter 5, a computational procedure is presented for time-efficient prediction of the load capacity of structures with varying ductility and also of the pre-failure behaviour of highly indeterminate structures. Then, Chapter 6 develops a technique for detailing of the structure when the load capacity is known.

Appendix 4A

Derivation of Interfacial Stress Equations

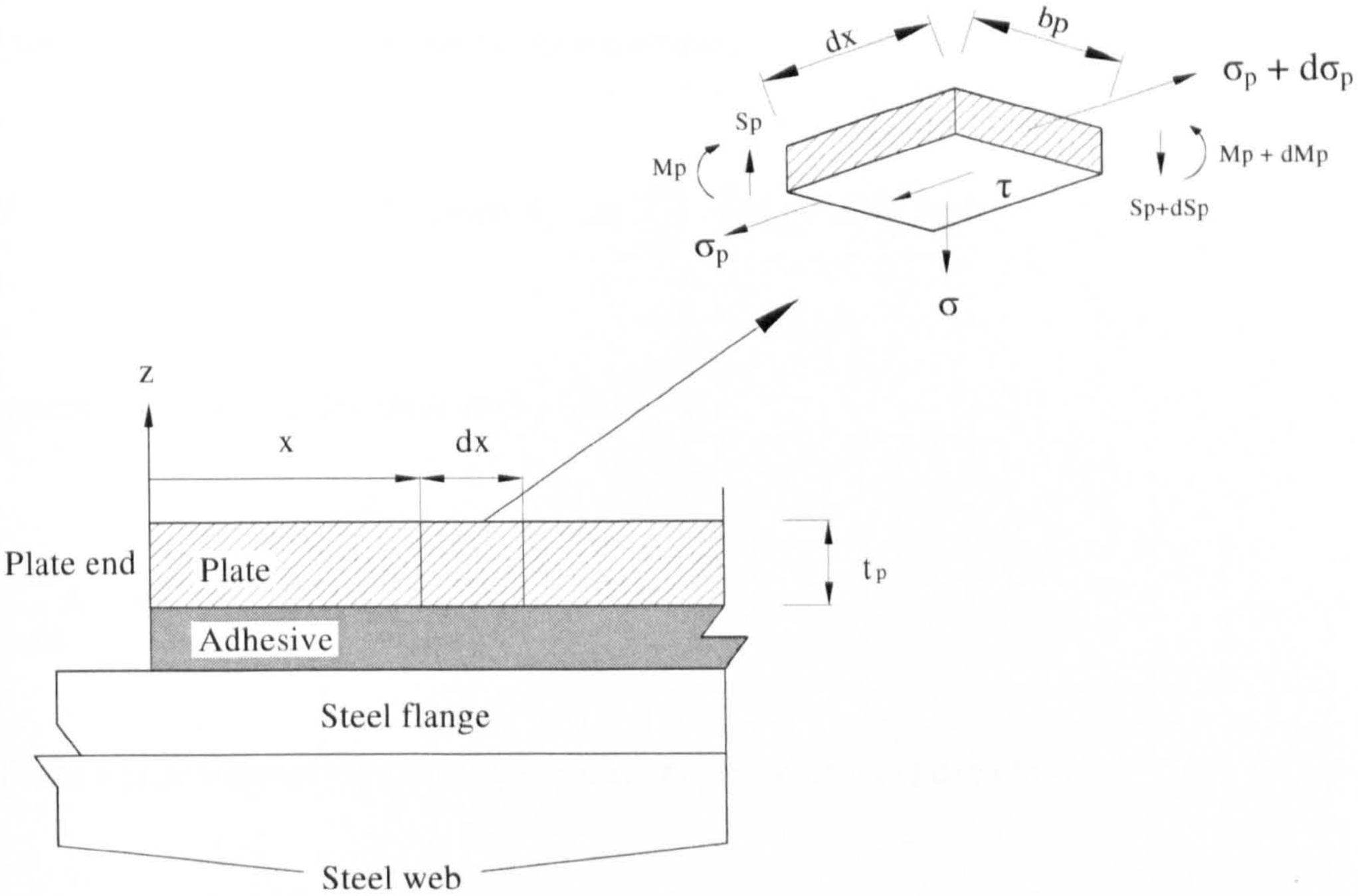

Figure 4A-1 - Differential section of the CFRP-plated steel beam

Take the infinitesimal plate element shown in Figure 4A-1. Equilibrium of the element in the longitudinal (x) direction gives:

$$(\sigma_p + d\sigma_p) \cdot b_p \cdot t_p = \sigma_p \cdot b_p \cdot t_p + \tau \cdot b_p \cdot dx \text{ and } \sigma_p = E_p \varepsilon_p$$

from which, τ can be obtained:

$$\tau = E_p t_p \frac{d\varepsilon_p}{dx}$$

For an element of finite length Δx, it can be approximated as:

$$\tau = E_p t_p \frac{\Delta\varepsilon_p}{\Delta x}$$

Consider moment equilibrium of plate element,

$$\tau \cdot b_p \cdot dx \cdot \frac{t_p}{2} + S_p \cdot dx + M_p - \sigma \cdot b_p \cdot dx \cdot \frac{dx}{2} - \left(M_p + dM_p\right) = 0$$

Ignore the second order term $\sigma \cdot b_p \cdot dx \cdot \frac{dx}{2}$,

$$\frac{dM_p}{dx} = S_p + \frac{\tau \cdot b_p \cdot t_p}{2}$$

From equilibrium of the plate element in the transverse (z) direction,

$$S_p - \sigma \cdot b_p \cdot dx - \left(S_p + dS_p\right) = 0$$

σ is then expressed as:

$$\sigma = -\frac{1}{b_p}\frac{dS_p}{dx} = -\frac{1}{b_p}\frac{d^2M_p}{dx^2} + \frac{t_p}{2}\cdot\frac{d\tau}{dx}$$

From local bending of the plate,

$$M_p = \frac{\sigma_z \cdot I_p}{y} = \frac{E_p \cdot \varepsilon_z \cdot I_p}{y} = E_p \cdot I_p \cdot \phi_p$$

Differentiate the above equation twice,

$$\frac{dM_p}{dx} = E_p \cdot I_p \cdot \frac{d\phi_p}{dx}$$

$$\frac{d^2M_p}{dx^2} = E_p \cdot I_p \cdot \frac{d^2\phi_p}{dx^2}$$

Substitute the above expression into the expression for σ,

$$\sigma = -E_p \cdot I_p \cdot \frac{1}{b_p} \cdot \frac{d^2\phi_p}{dx^2} + \frac{\tau \cdot t_p}{2} = -\frac{E_p \cdot t_p^3}{12} \frac{d\phi_p^2}{dx^2} + \frac{t_p}{2} \cdot \frac{d\tau}{dx}$$

where ϕ_p is the local curvature of the plate and can be expressed as:

$$\phi_p = \frac{\varepsilon_{out} - \varepsilon_{in}}{t_p}$$

where ε_{out} and ε_{in} are outer and inner surface strains of the plate, respectively.

Substitute ϕ_p and rearrange, the average normal stress may be expressed as:

$$\sigma = -\frac{E_p \cdot t_p^3}{12} \frac{\Delta\phi_p^2}{\Delta x^2} + \frac{t_p}{2} \cdot \frac{\Delta\tau}{\Delta x}$$

Appendix 4B

Loads from load cell readings

Three load cells were used to check how closely equilibrium was satisfied. Load cell 1 gives the total applied load, while load cells 2 and 3 record the centre and left end support reactions, respectively. The loads from all three load cell readings are given at each load step in Tables 4B-1 (a) to (d) for specimens B1 – B4, respectively.

Load step	Total applied load (Load cell 1) kN	Centre support reaction (Load cell 2) kN	Left end support reaction (Load cell 3) kN
1	0	0	0
2	60.73	39.42	11.6
3	95.03	62.85	17.7
4	135.46	90.73	24.7
5	181.49	122.69	32.2
6	224.2	152.35	40.48
7	264.27	180.93	47.235
8	304.88	210.05	54.453
9	333.06	230.5	58.21

(a) Specimen B1

Load step	Total applied load (Load cell 1) kN	Centre support reaction (Load cell 2) kN	Left end support reaction (Load cell 3) kN
1	0	0	0
2	57.4	37.51	11.42
3	113.23	75.03	20.56
4	174.49	116.75	31.98
5	238.72	160.93	45.68
6	289.83	195.47	54.82
7	350.03	236.49	66.24
8	363.86	245.08	68.53
9	382.41	256.82	70.81
10	387.84	259.63	73.1

(b) Specimen B2

Load step	Total applied load (Load cell 1) kN	Centre support reaction (Load cell 2) kN	Left end support reaction (Load cell 3) kN
1	0	0	0
2	25.24	17.15	4.499
3	47.49	33.08	8.998
4	69.92	49.36	11.247
5	92	65.46	15.746
6	113.73	80.86	20.245
7	135.28	96.09	22.495
8	157.54	112.01	26.994
9	180.49	128.29	31.493
10	203.27	144.22	33.742
11	225.18	159.62	38.241
12	239.55	169.77	40.491
13	259.87	184.12	42.74
14	278.8	197.25	44.99
15	301.4	213.17	49.489
16	319.98	226.3	53.988
17	339.78	240.3	56.237
18	353.8	250.1	58.487
19	372.37	263.05	62.986
20	383.06	270.23	62.986
21	397.08	280.03	65.235
22	403.21	284.06	65.235
23	412.33	289.66	67.485
24	418.28	293.16	67.485
25	432.65	298.93	69.734
26	442.12	301.73	69.734
27	453.33	305.06	71.984

(c) Specimen B3

Load step	Total applied load (Load cell 1) kN	Centre support reaction (Load cell 2) kN	Left end support reaction (Load cell 3) kN
1	0	0	0
2	22.79	15.4	4.499
3	42.41	28.88	6.748
4	65.72	44.98	11.247
5	102.34	69.83	17.996
6	133.18	91.01	24.744
7	168.75	115.16	29.243
8	162.1	110.26	26.994
9	225.98	151.77	37.862
10	247.43	169.24	42.74
11	293.35	203.02	51.738
12	277.05	194.27	47.239
13	315.42	221.22	53.988
14	370.97	260.78	62.986
15	384.64	270.75	65.235
16	402.16	283.71	67.485
17	411.8	290.53	69.734

(d) Specimen B4

Table 4B-1 - Loads from load cell readings

Chapter 5

Analysis of Ductility-Deficient Indeterminate Structures

5.1 Introduction

So far in this thesis, both the theoretical analysis in Chapter 3 and the experimental work in Chapter 4 have focused on FRP-plated 2-span continuous steel members. One other issue identified in Chapters 1 and 2 was that design using the procedure for traditional statically indeterminate reinforced concrete (RC) structures (as outlined in Chapter 1 and reproduced in Figure 5-1(a)) may be unsafe for ductility-deficient indeterminate structures such as steel over-reinforced or FRP-strengthened RC structures. An alternative approach is needed for these latter structures.

One such approach, outlined in Chapter 1 and reproduced in Figure 5-1(b), entails an iterative loop where analysis is conducted to quantify the load capacity of the detailed structure, with any deficiency in capacity triggering a re-detailing of the structure. This chapter focuses on quantifying the load capacity by presenting a computational technique for time-efficient prediction of ultimate loads of indeterminate members of varying ductility. Re-detailing of the structure will be addressed in Chapter 6.

In what follows, the idea of stiffness-moment convergence at the ultimate limit state which underpins the present capacity analysis is first introduced, after which an iterative procedure based on submission of section stiffness of the structure into linear elastic analysis will be presented. The procedure is then illustrated by way of examples including a ductility-compromised frame and multi-span continuous beams, which possess varying levels of ductility. Finally, this procedure is extended to incorporate effects of states of self-stress and to investigate behaviours in the pre-failure non-linear regime.

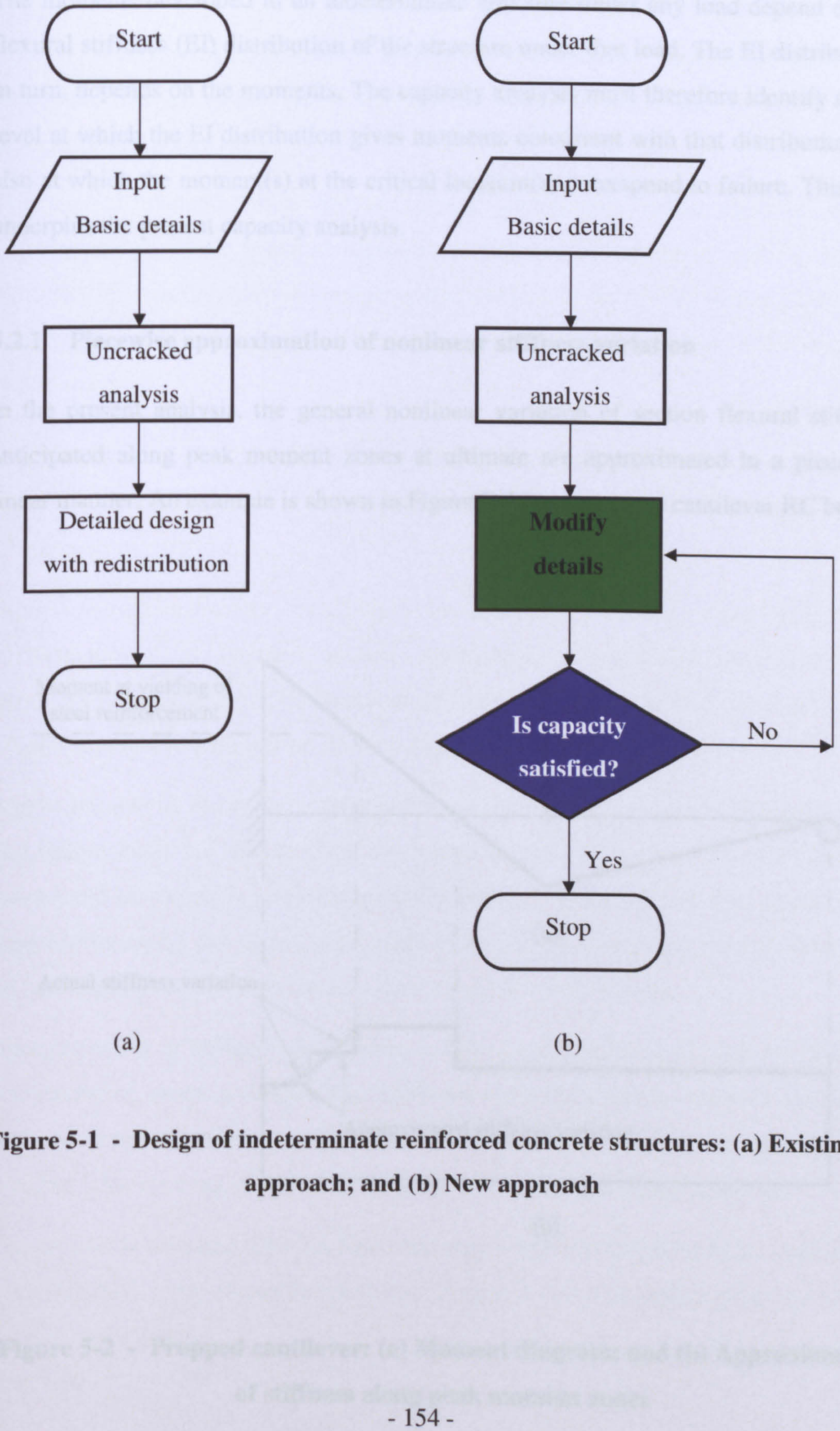

Figure 5-1 - Design of indeterminate reinforced concrete structures: (a) Existing approach; and (b) New approach

5.2 Capacity Analysis of Ductility-Deficient Structures

Any proposed analysis for load capacity must apply whatever the structure's ductility. The moments developed in an indeterminate structure under any load depend on the flexural stiffness (EI) distribution of the structure under that load. The EI distribution, in turn, depends on the moments. The capacity analysis must therefore identify a load level at which the EI distribution gives moments consistent with that distribution and also at which the moment(s) at the critical location(s) correspond to failure. This idea underpins the present capacity analysis.

5.2.1 Piecewise approximation of nonlinear stiffness variation

In the present analysis, the general nonlinear variation of section flexural stiffness anticipated along peak moment zones at ultimate are approximated in a piecewise linear manner. An example is shown in Figure 5-2 for a propped cantilever RC beam.

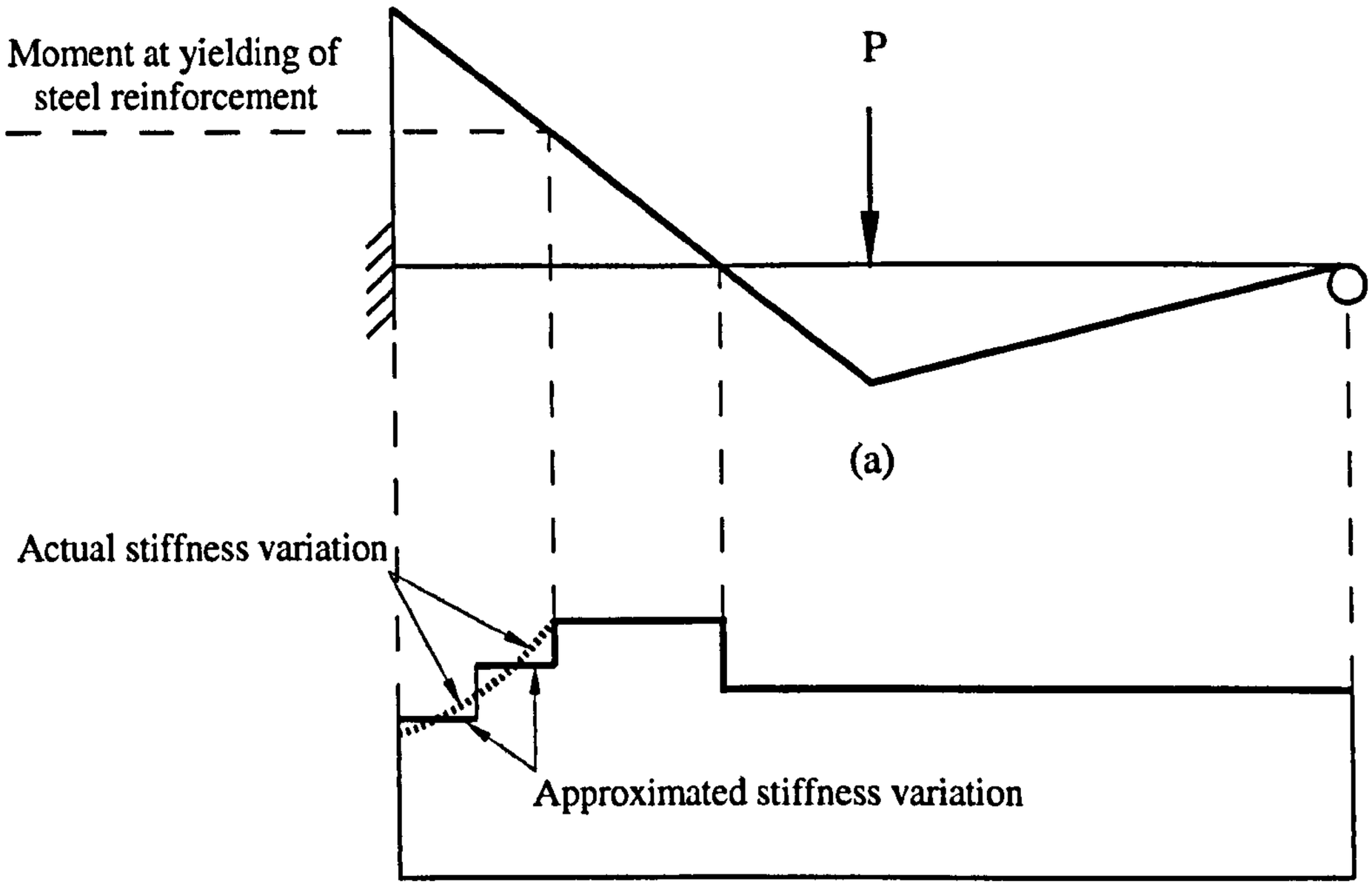

Figure 5-2 - Propped cantilever: (a) Moment diagram; and (b) Approximation of stiffness along peak moment zones

5.2.2 Iterative computation procedure for capacity analysis

An iterative procedure is adopted for the capacity analysis. A flow chart of the iterative procedure is given in Figure 5-3. The key steps are explained in detail below:

- Initially, a constant EI distribution is used for convenience. Analysis is carried out under an arbitrary magnitude of load for the prescribed load pattern to obtain the moment distribution.

- The critical moment (here defined as that giving the highest ratio relative to corresponding section moment capacity) is factored to equate to section moment capacity. The critical moment section is also defined as the critical section. The factor used to achieve this is also applied to the entire moment distribution of the structure, and to the load.

- A trial-and-error method may have to be performed in respect of non-critical peak moment(s) while maintaining the moment constant at the critical section in an attempt to achieve convergence.

- From moment-curvature relations, cracked/yield stiffness (EI) distribution corresponding to the factored moment distribution is obtained. The general nonlinear variation of section flexural stiffness anticipated along peak moment zones at ultimate is approximated in a piecewise linear manner.

- Bigger number of linear steps gives better approximations to the true EI distributions and failure loads but also requires more time to update the input information in the subsequent analyses. A good compromise between accuracy and time-efficiency is achieved by using 2-4 steps (along each ascending or descending branch) depending on how rapidly the stiffness changes over the peak moment zone;

- Approximation of stiffness distribution is input to the linear beam analysis to obtain corresponding moment distribution. Different mesh sizes may be used for the various stiffness zones to ensure comparable element stiffnesses so any ill-conditioning is avoided. This moment distribution is factored to satisfy the failure condition.

- The process is repeated until the EI-moment convergence and the failure condition are both satisfied. A prescribed tolerance on change in the load capacity may be used to test for convergence.

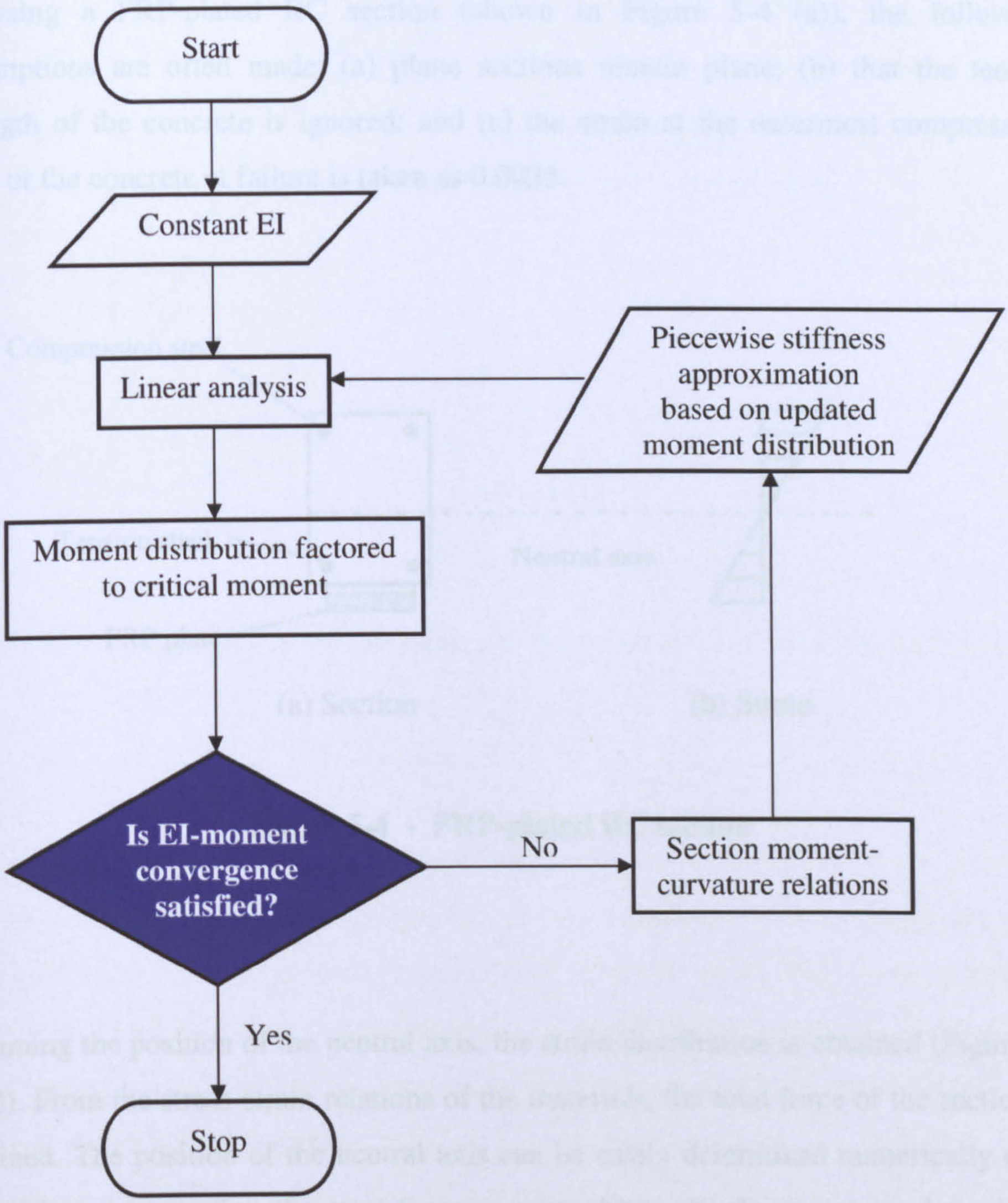

Figure 5-3 - Proposed capacity analysis procedure

5.2.3 Moment-curvature relations of FRP-plated concrete sections

The EI values are the secant gradients of the moment-curvature relations. When analysing a FRP-plated RC section (shown in Figure 5-4 (a)), the following assumptions are often made: (a) plane sections remain plane; (b) that the tensile strength of the concrete is ignored; and (c) the strain at the outermost compression fibre of the concrete at failure is taken as 0.0035.

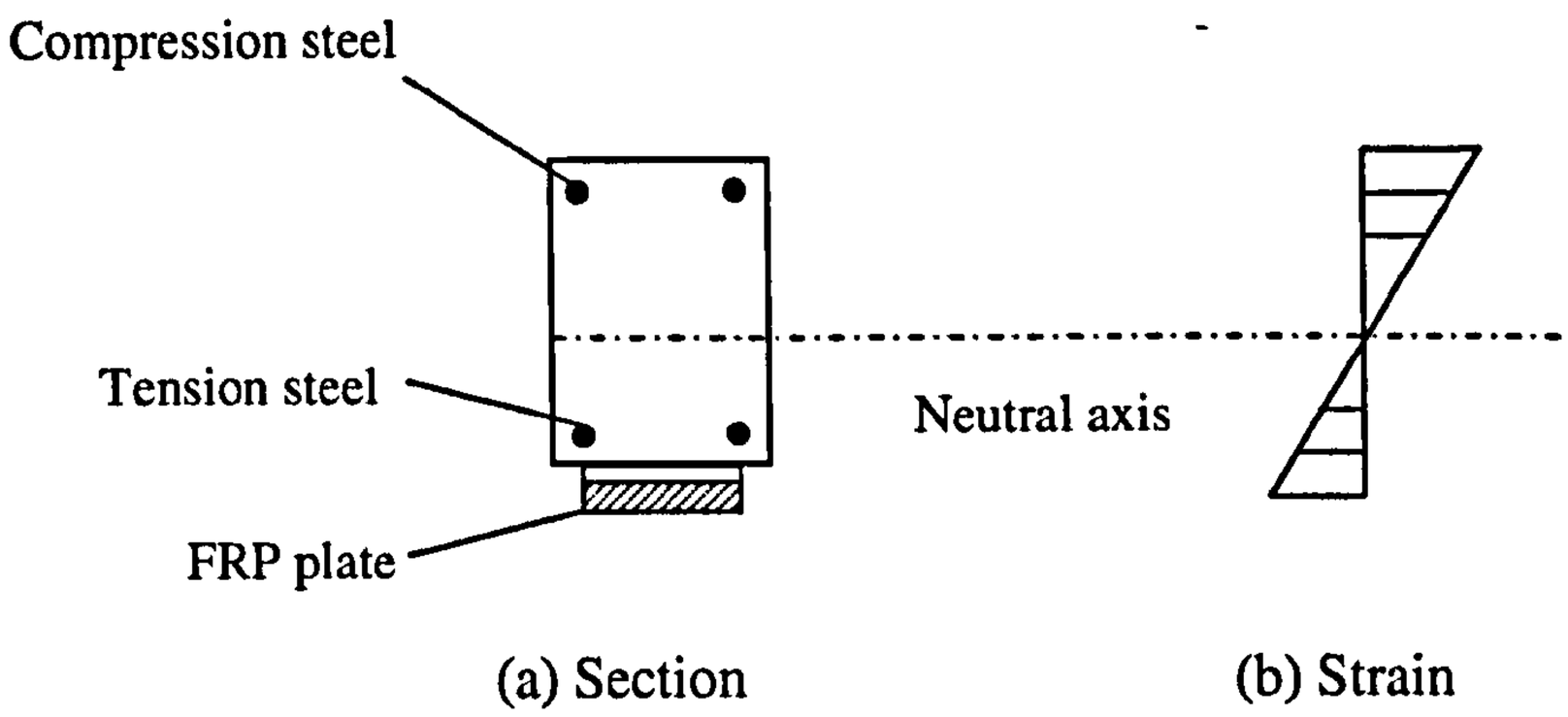

Figure 5-4 - FRP-plated RC section

Assuming the position of the neutral axis, the strain distribution is obtained (Figure 5-4 (b)). From the stress-strain relations of the materials, the total force of the section is obtained. The position of the neutral axis can be easily determined numerically on a spreadsheet by equating the total force to zero. Alternatively, it can be determined analytically as in Sebastian (2002). The bending moment and curvature are then obtained based on the actual position of the neutral axis.

The moment-curvature relations used henceforth are based on general non-linear or multi-linear material behaviours for the concrete, steel and FRP. These relations can be found in and have been verified using published test data in Sebastian (2002). An example is shown in Figure 5-5 for the moment-curvature relations of the section of the beam E4 in El-Refaie *et al.* (2003b).

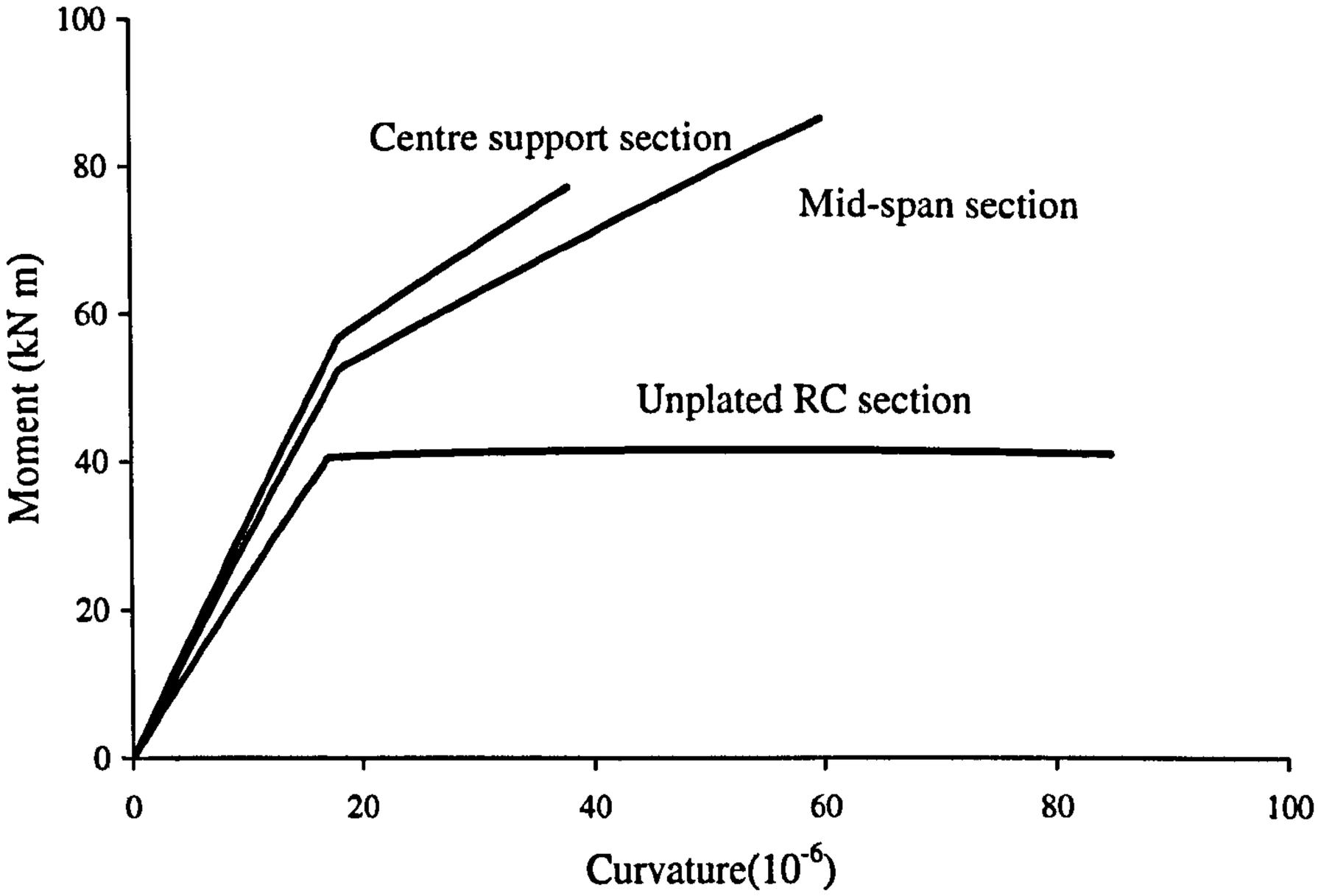

Figure 5-5 - Moment-curvature relations for beam E4 in El-Refaie *et al.* (2003b)

Prakhya and Morley (1990) have comprehensively demonstrated how these moment-curvature relations can be influenced by tension stiffening in the cracked concrete. Such influence is not considered in the present analysis. Also, beam spans are likely to contain zones of differing reinforcement (as outlined in Chapter 3). In the linear beam analysis, appropriate moment-curvature relations should be obtained and assigned to these various zones.

5.2.4 Verification study

In this section, this procedure is applied to beam E4 in El-Refaie *et al.* (2003b) to obtain the load capacity. The details of the beam were given in Chapter 3 and shown again in Figure 5-6. The beam failed by peeling failure of the FRP plate over the centre support section. Therefore, the centre support section moment reported in the paper at failure is taken as the ultimate moment in the present analysis.

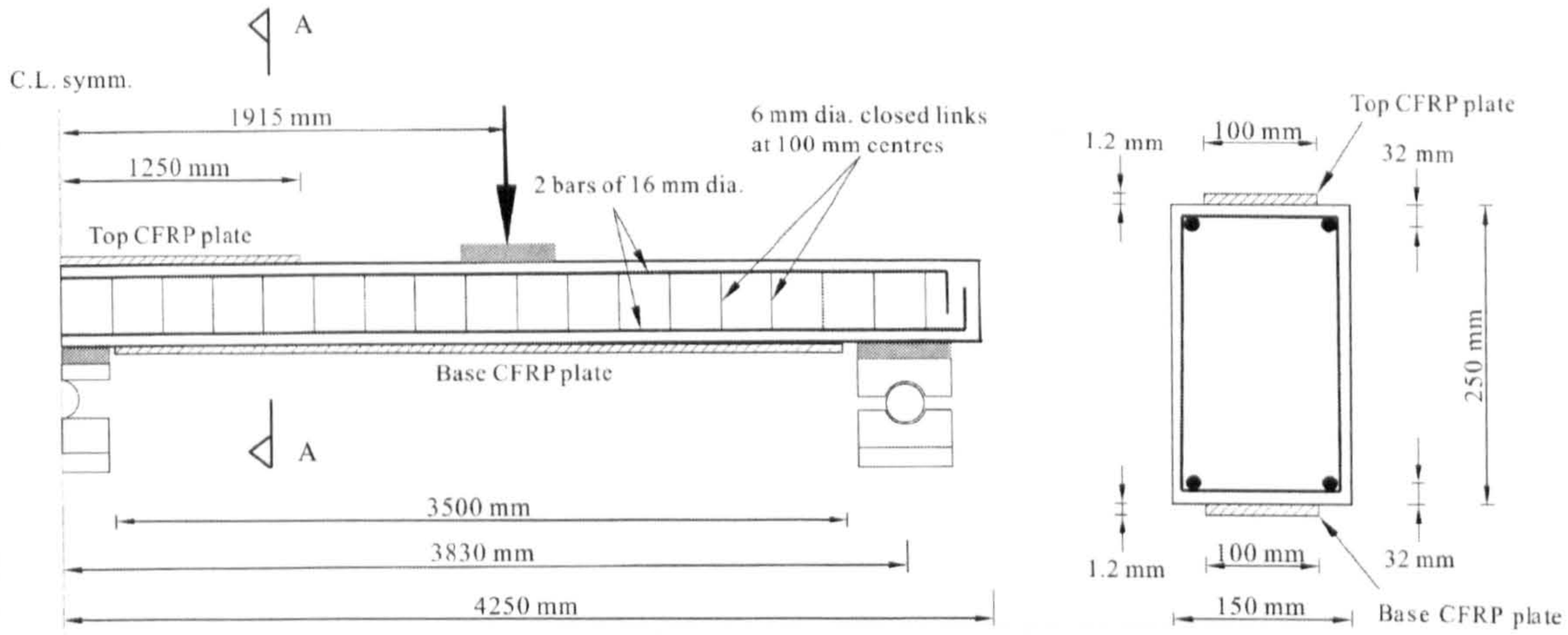

(a) Elevation (b) Section A-A

Figure 5-6 - Test details (E4 in El-Refaie *et al.* 2003b)

The ultimate load obtained from the present analysis is 220 kN compared to 231 kN from the test data. The results converged after 6 iterations. Figure 5-7 shows the variation of normalised predicted failure load with iterations. The stiffness variation along the right span after the final iteration is shown in Figure 5-8 compared with that obtained from the moment diagram reported by El-Refaie *et al.* (2003b) and corresponding moment-curvature relations shown in Figure 5-5. The good agreement between the predicted and experimental results gives confidence in the piecewise linear approximation of the nonlinear stiffness variation.

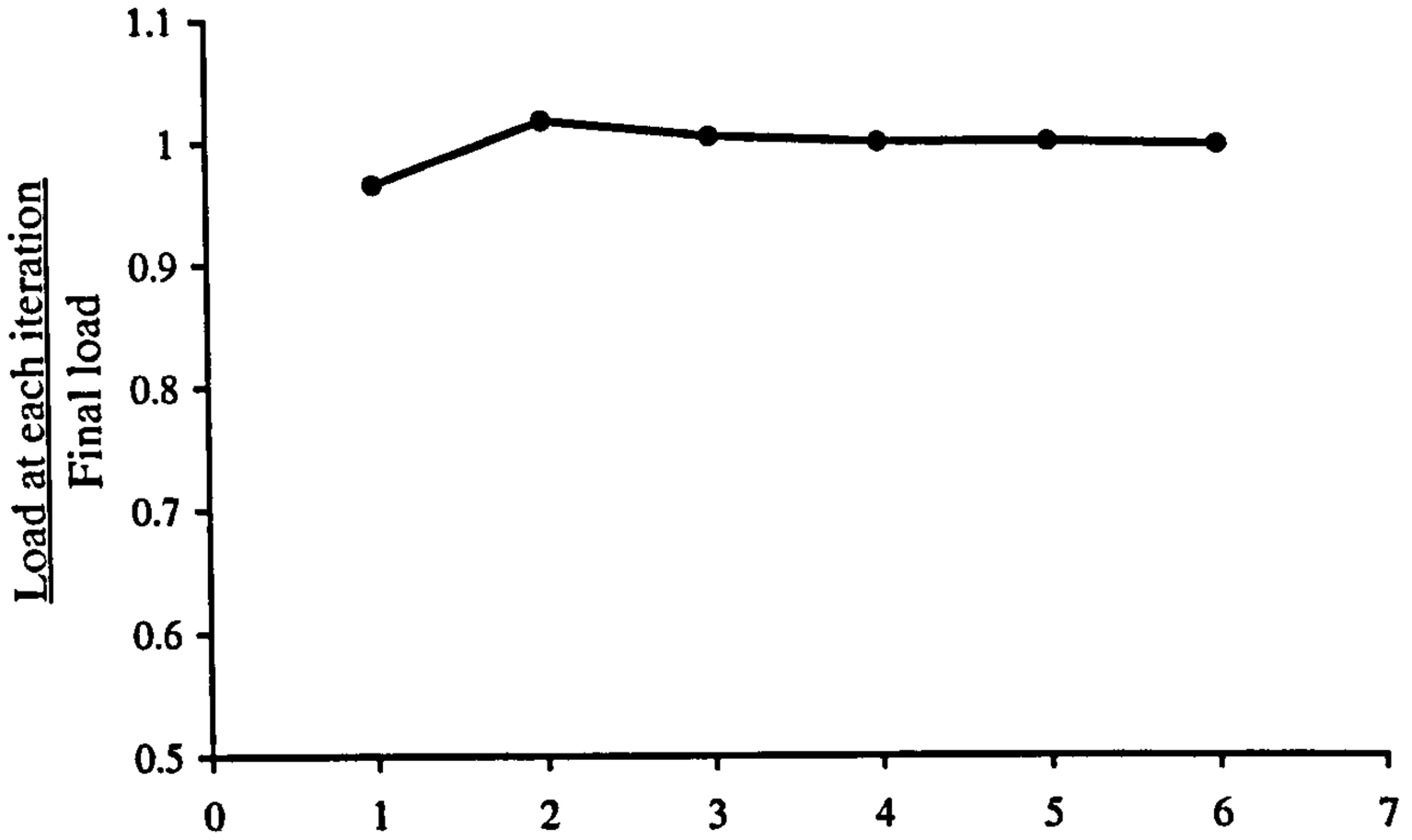

Figure 5-7 - Variation of predicted failure loads with iterations

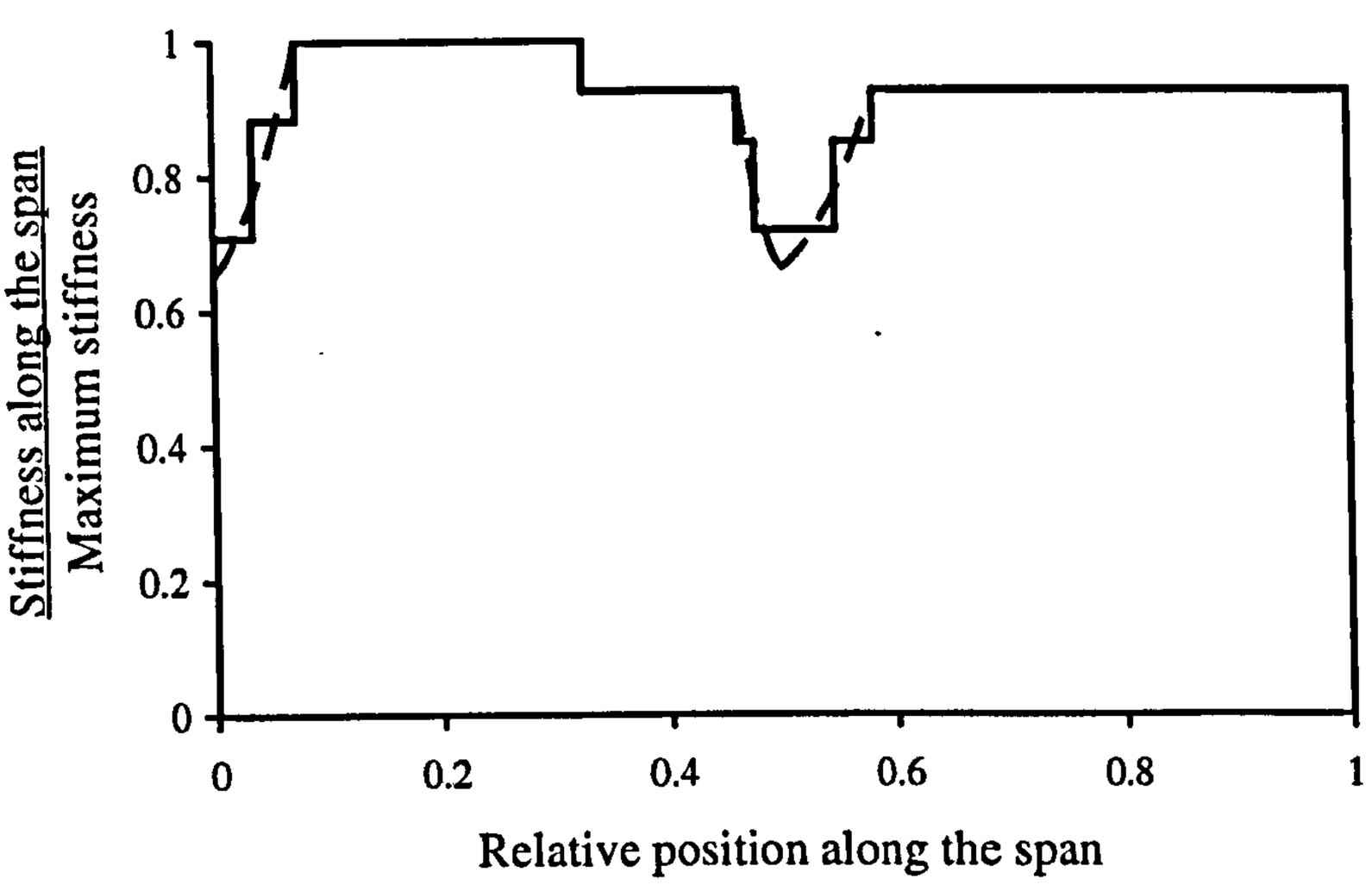

Figure 5-8 - Stiffness variation (El-Refaie *et al.* 2003b)

In what follows, the procedure is applied to a number of more complex structures, including a ductility-compromised frame and multi-span continuous beams, which possess various levels of ductility, to further demonstrate its efficiency.

5.3 Analytical study

In this section, the above proposed computational procedure is applied to three different structures of differing ductility, reinforced with either strain hardening steel or with fibre reinforced polymer (FRP) and perfectly plastic steel. Two continuous beam structures with different boundary conditions and a frame are considered.

In the following examples, both the steel and FRP are of Young's modulus 200 kN/mm^2, while the steel is of yield stress 460 N/mm^2 and is perfectly plastic unless stated otherwise. The FRP is assumed to be of rupture stress in excess of the maximum FRP stresses developed at predicted failure of the structures concerned. Also, sufficient anchorage to prevent separation of the FRP from the concrete is assumed, so that failure always occurs by crushing of the concrete.

5.3.1 Example 1

The first example is shown in Figure 5-9 and comprises a 300 mm wide, two-span continuous beam with rotationally free ends. All dimensions of Figure 5-9 are in mm. Only embedded steel reinforcement with a strain hardening modulus of 5 kN/mm^2 is used. The structure, but not the load – a UDL on one span and a point load of half the UDL at the other mid-span – is symmetric about the centre support. The hog and sag steel areas are 1950 mm^2 and 1350 mm^2 respectively. Moment-curvature relations for the different reinforced sections can be seen in Figure 5-10. 'D' refers to doubly reinforced sections, 'H' to a hogging section, 'S' to a sagging section. Hence 'DS' refers to a doubly reinforced section in sagging.

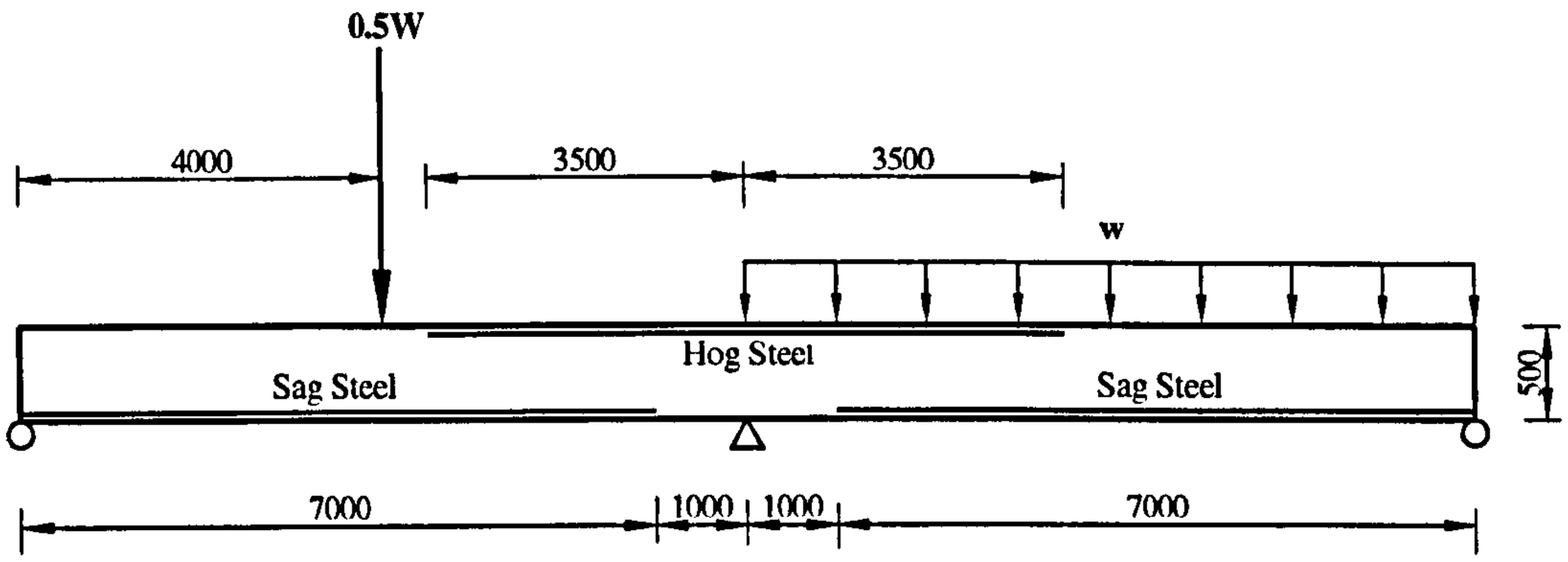

Beam of 300mm width

Figure 5-9 - Two-span continuous beam with rotationally free ends

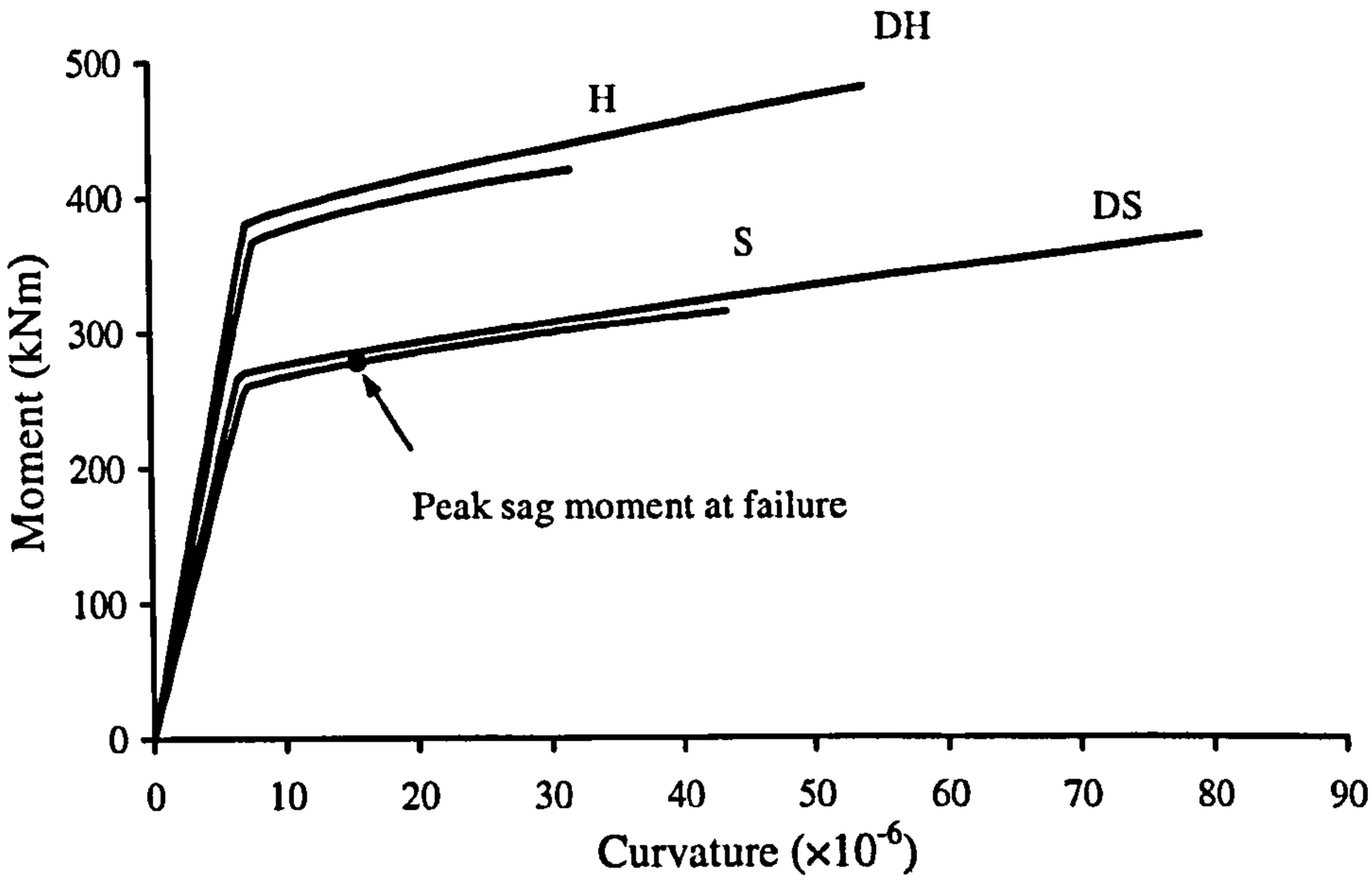

Figure 5-10 - Moment-curvature relations for Beam 1 (ductile)

The analysis predicted moment failure over the central support at 58 kN/m UDL. Ten iterations gave convergence onto this load. This convergence coincided with attainment of moment-EI consistency and with the failure condition being satisfied. The critical section is the centre support section. At failure, a maximum of 88.3% of the sag moment capacity was activated within the right span. The corresponding point

is shown on the moment-curvature curve in Figure 5-10. Linear analysis based on constant stiffness distribution along the spans of the beam, which is common in conventional design of concrete structures, gives a failure load of 60 kN/m. Linear analysis based on the different stiffness zones in the linear regime (see Chapter 3) gives a failure load of *circa* 56 kN/m. Clearly, ignoring the actual stiffness variation along the spans overestimates the load capacity of the structure in this case. On the other hand, plastic analysis – assuming that both the hog and sag moment capacities were activated – gives a failure load of 63 kN/m. The deviation of the failure load for plastic analysis is given in Appendix 5A. Over 92% of the plastic capacity is actually achieved for the structure compared to less than 89% from the linear analysis, suggesting that there *is* some level of ductility in the FRP-plated structure.

Figure 5-11 shows the variation of normalised predicted failure load with iterations. Palpable oscillations of predicted load occurred during the first five iterations, indicating the process of identifying the critical section (the centre support section in this case), with some stability thereafter. Figure 5-12 shows, for iteration 5, the normalised EI distribution along the normalised length of the member. Extensive steel yield up to concrete crushing over the centre support and lesser steel yield not up to concrete crushing within the mid-span under UDL account for the reduced EI values in those zones. The narrow zone of low EI over the centre support is attributable to the rapid fall-off of moment there, while the yield zone in the UDL mid-span region is wider owing to the low change of high moment along the parabolic moment variation.

Figure 5-11 - Variation of predicted failure load with iterations for Beam 1

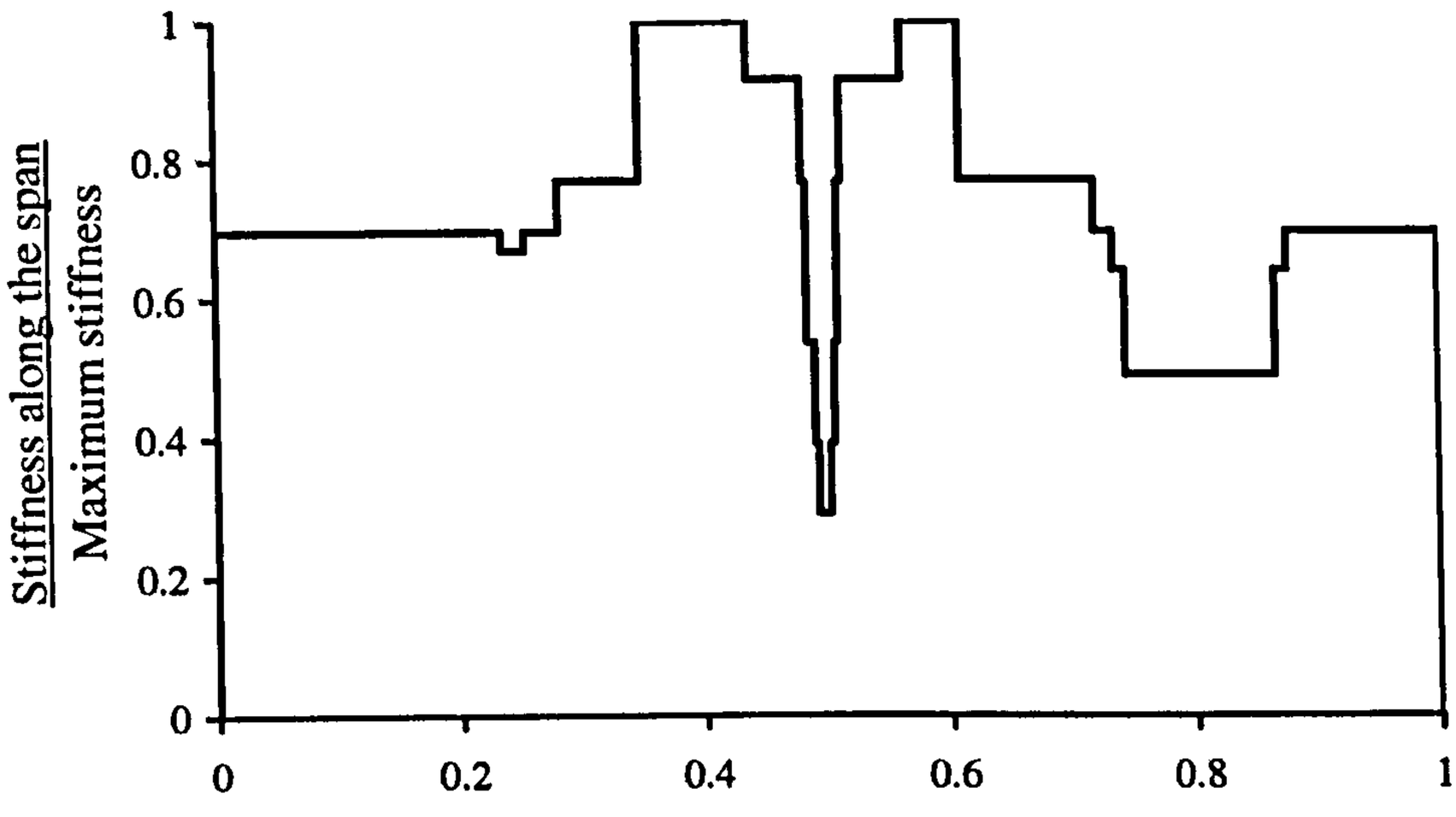

Figure 5-12 - Normalised EI distribution at convergence for Beam 1

5.3.2 Examples 2 and 3

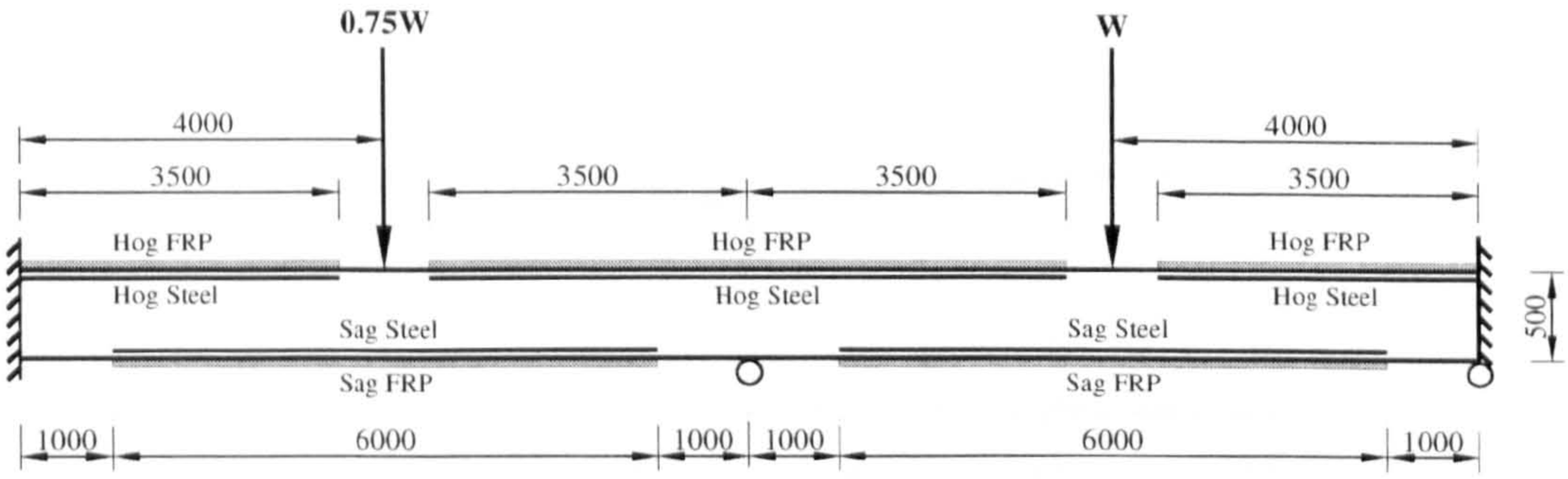

Beam of 300mm width

Figure 5-13 - Two-span continuous beam with encastered ends

This example, shown in Figure 5-13, again comprises a 300 mm wide, two-span continuous member, but this time with encastered ends and is reinforced with both steel and FRP. Again, the structure but not the loading is symmetric about the centre support. The use of a point load at each mid-span – rather than a UDL and a point load as in Example 1 – make for different redistribution characteristics after first yield relative to Example 1. This is accentuated by the different ratio (0.75) between the two point loads relative to the value (0.5) used in example 1. The hog FRP reinforcements at the ends are assumed to be adequately anchored (say, by embedment in the walls or other structures which provide the end restraints) to avoid FRP-steel separation. The hog and sag steel areas are 2550 mm^2 and 750 mm^2 respectively, while the hog and sag FRP areas are 36 mm^2 and 15 mm^2. These modest FRP areas give slightly rising moment-curvature characteristics after steel yield. Figure 5-14 shows that the hogging sections ('H') have short ductility near-plateaux while the mid-span sections are of significant ductility.

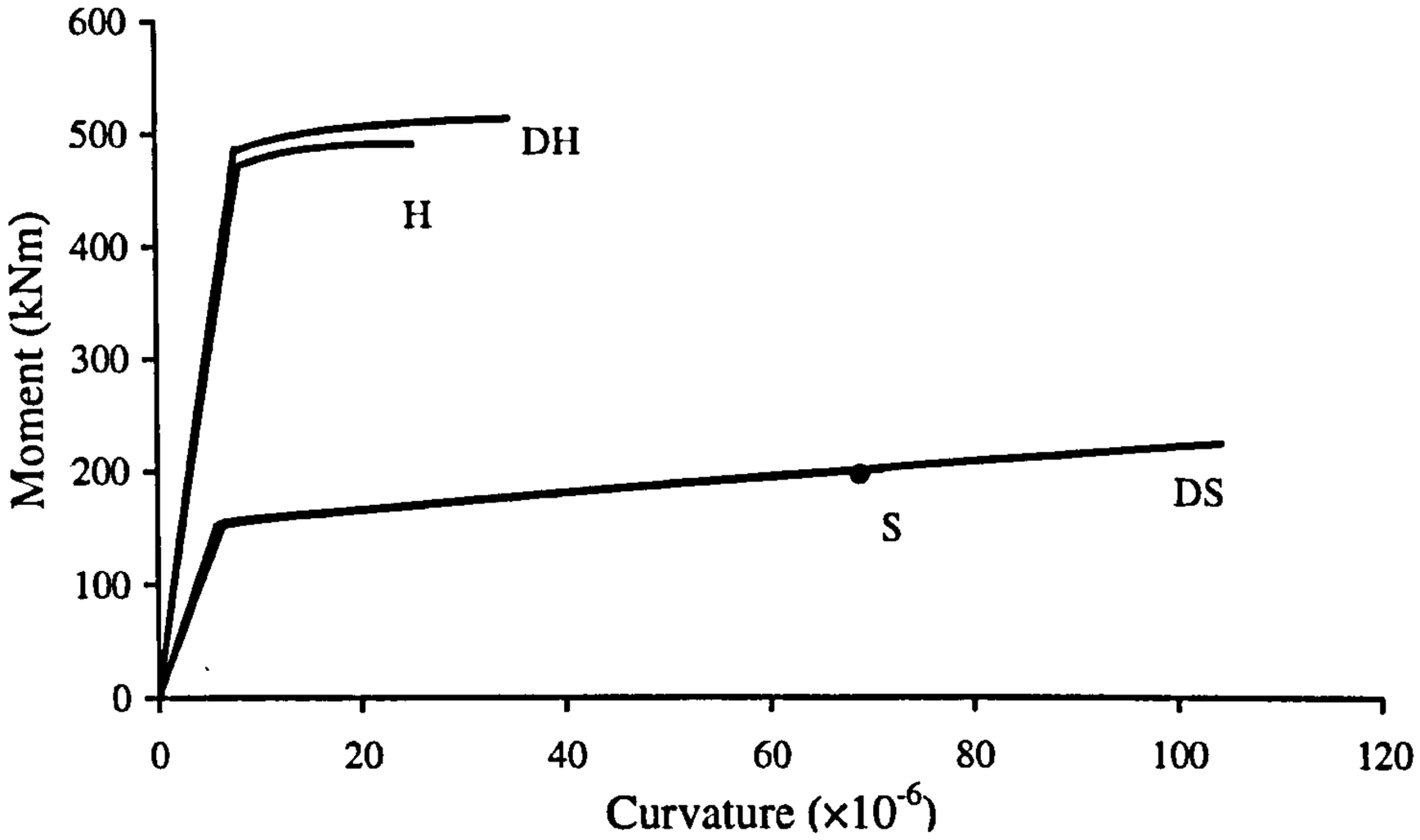

Figure 5-14 - Moment-curvature relations for Beam 2 (ductile)

Figure 5-15 shows that the analysis results oscillated significantly for the first six iterations, with convergence from the 7th to the 8th iteration. Figure 5-16 gives the normalised EI distribution along the structure at the final predicted failure load of 312 kN, with predicted failure over the end support for the more heavily loaded span, which is the critical section. Particular care was taken with the element mesh in zones of rapidly varying EI value to avoid ill-conditioning. This EI distribution represents extensive steel yielding at the outer support for the more heavily loaded span and also at both mid-span locations owing to the high sag moments generated by the point loads, the effect being more pronounced in the more heavily loaded span. Thus the significant length of the near-plateau in the more heavily load mid-span zone permitted some ductile behaviour.

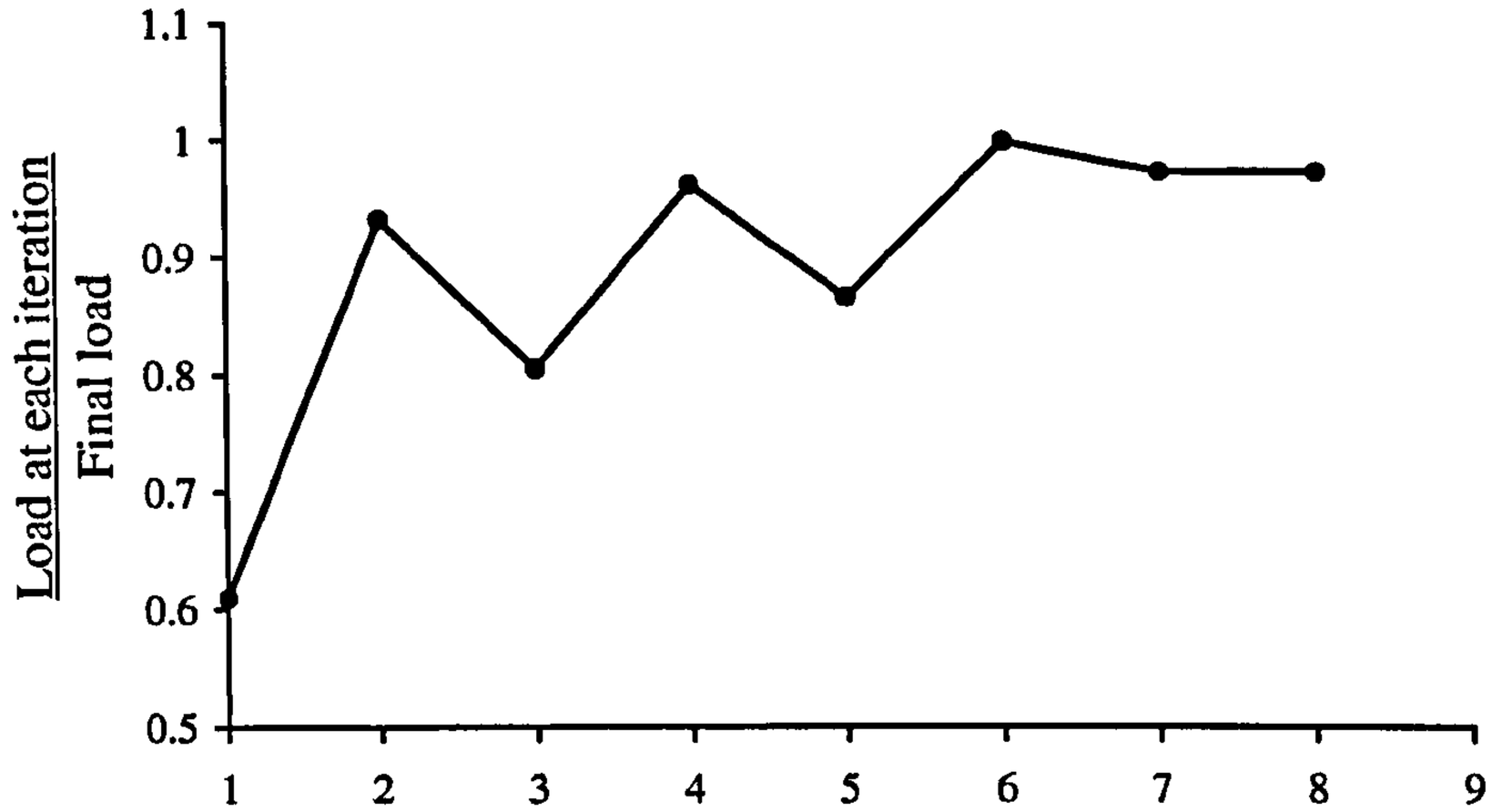

Figure 5-15 - Variation of predicted failure loads with iterations for Beam 2

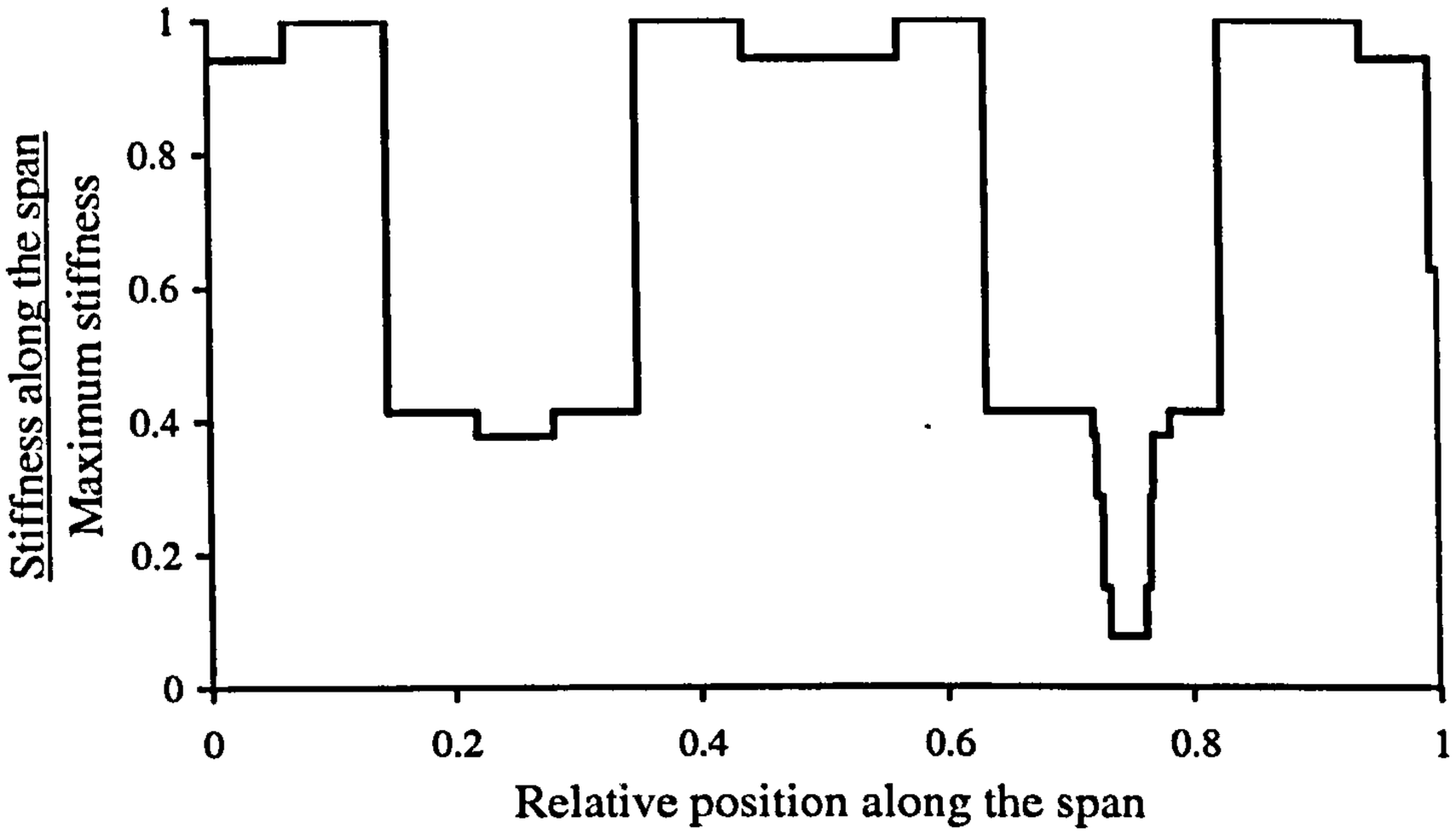

Figure 5-16 - Normalised EI distribution at convergence for Beam 2

If, instead, the member is FRP strengthened to a significantly higher extent by increasing the FRP areas to 200 mm^2 and 350 mm^2 for hog and sag respectively, giving the significantly strain hardened moment-curvature relations of Figure 5-17, then the convergence characteristics of the iterative procedure change to that of Figure

5-18. Fewer iterations are needed for convergence than previously, with lesser fluctuation of the predicted failure load (finally 492 kN). The normalised EI distribution at iteration 3, *en rout* to convergence is given in Figure 5-19.

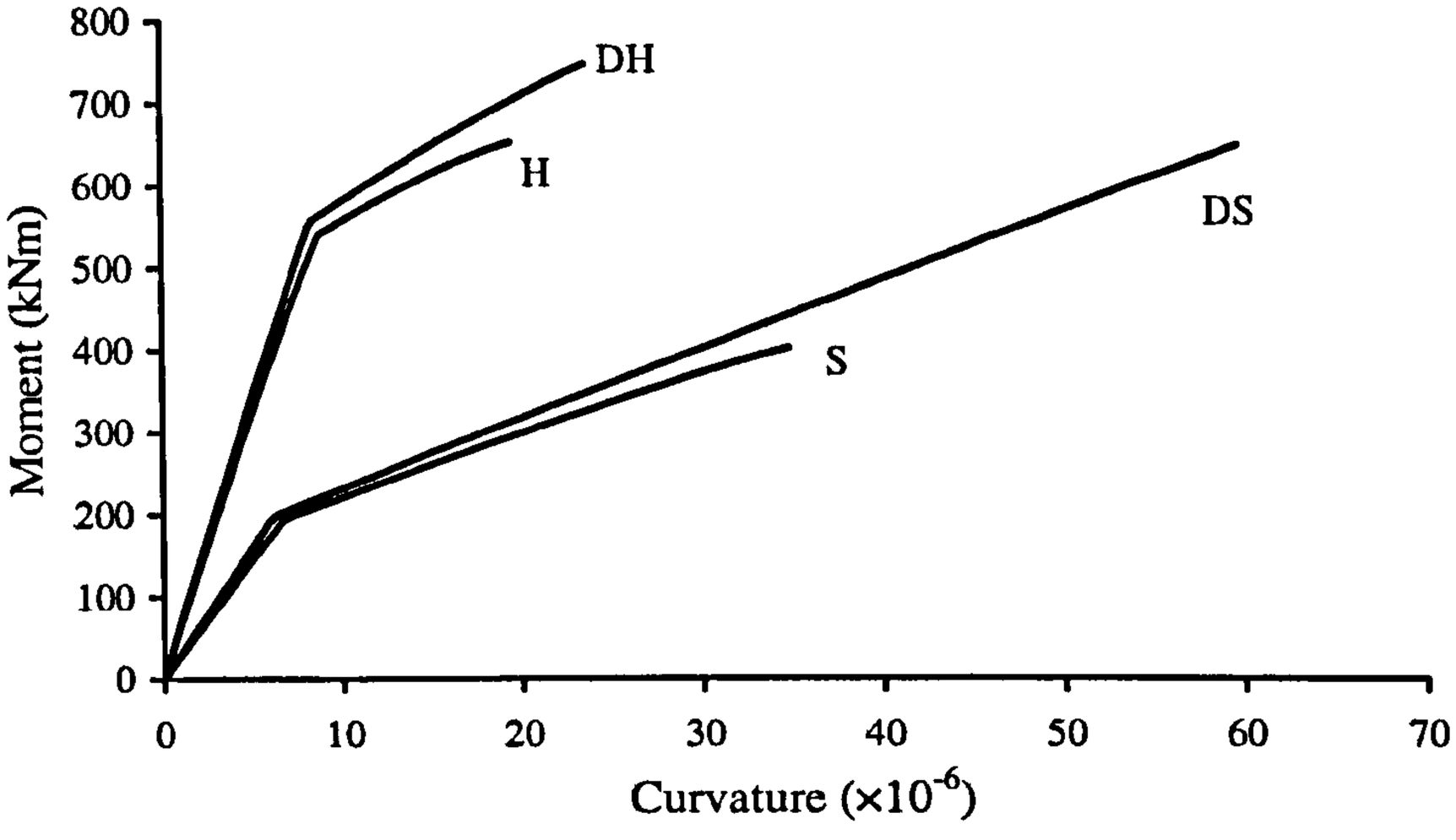

Figure 5-17 - Moment-curvature relations for Beam 3 with non-ductile sections

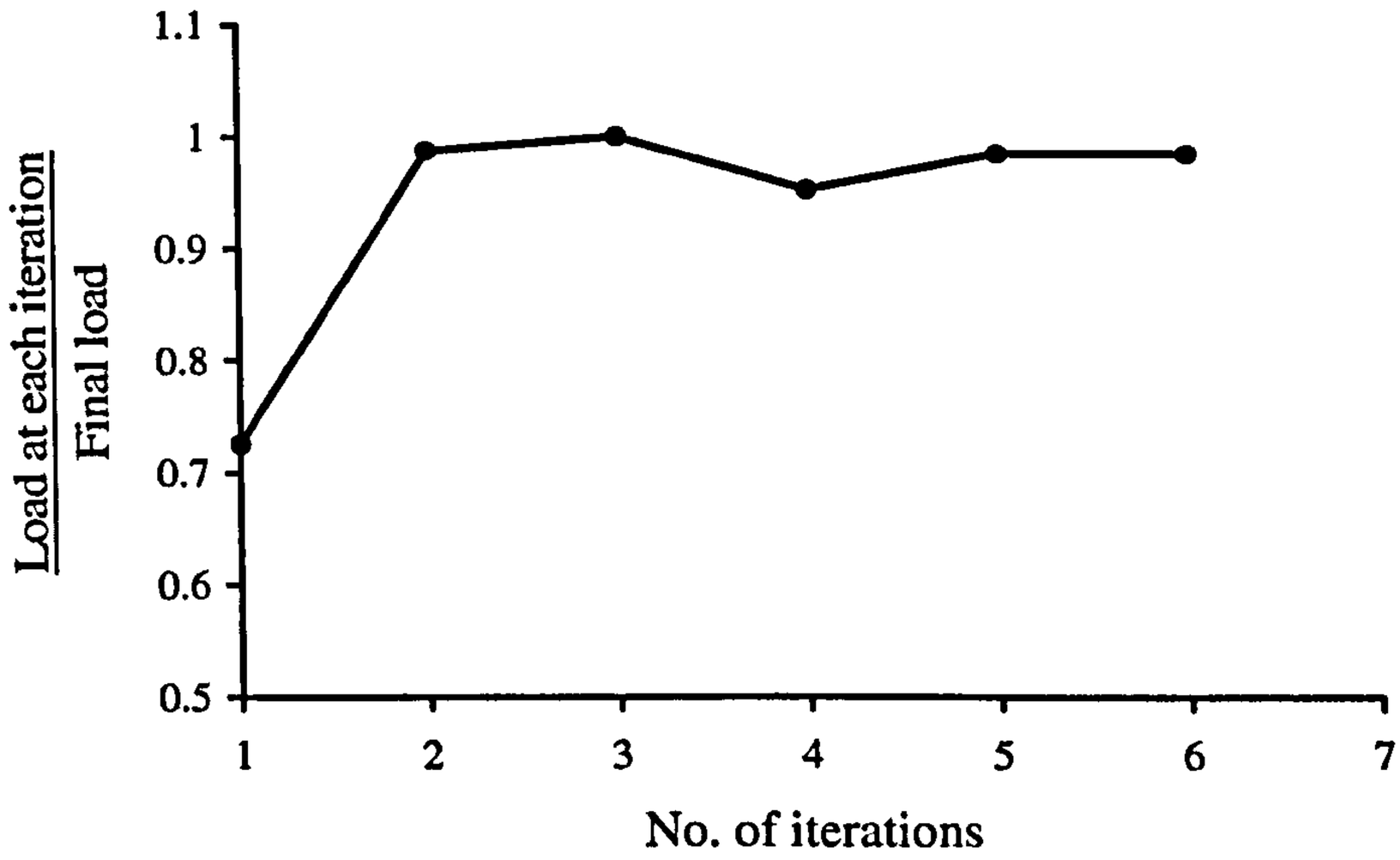

Figure 5-18 - Variation of predicted failure load with iterations for Beam 3

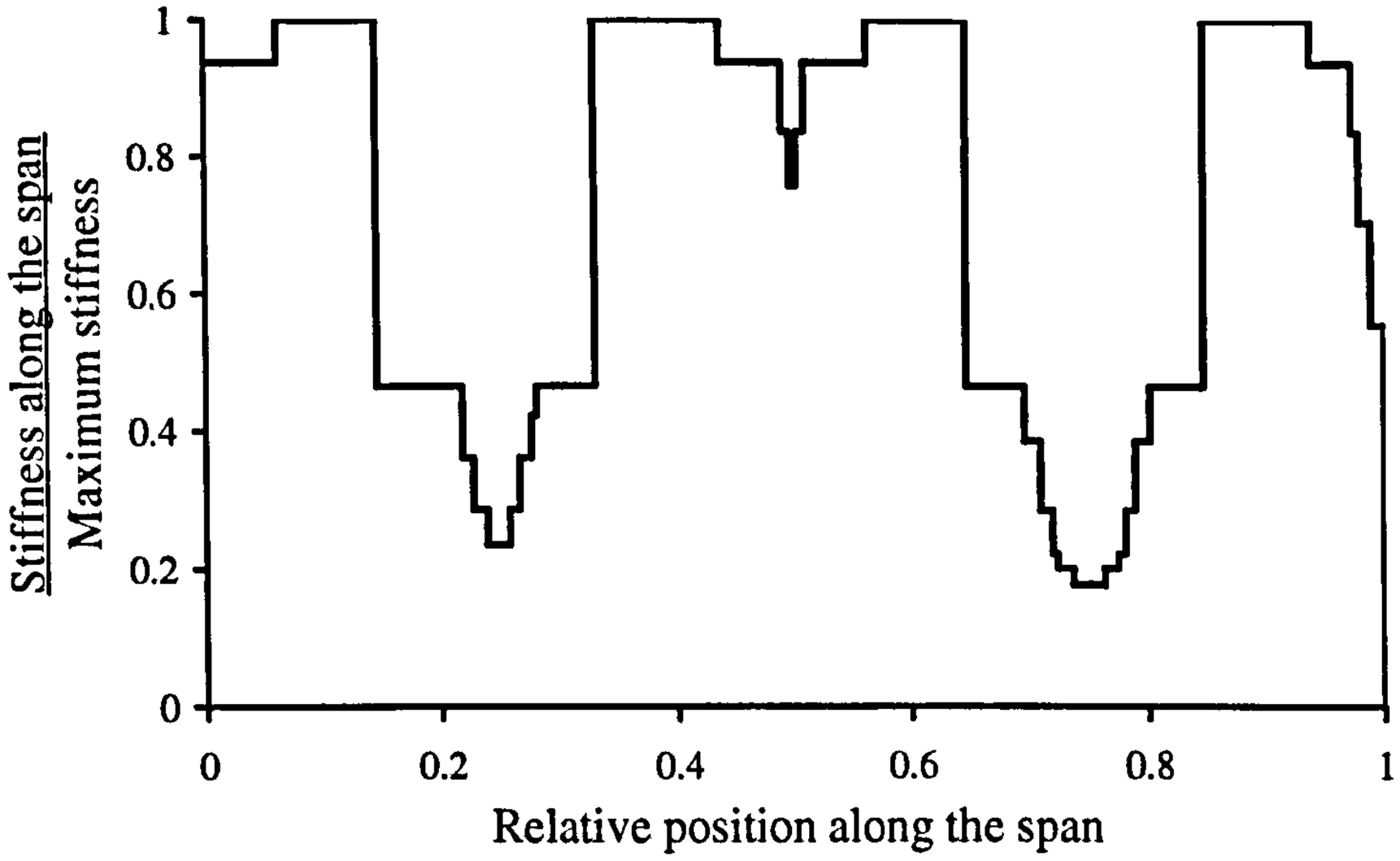

Figure 5-19 - Normalised EI distribution after iteration 3 for Beam 3

5.3.3 Example 4

A 300 mm wide steel and FRP RC frame under horizontal and vertical loads is considered in the final example, see Figure 5-20. Again, adequate anchorage of the FRP is assumed on both the beams and columns. The FRP and steel areas are given in brackets next to the relevant labels in the Figure. The significant FRP reinforcing leads to largely cracked linear behaviour up to failure. In this case only four iterations are needed to converge onto a failure state (predicted at 640 kN) as shown in Figure 5-21. Indeed, the second iteration is quite close to that final state and the iterations are stable thereafter, as may be expected from the minimal deviation from linear (although cracked) behaviour exhibited by this frame at the maximum moment sections.

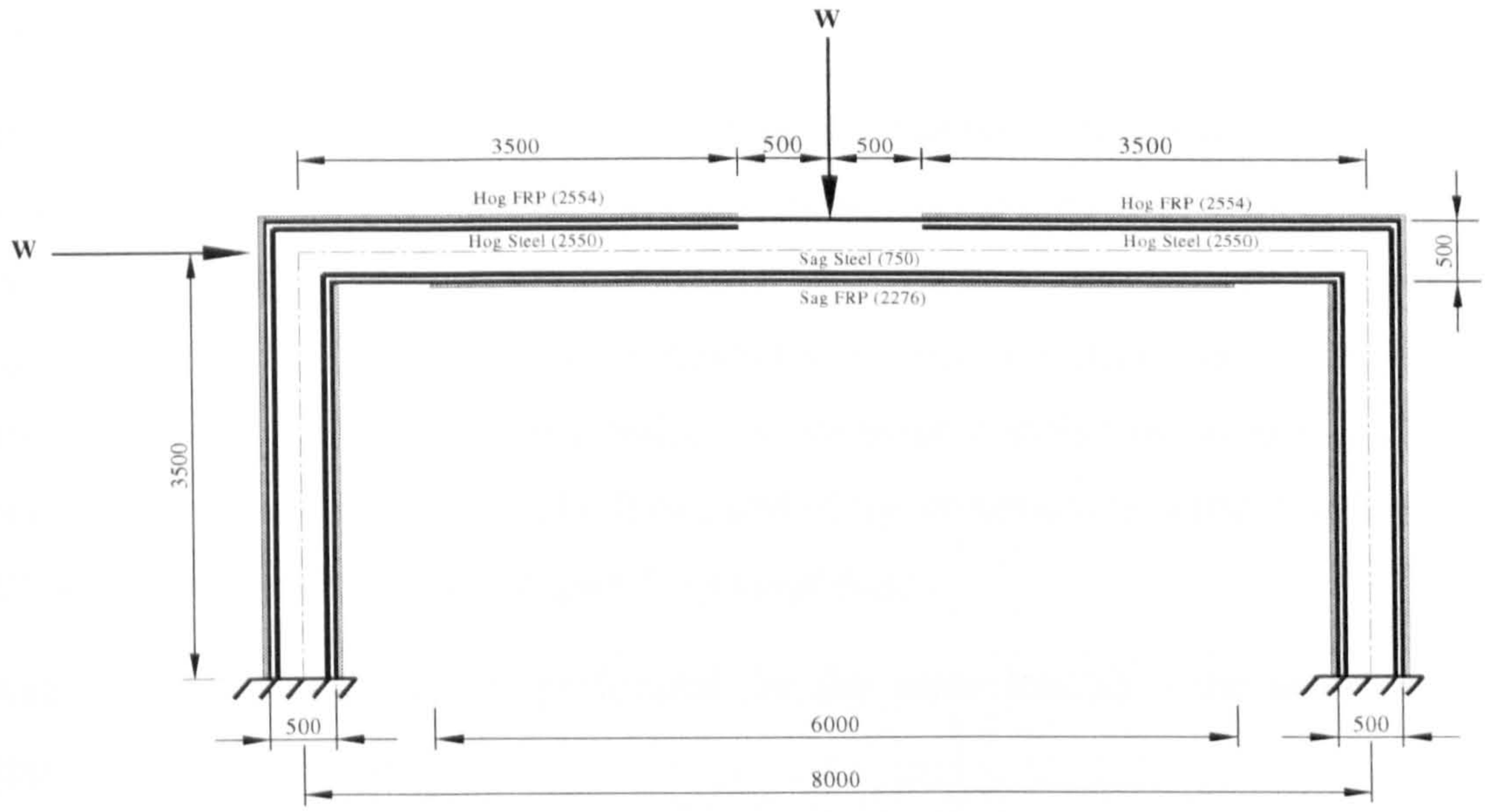

Frame of 300mm constant width

Figure 5-20 - Frame with encastered feet

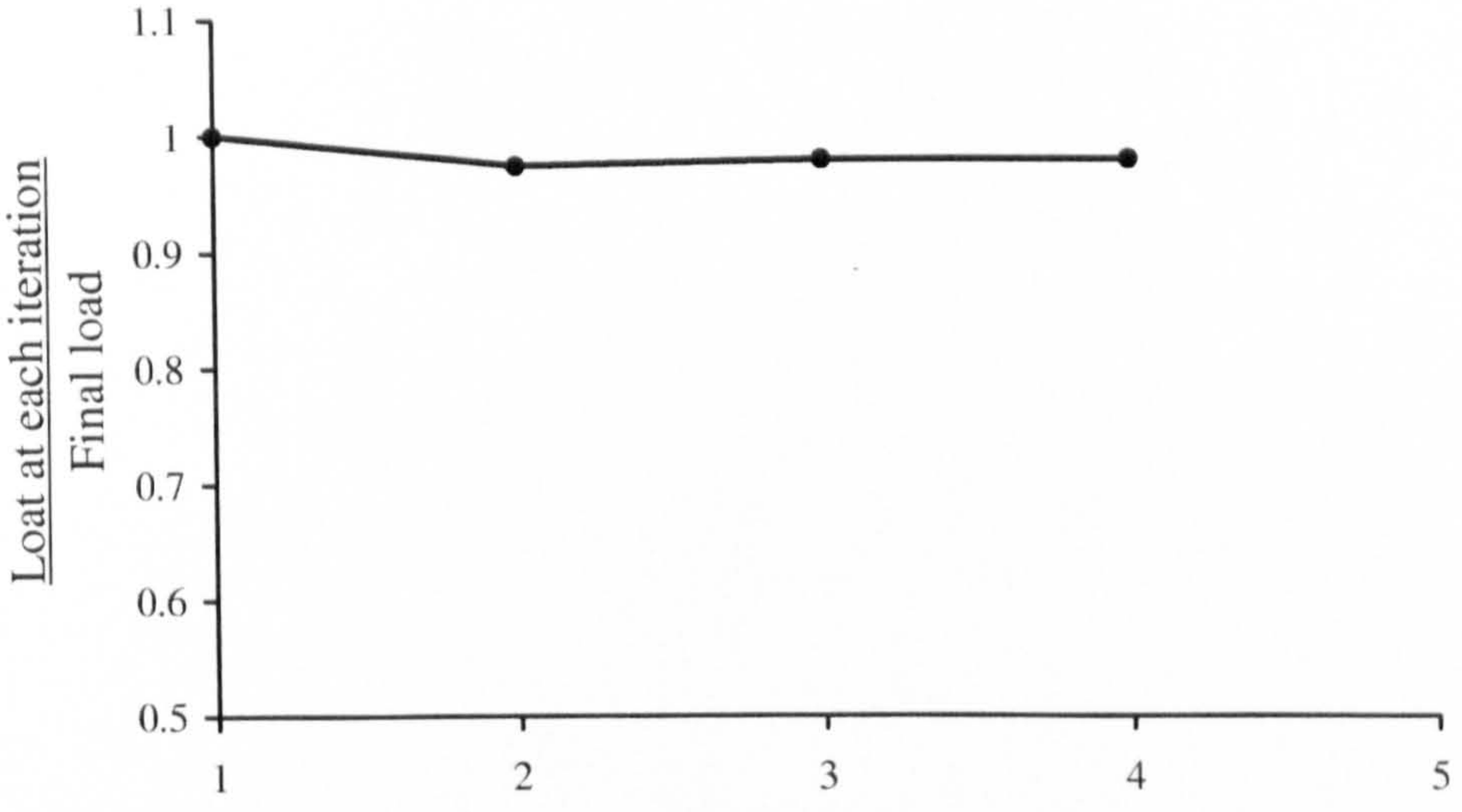

Figure 5-21 - Variation of predicted failure load with iterations for Example 4

5.3.4 Discussions

In the previous section, a computational procedure has been illustrated by examples to determine from known geometric property and/or reinforcement details the ultimate load capacity of indeterminate structures of differing ductility. The same principles can be applied to investigate the behaviours of such structures in the pre-failure nonlinear regime, that is, to determine the moment distribution at any load level before ultimate failure occurs. The flow chart of the procedure is outlined in Figure 5-22, which is similar to that in Figure 5-3 except that:

- Analysis at each iteration is performed for the same load(s) – the actual load(s) applied on the structure;
- The process is repeated until the EI-moment convergence is obtained for the same given load(s) rather than at failure for determining the ultimate load capacity.
- A prescribed tolerance is set on change in the peak moment rather than on the ultimate load(s) to test for convergence.

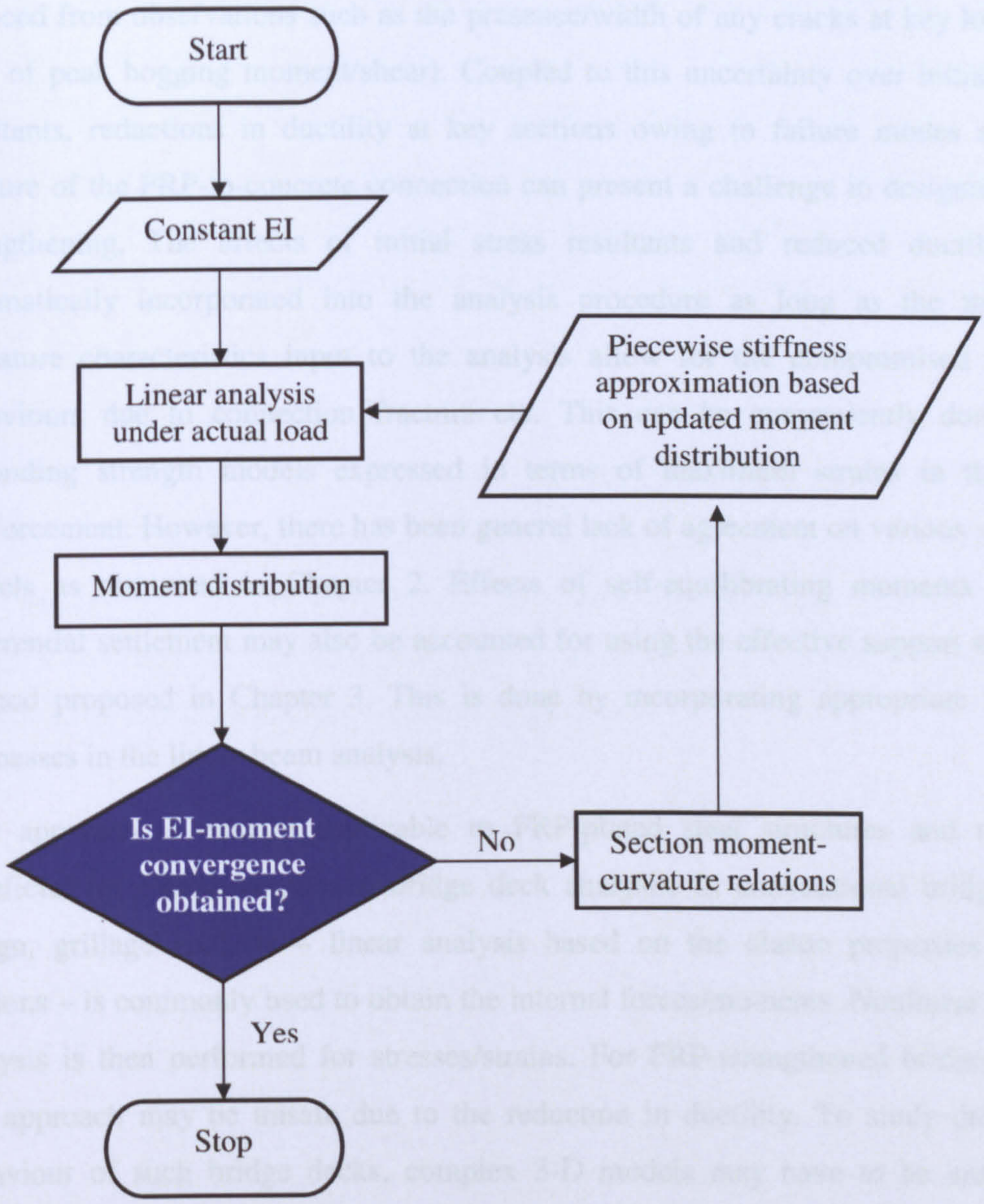

Figure 5-22 - Proposed procedure for prediction of nonlinear behaviour

FRP strengthening of an existing indeterminate structure must consider initial stress resultants owing to factors such as differential settlement (Sebastian 2002). These initial stress resultants can be difficult to quantify, although their severity may be deduced from observations such as the presence/width of any cracks at key locations (e.g. of peak hogging moment/shear). Coupled to this uncertainty over initial stress resultants, reductions in ductility at key sections owing to failure modes such as fracture of the FRP-to-concrete connection can present a challenge in designing FRP strengthening. The effects of initial stress resultants and reduced ductility are automatically incorporated into the analysis procedure as long as the moment-curvature characteristics input to the analysis allow for the compromised section behaviours due to connection fracture etc. This can be conveniently done with debonding strength models expressed in terms of maximum strains in the FRP reinforcement. However, there has been general lack of agreement on various strength models as discussed in Chapter 2. Effects of self-equilibrating moments due to differential settlement may also be accounted for using the effective support stiffness method proposed in Chapter 3. This is done by incorporating appropriate support stiffnesses in the linear beam analysis.

This approach is equally applicable to FRP-plated steel structures and may be beneficial for FRP-strengthened bridge deck analysis. In conventional bridge deck design, grillage analysis – linear analysis based on the elastic properties of the sections – is commonly used to obtain the internal forces/moments. Nonlinear section analysis is then performed for stresses/strains. For FRP-strengthened bridge decks, this approach may be unsafe due to the reduction in ductility. To study the actual behaviour of such bridge decks, complex 3-D models may have to be employed, which is costly and time-consuming, or even not possible as access to complex nonlinear structural software is limited in some design offices.

Finally, the structure will have to be re-detailed in case of any deficiency from the capacity analysis. In chapter 6, issues relating to re-detailing of the structure will be addressed and the complete analysis-design procedure presented.

5.4 Conclusions

In this chapter, a new approach based on an iterative computational technique has been proposed for analysis of indeterminate structures. The computational technique has been illustrated by way of examples which cover a range of structural ductility under different types of loading. Attainment of convergence in each case thus suggests that this may well constitute a reliable technique for time-efficient prediction of load capacities of highly indeterminate RC structures. As linear beam analysis can be performed on standard structural analysis software, the method may be widely used.

The procedure may be extended to investigate behaviours of the structure in the pre-failure nonlinear regime. Also, it is applicable to FRP-plated steel structures and able to accommodate states of self stresses and self-equilibrating moments due to differential settlement.

The structure will have to be re-detailed in case of any deficiency from the capacity analysis. In chapter 6, issues relating to re-detailing of the structure will be addressed and the complete analysis-design procedure presented.

Appendix 5A

Derivation of failure load for Plastic Analysis

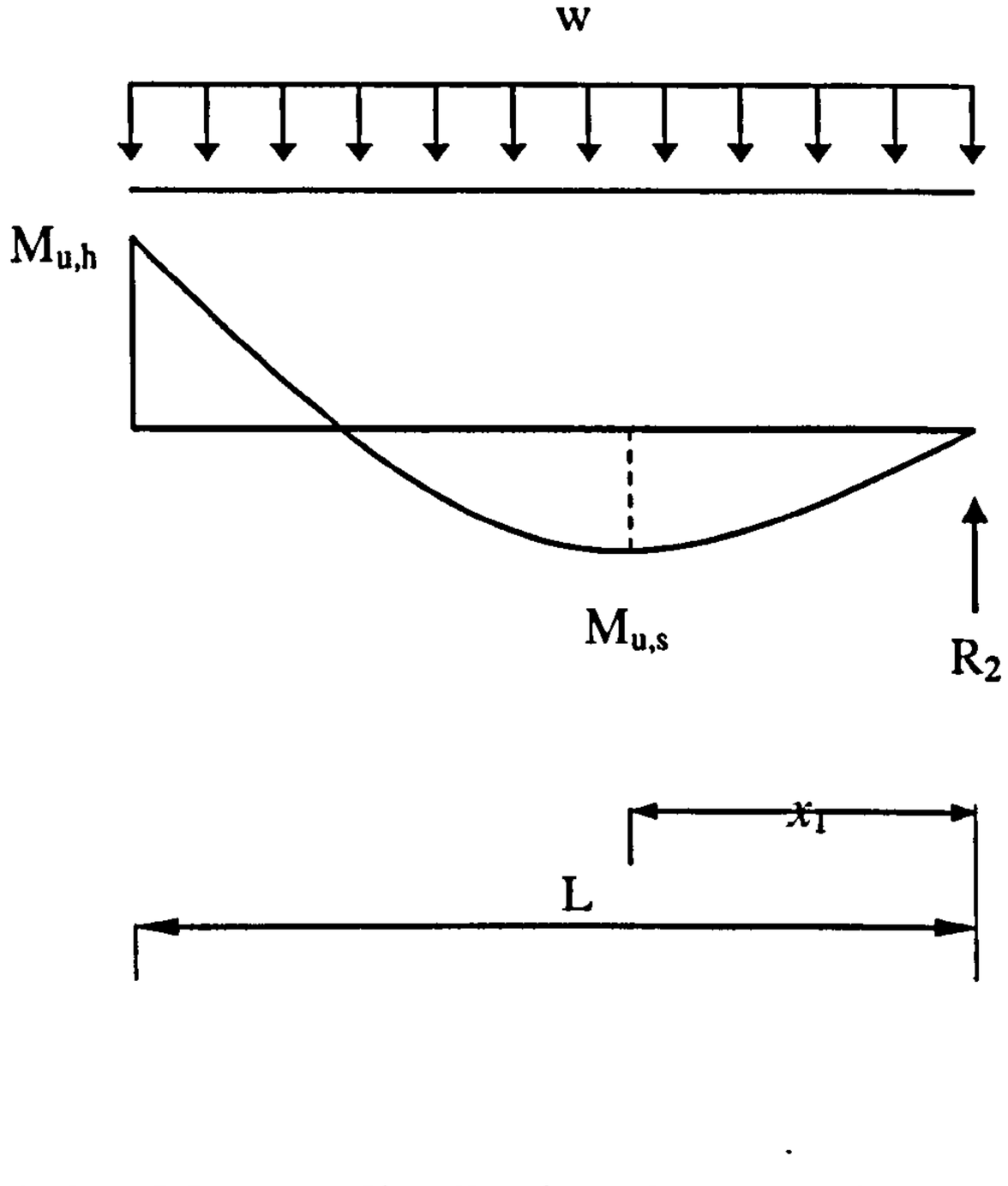

Figure 5A-2 - Moment distribution along the right span of the beam in Example 1 for plastic analysis

The failure load for plastic analysis can be obtained from the equations below, which are based on equilibrium of the span shown in Figure 5A-1.

$$M_{u1} = \frac{w \cdot L^2}{2} - R_2 \cdot L$$

$$M_{u2} = R_2 \cdot x_1 - \frac{w \cdot x_1^2}{2}$$

where L is the length of the right span; R_2 is the reaction force at the end support; $x_1 = \frac{R_2}{w}$ and is the distance from the end support to the maximum sag moment section along the span; $M_{u,h}$ and $M_{u,s}$ are the ultimate hog and sag moment capacities, respectively.

Chapter 6

Analysis-Design of Ductility-Deficient Indeterminate Structures

6.1 Introduction

It was identified in Chapter 2 that a new design approach is needed for ductility-deficient indeterminate structures. Any alternative approach must be capable of: (a) rapid prediction of the load capacity of a structure with given reinforcement details; and (b) time-efficient detailing of a structure to the given design load capacity.

Chapter 5 has presented a computational technique for time-efficient prediction of the ultimate loads of indeterminate structures. It is now logical to develop a technique for detailing the structure when the design load capacity is known, irrespective of the ductility capacity of the finally detailed structure. To that end, the present chapter presents an iterative procedure entailing multiple detailing and ultimate analysis sequences to create an analysis-design process for ductility-deficient indeterminate structures.

In what follows, an iterative detailing procedure is first introduced and incorporated into the proposed analysis-design process together with the capacity analysis presented in Chapter 5. The design procedure is then illustrated by way of examples including a FRP-plated continuous RC beam which is ductility-deficient, a continuous RC beam which is of sufficient ductility for the traditional design approach to be applied, and a three-storey three-span (3×3) plane frame strengthened with FRP sheets.

6.2 New analysis-design procedure

The detailing procedure is based on constantly updating the reinforcement details to enable the structure to carry the updated moment distribution. The final reinforcement layout must provide adequate moment capacity for the moment distribution obtained from analyses based on a stiffness distribution along the structure including the effects of that very reinforcement layout. Any change in reinforcement details will affect both the section moment capacity, and the stiffness variation (therefore the moment distribution under a given load), so an iterative process has to be employed.

Shown in Figure 6-1 is the flowchart of the process incorporated into the proposed design procedure. The following points should be noted in respect of the flowchart:

- Basic details are either known (section properties and existing steel reinforcement layout for strengthening design) or assumed to have been determined from preliminary analysis (section width and height and concrete cover depth for steel RC design).

- For convenience, analysis at the ultimate limit state (ULS) is first performed assuming constant EI distribution to obtain the moment distribution.

- Reinforcement from the available sizes (as the steel reinforcement bars and FRP plates normally come in discrete sizes) is then detailed to the moment distribution. For each reinforcement details tried, the ultimate moment of the section is stored in a section moment capacity 'bank' for any further use.

- The moment-curvature relations of the sections are obtained. Subsequent analyses are based on section properties including effects of cracking, concrete compression softening and steel yield.

- The load capacity of the detailed structure and the corresponding moment distribution are obtained using the iterative procedure presented in Chapter 5.

- If the load capacity of the detailed structure is deficient (excessive), the peak moments are to be scaled up (down) by the ratio of the design load capacity to the current (deficient or excessive) load capacity. The reinforcement details are then updated (first refer to the section moment capacity 'bank') at all peak moment locations to provide required (scaled up) moment capacities.

- Continuation of the process will lead to reinforcement accumulating at certain locations, which, in turn, attracts more reinforcement; while amount of reinforcement will keep decreasing at other locations. This may get to a stage where updating the reinforcement details will lead to little change in the load capacity of the structure. For instance, the section moment capacity at the location(s) where the reinforcement was being reduced dropped to such a level that it becomes the critical section and therefore controls the load capacity of the structure. If this is the case, measures need to be taken, for example, to keep constant or increase the reinforcement at that location.

- The process continues until the design load capacity is computationally achieved by the detailed structure.

  The proposed procedure applies to structures of varying levels of ductility. In the following section, it is illustrated by way of examples, including a FRP-plated continuous RC beam, a continuous RC beam and a three-storey three-span plane frame.

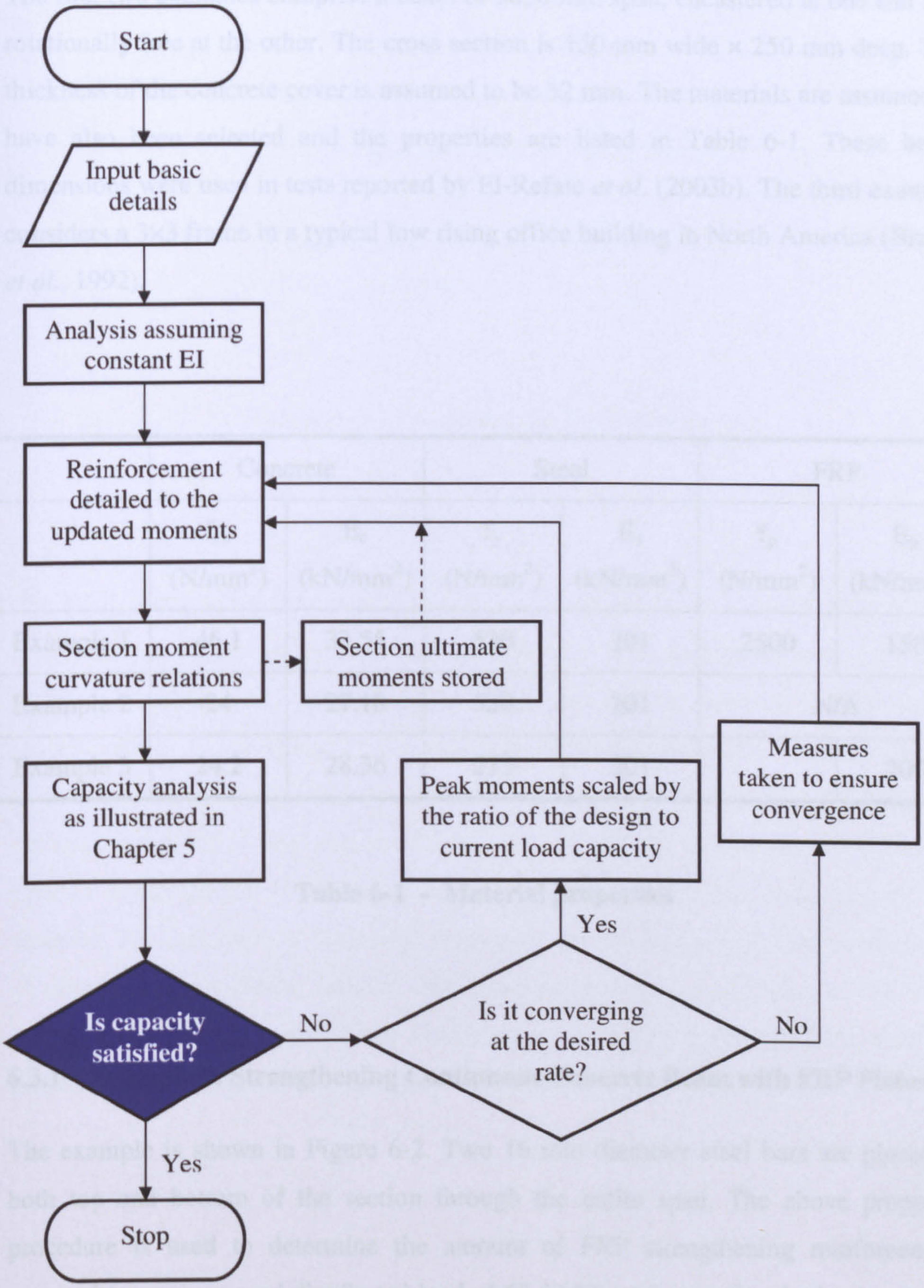

Figure 6-1 - Proposed Iterative Approach

6.3 Design Examples

The first two examples comprise a beam of 3830 mm span, encastered at one end and rotationally free at the other. The cross section is 150 mm wide × 250 mm deep. The thickness of the concrete cover is assumed to be 32 mm. The materials are assumed to have also been selected and the properties are listed in Table 6-1. These beam dimensions were used in tests reported by El-Refaie *et al.* (2003b). The third example considers a 3×3 frame in a typical low rising office building in North America (Bracci *et al.*, 1992).

	Concrete		Steel		FRP	
	f_{cu} (N/mm^2)	E_c (kN/mm^2)	f_y (N/mm^2)	E_s (kN/mm^2)	f_p (N/mm^2)	E_p (kN/mm^2)
Example 1	46.1	33.55	520	201	2500	150
Example 2	24	27.18	520	201	N/A	
Example 3	24.2	28.36	275	201		200

Table 6-1 - Material properties

6.3.1 Example 1: Strengthening Continuous Concrete Beam with FRP Plates

The example is shown in Figure 6-2. Two 16 mm diameter steel bars are placed at both top and bottom of the section through the entire span. The above proposed procedure is used to determine the amount of FRP strengthening reinforcement required for an increased distributed load of 67.5 kN/m (about twice the load capacity of the original RC beam).

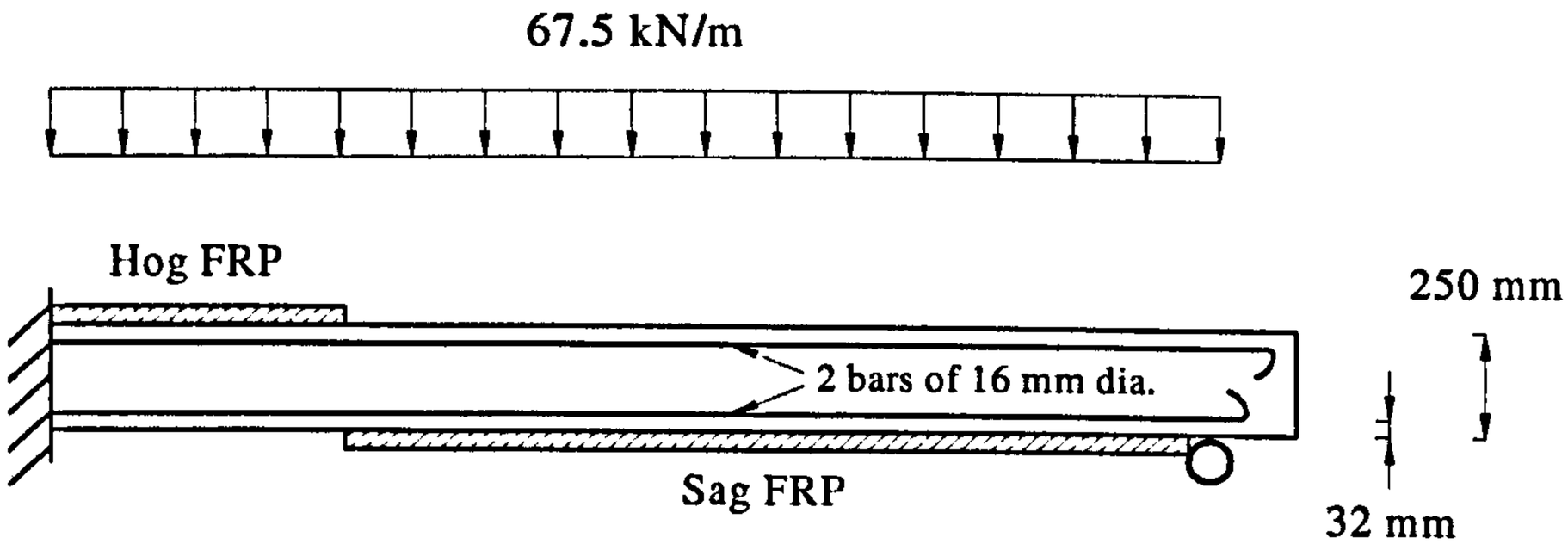

Figure 6-2 - Beam details for Example 1

The FRP plates are assumed to be curtailed at the points of contraflexure so that reinforcement details are constant but not identical through the hog and sag zones. Sufficient anchorage to prevent separation of the FRP is assumed so that failure always occurs by crushing of the concrete. The experimentally verified flexural constitutive models suggested in Sebastian (2002) are used to obtain the moment-curvature relations of FRP-plated RC sections. The models in Sebastian (2002) cover various combinations of the states of the reinforcing materials, both internal and external. The derivation of the model is given in the Appendix 6A for the combination of elastic-perfectly plastic internal steel reinforcement and elastic plating, which, in essence, is a special case of the models in the original paper. Typical moment-curvature relations are shown in Figure 6-3 for the FRP-plated RC sections.

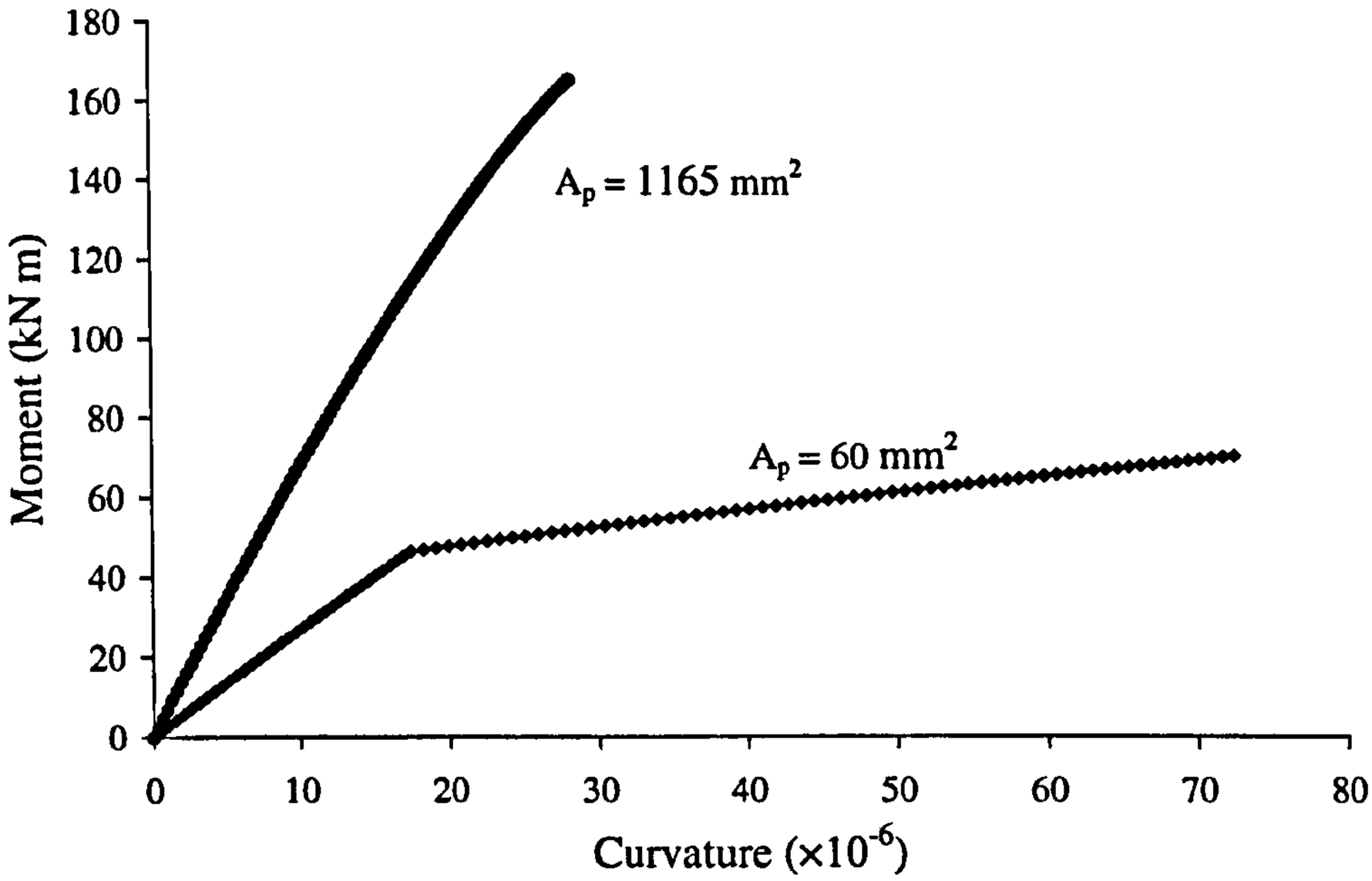

Figure 6-3 - Moment-curvature relationship for FRP-plated RC sections

Initially, the reinforcement was detailed to the moment diagram obtained from analysis assuming constant EI. More reinforcement was required in the hog zone compared to that in the sag zone, which results in a bigger moment at the encastered end. This, in turn, requires even more reinforcement in the hog zone. The iteration continued till a 4th cycle (Figure 6-4), where the load capacity was found to be diverging from rather than converging onto the design load. An alternative measure needs to be taken to ensure convergence.

It has been observed that the maximum sag moment section became the critical section at this stage that controls the load carrying capacity of the structure. Also, any more increase in FRP reinforcement in the hog zone does not lead to significant increase in the section moment capacity. It is therefore logical to provide a stronger section for the sag zone, although in doing so, the moment requirement in the sag zone also increases.

The reinforcement in the hog zone was then kept constant and the reinforcement in the sag zone was increased so that the moment at the encastered end could be reduced. Convergence was attained after eight iterations (Figure 6-4). The final FRP reinforcement areas for the hog and sag zones are 1165 mm^2 and 60 mm^2, respectively.

The reinforcement areas determined at each iteration are listed in Table 6-2 and also plotted in Figure 6-5.

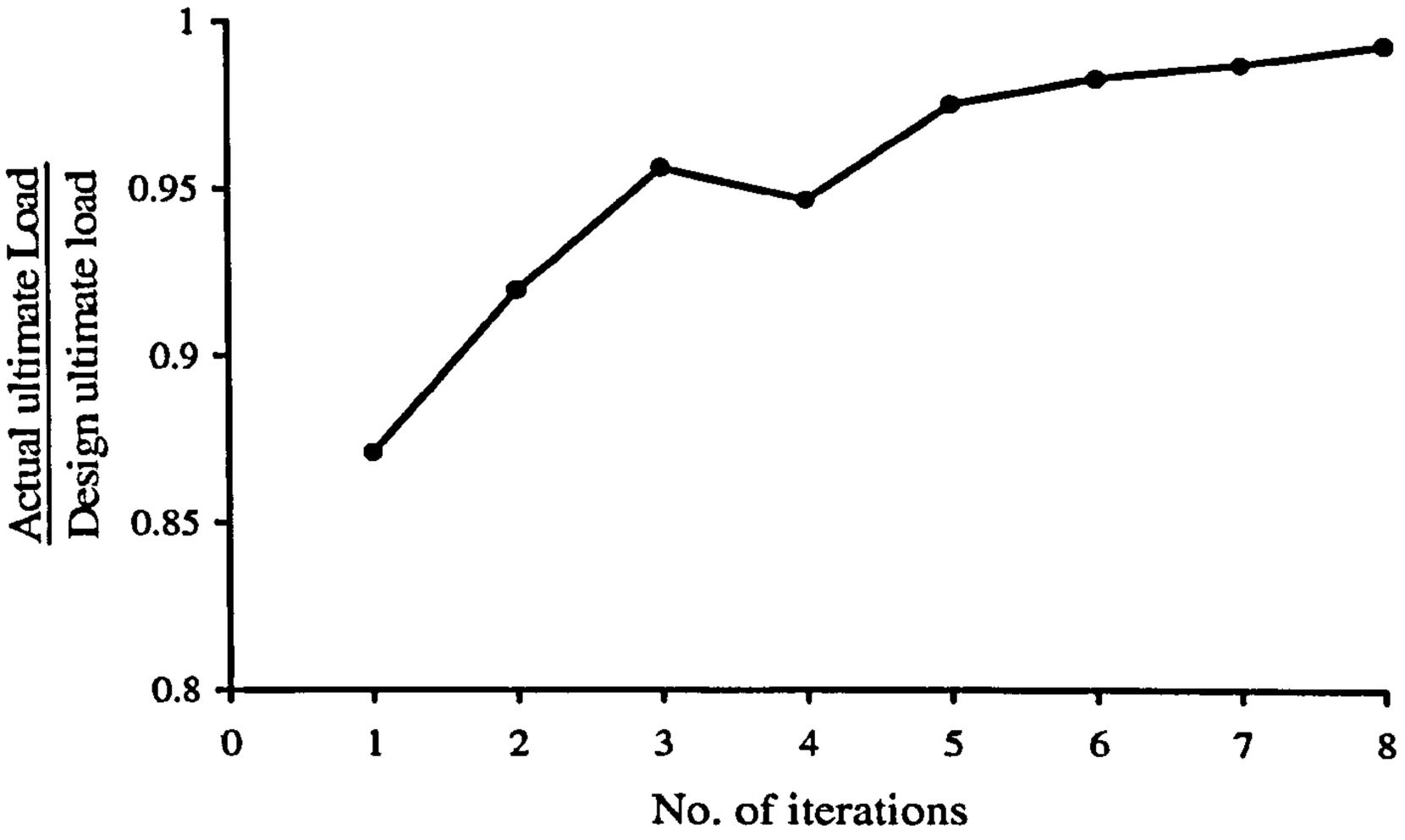

Figure 6-4 - Variation of predicted failure loads with iterations

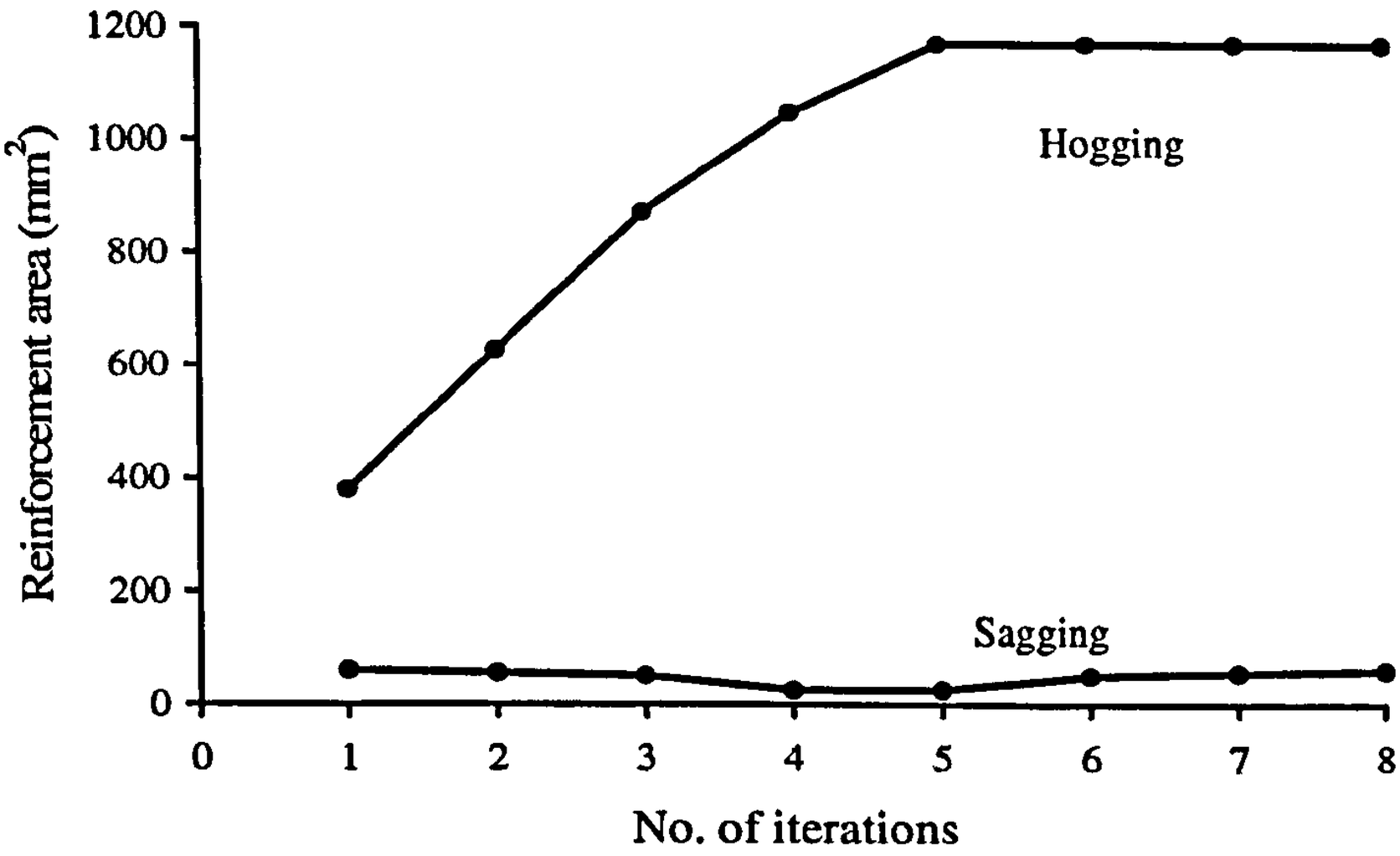

Figure 6-5 - Variation of FRP reinforcement areas with iterations

Iteration	$A_{p,hog}$ (mm^2)	P.o.C (mm)	$A_{p,sag}$ (mm^2)	$\overline{P_u}$
1	380	1098	60	0.871
2	625	1189	55	0.920
3	870	1250	50	0.957
4	1045	1313	25	0.947
5	1165	1275	25	0.976
6	1165	1299	50	0.984
7	1165	1296	55	0.988
8	1165	1273	60	0.996

Note: P.o.C = Point of contraflexure from the encastered end; $\overline{P_u}$ = non-dimensional load capacity as relative to the design load.

Table 6-2 - FRP reinforcement details and load capacity at each iteration

In design to existing design guidance such as TR 55 (Concrete Society 2004), detailing is essentially based on moment distribution from analysis performed on constant EI (with the reinforcement details at Iteration 1). In this case, the actual load capacity of the so-detailed beam is 58.8 kN/m, representing a 12.9% deficiency for the design load capacity of 67.5 kN/m. This significant disparity is also reflected in comparing the final moment distribution with that from analysis based on constant EI (Figure 6-6).

This deficiency may be compensated, however, by limiting the minimum strain in the tensile steel reinforcement to ensure that the section has sufficient plasticity, and by the use of bigger material factors for the FRP to account for the novel nature of its use in structural engineering applications. These make it difficult to make direct comparisons with the present approach.

Design against debonding could be readily incorporated in the evaluation of moment-curvature relations using the limiting strain approach, as has been discussed in Chapter 5. In assessing FRP-plated structures where the FRP has partly debonded from the concrete, the FRP plate can normally be ignored in obtaining the moment-curvature relations for the section as they are usually thin and subject to potential buckling if they are in compression. The corresponding stiffness is then used for the part of the structure over which debond has occurred.

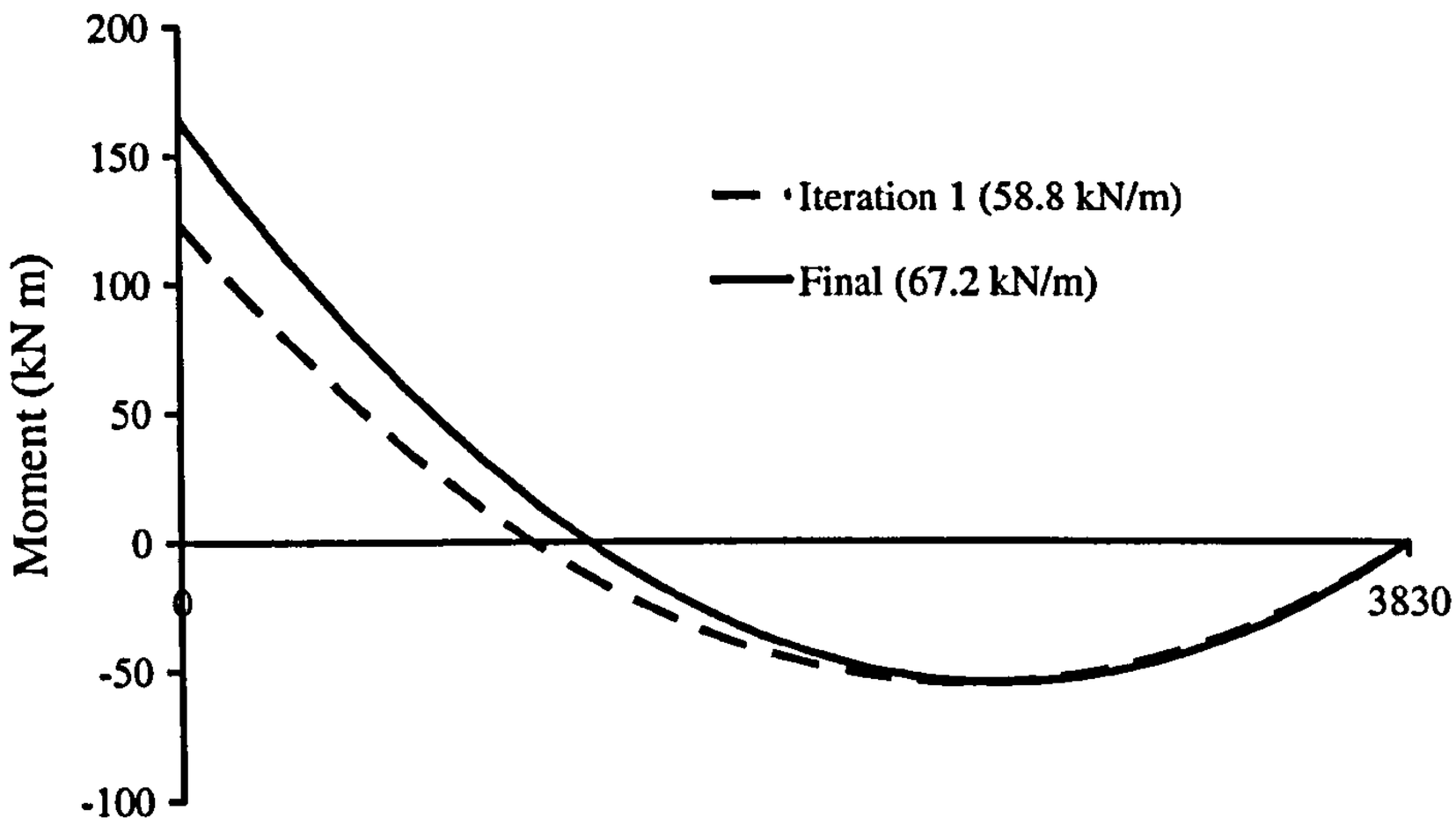

Figure 6-6 - Ultimate moment diagram

6.3.2 Example 2: Steel Reinforcement for Steel RC Beam

The proposed procedure also applies to traditional RC beam design, as will be shown in this example. The beam is shown in Figure 6-7. The above proposed procedure is used to determine the amount of steel reinforcement required to sustain a 75 kN load acting at mid-span. But before proceeding any further, the concept of hinge length is first introduced.

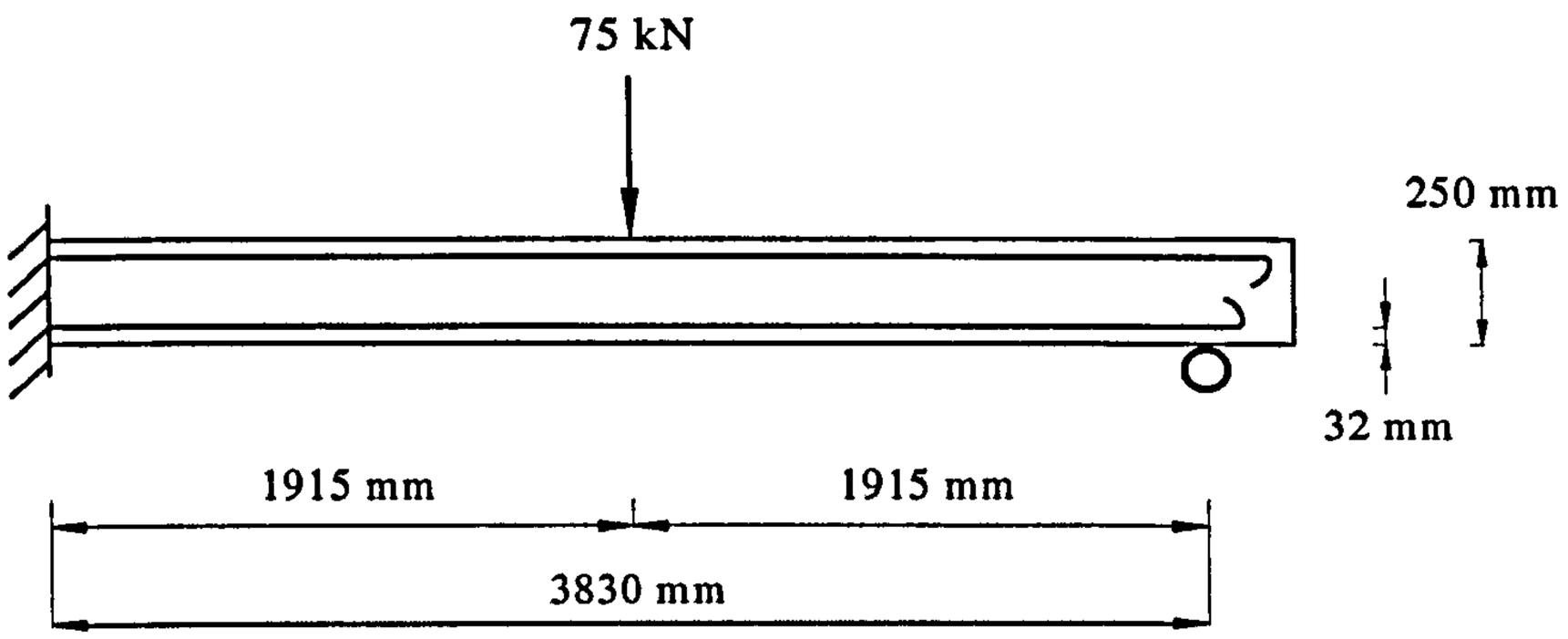

Figure 6-7 - Beam details for Example 2

6.3.2.1 The hinge length concept

Imagine the load is gradually applied until the moment capacity (M_u) is just reached at the maximum moment location, in this case the encastred end. On further loading, the curvature increases, but only at the point of encastred end. So there will be a hinge, but of zero length. This is the so-called 'zero hinge length concept' (Oehlers *et al.* 2007). To be able to determine the rotation at this hinge, the concept of 'hinge length' is commonly adopted. The rotation at the hinge is given as the product of the hinge length and the change in curvature.

The hinge length concept is also used in the current example to accommodate any rotation at the hinge. Failure is deemed to occur when the moment capacity (M_u) is reached at a section from the analysis assuming constant stiffness of $(EI)_B$, which is defined as the secant stiffness of the moment-curvature plot at concrete crushing (point B in Figure 6-8), over a distance equal to the hinge length (l_p). Shown in Figure 6-8 are the moment diagram and the corresponding stiffness variation along the span of an encastered beam at ultimate.

This may seem to conflict with the representation of nonlinear stiffness variations in Chapter 5. However, these are two different concepts. In chapter 5, the piecewise constant stiffness distribution is used to approximate the *actual* nonlinear stiffness variation, whereas here, the hinge length is a pure mathematical concept to enable the determination of the rotation and the analysis to be carried out. The introduction of hinge length essentially represents the allowance of the section to redistribute moment

through rotation. In Chapter 5, the hinge length is taken as zero, so effectively, moment redistribution due to rotation of the section is not allowed.

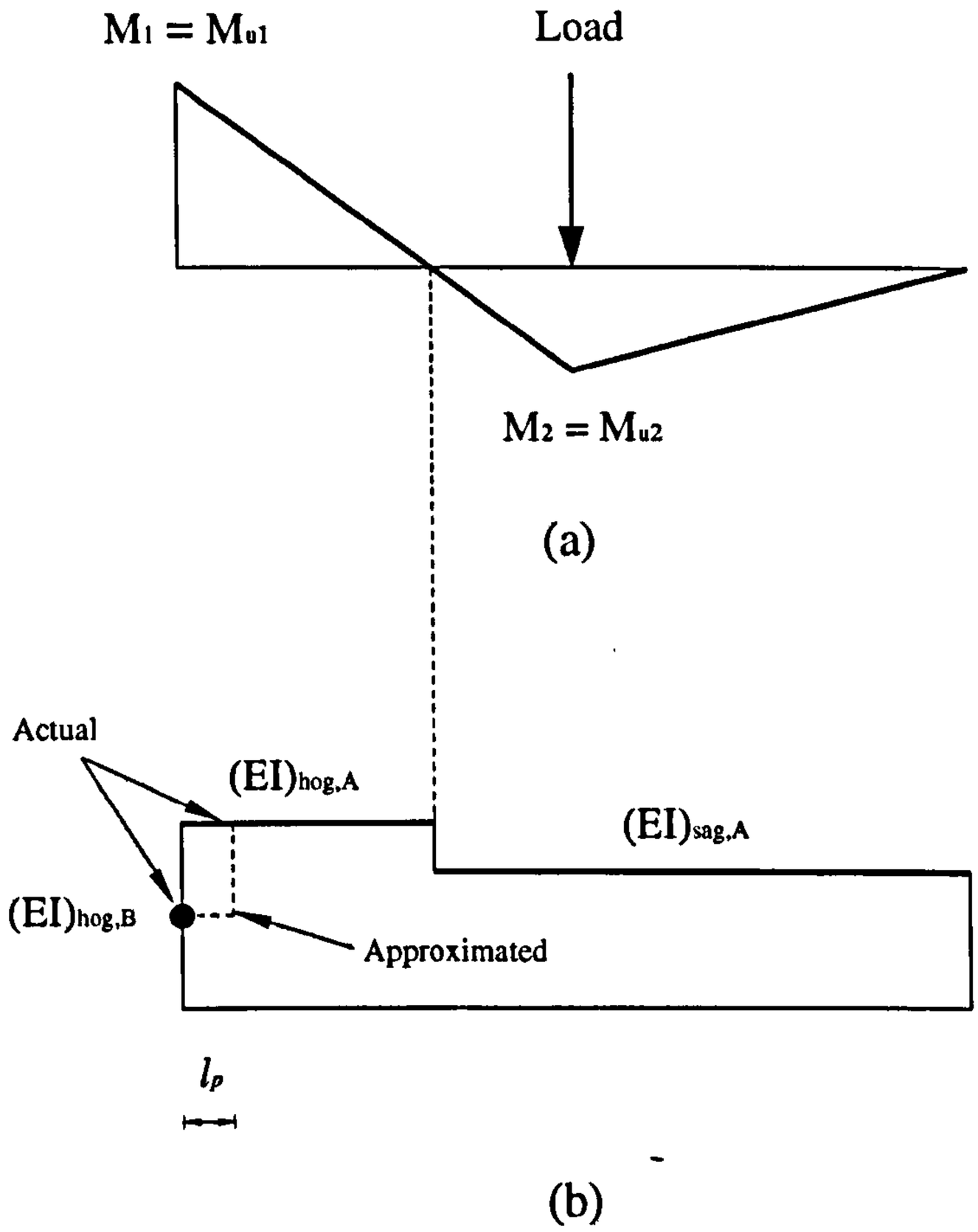

Figure 6-8 - Propped cantilever under a point load at mid-span: (a) Moment diagram; and (b) Stiffness variation along the span

The value of the hinge length, however, cannot be directly determined through numerical modelling, and is generally determined empirically (Oehlers *et al.* 2008). Also, there is big variation between values proposed in the literature, as point out by Oehlers *et al.* (2008). Here, the hinge length proposed by Mattock (1967) is adopted and given as follows

$$l_p = 0.5h + 0.05z \quad (6\text{-}1)$$

where h is the beam depth and z is the shear span. In the current example, the (equivalent) shear span z is taken as the distance between the location of the maximum moment and the nearest point of contraflexure, as suggested in Aoyagi and Endo (1993).

6.3.2.2 Design Procedure

Step 1: Detail to moment distribution from analysis based on constant EI

From analysis based on constant EI distribution, the peak moments and location of the point of contraflexure can be obtained. In this case, $M_1 = 53.9$ kN m; $M_2 = 44.9$ kN m; and the distance to the point of contraflexure from the fixed end is 1044.5 mm.

In selecting the steel reinforcement bars, two identical steel bars for the tension as well as compression reinforcement if required are used in all cases.

A_{st} (mm^2) / A_{sc} (mm^2)	157 (2 no. Φ10 bars)	226 (2 no. Φ12 bars)	402 (2 no. Φ16 bars)	628 (2 no. Φ20 bars)
0	27.3	37.6	58.9	74.4
101 (2 no. Φ8 bars)		36.0	57.9	79.5
157 (2 no. Φ10 bars)			57.2	80.4

Table 6-3 - Section moment capacity stored for any further use

Different steel reinforcement bars are tried until it gives a moment capacity that is bigger than (but close to) the requirement moment capacity. *In this case, two no. of 16* mm diameter bars are used for both the hog and sag zones. The section moment capacities of all tried reinforcement details are stored for any further use. The results are shown in Table 6-3.

Step 2: Construct the moment-curvature relations of the section(s)

The moment-curvature relations are shown in Figure 6-9 for the section (hog and sag sections are effectively the same here). In the present analysis, they are approximated as being bilinear – the first leg between zero moment and steel yield (point A in Figure 6-9) and the second leg between steel yield and concrete crushing ($\varepsilon_c = 0035$).

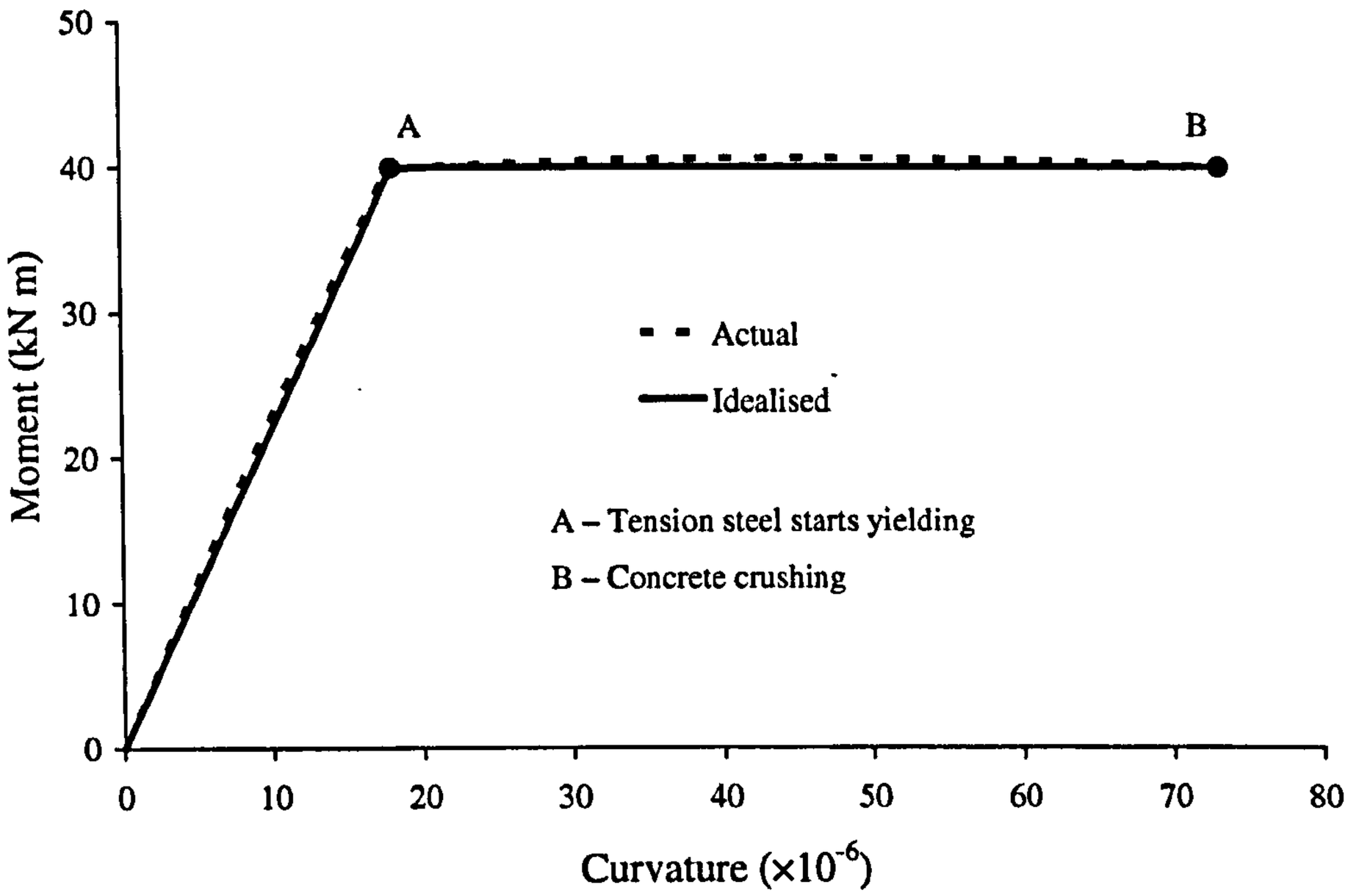

Figure 6-9 - Moment-curvature relations for steel RC section

Step 3: Obtain the load carrying capacity of the section based on the actual stiffness distribution

Based on the expression by Mattock (1967) for hinge length and failure criteria specified in the previous section, the actual load carrying capacity of the section can be obtained following the procedure set out in Chapter 5. One iteration gives the ultimate load of 91.4 kN. Further check demonstrates that the reinforcement can not be reduced due to the discrete bar sizes.

As discussed in the previous section, the introduction of hinge length essentially allows the section to redistribute moment through rotation. Also noted is that there is big variation between values proposed in the literature. Here, the moment distribution of the structure at ultimate is evaluated for a range of hinge length values so moment redistribution through rotation at the hinge can be demonstrated. The results are shown in Figure 6-10. The corresponding ultimate loads are also given.

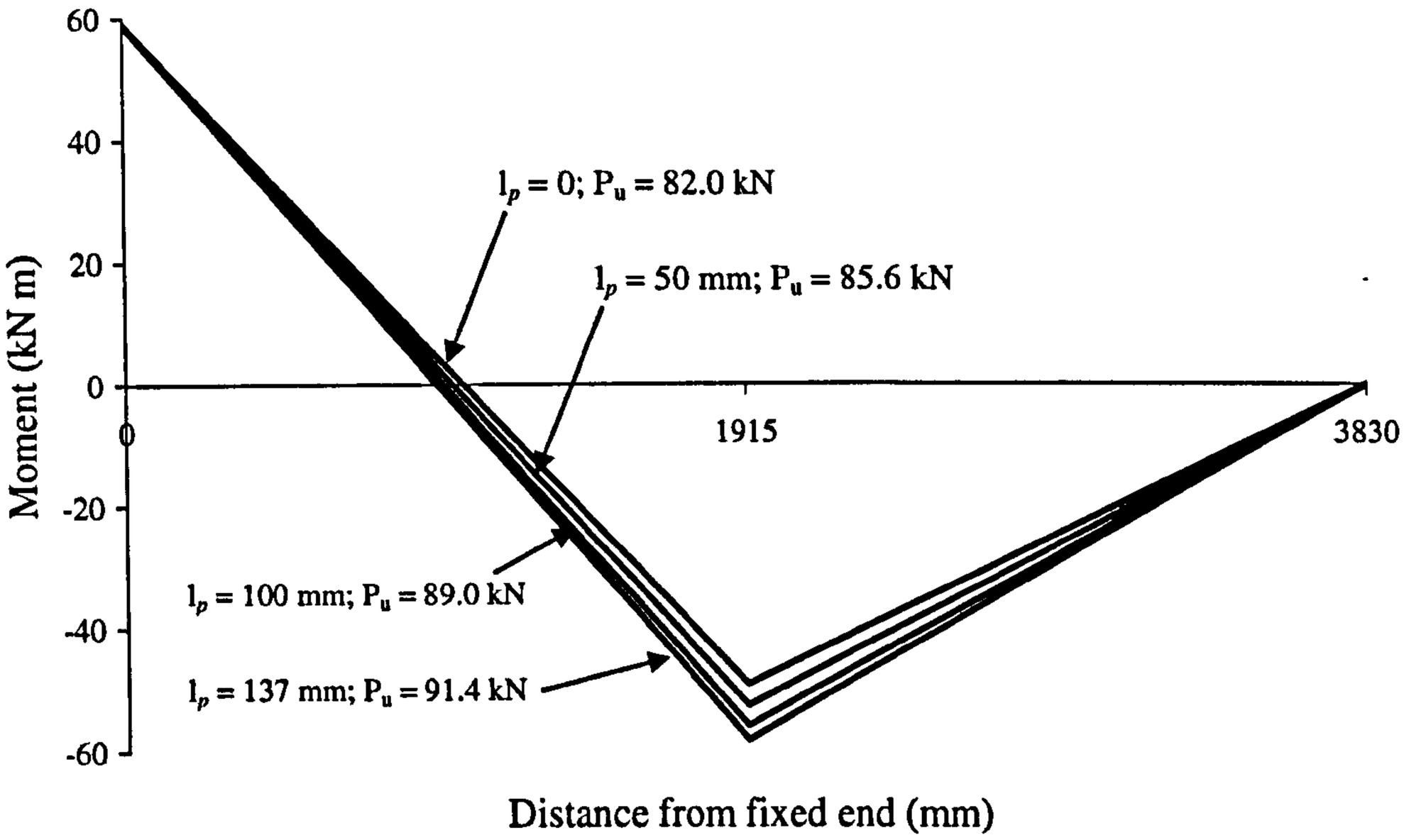

Figure 6-10 - Moment distribution at ultimate

It can be seen that when a bigger hinge length is adopted, the structure is able to take more load by increasing the bending moment at mid-span. When the hinge length increases from zero, which allows no moment redistribution through rotation at the hinge, to 137 mm from the Mottack (1967) expression, the mid-span moment has increased by 18.3% and the ultimate load by 11.4%.

In conventional design codes such as Eurocode 2 (BS EN 1992), ductility requirement is often implicitly embedded by, for example, limiting the amount of compression steel reinforcement so that the depth of the neutral axis is limited to 0.45 × the effective depth of the section. Also inherent in the design procedure are material partial safety factors to take into account any uncertainty in material properties. These factors have made it difficult to make direct comparison between the present approach and that in the code. However, this example has clearly illustrated that the proposed design approach is equally applicable to traditional RC beams, which are of sufficient ductility.

6.3.3 Example 3: Strengthening a 3×3 steel RC frame with FRP sheets

This example considers a 3×3 frame (Figure 6-11) in a typical low rising office building in North America (Bracci *et al.*, 1992). The load pattern in Figure 6-11 is adopted to simulate the worst loading effects on the span in consideration, with equal (factored) live and dead load. Wind loading is ignored as is the case in the original example. The cross section dimensions and reinforcement details of the original frame, which are modified from the original for the purpose of this example, are shown in Figure 6-12. All concrete cover is 40 mm. The materials properties are as given in Table 6.1.

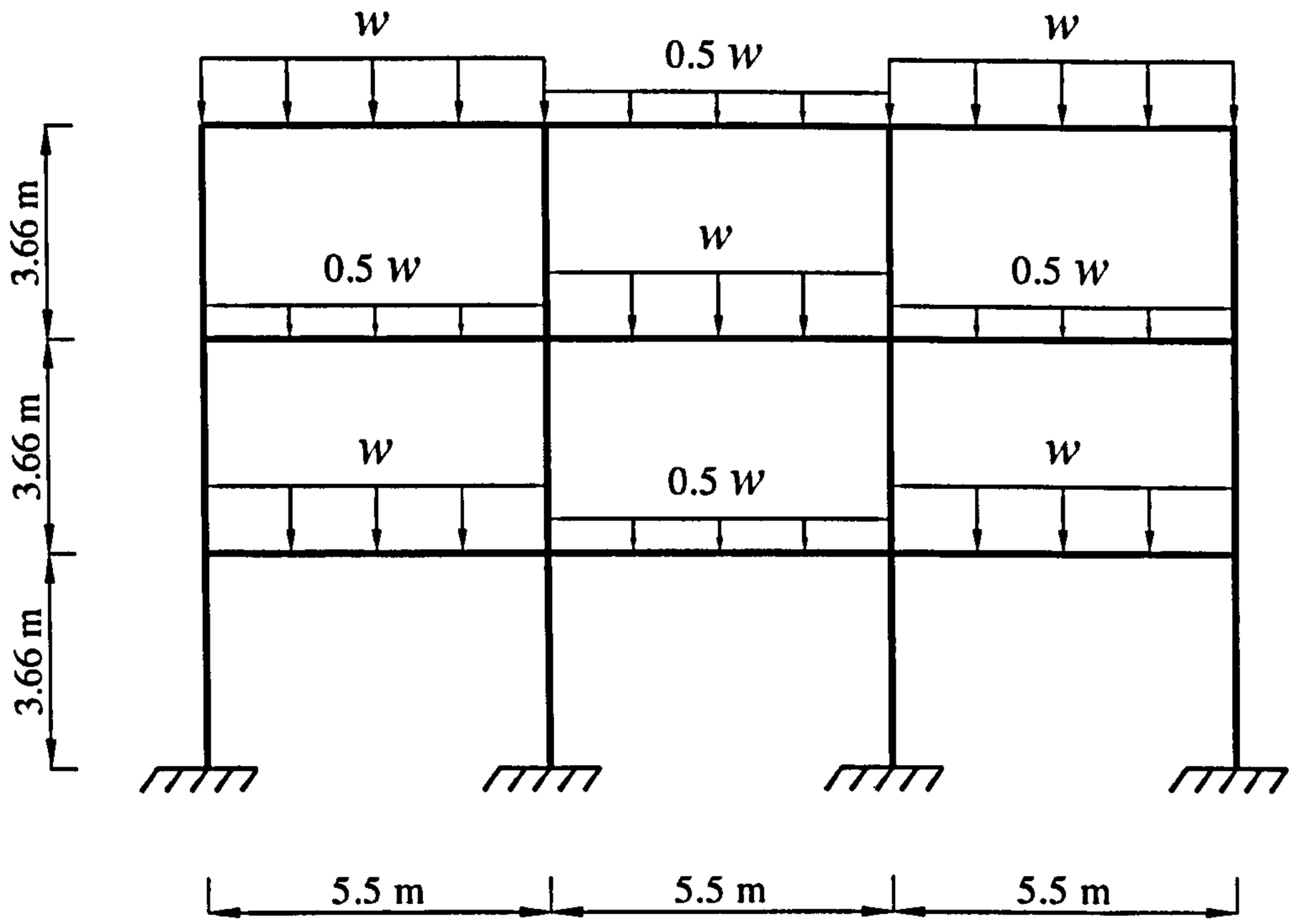

Figure 6-11 - Example 3

During a recent service installation, the 2 no. 16 mm diameter reinforcement bars were damaged at the bottom of the mid-bay second-floor beam. The subsequent reinforcement details for the sagging zone of the damaged span are as shown in Figure 6-32 (c). Using the procedure set out in Chapter 5, the load carrying capacity of the weakened structure is $w = 29.5$ kN/m. The proposed procedure is used to assess the effectiveness FRP-strengthening to restore the load carrying capacity ($w = 50$ kN/m with failure at the maximum sag moment section of the span in consideration) of the frame.

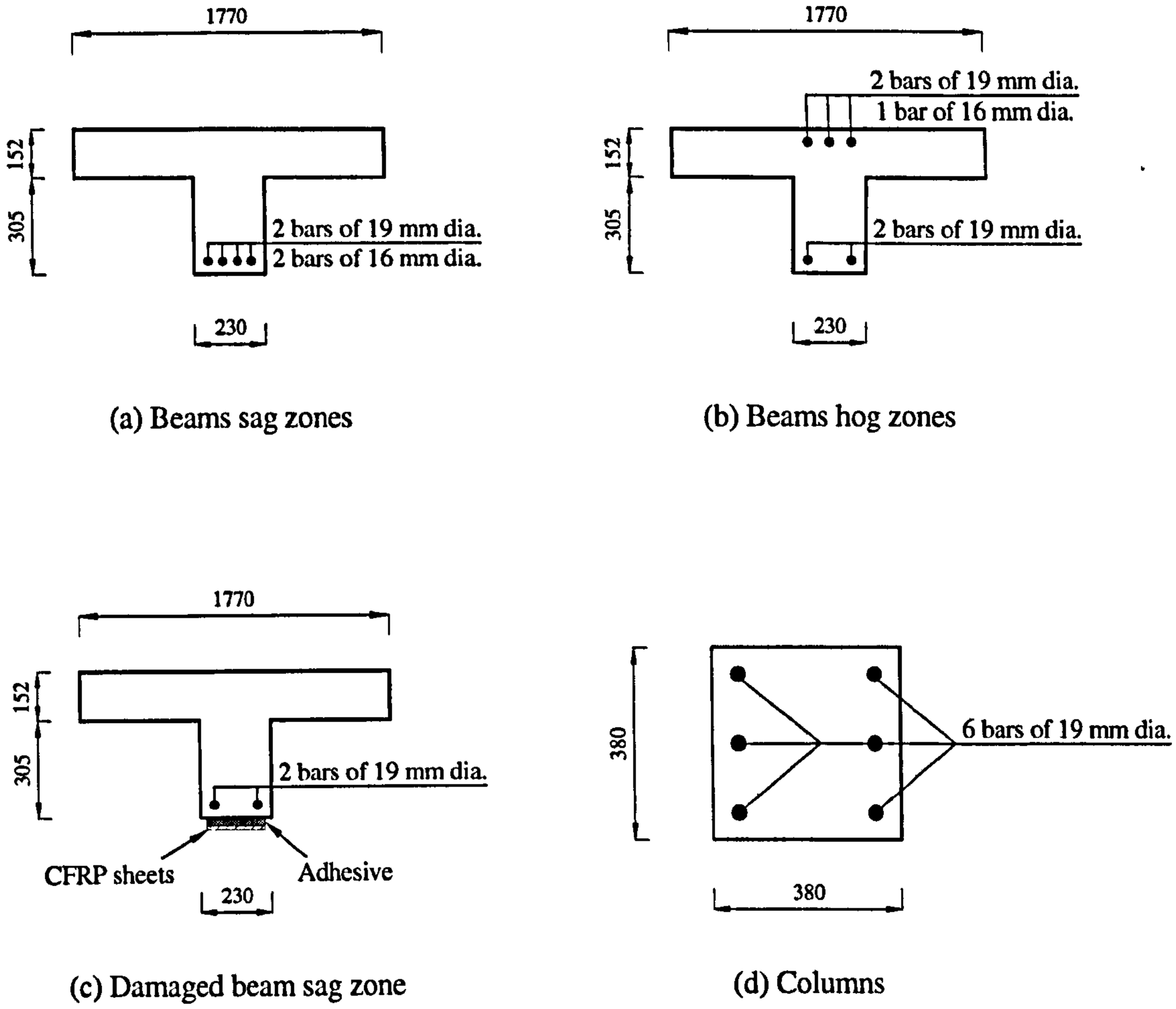

Figure 6-12 - Cross section and reinforcement details

Step 1: Existing strain at the time of strengthening

The strengthening work is assumed to be undertaken from the first floor during a weekend closure of the building. The loads on the frame at the time of strengthening, shown in Figure 6-13 with a bigger load on the mid-bay first-floor beam to account for the additional construction load, induce pre-existing strains in the concrete adjacent to the plate/sheet, but not in the plate/sheet itself. Both the ductility and strength of the plated section appreciably sensitive to pre-existing strains (Sebastian 2002) and should be properly accounted for in deriving the moment-curvature relations of the FRP-plated RC section.

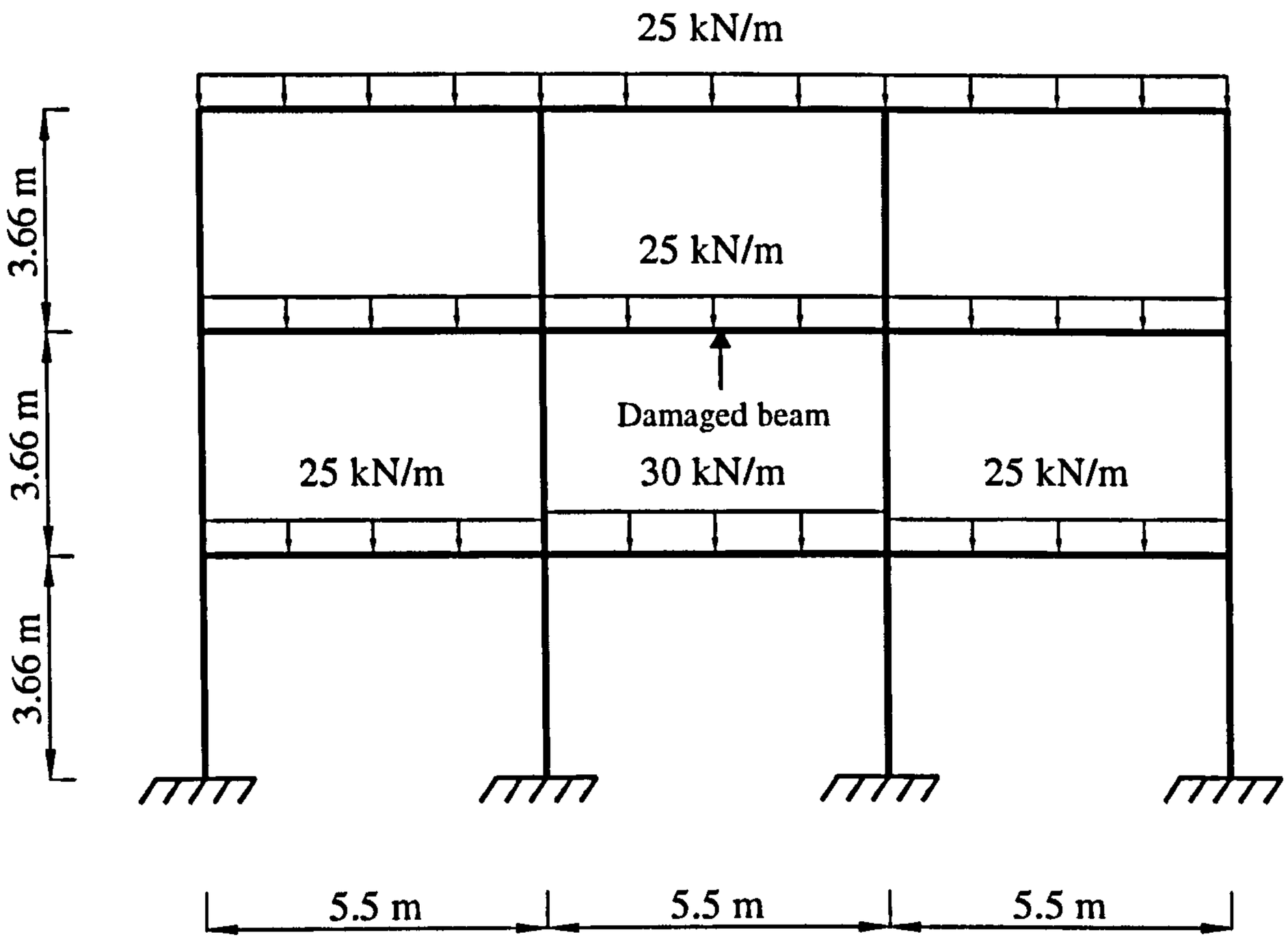

Figure 6-13 - Loading at the time of strengthening

For the purpose of this example, the pre-existing strain at the maximum sag moment section along the mid-bay second-floor beam is used in obtaining the moment-curvature relations of the FRP-plated RC sections over the entire sag zone of the strengthened beam. All sections were found to be in the elastic range, so when the pre-existing strain has been taken into consideration in obtaining the moment-curvature relations of the FRP-plated RC sections, the loads shown in Figure 6-11 - instead of the two-staged loading process for before- and after-strengthening – can be used for the subsequent design.

Step 2: Construct section moment capacity table

External FRP strengthening is most efficient when applied to under-reinforced sections. This is confirmed in this case. It was found that the application of a small amount of FRP reinforcement would lead to a significant increase in the section moment capacity. FRP sheets (nominal thickness of 0.17 mm and 100 mm wide) are

subsequently used in stead of thicker FRP plates. Shown in Table 6-4 are the section moment capacities for various amount of FRP reinforcement together with the relative sectional stiffness to the un-strengthened section.

No. of layers of CFRP sheets	Section moment capacity (kN m)	Relative elastic section stiffness to the unstrengthened RC section
0	64.7	1
1	102.7	1.017
2	138.4	1.034
3	172.3	1.050

Table 6-4 - Section moment capacity of FRP-plated RC sections

It is clear that a small amount of FRP reinforcement will lead to a significant increase in the section moment capacity. However, due to the relatively small amount of FRP reinforcement, there is little difference in the section stiffness prior to steel yielding. This will have a big impact on the effectiveness of FRP-strengthening in this case, as will be discussed later in the section.

Step 3: Detail to moment distribution from analysis based on constant EI

From analysis based on constant EI distribution, the peak moments and location of the point of contraflexure can be obtained. In this case, the maximum sag moment over the damaged span is 116.2 kN m. Refer to Table 6-32, 2 layers of 0.17mm thick CFRP sheets are used.

As the load pattern in Figure 6-31 represents the worst case scenario for the sag moment of the damaged span, the other parts of the frame are expected be capable of sustaining the design load without any need for strengthening. Therefore, the FRP reinforcement is only updated for the sagging zone of the damaged beam.

For the RC sections within the rest of the frame where the moment under the design load reaches/exceeds its moment capacity, the hinge length concept introduced in previous sections is used to accommodate any moment redistribution after steel yielding. The failure criteria defined in the previous section is also applied to determine any failure that might occur at any of these sections.

Step 4: Construct the moment-curvature relations of the section(s)

The moment-curvature relations are shown in Figure 6-14 for the damaged RC sections, taking account of the pre-existing strain discussed in Step 2 for the FRP-strengthened section. The figure has further illustrated the significant effect on the section moment capacity and much less so on the section stiffnesses.

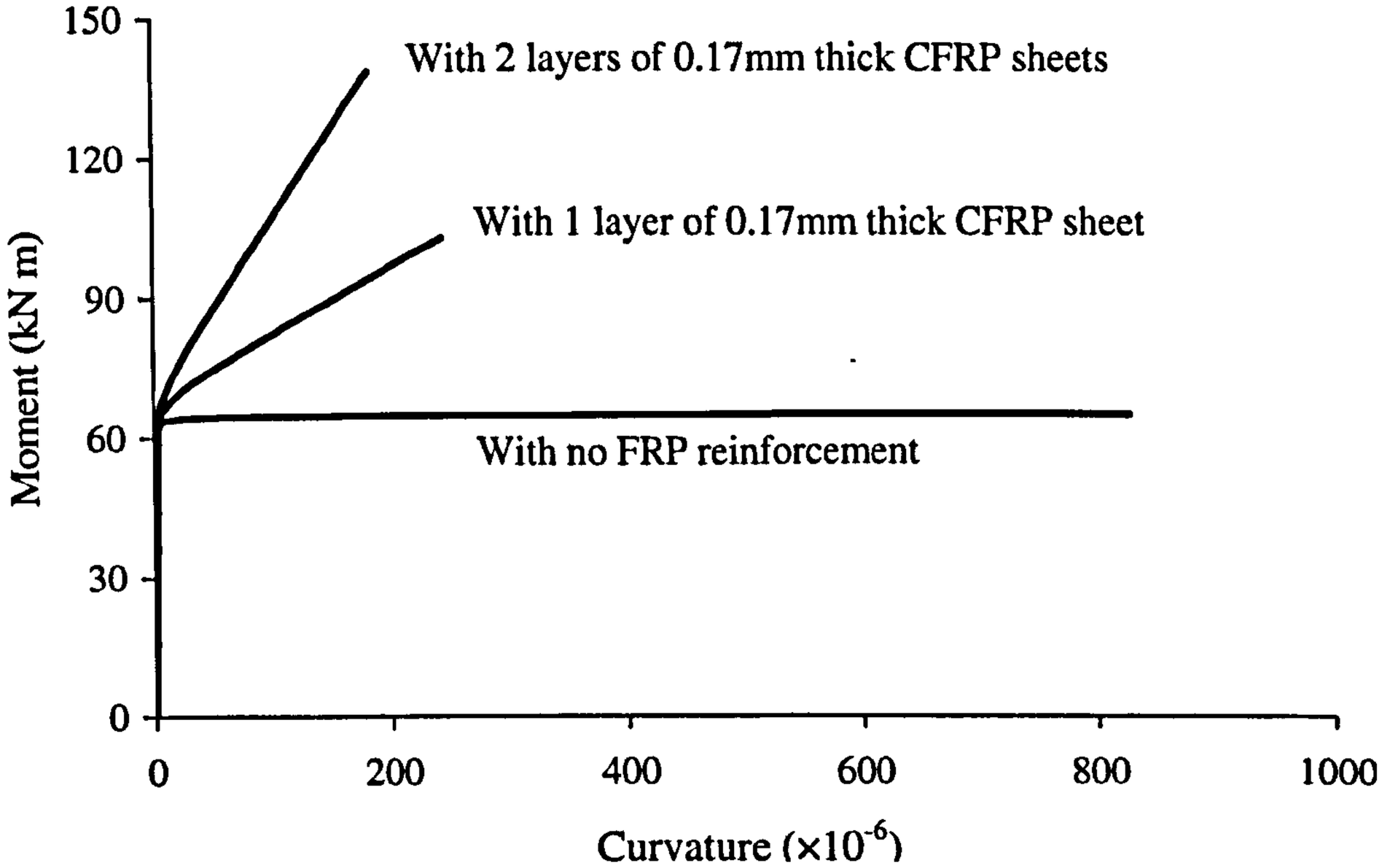

Figure 6-14 - Moment-curvature relations for the damaged RC sections

Step 5: Obtain the load carrying capacity of the frame based on the actual stiffness distribution

Following the procedure set out in Chapter 5, the load carrying capacity of the strengthened frame is w = 46.5 kN/m, with the maximum hog moment section along the strengthened beam being the critical section. This suggests that design based on constant EI distribution would have led to a 9.2% capacity deficiency in the structure. The lower stiffness of the FRP-strengthened section (which is comparable to that of the damaged section) compared to that of the original steel RC section means that the hog zone will attract more moment than the original design. At the end, the structure failed at the maximum hog moment sections. The stiffness profile along the strengthened span is shown in Figure 6-15.

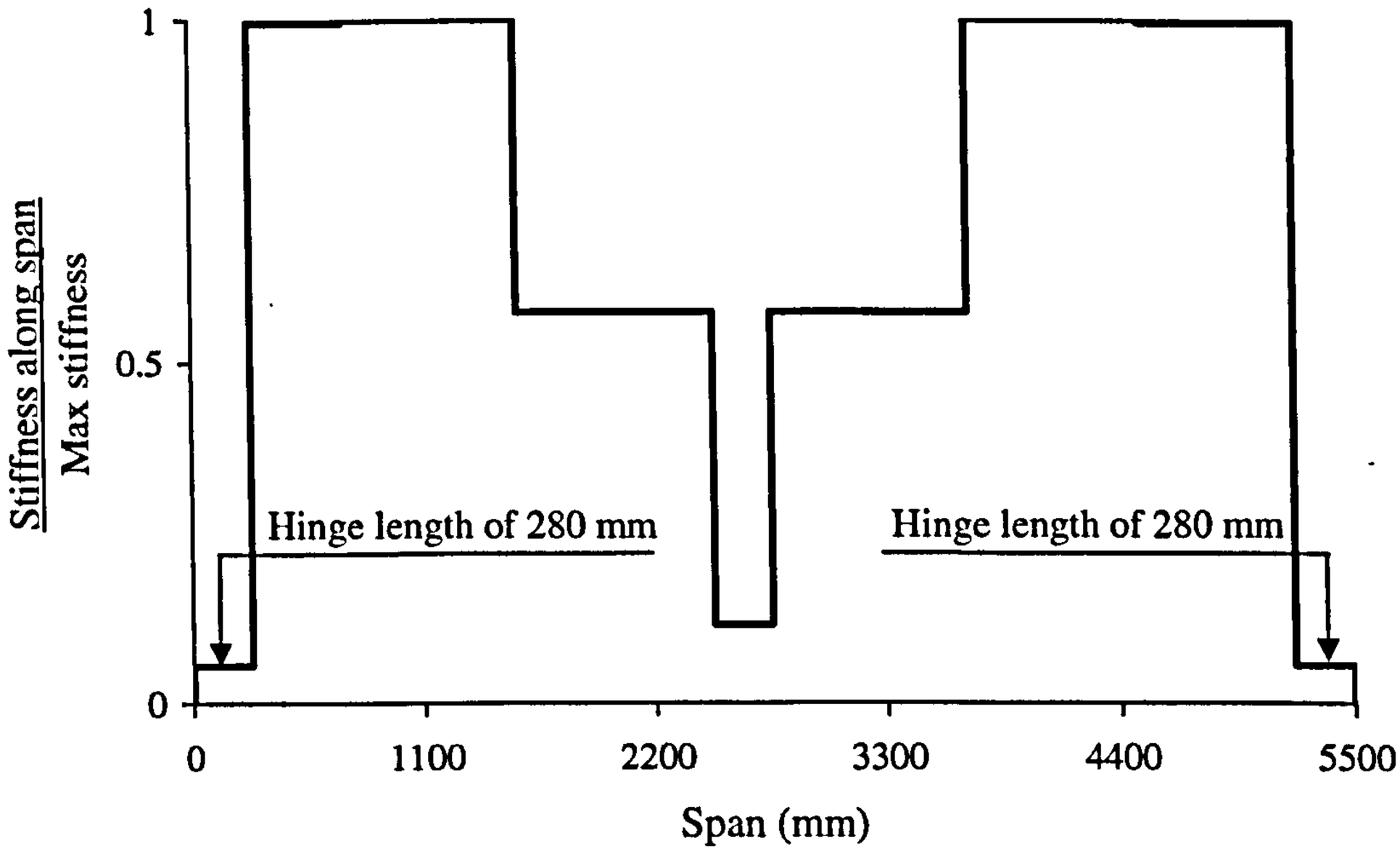

Figure 6-15 - Stiffness variation along the strengthened span

Based on the final moment distribution, 1 no. of 0.17 mm thick CFRP sheet is then used. The procedure in Chapter 5 has given a failure load at w = 38.8 kN/m. Also, further check on the ultimate load of the structure with more CFRP reinforcement shows little improvement, unless the amount of FRP is such that it will lead to significant increase in the section stiffness. Then, that means more 'waste' of section moment capacity. An alternative is to strengthen the hog sections within the damaged span, but considerations such as the difficulties in applying CFRP sheets/plates at the beam-column joints and the need to keep a level floor surface often leave the FRP-strengthening an unfavourable option.

The proposed design procedure is used in this example to assess the effectiveness of using FRP sheets/plates to restore the load carrying capacity of a 3×3 frame. In this particular example, the use of FRP strengthening is very effective up to a design load of around 46.5 kN/m. Beyond this point, any additional FRP strengthening will not lead to any significant increase in the load capacity of the structure as the maximum hog moment sections within the span became the critical section. Although the hog moment sections can also be strengthened with FRP plating, practical considerations often leave this an unfavourable option, which is therefore not pursued further in the example. It became clear that the impact on both the section moment capacity and the section stiffness should be considered in proposing FRP strengthening.

6.4 Conclusions and Discussions

An iterative procedure has been developed entailing multiple detailing and ultimate analysis loops for the structure to create an analysis-design process for ductility-deficient indeterminate structures. The new analysis-design process has been illustrated by way of examples including a FRP-plated continuous RC beam and a traditional RC continuous beam. The procedure is also used in strengthening a 3×3 frame to restore its load carrying capacity. Quick attainment of reinforcement details in all cases suggest that this may well constitute a design procedure applicable to structures of varying levels of ductility. Design based on constant EI may lead to structures with a load deficiency of 12.9% and 9.2% for Examples 1 and 3, respectively.

In designing the traditional RC continuous beam, the concept of hinge length was introduced. Its introduction provides a useful tool to allow moment redistribution through rotation at hinges and therefore the structure to take more loads. In this particular example, when the hinge length increases from zero, which allows no moment redistribution through rotation at the hinge, to 137 mm from the Mottack (1967) expression, the mid-span moment has increased by 18.3% and the ultimate load by 11.4%.

In the third example, it is considered that FRP strengthening is very effective up to a design load of 46.5 kN/m, beyond which any additional FRP strengthening will not lead to any significant increase in the load capacity of the structure. It is important that the impact on both the section moment capacity and the section stiffness should be considered in proposing FRP strengthening.

The new design approach is based on linear simulation of stiffness profiles of the member and clear defining of the failure point in the moment-curvature plot. Although the examples in this chapter have assumed that failure occurs due to concrete crushing, debonding failure may also be included by incorporating debonding strength models – especially those of limiting strain in the FRP plates – into the analysis. However, as have been highlighted in Chapter 2, large disparity exists between various debonding strength models and agreement remains to be reached.

Finally, the current analysis-design approach is applicable to structures of varying levels of ductility. However, the availability of such an approach does not discount but indeed highlight the significance of ductility in structural designs. Ductility should always remain an important consideration to structural designers, as it allows for stress redistribution in statically indeterminate structures and provides warning of impending failures.

Appendix 6A

Derivation of Flexural Constitutive Models

6A.1 Constitutive Behaviour of Materials

6A.1.1 Constitutive behaviour of concrete

Concrete is assumed to possess no tensile strength. In compression, the uniaxial behaviour of concrete is represented as follows:

$$\sigma_c = E_c\varepsilon_c - \frac{1}{f_{cu}}\cdot\left(\frac{E_c\varepsilon_c}{2}\right)^2 \qquad (6A\text{-}1)$$

for

$$0 \leqslant \varepsilon_c \leqslant 0.0035$$

where σ_c = compressive stress in the concrete; f_{cu} = uniaxial cube strength of the concrete; E_c = Young's modulus of the concrete; and ε_c (taken positive when compressive) = strain in the concrete. Crushing is assumed to occur at the compressive strain of 0.0035. E_c is derived, using standard elastic expressions, for the bulk modulus (K_0) and shear modulus (G_0) of the concrete at zero deformation, as follows:

$$E_c = \frac{9K_0G_0}{3K_0 + G_0} \qquad (6A\text{-}2)$$

The following Kotsovos (1979) expressions have been used for the bulk and shear moduli:

$$K_0 = 11000 + 3.2\left(f_c'\right)^2 \qquad (6A\text{-}3)$$

and

$$G_0 = 9224 + 136f_c' + 3.296\times10^{-12}\left(f_c'\right)^{8.273} \qquad (6A\text{-}4)$$

where f_c' = uniaxial cylinder strength of concrete, taken as 0.85 f_{cu}.

6A.1.2 Constitutive behaviour of internal steel and FRP plating

For the internal steel, a linearly elastic region followed by a region of constant yield stress is assumed. E_s and f_y are the initial Young's modulus and the yield stress, respectively. The FRP plate material is linearly elastic up to rupture, with a Young's modulus E_p.

6A.2 Assumptions of Analytical Procedure

A linear through-depth strain distribution in the RC section through to the plating is assumed. The modification made in the original paper to take account of the pre-existing strain is omitted here, assuming that there is no pre-existing strain in the members. All safety factors are set to be 1.

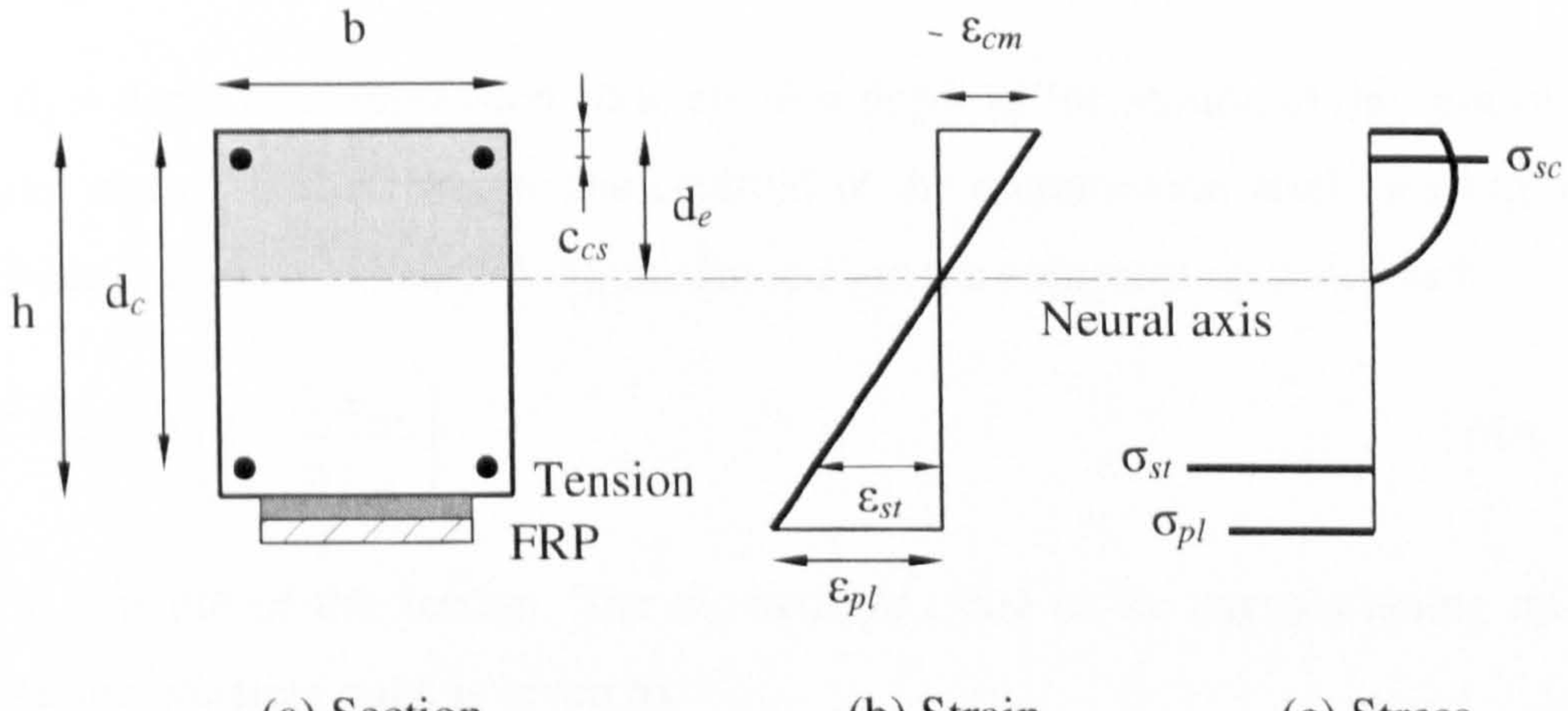

Figure 6A-1 - Through depth strains and stresses in plated reinforced concrete section

6A.3 Development of Analysis for Plated Reinforced Concrete Rectangular section

At section flexural failure, it is assumed that the compression steel is elastic, but that yielding of the internal tension steel is permitted.

6A.3.1 Fundamental equations

The relevant strain and stress distributions are given in Fig. 6A-1 (b) and (c). Using Fig. 6A-1 (b), the strain in the compression concrete at a distance x from the neutral axis (ε_{cx}), and the strain in the bonded plate (ε_{pl}), can all be expressed in terms of the strain in the extreme compression concrete fibre (ε_{cm}) as follows:

$$\varepsilon_{cx} = \frac{x}{d_c}\varepsilon_{cm} \tag{6A-5}$$

$$\varepsilon_{cs} = \frac{d_c - c_{cs}}{d_c}\varepsilon_{cm} \tag{6A-6}$$

and

$$\varepsilon_{pl} = \frac{h - d_c}{d_c}\varepsilon_{cm} \tag{6A-7}$$

where d_c = depth of compression concrete; h = depth of the section to the centroid of the plate; and c_{cs} is the cover to the centroid of the compression steel [see Fig. 6A-1(a). Using Eqs. (6A-1) and (6A-5), the force F_c in the compression concrete is

$$F_c = \frac{d_c b E_c \varepsilon_{cm}}{2}\left(1 - \frac{E_c \varepsilon_{cm}}{6 f_{cu}}\right) \tag{6A-7}$$

where b = width of the section. The moment, M_c, due to the stresses acting on the compression concrete only, is given by:

$$M_c = d_c^2 b_w E_c \varepsilon_{cm}\left(\frac{1}{3} - \frac{E_c \varepsilon_{cm}}{16 f_{cu}}\right) \tag{6A-8}$$

If the internal tension steel is elastic, the forces F_{st}, F_{sc}, in the internal tension and compression steel reinforcements, respectively, and the moments M_{st}, M_{sc} of these forces about the section neutral axis are

$$F_{st} = A_{st} E_s \frac{d_e - d_c}{d_c} \varepsilon_{cm} \tag{6A-9}$$

$$F_{sc} = A_{sc} E_s \frac{d_c - c_{cs}}{d_c} \varepsilon_{cm} \tag{6A-10}$$

$$M_{st} = (d_e - d_c) F_{st} = A_{st} E_s \frac{(d_e - d_c)^2}{d_c} \varepsilon_{cm} \tag{6A-11}$$

$$M_{sc} = A_{sc} E_s \frac{(d_c - c_{cs})^2}{d_c} \varepsilon_{cm} \tag{6A-12}$$

where A_{st}, A_{sc} = areas of the internal tension and compression steels; d_e = the depth to the centroid of the internal tension steel.

Similarly, the force F_p in the plate, and the moment M_p due to this force are as follows:

$$F_p = A_p E_p \frac{(h - d_c)}{d_c} \varepsilon_{cm} \tag{6A-13}$$

$$M_p = (h - d_c) A_p E_p \frac{(h - d_c)}{d_c} \varepsilon_{cm} \tag{6A-14}$$

where A_p = the area of the bonded plate.

If the strain in the internal tension steel falls within the plastic region, the expression for F_{st}, M_s are

$$F_{st} = A_{st} f_y \tag{6A-15}$$

$$M_{st} = A_{st} f_y (d_e - d_c) \tag{6A-16}$$

Equilibrium requires that

$$F_{st} + F_p = F_{sc} + F_c \tag{6A-17}$$

This will give the depth of the neutral axis (d_e).

The total moment M_{tot} on the section to be

$$M_{tot} = M_{st} + M_{sc} + M_p + M_c \tag{6A-18}$$

The moment-curvature relations for the section can be obtained.

Chapter 7

Conclusions

This chapter summarises the issues addressed throughout this thesis, and outlines the main findings of the work. Finally, suggestions are made for extension of this work.

7.1 Summary

There is currently a significant requirement for enhancement of existing – both reinforced concrete (RC) and metallic – structures. Due largely to the economic advantages of enhancing over demolition and rebuilding of these existing structures, a number of structural strengthening methods have been developed. This thesis is concerned with one of these strengthening methods, namely flexural strengthening via external adhesive bonding, to the existing structure, of unidirectional FRP reinforcing plates. In particular, this thesis focuses on FRP-plated indeterminate structures – an important area that so far has not received much attention.

A survey of the literature identified that there was considerable scope for further research to achieve the following:

- The implications of premature debonding failures on the ductility of FRP-plated structures have been noted by many researchers. Although various strength models have been developed for debonding failures, there is high level of dispersion in the results so thorough understanding of their mechanisms is still to gained;
- Design using procedure for traditional statically indeterminate reinforced concrete (RC) structures may be unsafe for FRP-plated RC structures. And quantification of the ductility of FRP-plated structures remains largely an unresolved issue. Design

- guidance documents currently available either limit the strengthening level of the FRP reinforcement to provide sufficient ductility of the strengthened structure or use a bigger safety factor to compensate for the reduction in ductility;
- Most of the work to date has focused on the application of FRP reinforcement to one-span simply supported members. Research – both analytical and experimental – into FRP-plated indeterminate (particularly metallic) structures is limited. The development of self-equilibrating moments and their potential effects in the indeterminate spans have not thus far been addressed;
- Most research to date has focused on FRP-plated RC structures and less work has been conducted on FRP-plated metallic structures. Virtually no documents have been found on the general behaviour of FRP-plated indeterminate metallic structures.

In order to investigate these issues, analyses were conducted on 2-span FRP-plated continuous members, to investigate the mechanics of the development of self-equilibrating moments, due to support settlements. Parametric studies were carried out to illustrate how certain ranges of the stiffness ratios can give rise to significant self-equilibrating moment effects including early nonlinearity and contraflexure shift.

In addition, four 2-span FRP-plated steel-I beams were fabricated and tested to failure at the Structures Lab at University of Bristol. As one of the novel tests of its kind, the main aspects of investigation include those related to FRP plated thin-walled metallic structures such as buckling, plate debonding, interfacial strain and (average) interfacial stresses in the adhesive, and those specific to structural indeterminacy such as support deformations, stiffness variations along the member, and migration of point of contraflexure. The main parameters varied between specimens include layout of plates and plate thicknesses. Some novel measures were taken to prevent local buckling.

A computational technique was presented for time-efficient prediction of ultimate loads of indeterminate members of varying ductility, which is then incorporated into an iterative procedure entailing multiple detailing and ultimate analysis loops for the structure to create a design process for ductility-deficient indeterminate structures.

7.2 Conclusions

From the results of the work presented in this thesis, the following points should be highlighted:

- The moments developed in a 2-span continuous structure depend not only on the support-to-member stiffness *ratios* but also on the distribution of stiffness along the member. A 'sensitive zone' ($\beta = 0 - 60$) exists for support stiffnesses where particular care should be taken for test set-up in the lab and also for bridges in practice.
- The use of effective support stiffnesses gives good prediction of self-equilibrating moments developed due to differential settlement under both ultimate and service loads. The proposed deflection-based approach has proven to be satisfactory in estimating the support stiffnesses.
- Linear variation along the segment nearest to the centre support (Z4) was assumed for the ULS analysis. Change in section stiffness at the centre support leads to a gradual change in the centre support moment.
- For beams subject to point load, both the length and the stiffness of the segment nearest the centre support have a significant effect on the moment distribution along the span.
- For a beam of given stiffness profile subjected to a point load with constant support stiffness ratio, a point exists along the beam where there is no self-equilibrating moment. On the one side of the point closer to the centre support, the self-equilibrating moment increases the moment at the centre support section; on the other side of the point, it decreases the moment at the centre support section.
- Of the four tested specimens, two (B1 and B2) failed by loss of stability induced by local buckling and one (B4) failed by plate separation from the steel beam.
- Some debonding was observed at the compression end of specimen B1 and sudden separation occurred with specimen B4. In both cases, debonding occurred at the interfaces (steel/adhesive interface for B4 and adhesive/plate interface for B1) in contrast to common failure in the concrete cover in FRP-strengthened RC beams.
- Adhesive bonding the steel stiffeners to the test beam has worked very efficiently to prevent local flange/web buckling. It was most effective when the stiffeners were placed directly at the sections where load were applied or at the supports. Local

buckling was prevented up to a load of at least 36% higher than the failure load for the beam of similar section but without any stiffeners. This technique is an alternative to welding and allows for safe application of strain gauging at the section of stiffening;

- Through thickness variation and/or local bending, are important in the evaluation of the average bond stresses, especially when thick FRP plates are used. Using outer surface strains only (which is common in practice) could lead to unreasonable prediction of interfacial shear stresses.

- There is significant variation in material properties in the steel. However, the idealised elastic-perfectly plastic characteristic commonly taken for steel has shown to be satisfactory. Residual stresses may also be present in the steel and should be properly accounted for in corresponding section analysis.

- Section stiffness obtained from the strain distribution across plated sections (and therefore is bond slip analysis) are compared with results from rigid bond analyses. The generally good comparison for various plate thicknesses ranging 1.5 to 16 mm suggests that rigid bond analyses can be used to calculate section stiffnesses.

- The general nonlinear stiffness variation can be approximated in a piecewise linear manner. The choice of the number of linear stiffness pieces depends on how rapidly the stiffness changes and the precision level specified. A 2-to-5-piece linear stiffness approximation generally gives sufficient representation of the nonlinear stiffness variation;

- This technique has been illustrated by way of examples, which cover a wide range of structural ductility under different types of loading. Convergence was attained after 4-8 iterations in all cases, suggesting that standard structural analysis software for linear beam analysis may well be used confidently for analysing nonlinear problems;

- An iterative procedure has been developed entailing multiple detailing and ultimate analysis loops for the structure to create a design process for ductility-deficient indeterminate structures. The new analysis-design process has been illustrated by way of examples including a FRP-plated continuous RC beam and a traditional RC continuous beam. The procedure is also used in strengthening a 3×3 frame to restore its load carrying capacity. Quick attainment of reinforcement details in all cases suggest that this may well constitute a design procedure applicable to structures of

varying levels of ductility. Design based on constant EI may lead to structures with a load deficiency of 12.9% and 9.2% for Examples 1 and 3, respectively;

- In designing the traditional RC continuous beam, the concept of hinge length was introduced. Its introduction provides a useful tool to allow moment redistribution through rotation at hinges and therefore the structure to take more loads. In this particular example, when the hinge length increases from zero, which allows no moment redistribution through rotation at the hinge, to 137 mm from the Mottack (1967) expression, the mid-span moment has increased by 18.3% and the ultimate load by 11.4%.

7.3 Future work

The following ideas may form the basis of extension of this research:

- More test data is required on FRP-plated indeterminate (especially metallic) structures to gain further understanding of the influences of the applications of FRP reinforcement on the ductility and general behaviour of such structures.
- Debonding strength models – especially those of limiting strain in the FRP plates – should be incorporated into the proposed procedure to accommodate design against premature debonding failures.
- The process to submit EI distributions to linear beam analysis should be automated in order for this technique to be practically applicable in real design environments.
- Different structures such as multi-span beams or frames and multiple load cases should be considered for the application of the proposed design procedure.

References

[1] Adhikary, B. B. and Mutsuyoshi, H., "Study on the bond between concrete and externally bonded CFRP sheet", *Proc. 5th International Conference on Fibre-reinforced Plastics for Reinforced Concrete Structures (FRPRCS-5)*, Cambridge, UK, 2001, pp.371-378. ISBN 0727730290.

[2] Ahmed, O. and Van Gemert, D., "Effect of longitudinal carbon fiber reinforced plastic laminates on shear capacity of reinforced concrete beams", *Proc. 4th International Symposium on Fibre-reinforced Plastics for Reinforced Concrete Structures (FRPRCS-4)*, Baltimore, USA, 1999, pp.933-943.

[3] Alexander, J. G. S. and Cheng, J. J. R., "Field application and studies of using CFRP sheets to strengthen concrete bridge girders", *Advanced Composite Materials in Bridges and Structures*, Canadian Society for Civil Engineering, Montreal, 1996, pp.465-472.

[4] Alkhrdaji T, Nanni A., Chen G. and Barker M., "Upgrading the transportation infrastructure: solid RC decks strengthened with FRP", *ACI Concrete International*, 1999, Vol. 21, No. 10, pp.37-41.

[5] Al-Saidy, A. H., Klaiber, F. W. and Wipf, T. J., "Repair of steel composite beams with carbon fibre-reinforced polymer plates", *ASCE Journal of composites for construction*, 2004, Vol. 8, No. 2, pp.163-172.

[6] American Concrete Institute (ACI). "Guide for the design and construction of externally bonded FRP systems for strengthening concrete structures", *ACI 440.2R-08*, ACI Committee 440, 2008, Detroit, USA. ISBN 9780870312854.

[7] American Concrete Institute (ACI), "Building code requirementsfor structural concrete and commentary", *ACI 318-05*, ACI Committee 318, 2005, Farmington Hills, Michigan. ISBN 0870311719.

[8] American Concrete Institute (ACI), "Guide for the design and construction of concrete reinforced with FRP bars", *ACI 440.1R-03*, ACI Committee 440, 2003, Farmington Hills, Michigan. ISBN 0870311182.

[9] American Concrete Institute (ACI), "Guide for the design and construction of concrete reinforced with FRP bars", Proposed revisions, ACI Committee 440, 2004, Farmington Hills, Michigan.

[10] American Society of Civil Engineers (ASCE), "Bridges", *The 2005 Report card for America's Infrastructure*, American Society of Civil Engineers, 2005, pp.3.

[11] Aoyagi, Y. and Endo, T., "Shear strength in corner region of reinforced concrete duct type structures to be embedded in soil", *Proc. 12th International Conference on Structural Mechanics in Reactor Technology (SMiRT-12)*, Stuttgart, Germany, 1993, pp.289-294.

[12] Aram, M. R., Czaderski, C. and Motavalli, M., "Effects of gradually anchored prestressed CFRP strips bonded on prestressed concrete beams", *ASCE Journal of Composites for Construction*, 2008, Vol. 12, No. 1, pp.25-34.

[13] Arduini, M. and Nanni, A., "Behaviour of precracked RC beams strengthened with carbon FRP sheets", *ASCE Journal of Composites for Construction*, 1997, Vol. 1, No. 2, pp.63-70.

[14] Ashour A. F., El-Refaie S. A., and Garrity S. W., "Flexural strengthening of RC continuous beams using CFRP laminates", *Cement and Concrete Composites*, 2004, Vol. 26, No. 7, pp.765–775.

[15] Bahn, B. and Harichandran, R. S., "Flexural behaviour of reinforced concrete beams strengthened with CFRP sheets and epoxy mortar", *ASCE Journal of Composites for Construction*, 2008, Vol. 12, No. 4, pp.387-395.

[16] Benachour, A., Benyoucef, S., Tounsi, A. and Bedia, E. A. A., "Interfacial stress analysis of steel beams reinforced with bonded prestressed FRP plate", Engineering Structures, 2008, Vol. 30, No. 11, pp.3305-3315.

[17] Bencardino, F., Spadea, G. and Swamy, R. N., "Strength and ductility of reinforced concrete beams externally reinforced with carbon fiber fabric", *ACI Structural Journal*, 2002, Vol. 99, No. 2, pp.163-171.

[18] Bisby, L. A., Dent, A. J. S. and Green, M. F., "Comparison of confinement models for fiber-reinforced-polymer-wrapped concrete", *ACI Structural Journal*, 2005, Vol. 102, No. 1, pp.62-72.

[19] Bischoff, P. H., "Deflection calculation of FRP reinforced concrete beams based on modifications to the existing Branson Equation", *ASCE Journal of Composites for Construction*, 2007, Vol.11, No. 1, pp.4-14.

[20] Bizindavyi, B. L. and Neale, K. W., "Transfer lengths and bond strengths for composites bonded to concrete", *ASCE Journal of Composites for Construction*, 1999, Vol. 3, No. 4, pp.153-160.

[21] Blaschko, M., Niedermeier, R. and Ailch, K., "Bond failure modes of flexural members strengthened with FRP", *Proc. 2nd International Conference on Composites in Infrastructure*, Arizona, USA, 1998, pp.315-327

[22] Bonacci, J. F. and Maalej, M., "Externally bonded FRP for service-life extension of RC infrastructure", *Journal of Infrastructure Systems*, ASCE, 2000, Vol. 6, No. 1, pp.41-51.

[23] Bonacci, J. F. and Maalej, M. "Behavioral trends of RC beams strengthened with externally bonded FRP", *ASCE Journal of Composites for Construction*, 2001, Vol. 5, No. 2, pp.102-113.

[24] Bracci, J. M., Reinborn, A. M. and Mander, J. B., "Seismic resistance of reinforced concrete frame structures designed only for gravity loads: Part I – Design and properties of a one-third scale model structure", *National Centre for Earthquake Engineering Research (NCEER) Technical Report NCEER-92-0027*, State University of New York, Buffalo, New York, USA, 1992.

[25] British Standards Institution. "Structural use of concrete—Part 1", *BS 8110*, BSI, London, 1995.

[26] Brosens, K and Van Gemert, D., "Anchoring stress between concrete and carbon fiber reinforced laminates", *Proc. 3rd International Symposium on Fibre-reinforced Plastics for Reinforced Concrete Structures (FRPRCS-3)*, Sapporo, Japan, 1997, pp.271-278.

[27] Cadei, J. (ed), "Strengthening of Metallic structures using FRPs", *CIRIA Report C595*, Construction Industry Research and Information Association, 2004, London. ISBN 0860175952.

[28] Canadian Standards Association, "Code for the design of concrete structures for buildings", *CAN-A23.2*, CSA, 1994.

[29] Canadian Standards Association, "Design and construction of building components with fibre-reinforced polymers", *Concrete design handbook: Canadian Standard S806-02*, CSA, 2002, Toronto.

[30] Chajes, M. J., Thomson, T. A., Januszka, T. F. and Finch, W. W., "Flexural strengthening of concrete beams using externally bonded composite materials", *Construction and Building Materials*, 1994, Vol. 8, No. 3, pp.191-201.

[31] Chaallal, O., Nollet, M.J. and Perraton, D., "Strengthening of reinforced concrete beams with externally bonded fiber-reinforced-plastic plates: Design guidelines for shear and flexure", *Canadian Journal of Civil Engineering*, 1998, Vol. 25, No. 4, pp.692-704.

[32] Chen, J.F. and Teng, J.G., "Anchorage strength models for FRP and steel plates bonded to concrete", *ASCE Journal of Structural Engineering*, 2001, Vol. 127, No. 7, pp.784-791.

[33] Coccia, S., Ianniruberto, U. and Rinaldi, Z., "Redistribution of bending moments in continuous reinforced concrete beams strengthened with fiber-reinforced polymer", *ACI Structural Journal*, 2008, Vol. 105, No. 3, pp.318-326.

[34] Colotti, V., Spadea, G. and Swamy, R. N., "Structural model to predict the failure behaviour of plated reinforced concrete beams", *ASCE Journal of Composites for Construction*, 2004, Vol. 8, No. 2, pp.104-122.

[35] Colombi, P. and Poggi, C., "An experimental, analytical and numerical study of the static behaviour of steel beams reinforced by pultruded CFRP strips", *Composites, Part B*, 2006, Vol. 37, No.1, pp.64-73.

[36] Concrete Society, "Design guidance for strengthening concrete structures using fiber composite materials", *Technical Report 55*, The Concrete Society, 2004, Surrey, UK. ISBN 1904482147.

[37] Dai, J.G., Ueda, T. and Sato, Y. "Development of the nonlinear bond stress-slip model of fiber reinforced plastics sheet-concrete interfaces with a simple method", *ASCE Journal of Composites for Construction*, 2005, Vol. 9, No. 1, pp.52-62.

[38] Debernardi, P. G. and Taliano, M., "Evaluation of rotation capacity for reinforced concrete beams", *ACI Structural Journal*, 2002, Vol. 99, No. 3, pp.360-368.

[39] De Lorenzis, L., Miller, B. and Nanni, A., "Bond of FRP laminates to concrete", *ACI Material Journal*, 2001, Vol. 98, No. 3, pp.256-264.

[40] De Lorenzis L., Galati D. and La Tegola A., "Stiffness and ductility of fibre-reinforced polymer-strengthened reinforced concrete beams" *Proceedings of the Institution of Civil Engineers, Structures and Buildings*, 2004, Vol. 157, No. 1, pp.31-51.

[41] Deng, J., Lee, M. M. K. and Moy, S. S. J., "Stress analysis of steel beams reinforced with a bonded CFRP plate", *Composites, Structures*, 2004, Vol. 65, No. 2, pp.205-215.

[42] Duthinh D. and Starnes M., "Strength and ductility of concrete beams reinforced with carbon fibre-reinforced polymer plates and steel", *ASCE Journal of Composites for Construction*, 2004, Vol. 8, No. 1, pp.59-69.

[43] Edberg, W., Mertz, D. and Gillespie Jr., J., "Rehabilitation of steel beams using composite materials", *Proc. The Materials Engineering Conference, Materials for the New Millennium*, ASCE, New York, USA, 1996, pp.502-508.

[44] El Damatty, A. A., Abushagur, M. and Youssef, M. A., "Experimental and analytical investigation of steel beams rehabilitated using GFRP sheets", *Steel and Composite Structures*, 2003, Vol. 3, No. 6, pp.421-438.

[45] El-Hacha, R., Wight, R. G. and Green, M. F., "Prestressed fibre-reinforced polymer laminates for strengthening structures." *Progress in Structural Engineering and Materials*, 2001, Vol. 3, No. 2, pp.111-121.

[46] El-Hacha, R., Wight, R. G. and Green, M. F., "Prestressed carbon fiber reinforced polymer sheets for strengthening concrete beams at room and low

temperatures." *ASCE Journal of Composites for Construction*, 2004, Vol. 8, No. 1, pp.3-13.

[47] El-Mihilmy, M. T. and Tedesco, J. W., "Prediction of anchorage failure for reinforced concrete beams strengthened with fiber-reinforced polymer plates", *ACI Structural Journal*, 2001, Vol. 98, No. 3, pp.301-314.

[48] El-Refaie S. A., Ashour A. F. and Garrity S. W., "Strengthening of reinforced concrete continuous beams with CFRP composites", *Structural Engineering, Mechanics and Computation*, 2001, Vol. 2, pp.1591-1598.

[49] El-Refaie S. A., Ashour A. F. and Garrity S. W., "Sagging and hogging strengthening of continuous reinforced concrete beams using carbon fibre-reinforced polymer sheets", *ACI Structural Journal*, 2003a, Vol. 100, No. 4, pp.446-453.

[50] El-Refaie S. A., Ashour A. F. and Garrity S. W., "CFRP strengthened continuous concrete beams", *Proceedings of the Institute of Civil Engineers, Structures and Buildings*, 2003b, Vol. 156, No. 4, pp.395-404.

[51] Elsayed, W., Ebead, U. A. and Neale, K. W., "Interfacial behaviour and debonding failures in FRP-strengthened concrete slabs", *ASCE Journal of Composites for Construction*, 2007, Vol. 11, No. 6, pp.619-628.

[52] Esfahani, M. R., Kianoush, M. R. and Tajari, A. R., "Flexural behaviour of reinforced concrete beams strengthened by CFRP sheets", *Engineering Structures*, 2007, Vol. 29, No. 10, pp.2428-2444.

[53] European Convention for Constructional Steelwork, "Ultimate limit state calculation of sway frames with rigid joints", ECCS Technical Committee 8 – Structural Stability – Technical Working Group 8.2 – System, ECCS publication No. 33, ECCS, 1984, Brussels, Belgium.

[54] Fantilli, A. P., Ferretti, D., Iori, I. and Vallini, P., "Mechanical model for failure of compressed concrete in reinforced concrete beams", *ASCE Journal of Structural Engineering*, 2002, Vol. 128, No. 5, pp.637-645.

[55] Federation internationale du beton (fib). "Design and use of externally bonded FRP reinforcement for RC structures", *FIB Bulletin No.14*, FIB Task Group 9.3, 2001, Lausanne, Switzerland. ISBN 9782883940543

[56] Ferrier, E., Ennaceur, C., Bigaud, D. and Hamelin, P., "Prestressed externally bonded FRP reinforcement for RC beams", *Proc. 5th International Conference on Fibre-reinforced Plastics for Reinforced Concrete Structures (FRPRCS-5)*, Cambridge, UK, 2001, pp. 271-280. ISBN 0727730290.

[57] Gao, B., Kim, J. K. and Leung, C. K. Y., "Effects of rubber modifier on mechanical properties of interface between CFRP and concrete", *Composites Science and Technology*, 2003, Vol. 63, No. 6, pp.883-892.

[58] Gao, B., Kim, J. K. and Leung, C. K. Y., "Experimental study on RC beams with FRP strips bonded with rubber modified resins", *Composites Science and Technology*, 2004, Vol. 64, No. 16, pp.2557-2564.

[59] Gao, B., Kim, J. K. and Leung, C. K. Y., "Optimisation of tapered end design for FRP strips bonded to RC beams", *Composites Science and Technology*, 2006a, Vol. 66, No. 10, pp.1266-1273.

[60] Gao, B., Kim, J. K. and Leung, C. K. Y., "Strengthening efficiency of taper ended FRP strips bonded to RC beams", *Composites Science and Technology*, 2006b, Vol. 66, No. 13, pp.2257-2264.

[61] Garden, H. N., Hollaway, L. C. and Thorne, A. M., "A preliminary evaluation of carbon fibre reinforced polymer plates for strengthening reinforced concrete members", *Proceedings of the Institute of Civil Engineers, Structures and Buildings*, 1997, Vol. 123, pp.127-142.

[62] Garden, H. N. and Hollaway, L. C., "An experimental study of the influence of plate end anchorage of carbon fibre composite plates used to strengthen reinforced concrete beams", *Composites, Structures*, 1998, Vol. 42, No. 2, pp.175-188.

[63] Gentile C and Rizkalla S., "Flexural strengthening of timber beams using FRP", *Technical Report*, ISIS Canada, University of Manitoba, Winnipeg, Manitoba, Canada, 1999.

[64] Grace N. F., Soliman A. K., Abdel-Sayed G. and Saleh K. R., "Behaviour and ductility of simple and continuous FRP reinforced beams", *ASCE Journal of Composites for Construction*, 1998, Vol. 2, No. 4, pp.186-194.

[65] Grace N. F., Soliman A. K., Abdel-Sayed G. and Saleh K. R., "Strengthening of continuous beams using fibre reinforced polymer laminates", *Proc. 4th International Symposium on Fibre Reinforced Polymer Reinforcement for Reinforced Concrete Structures (FRPRCS-4)*, Baltimore, 1999, pp.647-657.

[66] Gravina, R. J. and Smith, S. T., "Flexural behaviour of indeterminate concrete beams reinforced with FRP bars", *Engineering Structures*, 2008, Vol. 30, No. 9, pp.2370-2380.

[67] Habeeb M. N. and Ashour A. F., "Flexural behaviour of continuous GFRP reinforced concrete beams." *ASCE Journal of Composites for Construction*, 2008, Vol. 12, No. 2, pp.115-124.

[68] Harmon, T.G., Kim, Y.J., Kardos, J., Johnson, T. and Stark, A., "Bond of surface mounted fiber-reinforced polymer reinforcement for concrete structures", *ACI Structural Journal*, 2003, Vol. 100, No. 5, pp.557-564.

[69] Highways Agency, "Strengthening highway bridges using externally bonded fibre reinforced polymer", BD 85/08, Design Manual for Roads and Bridges, Vol. 1, Section 3, Part 18, 2008.

[70] Hiroyuki, Y. and Wu, Z., "Analysis of debonding fracture properties of CFS strengthened member subject to tension", *Proc. 3rd International Symposium on Fibre-reinforced Plastics for Reinforced Concrete Structures (FRPRCS-3)*, Japan Concrete Institute, Sapporo, 1997, Issue 1, pp.287–294.

[71] Hogue T, Cornforth R, Nanni A., "Myriad convention center floor system reinforcement", *Proc. 4th International Conference on Fibre-reinforced Plastics for Reinforced Concrete Structures (FRPRCS-4)*, Baltimore, USA, 1999, pp.751-765.

[72] Hollaway, L. C., "Polymer composites for civil and structural engineering", Blackie Academic and Professional, Glasgow, Scotland, 1993.

[73] Hollaway, L. C. and Leeming, M. B. (ed.), "Strengthening of reinforced concrete structures (using externally-bonded FRP composites in Structural and Civil Engineering)", Woodhead, Cambridge, UK, 2001. ISBN 1855733781.

[74] Hollaway, L. C. and Cadei, J., "Progress in the technique of upgrading metallic structures with advanced polymer composites." *Progress of Structural Engineering Materials*, 2002, Vol. 4, No.2, pp.131-148.

[75] Hooks, J. M. and Cooper, J. D., "Application of FRP composites for bridge rehabilitation and strengthening in the USA", *Proceedings of Tenth International Conference on Structural Faults and Repair – 2003*, Technics Press, Edinburgh, 2003, available as CD.

[76] Hutchinson A. R. and Rahimi, H., "Behaviour of reinforced concrete beams with externally bonded fibre reinforced plastics", *Proc. 5th International Conference on Structural Faults and Repair,* June/July, University of Edinburgh, 1993, Vol. 3, pp.221-228.

[77] Hutchinson A. R. and Rahimi, H., "Flexural strengthening of concrete beams with externally bonded FRP reinforcement", *Proc. 2nd International Conference on Advanced Composite Materials in Bridges and Structures,* Canadian Society for Civil Engineering, Montreal, 1996, August, 1996.

[78] Irwin, R. W. and Rahman, A., "FRP strengthening of concrete structures – design constraints and practical effects on construction detailing." *NZ Concrete Society Conference*, Wairakei, NZ, 2002.

[79] ISIS Canada, "Impact of ISIS Canada", *ISIS Canada Research Network Annual Report*, 2005, pp.6.

[80] ISIS Canada, "Innovator", *Newsletter of the Canadian Network of Centres of Excellence on Intelligent Sensing for Innovative Structures*, August 2008.

[81] Izumo, K. M., Saeki, N., Asamizu, T. and Shimura, K., "Strengthening reinforced concrete beams using prestressed fiber sheets", *Proc. 3rd International Symposium on Fibre-reinforced Plastics for Reinforced Concrete Structures (FRPRCS-3)*, Sapporo, Japan, 1997, pp.379-386.

[82] Jansze, W., "Strengthening of RC members in bending by externally bonded steel plates", Ph.D. thesis, 1997, Delft University of Technology, Delft, The Netherlands.

[83] Japan Society of Civil Engineers (JSCE), "Recommendations for upgrading of concrete structures with use of continuous fiber sheets", *JSCE Concrete Engineering Series No.41*, 2001, Japan. ISBN 4810603555.

[84] Jeppsson, J. and Thelandersson, S., "Behaviour of reinforced concrete beams with loss of bond at longitudinal reinforcement", *ASCE Journal of Structural Engineering*, 2003, Vol. 129, No. 10, pp.1376-1383.

[85] Jones, R., Swamy, R. N., Bloxham, J. and Bouderbalah, A., "Composite behaviour of concrete beams with epoxy bonded external reinforcement", *International Journal of Cement Composites*, 1980, Vol. 2, No. 2, pp.91-107.

[86] Karbhari V. M. and Shulley, S. B., "Use of composites for rehabilitation of steel structures— Determination of bond durability", *Journal of Materials in Civil Engineering*, 1995, Vol. 7, No. 4, pp.239–245.

[87] Khalifa, A., Gold, W. J., Nanni, A. and Aziz, A., "Contribution of externally bonded FRP to shear capacity of RC flexural members", *ASCE Journal of Composites for Construction*, 1998, Vol. 2, No. 4, pp.195-203.

[88] Kliger, H., "Repair of parking structures", *FRP International*, 1996, Vol. IV, Issue 4, pp.3-4.

[89] Kotsovos, M. D., "A mathematical description of the deformation behaviour of concrete under complex loading", *Magazine of Concrete Research*, 1979, Vol. 31, No. 107, pp.77-90.

[90] Lamanna, A. J., Bank, L. C. and Scott, D. W., "Flexural strengthening of reinforced concrete beams by mechanically attaching fiber-reinforced polymer strips", *ASCE Journal of Composites for Construction*, 2004, Vol. 8, No. 3, pp.203-210.

[91] Lees J. M. and Burgoyne C. J., "Experimental study of the influence of bond on the flexural behaviour of concrete beams pre-tensioned with aramid fibre reinforced plastics", *ACI Structural Journal*, 1999, Vol. 96, No. 3, pp.377-385.

[92] Lenwari, A., Thepchatri, T. and Albrecht, P., "Flexural Response of Steel Beams Strengthened with Partial-Length CFRP Plates", *ASCE Journal of Composites for Construction*, 2005, Vol. 9, No. 4, pp.296-303.

[93] Lenwari, A., Thepchatri, T. and Albrecht, P., "Debonding Strength of Steel Beams Strengthened with CFRP Plates", *ASCE Journal of Composites for Construction*, 2006, Vol. 10, No. 1, pp.69-78.

[94] Leung, C.K.Y., "Delamination failure in concrete beams retrofitted with a bonded plate", ASCE Journal of Materials in Civil Engineering, 2001, Vol. 13, No. 2, pp.106-113.

[95] Leung, C. K. Y. and Tung, W. K., "A three-parameter model for debonding of FRP from concrete substrate", *Proceedings of the International Conference on FRP Composites in Civil Engineering*, Hong Kong, China, 2001, pp.272–373.

[96] Liu I. S. T., Oehlers D. J. and Seracino R., "Tests on the ductility of reinforced concrete beams retrofitted with FRP and steel near-surface mounted plates", *ASCE Journal of Composites for Construction*, 2006, Vol. 10, No. 2, pp.106-114.

[97] Liu, X., Silva, P. F. and Nanni, A., "Rehabilitation of steel bridge members with FRP composite materials", *Proc., International Conference on Composites in Construction*, Porto, Portugal, 2001, pp.613-617.

[98] Lu, X.Z., Teng, J.G., Ye, L.P. and Jiang, J.J., "Bond-slip models for FRP sheets/plates bonded to concrete", 2005, *Engineering Structures*, Vol. 27, No. 6, pp.920-937.

[99] Luke, S., "The use of carbon fibre plates for the strengthening of two metallic bridges of an historic nature in the UK." *Proc., International Conference on FRP Composites in Civil Engineering*, Hong Kong, China, 2001, Vol. 2, pp.975–983.

[100] Luke, S., Godman, S. and Hamnevoll, H., "Strengthening the Qafco Prill Tower, Qatar, with FRP plates", *Concrete*, 2002, pp.32-33.

[101] Luke, S. and Canning L., "Strengthening of highway and railway bridge structures with FRP composites - Case studies." *Advanced polymer composites for structural applications in construction (ACIC 2004)*, Surrey, UK, 2004, pp.747-754.

[102] Maeda, T., Asano, Y., Sato, Y., Ueda, T. and Kakuta, Y., "A study on bond mechanism of carbon fiber sheet", *Proc. 3rd International Symposium on*

Fibre-reinforced Plastics for Reinforced Concrete Structures (FRPRCS-3), Sapporo, Japan, 1997, pp.279-285.

[103] Martin, J. A., Lamanna, A. J., "Performance of mechanically fastened FRP strengthened concrete beams in flexure", *ASCE Journal of Composites for Construction*, 2008, Vol. 12, No. 3, pp.257-265.

[104] Matthys, S., "Structural behaviour and design of concrete members strengthened with externally bonded FRP reinforcement", Ph.D. thesis, 2000, Ghent University, Ghent, Belgium.

[105] Mattock, A. H., "Discussion of rotational capacity of reinforced concrete beams, by W. D. G. Corley.", *ASCE Journal of Structural Division*, 1967, Vol. 93, No. 2, pp.519-522.

[106] Meier, U. and Kaiser H. P., "Strengthening of structures with CFRP laminates", *Proc. Specialty Conference on Advanced Composite Materials in Civil Engineering Structures*, LA, USA, 1991, pp.224-232.

[107] Meier, U., Deuring, M., Meier, H. and Schwegler, G., "CFRP bonded sheets", *Fibre-Reinforced-Plastic (FRP) Reinforcement for Concrete Structures: Properties and Applications*, Elsevier Science, Amsterdam, The Netherlands, 1993.

[108] Meier, U., "Strengthening of structures using carbon fibre/epoxy composites", *Construction and Building Materials*, 1995, Vol. 9, No. 6, pp.341-351.

[109] Mertz, D. R. and Gillespie Jr., J. W., "Rehabilitation of steel bridge girders through the application of advanced composite materials (Contract NCHRP-93-ID011)", Washington, D.C.: Transportation Research Board, 1996.

[110] Miller, T. C., Chajes, M. J., Mertz, D. R. and Hastings, J. N., "Strengthening of a steel bridge girder using CFRP plates", *ASCE Journal of Bridge Engineering*, 2001, Vol. 6, No. 6, pp. 514-522.

[111] Mota, C., Alminar, S., and Svecova, D., "Critical review of deflection formulas for FRP-RC members", *ASCE Journal of Composites for Construction*, 2006, Vol. 10, No. 3, pp.183-194.

[112] Mosallam, A. S., Evaluation and construction of composite strengthening systems for the Sauvie Island Bridge", *Proc. 2nd International Conference on*

FRP composites in Civil Engineering (CICE 2004), Adelaide, Australia, 2004, pp.715-723.

[113] Moy S. S. J. (ed.), "ICE Design and Practice Guide. FRP composites – Life Extension and Strengthening of Metallic Structures", Thomas Telford, 2001, London. ISBN 9780727730091.

[114] Moy, S. S. J. and Bloodworth, A. G., "Strengthening a steel bridge with CFRP composites", *Proc. Instn Civ. Engrs Structus & Bldgs*, 2007, Vol. 160, pp.81-93.

[115] Naaman, A. E. and Jeong, S. M., "Structural ductility of concrete beams with FRP tendons", *Non-metallic (FRP) Reinforcement for Concrete Structures*, E & FN Spon, London, 1995, pp.379-401.

[116] Naaman, A. E., Park, S. Y., Lopez, M. M., Stankiewicz and Pinkerton, L., "Repair and strengthening of RC beams using CFRP laminates", *University of Michigan Rep. No. UMCEE 99-04, 97-12, 98-21, 98-38, 98-39*, Ann Arbor, Mich., 1999.

[117] Nanni, A., Alkhrdaji, T., Barker, M., Chen, G., Mayo, R., and Yang, X. Overview of testing to failure program of a highway bridge strengthened with FRP composites", *Proc. 4th International Symposium on Fibre-reinforced Plastics for Reinforced Concrete Structures (FRPRCS-4)*, Baltimore, USA, 1999, pp.725-735.

[118] Neale, K., "Strengthening reinforced concrete structures with externally-bonded fibre reinforced polymers (FRPs)", ISIS Canada Design Manual No. 4, 2001.

[119] Neubauer, U. and Rostasy, F. S., "Design aspects of concrete structures strengthened with externally bonded CFRP-plates", *Concrete and Composites, Proc. 7th International Conference on Structural Faults and Repair*, 1997, Vol. 2, pp.109-118.

[120] Nordin, H. and Taljsten, B., "Concrete beams strengthened with prestressed near surface mounted CFRP." *ASCE Journal of Composites for Construction*, 2006, Vol. 10, No. 1, pp.60-68.

[121] Niu, H.D. and Wu, Z.S., "Prediction of debonding failure load due to flexural cracks of concrete for FRP-strengthened structures", *Proc. 5th International Conference on Fibre-reinforced Plastics for Reinforced Concrete Structures (FRPRCS-5)*, Cambridge, UK, 2001, pp.361-370.

[122] Oehlers, D.J., "Reinforced concrete beams with plates glued to their soffits", *ASCE Journal of Structural Engineering*, 1992, Vol. 118, No. 8, pp.2023-2038.

[123] Oehlers D. J., Ju G., Liu I. S. T. and Seracino R., "Moment redistribution in continuous plated RC flexural members. Part 1: neutral axis depth approach and tests", *Engineering Structures*, 2004a, Vol. 26, pp.2197-2207.

[124] Oehlers D. J., Liu I. S. T., Ju G. and Seracino R., "Moment redistribution in continuous plated RC flexural members. Part 2: flexural rigidity approach", *Engineering Structures*, 2004b, Vol. 26, pp.2209-2218.

[125] Oehlers D. J. and Seracino R., "*Design of FRP and steel plated RC structures: retrofitting beams and slabs for strength, stiffness and ductility*", Elsevier, 2004c, Oxford, UK.

[126] Oehlers, D. J., Griffith, M. C. and Mohamed Ali, M. S., "Ductility components and limits of FRP-plated RC structures", *Construction and Building Materials*, 2008, in press.

[127] Pan, J. L. and Leung C. K. Y., "Effect of end tapering on crack induced FRP debonding from the concrete substrate", *ASCE Journal of Composites for Construction*, 2008, Vol. 12, No. 1, pp.15-24.

[128] Patnaik, A.K. and Bauer, C. L., "Strengthening of steel beams with carbon FRP laminates", *Proc. 4th International conference on Advanced Composite Materials in Bridges and Structures*, Calgary, Alberta, Canada, 2004, pp.1-8.

[129] Pham, H. and Al-Mahaidi, R., "Experimental investigation into flexural retrofitting of reinforced concrete bridge beams using FRP composites", *Journal of Composite Structures*, 2004, No. 66, pp.617-625.

[130] Phares, B. M., Wipf, T. J., Klaiber, F. W., Abu-Hawash, A. and Lee, Y. S., "Strengthening of steel girder bridges using FRP", *Proc., Mid-Continent Transportation Research Symposium*, Ames, Iowa, 2003, pp.1-12.

[131] Prakkhya, G. K. and Morley, C. T. M., "Tension stiffening and moment-curvature relations of reinforced concrete elements", 1990, Vol. 87, No. 5, pp.597-605.

[132] Quantrill, R. J., Hollaway, L.C. and Thorne, A. M., "Experimental and analytical Iinvestigation of FRP strengthened beam response: Part I", *Magazine of Concrete Research*, 1996, Vol. 48, No. 177, pp.331-342.

[133] Quantrill, R. J. and Hollaway, L. C., "The flexural rehabilitation of reinforced concrete beams by the use of prestressed advanced composite plates", *Composites Science and Technology*, Vol. 58, No. 8, 1998, pp.1259-1275.

[134] Quattlebaum, J., Harris, K. and Petrou, M., "Comparison of three flexural retrofit systems under monotonic and fatigue loads", *ASCE Journal of Bridge Engineering*, 2005, Vol. 10, No. 6, pp.731-740.

[135] Rahimi, H. and Hutchinson, A., "Concrete beams strengthened with externally bonded FRP plates", *ASCE Journal of Composites for Construction*, 2001, Vol. 5, No. 1, pp.44–56.

[136] Raoof, M. and Zhang, S., "An insight into the structural behaviour of reinforced concrete beams with externally bonded plates", *Proceedings of the. Institution of Civil Engineers, Structures and Buildings*, 1997, Vol. 122, pp. 477-492.

[137] Raoof, M. and Hassanen, M. A. H., "Peeling failure of reinforced concrete beams with fiber-reinforced plastic or steel plates glued to their soffits", *Proceedings of the. Institution of Civil Engineers, Structures and Buildings*, 2000, Vol. 140, pp.291-305.

[138] Razaqpur, A. G., Svecova, D., and Cheung, M. S., "Rational method for calculating deflection of fibre-reinforced polymer reinforced beams." *ACI Structural Journal*, 2000, Vol. 97, No. 1, pp.175-184.

[139] Ritchie, P. A., Thomas, D. A., Lu, L. W. and Connelly, G. M., "External reinforcement of concrete beams using fiber reinforced plastic", *ACI Structural Journal*, 1991, Vol. 88, No. 4, pp.490-500.

[140] Rizkalla, S. and Mufti, A., "Reinforcing concrete structures with fibre reinforced polymers", *Design manual No. 3*, 2001, ISIS Canada, Winnipeg, Canada.

[141] Rizkalla, S., Dawood, M. and Shahawy, M., "Fiber-reinforced polymers for transportation and civil engineering infrastructure", *Transportation Research Circular No. E-C104*, September, 2006, pp.121-145.

[142] Roberts T. M., "Approximate analysis of shear and normal stress concentrations in the adhesive layer of plated RC beams. *The Structural Engineer*, 1989, Vol. 67, No. 12, pp.229-233.

[143] Rosenboom, O. and Rizkalla, S., "Modelling of IC debonding of FRP-strengthened concrete flexural members." *ASCE Journal of Composites for Construction*, 2008, Vol. 12, No. 2, pp.168-179.

[144] Saadatmanesh, H. and Ehsani, M., "RC beams strengthened with GFRP plates: Part I: Experimental Study", *ASCE Journal of Structural Engineering*, 1991, Vol. 117, No. 11, pp.3417-3433.

[145] Saadatmanesh, H. and Malek, A.M., "Design guidelines for flexural strengthening of RC beams with FRP plates", *ASCE Journal of Composites for Construction*, 1998, Vol. 2, No. 4, pp.158-164.

[146] Said, H. and Wu, Z., "Evaluating and proposing models of predicting IC debonding failure." *Journal of Composites for Construction*, 2008, Vol. 12, No. 3, pp.284-299.

[147] Sayed-Ahmed, E. Y., "Numerical investigation into strengthening steel I-section beams using CFRP strips", *Structures Congress 2006*, 2006, pp.1-8.

[148] Saxena, P., Toutanji, H., and Noumowe, A., "Failure analysis of FRP-strengthened RC beams", *ASCE Journal of Composites for Construction*, 2008, Vol. 12, No. 1, pp.2-14.

[149] Schnerch, D. and Rizkalla, S., "Strengthening of steel bridges with high modulus CFRP strips", *ASCE Journal of Bridge Engineering*, 2008, Vol. 13, No. 2, pp.192-201.

[150] Schuman, P., Karbhari, V. M., Seible, F., and Sikorsky, C., "Rehabilitation of a multi-span bridge using FRP composite materials", *Proc. International*

Conference on High Performance Materials in Bridges 2003, Kona, Hawaii, USA, pp.374-385.

[151] Sebastian, W.M., "Significance of mid-span debonding failure in FRP-plated RC beams", ASCE Journal of Structural Engineering, 2001, Vol. 127, No. 7, pp. 792-798.

[152] Sebastian W. M, "Sensitivities of strength and ductility of plated reinforced concrete sections to pre-existing strains", *ASCE Journal of Structural Engineering*, 2002, Vol. 128, No. 5, pp.624-636.

[153] Sebastian W. M., "Nonlinear influence of contraflexure migration on near-curtailment stresses in hyperstatic FRP-laminated steel members", *Computers and Structures*, 2003, 81, pp.1619-1632.

[154] Sebastian W. M., "Design of FRP strengthening in metal yield zones", *Proceedings of the Institute of Civil Engineers, Structures and Buildings*, 2005, Vol. 158, No. 5, pp.303-310.

[155] Sebastian W. M., "Performance implications of imperfectly plastic material in metallic structures with non-metallic reinforcement", *ASCE Journal of Structural Engineering*, 2006a, Vol. 132, No. 2, pp.237-243.

[156] Sebastian W. M., "Optimisation of flexural stiffness profiles to compensate for reduced ductility in hyperstatic reinforced concrete structures", *Engineering Structures*, 2006b, Vol. 28, No. 6, pp.893-902.

[157] Sebastian, W. and Luke, S., "Interface failure mechanics of elastically (advanced composite) reinforced steel members", *ASCE Journal of Structural Engineering*, 2007, Vol. 133, No. 5, pp.683-694.

[158] Seim, W., Hörman, M., Karbhari, V. and Seible, F., "External FRP poststrengthening of scaled concrete slabs", *ASCE Journal of Composites for Constructions*, 2001, Vol. 5, No. 2, pp.67-75.

[159] Sen, R., Liby, L., Spillett, K. and Mullins, G., "Strengthening steel composite bridge members using CFRP laminates". *Proc. 2nd International symposium on Non-Metallic (FRP) Reinforcement for Concrete Structures (FRPRCS-2)*, London, UK, 1995, pp551-558.

[160] Sen, R., Liby, L. and Mullins, G., "Strengthening steel bridge sections using CFRP laminates", *Composites, Part B*, 2001, Vol. 32, No.4, pp.309-322.

[161] Seracino, R., "Axial intermediate crack debonding of plates glued to concrete surfaces", *Proceedings of the International Conference on FRP Composites in Civil Engineering*, Hong Kong, China, 2001, pp.365–372.

[162] Sharma A. K., "Tests of reinforced concrete continuous beams repaired with and without fibre-ferrocement", *ACI Concrete International*, 1992, Vol. 14, No. 3, pp.36-40.

[163] Sharif, A., Al-Sulaimani, G. J., Basunbul, I. A., Baluch, M. H. and Chaleb, B. N. "Strengthening of initially loaded reinforced concrete beams using FRP plates", *ACI Structural Journal*, 1994, Vol. 91, No. 2, pp.160-168.

[164] Smith, S.T., Teng, J.G. and Chen, J.F., "Debonding in FRP plated RC beams induced by intermediate cracking", *Proc. ACUN-3 International Composites Conference: Technology Convergence in Composite Applications*, Sydney, Australia, 2001, pp. 67-72.

[165] Smith, S.T. and Teng, J.G., "FRP strengthened RC beams – I: Review of debonding strength models", *Engineering Structures*, 2002a, Vol. 24, No. 4, pp. 385-395.

[166] Smith, S.T. and Teng, J.G., "FRP strengthened RC beams – II: Assessment of debonding strength models", *Engineering Structures*, 2002b, Vol. 24, No. 4, pp. 397-417.

[167] Spadea G., Swamy R. N. and Bencardino F., "Strength and ductility of RC beams reparied with bonded CFRP laminates", *ASCE Journal of Bridge Engineering*, 2001, Vol. 6, No. 5, pp.349-355.

[168] Standards Australia, "Australian Concrete Structures Standard AS 3600", Sydney, Australia, 1994.

[169] Stocklin, L. and Meier, U., "Strength of concrete structures with prestressed and gradually anchored CFRP strips", *Proc. 5th International Conference on Fibre-reinforced Plastics for Reinforced Concrete Structures (FRPRCS-5)*, Cambridge, UK, 2001, pp.291-296. ISBN 0727730290.

[170] Swamy, R. N. and Mukhopadhyaya, P., "Debonding of carbon-fibre-reinforced polymer plate from concrete beams", *Proc. Instn Civ. Engrs Structus & Bldgs*, 1999, Vol. 123, pp.301-317.

[171] Täljsten, B., "Plate bonding - Strengthening of existing concrete structures with epoxy bonded plates of steel or fibre reinforced plastics", PhD thesis, Luleå University of Technology, Sweden, 1994, 189 pp.

[172] Tann, D. B., Delpak, R. and Davies, P., "Ductility and deformability of fibre-reinforced polymer-strengthened reinforced concrete beams", *Proc. Instn Civ. Engrs Structus & Bldgs*, 2004, Vol. 157, pp.19-30.

[173] Tavakkolizadeh, M. and Saadatmanesh, H., "Strengthening of steel-concrete composite girders using carbon fiber reinforced polymer sheets", *ASCE Journal of Structural Engineering*, 2003, Vol. 129, No. 1, pp.30-40.

[174] Taylor, M. J., Luke, P. S., Collins, S. and Darby, J. J., "Using advanced composites in strengthening and rehabilitation of rail bridges", *Proc. 2nd International Conference on Railway Engineering*, London, 1999.

[175] Teng, J.G., Chen, J.F., Smith, S.T. and Lam, L., "FRP strengthened RC structures", John Wiley and Sons Ltd., 2002, Chichester, UK. ISBN 0471487066.

[176] Teng, J.G., Smith, S.T., Yao, J. and Chen, J.F., "Intermediate crack induced debonding in RC beams and slabs", *Construction and Building materials*, 2003, Vol. 17, No. 6, pp. 447-462.

[177] Teng, J.G., Lu, X.Z., Ye, L.P. and Jiang, J.J., "Recent research on intermediate crack-induced debonding in FRP strengthened RC beams", *Proc. 4th Advanced Composite Materials in Bridges and Structures (ACMBS-IV)*, Alberta, Canada, 2004, pp.1-12.

[178] Toutanji, H. A. and Saafi, M., "Flexural behavior of concrete beams reinforced with glass fiber-reinforced polymer (GFRP) bars", *ACI Structural Journal*, 2000, Vol. 97, No.5, pp.712–719.

[179] Toutanji, H., Zhao, L. and Anselm, E., "Verifications of design equations of beams externally strengthened with FRP composites", *ASCE Journal of Composites for Construction*, 2006, Vol. 10, No. 3, pp.254-264.

[180] Toutanji, H., Saxena, P., Zhao, L., and Ooi T., "Prediction of interfacial bond failure of FRP-concrete surface", *ASCE Journal of Composites for Construction*, 2007, Vol. 11, No. 4, pp.427-436.

[181] Toutanji, H., Han, M., Gilbert, J. and Matthys, S., "Behavior of large-scale rectangular columns confined with FRP composites", *ASCE Journal of Composites for Construction*, 2010, Vol. 14, No. 62, pp.62-71.

[182] Triantafillou, T. C. and Deskovic, N., "Innovative Prestressing with FRP Sheets: Mechanics of Short-Term Behavior", *ASCE Journal of Engineering Mechanics*, 1991, Vol. 117, No. 7, pp.1652-1672.

[183] Triantafillou, T. C., Deskovic, N., and Deuring, M., "Strengthening of concrete structures with prestressed fibre reinforced plastic sheets", *ACI Structural Journal*, 1992, Vol. 89, No. 3, pp.235-244.

[184] Tumialan, G., Serra, P., Nanni, A. and Belarbi, A., "Concrete cover delamination in reinforced concrete beams strengthened with carbon fiber reinforced polymer sheets", *Proc. 4th International Symposium on Fibre-reinforced Plastics for Reinforced Concrete Structures (FRPRCS-4)*, Baltimore, USA, 1999, pp. 725-735.

[185] Tumialan G, Tinazzi D, Myers J, Nanni A., "Field evaluation of masonry walls strengthened with FRP composites at the Malcolm Bliss Hospital", *Report CIES 99-8*, University of Missouri-Rolla, Rolla, MO, 1999.

[186] Ulaga, T., Vogel, T. and Meier, U., "Bilinear stress-slip model: Theoretical background and significance", *Proc., 6th International Symposium on Fiber-Reinforced Polymer Reinforcement for Reinforced Concrete Structures (FRPRCS-6)*, Singapore, 2003, pp.153-162. ISBN 9812384014.

[187] Varastehpour, H. and Hamelin, P., "Strengthening of concrete beams using fiber-reinforced plastics", *Materials and Structures*, 1997, Vol. 30, No. 3, pp.160-166.

[188] Wang, C.Y. and Ling, F.S., "Prediction for the debonding failure of cracked RC beams with externally bonded FRP sheets", Proc., *2nd International Conference on Composites in Infrastructure (ICCI'98)*, Tucson, Arizona, USA, 1998, pp.548-562.

[189] Wight, R. G., Green, M. F. and Erki, M. A., "Tapered transfer zones for prestressed FRP sheets", *Proceedings of the 1995 Annual Conference of the Canadian Society for Civil Engineering*, Ottawa, Canada, 1995, pp.1356-1364.

[190] Wight, R. G., Green, M. F. and Erki, M. A., "Prestressed FRP sheets for poststrengthening reinforced concrete beams", *ASCE Journal of Composites for Construction*, 2001, Vol. 5, No. 4, pp.214-220.

[191] Woo, S. K., Nam, J. W., Kim, J. H. J, Han, S. H. and Byun, K. J., " Suggestion of flexural capacity evaluation and prediction of prestressed CFRP strengthened design", *Engineering Structures*, 2008, Vol. 30, No. 12, pp.3751-3763.

[192] Wu, Z., Matsuzaki, T. and Tanabe, K., "Interface crack propagation in FRP-strengthened concrete structures", Proc., 3rd *Non-metallic (FRP) Reinforcement for Concrete Structures (FRPRCS-3)*, Sapporo, Japan, 1997, Vol. 1, pp.319-326.

[193] Wu, Z., Matsuzaki, T., Yokoyama, K. and Kanda, T., "Retrofitting method for reinforced concrete structures with externally prestressed FRP sheets", *Proc. 4th International Conference on Fibre-reinforced Plastics for Reinforced Concrete Structures (FRPRCS-4)*, Baltimore, USA, 1999, pp.751-765.

[194] Wu, Z.S. and Niu, H.D., "Study on debonding failure load of RC beams strengthened with FRP sheets", *JSCE Journal of Structural Engineering*, 2000, 46 (A), pp.1431-1441.

[195] Yang, Y. X., Yue, Q. R. and Hu, Y. C., "Experimental study on bond performance between carbon fiber sheets and concrete", *Journal of Buildings and Structures*, 2001, Vol. 22, No.3, pp.36-42 (in Chinese).

[196] Yost, J. R., Gross, S. P. and Dinehart, D. W., "Effective moment of inertia for glass fiber-reinforced polymer-reinforced concrete beams", *ACI Structural Journal*, 2003, Vol. 100, No. 6, pp.732–739.

[197] Youssef, M. A., "Analytical prediction of the linear and nonlinear behaviour of steel beams rehabilitated using FRP sheets", *Engineering Structures*, 2006, Vol. 28, No. 6, pp.903-911.

[198] Yuan, H. and Wu, Z. S., "Interfacial fracture theory in structures strengthened with composite of continuous fiber", *Proceedings of the Symposium of China and Japan, Science and Technology of the 21st Century*, Tokyo, Japan, 1999, pp.142-155.

[199] Yuan, H., Wu, Z. S. and Yoshizawa, H., "Theoretical solutions on interfacial stress transfer of externally bonded steel/composite laminates", *JSCE Journal of Structural Mechanics and Earthquake Engineering*, April, 2001 (In press).

[200] Zhao, L., "Characterization of RC beams strengthened with carbon fiber sheets", Graduation thesis, Department of Civil and Environmental Engineering, University of Alabama in Huntsville, Huntsville, Alabama, USA, 2005.

[201] Zhao X. L., Fernando D. and Al-Mahaidi R., CFRP strengthened RHS subjected to transverse end bearing force. *Engineering Structures*, 2006. Vol. 28, No. 11, pp.1555-1565.

[202] Zhao, X. L. and Zhang, L., "State of the art review on FRP strengthened steel structures", *Engineering Structures*, 2007, Vol. 29, No. 8, pp.1808-1823.

[203] Ziraba, Y.N., Baluch, M.H., Basunbul, I.A., Sharif, A.M., Azad, A.K. and Al-Sulaimani, G.J., "Guidelines towards the design of reinforced concrete beams with external plates", *ACI Structural Journal*, 1994, Vol. 91, No. 6, pp.639-646.